

**From supramolecular chemistry to crystal engineering using  
hydrogen- and halogen bonds**

by

Stefan Nirasher Lorenzo Andree

B.S., University of Colombo, 2011

AN ABSTRACT OF A DISSERTATION

submitted in partial fulfillment of the requirements for the degree

DOCTOR OF PHILOSOPHY

Department of Chemistry  
College of Arts and Sciences

KANSAS STATE UNIVERSITY  
Manhattan, Kansas

2018

## Abstract

A methodology for estimating hydrogen-bond preferences and binding affinities in solution, based on molecular electrostatic potential surfaces (MEPS), is presented using tritopic hydrogen bond acceptor and a series of aromatic carboxylic acids. The plot of calculated MEPS values against experimentally determined binding constants produces a goodness-of-fit of over 0.93 and a similar positive correlation is obtained between MEPS values and binding enthalpies.

A series of tritopic N-heterocyclic compounds were synthesized and subjected to systematic co-crystallizations with selected multi-topic aliphatic and aromatic carboxylic acids to determine if ditopic and tritopic donors formulate assemblies with desired stoichiometries. The co-crystals formed contained the COOH $\cdots$ Bzim synthon, and we observe vacant sites on the acceptor molecules.

A series of co-crystallizations between tritopic N-heterocyclic compounds and perfluoroiodoarenes were carried to map out structural landscapes. At least one potential binding site on the acceptor is left vacant on all the four structures obtained. The absence of halogen bonds to all sites can be ascribed primarily due to deactivation of the  $\sigma$ -hole on the iodo-arene donors and partially due to steric hindrance.

Four nonsteroidal anti-inflammatory (NSAID) drugs were chosen due to the presence of the COOH moiety, to establish if aqueous solubility can be modulated by systematic solubility measurements of the complex. Two different solids were obtained with a 1:1 and 1:3 stoichiometry. The solubility of the 1:1 co-crystal decreased by 12-fold compared to pure aspirin (3mg/mL at 20 °C) indicating that co-crystals can offer promising new solid forms of pharmaceutically relevant compounds.

A series of hydrogen- and halogen bonding Tröger's base derivatives were synthesized using aromatic N-heterocycles and the iodoethynyl functionality, followed by a series of co-crystallization between aliphatic dicarboxylic acids and symmetric ditopic acceptors. The results suggest that reducing the number of binding sites from three to two facilitates the formation of co-crystals with the desired stoichiometry. The results indicate that directed assembly can be achieved more easily when the molecular building blocks are conformationally rigid.

# **From supramolecular chemistry to crystal engineering using hydrogen- and halogen bonds**

by

Stefan Nirasher Lorenzo Andree

B.S., University of Colombo, 2011

A DISSERTATION

submitted in partial fulfillment of the requirements for the degree

DOCTOR OF PHILOSOPHY

Department of Chemistry  
College of Arts and Sciences

KANSAS STATE UNIVERSITY  
Manhattan, Kansas

2018

Approved by:

Major Professor  
Christer B. Aakeröy



# Copyright

© Stefan Andree 2018.

## Abstract

A methodology for estimating hydrogen-bond preferences and binding affinities in solution, based on molecular electrostatic potential surfaces (MEPS), is presented using tritopic hydrogen bond acceptor and a series of aromatic carboxylic acids. The plot of calculated MEPS values against experimentally determined binding constants produces a goodness-of-fit of over 0.93 and a similar positive correlation is obtained between MEPS values and binding enthalpies.

A series of tritopic N-heterocyclic compounds were synthesized and subjected to systematic co-crystallizations with selected multi-topic aliphatic and aromatic carboxylic acids to determine if ditopic and tritopic donors formulate assemblies with desired stoichiometries. The co-crystals formed contained the COOH $\cdots$ Bzim synthon, and we observe vacant sites on the acceptor molecules.

A series of co-crystallizations between tritopic N-heterocyclic compounds and perfluoroiodoarenes were carried to map out structural landscapes. At least one potential binding site on the acceptor is left vacant on all the four structures obtained. The absence of halogen bonds to all sites can be ascribed primarily due to deactivation of the  $\sigma$ -hole on the iodo-arene donors and partially due to steric hindrance.

Four nonsteroidal anti-inflammatory (NSAID) drugs were chosen due to the presence of the COOH moiety, to establish if aqueous solubility can be modulated by systematic solubility measurements of the complex. Two different solids were obtained with a 1:1 and 1:3 stoichiometry. The solubility of the 1:1 co-crystal decreased by 12-fold compared to pure aspirin (3mg/mL at 20 °C) indicating that co-crystals can offer promising new solid forms of pharmaceutically relevant compounds.

A series of hydrogen- and halogen bonding Tröger's base derivatives were synthesized using aromatic N-heterocycles and the iodoethynyl functionality, followed by a series of co-crystallization between aliphatic dicarboxylic acids and symmetric ditopic acceptors, respectively. The results suggest that reducing the number of binding sites from three to two facilitates the formation of co-crystals with the desired stoichiometry. The results indicate that directed assembly can be achieved more easily when the molecular building blocks are conformationally rigid.

# Table of Contents

List of Figures .....	xiv
List of Tables .....	xx
Acknowledgements .....	xxii
Dedication .....	xxiii
Chapter 1 - Introduction .....	1
1.1 Supramolecular chemistry .....	1
1.2 Supramolecular chemistry in solution .....	2
1.3 Concepts in supramolecular chemistry .....	4
1.3.1 Molecular self-assembly .....	4
1.3.2 Molecular recognition .....	5
1.4 Supramolecular interactions .....	6
1.4.1 Hydrogen-bond .....	7
1.4.2 Halogen bond .....	7
1.5 Solid-state supramolecular chemistry .....	8
1.5.1 Crystal engineering .....	9
1.6 Research overview .....	11
1.6.1 Overall challenge .....	11
1.6.2 Goals .....	12
1.7 References .....	13
Chapter 2 - Molecular electrostatic potentials as a quantitative measure of hydrogen bonding preferences in solution <sup>1</sup> .....	16
2.1 Introduction .....	16
2.2 Experimental .....	21
2.2.1 Molecular electrostatic potential surface calculations .....	21
2.2.2 Materials and methods .....	22
2.2.3 Synthesis .....	22
2.2.3.1 Synthesis of 1,3,5-tris(bromomethyl) benzene .....	22
2.2.3.2 Synthesis of 1,3,5-tris(imidazole-1-yl-methyl) benzene .....	23
2.2.4 Binding studies with ITC .....	24

2.2.4.1 Binding study of 1,3,5-tris(imidazole-1-yl-methyl) benzene and 3-nitrobenzoic acid.....	25
2.2.4.2 Binding study of 1,3,5-tris(imidazole-1-yl-methyl) benzene and 3-methoxybenzoic acid .....	25
2.2.4.3 Binding study of 1,3,5-tris(imidazole-1-yl-methyl) benzene and benzoic acid....	25
2.2.4.4 Binding study of 1,3,5-tris(imidazole-1-yl-methyl) benzene and 3-dimethylaminobenzoic acid .....	25
2.3 Results.....	26
2.4 Discussion.....	31
2.5 Conclusions <sup>1</sup> .....	38
2.6 References.....	39
Chapter 3 - Guiding tritopic nitrogen heterocycles and multitopic carboxylic acids into co-crystals via selective O—H···N hydrogen bonds .....	42
3.1 Introduction.....	42
3.2 Experimental .....	48
3.2.1 Molecular electrostatic potential surface calculations .....	48
3.2.2 Synthesis of tritopic acceptors .....	49
3.2.2.1 Synthesis of 1,3,5-tris(bromomethyl)-2,4,6-trimethylbenzene <sup>7</sup> ( <b>A</b> ).....	49
3.2.2.2 Synthesis of 1,3,5-tris(imidazole-1-yl-methyl)-2,4,6-trimethylbenzene <sup>8</sup> ( <b>A</b> ) .....	49
3.2.2.3 Synthesis of 1,3,5-tris(pyrazole-1-yl-methyl)-2,4,6-trimethyl benzene <sup>9</sup> ( <b>B</b> ).....	50
3.2.2.4 Synthesis of 1,3,5-tris(pyrazole -1-yl-methyl) benzene <sup>9</sup> ( <b>B'</b> ).....	51
3.2.2.5 Synthesis of 1,3,5-tris(3,5-dimethylpyrazole-1-yl-methyl)-2,4,6-trimethyl benzene <sup>9</sup> ( <b>C</b> ).....	51
3.2.2.6 Synthesis of 1,3,5-tris(3,5-dimethylpyrazole -1-yl-methyl) benzene ( <b>C'</b> ) .....	52
3.2.2.7 Synthesis of 1,3,5-tris(benzimidazole-1-yl-methyl)-2,4,6-trimethylbenzene <sup>8</sup> ( <b>D</b> )53	
3.2.2.8 Synthesis of 1,3,5-tris(benzimidazole -1-yl-methyl)benzene <sup>10</sup> ( <b>D'</b> ).....	54
3.2.2.9 Synthesis of 1,3,5-tris(5,6-dimethylbenzimidazole-1-yl-methyl)-2,4,6-trimethylbenzene <sup>11</sup> ( <b>E</b> ).....	54
3.2.2.10 Synthesis of 1,3,5-tris(5,6-dimethylbenzimidazole -1-yl-methyl)benzene ( <b>E'</b> ) 55	
3.2.3 Grinding experiments.....	56
3.2.4 Synthesis of co-crystals.....	56

3.2.4.1 Synthesis of 1,3,5-tris(benzimidazole -1-yl-methyl) benzene suberic acid hydrate acetonitrile, <b>D':SUB:ACN:H<sub>2</sub>O</b> (1:1:1:1) .....	56
3.2.4.2 Synthesis of 1,3,5-tris(5,6-dimethylbenziimidazole-1-yl-methyl)-2,4,6-trimethyl benzene succinic acid, <b>E:SUC</b> (1:1).....	57
3.2.4.3 Synthesis of 1,3,5-tris(5,6-dimethylbenziimidazole-1-yl-methyl)-2,4,6-trimethyl benzene terephthalic acid hydrate, <b>E:TPH:H<sub>2</sub>O</b> (1:1:1).....	57
3.2.4.4 Synthesis of 1,3,5-tris(5,6-dimethylbenziimidazole-1-yl-methyl)-2,4,6-trimethyl benzene trimesic acid, <b>E:TMS</b> (1:1) .....	57
3.2.5 CSD search.....	58
3.3 Results.....	59
3.3.1 Description of solid state architectures .....	63
3.3.1.1 Crystal structure of 1,3,5-tris(benzimidazole -1-yl-methyl) benzene suberic acid <sub>0.5</sub> hydrate acetonitrile.....	63
3.3.1.2 Crystal structure of 1,3,5-tris(5,6-dimethylbenziimidazole-1-yl-methyl)-2,4,6-trimethyl benzene succinic acid .....	64
3.3.1.3 Crystal structure of 1,3,5-tris(5,6-dimethylbenziimidazole-1-yl-methyl)-2,4,6-trimethyl benzene terephthalic acid hydrate .....	65
3.3.1.4 Crystal structure of 1,3,5-tris(5,6-dimethylbenziimidazole-1-yl-methyl)-2,4,6-trimethyl benzene trimesic acid .....	66
3.3.2 Crystal packing interactions observed in the crystal structures .....	67
3.3.2.1 Crystal structure of <b>D':SUB</b> and <b>E:SUC</b> .....	67
3.3.2.2 Crystal structure of <b>E:TPH</b> and <b>E:TMS</b> .....	68
3.4 Discussion.....	70
3.5 Conclusions.....	78
3.6 References.....	79
Chapter 4 - Structural examination of halogen-bonded co-crystals of tritopic acceptors <sup>1</sup> .....	82
4.1 Introduction.....	82
4.2 Experimental.....	85
4.2.1 Molecular electrostatic potential surface calculations .....	85
4.2.2 CSD search.....	86
4.2.3 Grinding experiments.....	86

4.2.4 Synthesis of co-crystals.....	86
4.2.5 X-ray crystallography .....	87
4.3 Results.....	87
4.3.1 Description of solid state architectures .....	91
4.3.2 Aromatic stacking .....	94
4.4 Discussion.....	96
4.5 Conclusions <sup>1</sup> .....	103
4.6 References.....	104
Chapter 5 - Co-crystal technology for drug development via O—H···N hydrogen bonds .	107
5.1 Introduction.....	107
5.2 Experimental.....	113
5.2.1 Synthesis .....	113
5.2.1.1 Synthesis of diclofenac <sup>12</sup> .....	113
5.2.1.2 Co-crystal synthesis via solvent assisted grinding experiments .....	114
5.2.2 Co-crystal experiments .....	114
5.2.2.1 Synthesis of 1,3,5-tris(5,6-dimethylbenzimidazole-1-yl-methyl)-2,4,6-trimethyl benzene tri aspirin, <b>E:(ASP)<sub>3</sub></b> .....	114
5.2.2.2 Synthesis of 1,3,5-tris(5,6-dimethylbenzimidazole-1-yl-methyl)-2,4,6-trimethyl benzene aspirin, <b>E:ASP</b> .....	115
5.2.3 Solubility studies.....	115
5.2.3.1 Preparation of co-crystals for solubility studies <sup>14</sup> .....	115
5.2.3.2 Preparation of standard series of salicylic acid for solubility studies of <b>E:ASP</b>	115
5.2.3.3 Time dependent study of aspirin hydrolysis .....	116
5.2.3.4 Aqueous solubility of <b>E:ASP</b> .....	116
5.2.4 Binding study of aspirin and 1,3,5-tris(imidazole-1-yl-methyl) benzene ( <b>A'</b> ) using isothermal titration calorimetry.....	116
5.3 Results and discussion .....	117
5.3.1 IR screening of solids resulting from solvent assisted grinding method .....	117
5.3.2 Crystal structure of <b>EH<sup>+</sup>:ASP<sup>-</sup>:(ASP)<sub>2</sub></b> .....	120
5.3.3 <sup>1</sup> H NMR of solid resulting from slow evaporation.....	121

5.3.4 IR and PXRD data analysis of solids resulting from solvothermal method and slow evaporation method.....	122
5.3.5 <sup>1</sup> H NMR and DSC data analysis of solid resulting from solvothermal method .....	125
5.3.6 Isothermal calorimetry .....	127
5.3.7 Aqueous solubility of co-crystal .....	128
5.4 Conclusions.....	132
5.5 References.....	133
Chapter 6 - A take on Trögers base as a potential hydrogen and halogen bond acceptors and donors .....	135
6.1 Introduction.....	135
6.2 Experimental.....	142
6.2.1 General.....	142
6.2.2 Electrostatic potential calculations .....	142
6.2.3 Synthesis .....	143
6.2.3.1 2,8-Diiodo-4,10-dimethyl-6H,12H-5,11-methanodibenzo[b,f]- diazocine <b>TBX1</b> <sup>8</sup> .....	143
6.2.3.2 2,8-Diiodo-6H,12H-5,11-methanodibenzo[b,f]- diazocine <b>TBY1</b> <sup>8</sup> .....	143
6.2.3.3 4,10-Dimethyl-2,8-bis[(trimethylsilyl)ethynyl]-6H,12H-5,11-methanodibenzo[b,f]- diazocine <b>TBX2</b> <sup>9</sup> .....	144
6.2.3.4 2,8-Bis[(trimethylsilyl)ethynyl]-6H,12H-5,11-methanodibenzo[b,f]-diazocine <b>TBY2</b> <sup>9</sup> .....	145
6.2.3.5 4,10-Dimethyl-2,8-bisethynyl-6H,12H-5,11-methanodibenzo[b,f]-diazocine <b>TBX3</b> <sup>10</sup> .....	145
6.2.3.6 2,8-Bisethynyl-6H,12H-5,11-methanodibenzo[b,f]-diazocine <b>TBY3</b> <sup>10</sup> .....	146
6.2.3.7 4,10-Dimethyl-2,8-diiodoethynyl-6H,12H-5,11-methanodibenzo[b,f]-diazocine <b>TBX4</b> <sup>11</sup> .....	147
6.2.3.8 2,8-Diiodoethynyl-6H,12H-5,11-methanodibenzo[b,f]-diazocine <b>TBY4</b> <sup>11</sup> .....	147
6.2.3.10 2,8-Bis-4-ethynylimidazole -6H,12H-5,11-methanodibenzo[b,f]-diazocine <b>TBX5</b> <sup>12</sup> .....	148
6.2.3.11 2,8-Bis-3-ethynylpyrazole-6H,12H-5,11-methanodibenzo[b,f]-diazocine <b>TBX6</b> <sup>12</sup> .....	149



6.2.3.12 2,8-Bis-5-ethynylpyrimidine-2-amino -6H,12H-5,11-methanodibenzo[b,f]- diazocine <b>TBX7</b> <sup>12</sup> .....	150
6.2.3.13 2,8-Bis-5-ethynylpyridine-6H,12H-5,11-methanodibenzo[b,f]-diazocine <b>TBX8</b> <sup>12</sup> .....	151
6.2.4 Grinding experiments.....	151
6.3 Results.....	152
6.3.1 MEP surface calculations.....	152
6.3.2 Covalent synthesis .....	153
6.3.2.1 Synthesis of <b>TBX1</b> .....	153
6.3.2.2 Synthesis of <b>TBX4</b> .....	153
6.3.3 IR stretching frequencies of ground mixtures.....	154
6.3.4 Description of solid state architectures .....	156
6.3.4.1 Crystal structure of 2, 8-diiodo-4,10-dimethyl-6H,12H-5,11-methanodibenzo [b,f]-diazocine ( <b>TBX1</b> ).....	156
6.3.4.2 Crystal structure of 4,10-dimethyl-2,8-bis[(trimethylsilyl)ethynyl]-6H,12H-5,11- methanodibenzo[b,f]-diazocine ( <b>TBX2</b> ).....	157
6.3.4.3 Crystal structure of 4,10-dimethyl-2,8-dipyridinethynyl-6H,12H-5,11- methanodibenzo[b,f]-diazocine ( <b>TBX8</b> ).....	159
6.3.4.4 Crystal structure of 4,10-dimethyl-2,8-diiodoethynyl-6H,12H-5,11- methanodibenzo[b,f]-diazocine tetramethylpyrazine ( <b>TBX4:A2</b> ) .....	160
6.3.4.4 Crystal structure of 4,10-dimethyl-2,8-diiodoethynyl-6H,12H-5,11- methanodibenzo[b,f]-diazocine 1,2-di(4-pyridyl)ethylene ( <b>TBX4:A6</b> ).....	161
6.4 Discussion.....	162
6.5 Conclusions.....	166
6.6 References.....	167
Chapter 7 - Conclusions and future work .....	169
Appendix A - <sup>1</sup> H NMR and <sup>13</sup> C NMR spectra .....	173

## List of Figures

Figure 1.1 Supramolecules formed by molecular recognition, binding through complementary shape and periodic arrangement resulting in a crystal lattice .....	1
Figure 1.2 Interaction of halogen bond donor with a triazole foldamer <sup>7</sup> .....	2
Figure 1.3 Ion-pair recognition based on halogen bonding to Recp(I) <sup>8</sup> .....	3
Figure 1.4 1-Haloperfluoroalkanes as catalysts for reductions of 2-substituted quinolines by Hantzsch ester <sup>9</sup> .....	3
Figure 1.5 Chemical structures of the keto (top) and enol (bottom) tautomers of UPy and their dimers <sup>10</sup> .....	4
Figure 1.6 Self-assembly between complementary molecules .....	5
Figure 1.7 Molecular recognition .....	6
Figure 1.8 Hydrogen bond donating and hydrogen bond accepting groups .....	7
Figure 1.9 Schematic diagram showing the formation of a halogen bond (R and D-molecular fragments or atoms; X-halogen atom; A-nucleophilic atom) .....	8
Figure 1.10 Green route crystal engineering .....	10
Figure 1.11 Generations of crystal engineering <sup>29</sup> .....	10
Figure 1.12 Photodimerized products of trans-cinammic acid .....	11
Figure 2.1 Molecular recognition .....	16
Figure 2.2 Schematic representation of the electrostatic solvent competition mode .....	17
Figure 2.3 Molecular electrostatic potential surface map on CHCl <sub>3</sub> .....	17
Figure 2.4 Scheme representing tritopic acceptor and donors employed in this study .....	19
Figure 2.5 A schematic of ITC cell and injection syringe and raw data from ITC experiment with binding isotherm <sup>21</sup> .....	20
Figure 2.6 Three possible outcomes when co-crystallizing monotopic donors with a tritopic acceptor .....	21
Figure 2.7 Calculated molecular electrostatic potential surface maps; ABEN = 3-diamino benzoic acid; HBEN = benzoic acid; MBEN = 3-methoxybenzoic acid; and NBEN = 3-nitrobenzoic acid .....	26
Figure 2.8 ITC profile between IM <sub>3</sub> (1.20 mM) and NBEN (0.150 mM) at 25°C .....	29
Figure 2.9 ITC profile between IM <sub>3</sub> (1.20 mM) and MBEN (0.150 mM) at 25°C .....	29

Figure 2.10 ITC profile between IM <sub>3</sub> (1.20 mM) and HBEN (0.150 mM) at 25°C .....	30
Figure 2.11 ITC profile between IM <sub>3</sub> (1.20 mM) and ABEN (0.150 mM) at 25°C .....	30
Figure 2.12 Plot of the association constant versus electrostatic potential on carboxyl H for the binding of IM <sub>3</sub> with benzoic acid derivatives .....	32
Figure 2.13 Plots of average $\Delta H$ versus electrostatic potential on carboxyl H for the binding of IM <sub>3</sub> with benzoic acid derivatives.....	34
Figure 2.14 Scatter plot of enthalpies $\Delta H$ and entropies $\Delta S$ for the binding of IM <sub>3</sub> with benzoic acid derivatives .....	36
Figure 2.15 Plot of the association constant versus pK <sub>a</sub> values of aromatic carboxylic acids for the binding of IM <sub>3</sub> with benzoic acid derivatives .....	37
Figure 2.16 Plots of average $\Delta H$ versus pK <sub>a</sub> values of aromatic carboxylic acids for the binding of IM <sub>3</sub> with benzoic acid derivatives .....	37
Figure 3.1 Supramolecular synthons in a co-crystal.....	43
Figure 3.2 Schematic showing some examples of observable synthons (a) COOH···imidazole (b) COOH···benzimidazole (c) COOH···pyrazole .....	44
Figure 3.3 The (a) COOH···imidazole and (b) COOH···benzimidazole synthons indicating the best and second-best hydrogen-bond donor/acceptor couples.....	44
Figure 3.4 Possible outcomes in this study in the presence of monotopic, flexible ditopic and rigid tritopic donors.....	45
Figure 3.5 Tritopic acceptors used in this study .....	46
Figure 3.6 Multitopic hydrogen bond donors used in this study .....	47
Figure 3.7 Ditopic acceptors used in the CSD study .....	58
Figure 3.8 Main interactions in the crystal structure of <b>D':SUB<sub>0.5</sub>:H<sub>2</sub>O:MeCN</b> .....	63
Figure 3.9 Main interactions in the crystal structure of <b>E:SUC</b> .....	64
Figure 3.10 Main interactions in the crystal structure of <b>E:TPH:H<sub>2</sub>O</b> .....	65
Figure 3.11 Main interactions in the crystal structure of <b>E:TMS</b> .....	66
Figure 3.12 Secondary C—H··· $\pi$ interactions observed for <b>E</b> in <b>E:SUC</b> .....	67
Figure 3.13 Secondary C—H··· $\pi$ interactions observed for <b>D'</b> in <b>D':SUB</b> .....	67
Figure 3.14 Overall packing interactions of (a) <b>E:SUC</b> and (b) <b>D':SUB</b> .....	68
Figure 3.15 Packing interactions of <b>E:TPH</b> (a) one dimensional (b) two dimensional (c) two dimensional space filling .....	69

Figure 3.16 Packing interactions of <b>E:TMS</b> (a) one dimensional (b) side view indicating acceptor donor stacking interactions (c) two dimensional.....	70
Figure 3.17 Full interaction maps showing steric hinderance at the vacant acceptor site in <b>D':SUB</b> .....	73
Figure 3.18 Alternative heteromeric O—H···N/C—H···O motif in (a) COOH···imidazole and (b) COOH···benzimidazole interactions.....	74
Figure 3.19 Intra-chain and structure directing inter-chain C—H···O interactions observed in <b>D':SUB</b> .....	75
Figure 3.20 Structure directing intramolecular chain C—H···O interactions observed in <b>E:SUC</b> (methyl substituent on benzene scaffold and hydrogens on succinic acid were removed for clarity).....	76
Figure 4.1 Electrostatic potential surface representing a halogen bond <sup>6</sup> .....	82
Figure 4.2 Tritopic acceptors used in this study .....	83
Figure 4.3 Halogen bond donor molecules used in this study .....	84
Figure 4.4 Main interactions in the crystal structure of <b>12XB:B</b> .....	92
Figure 4.5 Tetramer in the structure of <b>14XB:E</b> .....	92
Figure 4.6 (a) Tetramer in the crystal structure of <b>135XB:E:EtOAc</b> (b) Ethyl acetate wedged between benzimidazole arms .....	93
Figure 4.7 Primary halogen bond interactions in the structure of <b>135XB:A</b> .....	93
Figure 4.8 (a) Stacking interactions between the two components in the structure of <b>12XB:B</b> ; (b) Space filling representation of the packing showed in (a).....	94
Figure 4.9 (a) Stacking of donors in <b>12XB:B</b> (b) Stacking of donors in <b>135XB:A</b> ; (c) Close packing of donor molecules in <b>14XB:E</b> .....	95
Figure 4.10 Expected vs unexpected connectivity.....	97
Figure 4.11 <b>14XB</b> structures that failed to reach a full coordination. (a) TOJBOK, (b) TAWFEE, (c) VABNUJ .....	98
Figure 4.12 Halogen-bond distances and angles extracted from a CSD search on crystal containing sp <sup>2</sup> -hybridized nitrogen atoms as acceptors and (a) <b>135XB</b> , (b) <b>12XB</b> and (c) <b>14XB</b> , respectively. The colors indicate number of hits in each cell.....	99
Figure 4.13 Molecular geometries of the tritopic acceptor molecules in the crystal structures of <b>14XB:E</b> (top left), <b>12XB:B</b> (bottom left), <b>135XB:A</b> (top right), and <b>135XB:E:EtOAc</b>	

(bottom right). The crown conformation is only observed in the crystal structure of <b>135XB:E:EtOAc</b> , whereas the chair is present in the other three structures .....	101
Figure 4.14 $\sigma$ -hole bonding.....	102
Figure 4.15 Full interaction maps showing steric hinderance at the vacant donor site in <b>E:14XB</b> .....	103
Figure 5.1 API solid form classification according to the structure and composition.....	107
Figure 5.2 BCS classification of API's.....	109
Figure 5.3 Non-steroidal anti-inflammatory drugs .....	110
Figure 5.4 Schematic of tritopic acceptors used in the study .....	110
Figure 5.5 NSAID general structure .....	111
Figure 5.6 Two unique morphologies of <b>E</b> and <b>ASP</b> (a) ribbon-like and (b) columnar-like crystals .....	119
Figure 5.7 Asymmetric unit of the crystal resulting from <b>EH<sup>+</sup>:ASP<sup>-</sup>:(ASP)<sub>2</sub></b> .....	120
Figure 5.8 Tetramer in the crystal structure of <b>EH<sup>+</sup>:ASP<sup>-</sup>:(ASP)<sub>2</sub></b> .....	120
Figure 5.9 Dimers formed between (a) 2-carboxyphenolate ions (b) salicylic acids .....	121
Figure 5.10 <sup>1</sup> H NMR of ribbon-like crystal, where peaks denoted in red correspond to aspirin and peaks in cyan correspond to acceptor <b>E</b> .....	122
Figure 5.11 Top is the IR spectrum of <b>E:ASP</b> prepared from a solvothermal method and the bottom is the IR spectrum for single crystal of <b>E:ASP</b> .....	123
Figure 5.12 Overlaid IR spectrums of crystals resulting from slow evaporation of <b>E:ASP</b> in red and <b>EH<sup>+</sup>:ASP<sup>-</sup>:(ASP)<sub>2</sub></b> in cyan .....	123
Figure 5.13 Overlaid powder patterns of <b>E</b> , <b>ASP</b> , <b>E:ASP</b> , simulated <b>EH<sup>+</sup>:ASP<sup>-</sup>:(ASP)<sub>2</sub></b> and bulk (resulting from solvothermal method) .....	125
Figure 5.14 <sup>1</sup> H NMR of bulk <b>E:ASP</b> , where peaks denoted in red correspond to aspirin and peaks in cyan correspond to acceptor <b>E</b> .....	126
Figure 5.15 DSC thermograms for bulk solid <b>E:ASP</b> and aspirin by itself .....	127
Figure 5.16 ITC profile between A' (1.20 mM) and aspirin (0.150 mM) at 25°C .....	128
Figure 5.17 Alkaline hydrolysis of aspirin followed by acidification resulting in salicylic acid	129
Figure 5.18 Ultraviolet absorption spectra of aspirin in acidic solution before (black) and after (orange) hydrolysis .....	129
Figure 5.19 Effect of time on aspirin hydrolysis .....	130

Figure 5.20 Absorption maxima at 303 nm for salicylic acid at different concentrations.....	130
Figure 5.21 Absorption vs concentration plot of salicylic acid .....	131
Figure 5.22 Control experiment of acceptor <b>E</b> .....	131
Figure 5.23 Control experiment of acceptor <b>E</b> compared with before and after hydrolysis of aspirin.....	132
Figure 6.1 Tröger's base showing its two enantiomers.....	136
Figure 6.2 Tröger's base depicting its main moieties and possible adaptable locations.....	136
Figure 6.3 Aniline substitution for Tröger's base synthesis.....	137
Figure 6.4 Main precursors of 2,8-disubstituted analogues of Tröger's bases.....	138
Figure 6.5 2,8-Diiodo substituted Tröger's base analogue synthesized by Wärnmark and co- workers.....	138
Figure 6.6 Targeted Tröger's base halogen bond donors and hydrogen bond acceptors .....	139
Figure 6.7 Co-formers used in the study; symmetric ditopic acceptors and aliphatic dicarboxylic acids .....	139
Figure 6.8 Scheme of dihedral angles between aromatic rings of some structures reported in the CSD.....	140
Figure 6.9 Expected halogen-bonded supramolecular architecture .....	141
Figure 6.10 Synthetic route to <b>TBX4</b> .....	154
Figure 6.11 C—I··· $\pi$ and aromatic stacking interaction observed in <b>TBX1</b> .....	157
Figure 6.12 Discrete void space observed in overall packing of <b>TBX1</b> .....	157
Figure 6.13 C—H··· $\pi$ with ethynyl group and aromatic ring in <b>TBX2</b> .....	158
Figure 6.14 C—H···N interactions observed between methyl C—H and diazocine N in <b>TBX2</b> .....	158
Figure 6.15 Overall packing observed in <b>TBX2</b> .....	158
Figure 6.16 C—H··· $\pi$ and aromatic stacking interaction observed in <b>TBX8</b> .....	159
Figure 6.17 Bifurcated C—H···N type interactions in <b>TBX8</b> .....	159
Figure 6.18 Main interactions in the crystal structure of <b>TBX4:A2</b> .....	160
Figure 6.19 Main interactions in the crystal structure of <b>TBX4:A6</b> .....	161
Figure 6.20 IR spectra of <b>TBX5</b> and Tartaric acid and the co-crystal thereof .....	162
Figure 6.21 Scheme representing the reactivity of the methanodiazocine of the Tröger's base	163
Figure 6.22 Bond distance between diazocine nitrogens and CH <sub>2</sub> bridge .....	164

Figure 6.23 Expected 1-D zig-zag chains of (a) <b>TBX4:A2</b> and (b) <b>TBX4:A6</b> .....	165
Figure 7.1 Binding constant dependence on MEPS .....	169
Figure 7.2 Deactivated halogen bond donors compared to hydrogen bond donors.....	170
Figure 7.3 A flexible tritopic acceptor compared to a rigid ditopic donor .....	171
Figure 7.4 Asymmetric tritopic acceptors.....	171
Figure 7.5 Conformationally rigid tritopic acceptors .....	172

## List of Tables

Table 1.1 Strength scale of supramolecular interactions <sup>11</sup> .....	6
Table 2.1 95% confidence interval for association constants and thermodynamic parameters for benzoic acid derivatives and IM <sub>3</sub> .....	27
Table 2.2 Electrostatic potentials of donors (-COOH) and pK <sub>a</sub> values .....	27
Table 2.3 IR stretches for ground mixtures for respective acceptor and donors .....	28
Table 2.4 Association constants (K <sub>a</sub> ) and thermodynamic binding parameters for benzoic acid derivatives and IM <sub>3</sub> .....	28
Table 2.5 Averaged ΔH values for benzoic acid derivatives and IM <sub>3</sub> .....	34
Table 3.1 Molecular electrostatic potentials on hydrogen atoms adjacent to the nitrogen on the heterocyclic ring.....	59
Table 3.2 IR stretching frequencies (cm <sup>-1</sup> ) of the solids produced by combining tritopic acceptors with aliphatic dicarboxylic acids .....	59
Table 3.3 IR stretching frequencies (cm <sup>-1</sup> ) of the solids produced by combining tritopic acceptors with aromatic carboxylic acids .....	61
Table 3.4 Hydrogen bond geometries.....	62
Table 3.5 Percentage of occurrence of O—H···N stretch in grinding experiments with aliphatic dicarboxylic acids .....	71
Table 3.6 Percentage of occurrence of O—H···N stretch in grinding experiments with aromatic carboxylic acids .....	72
Table 3.7 Overall percentage of occurrence of O—H···N stretch in grinding experiments with acids .....	72
Table 3.8 Summary of CSD search on ditopic acceptors .....	76
Table 4.1 1 CSD-based summary of frequency of interactions to available halogen-bond donors and MEPs values.....	88
Table 4.2 Grinding results.....	88
Table 4.3 IR results between tritopic acceptors and halogen bond donors.....	89
Table 4.4 Crystallographic data .....	90
Table 4.5 Halogen-bond geometries .....	91
Table 4.6 C—I bond lengths of co-crystals <b>135XB:E:EtOAc</b> and <b>14XB:E</b> .....	100



Table 5.1 Solubility according to the US Pharmacopoeia <sup>6</sup> .....	108
Table 5.2 Sub-class structures of NSAID and type of COX being inhibited .....	111
Table 5.3 IR stretching frequencies (cm <sup>-1</sup> ) of the solids produced by combining tritopic acceptors with ibuprofen, naproxen, aspirin, diclofenac .....	118
Table 5.4 Co-crystal formation with ibuprofen, naproxen, aspirin, diclofenac and <b>A-E</b> .....	119
Table 6.1 Electrostatic surface potential energies for hydrogen bond acceptor and halogen bond donor Tröger's base derivatives .....	152
Table 6.2 Electrostatic surface potential energies for symmetric ditopic acceptors .....	153
Table 6.3 IR stretching frequencies (cm <sup>-1</sup> ) of the solids produced by combining Tröger's base derivatives <b>TBX5-TBX8</b> acceptors with aliphatic dicarboxylic acids .....	155
Table 6.4 IR stretching frequencies (cm <sup>-1</sup> ) of the solids produced by combining Tröger's base derivatives <b>TBX4</b> and <b>TBY4</b> donors with symmetric ditopic acceptors .....	156

## Acknowledgements

Ammi and Dada, THANK YOU for your unconditional love and blessings. To my loving brothers, Aaron, Gerard and Jerome, thank you. A special thank you to Amma, Thaththa, Akka and Ayya for all your love.

I would like to gratefully acknowledge my doctoral advisor and mentor, Dr. Christer Aakeröy, whose selflessness in attention and sacrifice of time and care got me through, during my time as a PhD student. Working under you was truly a privilege.

I would also like to thank my Ph.D. advisory committee, Dr. Christine Aikens, Dr. Emily McLaurin, Dr. Michael Kanost and Dr. Larry Erickson for their valuable time and inputs on this dissertation. A special thank you to Dr. Eric Maatta for being in my committee for three years and for all his support and encouragement.

I'm grateful to Dr. John Desper, Dr. Marijana Đaković and Dr. Abhijeet Sinha for solving the crystal structures for this dissertation.

A special gratitude is extended to Dr. Yasmin Patell, Dr. Leila Maurmann, Mr. Michael Hinton, Mr. Jim Hodgson, Mr. Ron Jackson, Mr. Tobe Eggers, Ms. Mary Dooley, Ms. Kimberly Ross and Ms. Lisa Percival.

Thank you to all my past and present friends of the Aakeröy group, colleagues from the department of chemistry; it was a pleasure to have shared my stay here at K-State with you all.

A very special gratitude is extended to Sandy, Jose and Eric.

## **Dedication**

*To my daughter!!!*

# Chapter 1 - Introduction

## 1.1 Supramolecular chemistry

Supramolecular chemistry is described as ‘chemistry beyond the molecule’, in which a ‘supermolecule’ is a species held together by non-covalent interactions between two or more covalent molecules or ions,<sup>1</sup> Figure 1.1. In the context of this discipline, chemical systems are broadly classified into two major categories.<sup>2</sup>

- molecular recognition in solution, and
- organized self-assembly in the solid state (crystal engineering)<sup>2-3</sup>

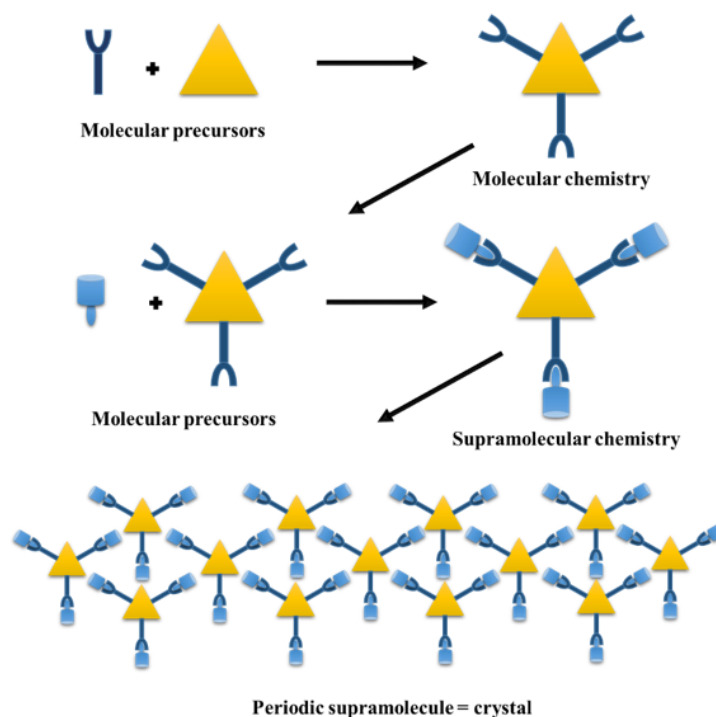


**Figure 1.1** Supramolecules formed by molecular recognition, binding through complementary shape and periodic arrangement resulting in a crystal lattice

## 1.2 Supramolecular chemistry in solution

Due to the competition between solute–solute, solvent–solvent, and solute–solvent interactions, molecular recognition events are heavily influenced by solvents.<sup>4</sup> The stability of a supramolecular complex in solution is quantified by the equilibrium constant or binding constant for the system.<sup>5</sup> The binding equilibrium becomes a competition reaction between these molecules and thus complicates the explicit quantification of these forces in solution.<sup>4,6</sup>

Recent advancement in supramolecular chemistry have appeared through carefully tailored multi component systems that can interact in a coherent manner to elicit a specific purpose. One such example uses halogen bonded templated self-assembly allowing a triazole-based foldamer to act as a tridentate halogen bond acceptor,<sup>7</sup> Figure 1.2. The cumulative effect of a tri-halogen bonded, preorganized structure displayed an association constant of  $3.2 \times 10^4 \text{ M}^{-1}$  in dichloromethane, which is very noteworthy for an uncharged organic donor and acceptors in solution.

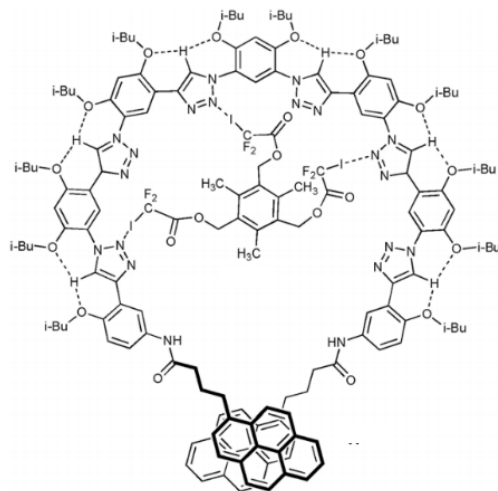


**Figure 1.2** Interaction of halogen bond donor with a triazole foldamer<sup>7</sup>

In another case, Resnati, Metrangolo and co-workers functionalized a preorganized receptor architecture with halogen bond donors as a means of ion pair recognition,<sup>8</sup> Figure 1.3. Even though the geometry of the receptor prevents it from acting as a multidentate halogen bond donor (monodentate halogen bond with the anion in solid state structure), it shows a roughly 20-fold increase in NaI affinity as determined by <sup>1</sup>H-NMR in CDCl<sub>3</sub> compared to the perfluorelated receptor.

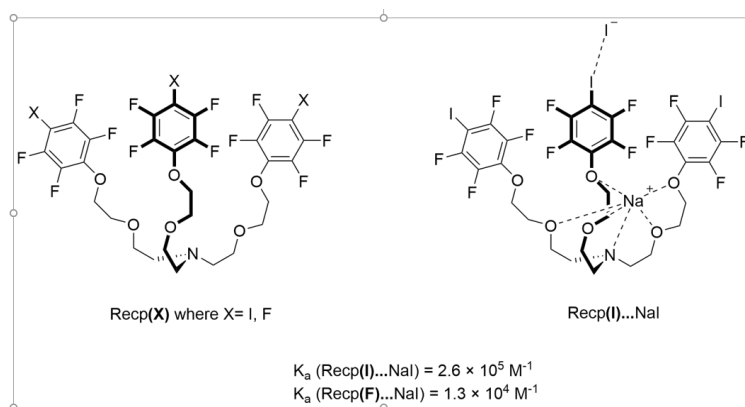


**Figure 1.3** Ion-pair recognition based on halogen bonding to Recp(I)<sup>8</sup>

Organic halogen bond donor mediated catalysis is a field not been extensively explored. Bolm and co-workers studied the reduction of 2-substituted quinolines by Hantzsch esters using 1-haloperfluoroalkanes as catalysts,<sup>9</sup> Figure 1.4. They suggested that the reaction mechanism involves an activation of the heterocycle by halogen bonding arising from a Hal–N interactions.

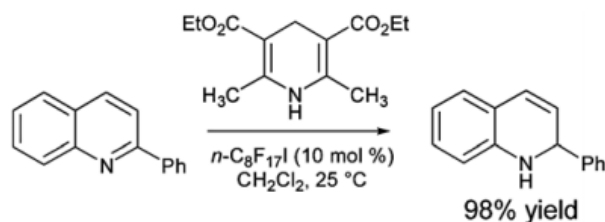


**Figure 1.4** 1-Haloperfluoroalkanes as catalysts for reductions of 2-substituted quinolines by Hantzsch ester<sup>9</sup>

Meijer and co-workers pointed out that the order of donor acceptor in the multiple hydrogen bonding arrays influenced the binding strength significantly, because of additional attractive secondary electrostatic interactions in hydrogen-bonded DDAA dimers,<sup>10</sup> Figure 1.5. The dimerization constant decreased as the polarity of the solvent increased showing a strong dependency on it.

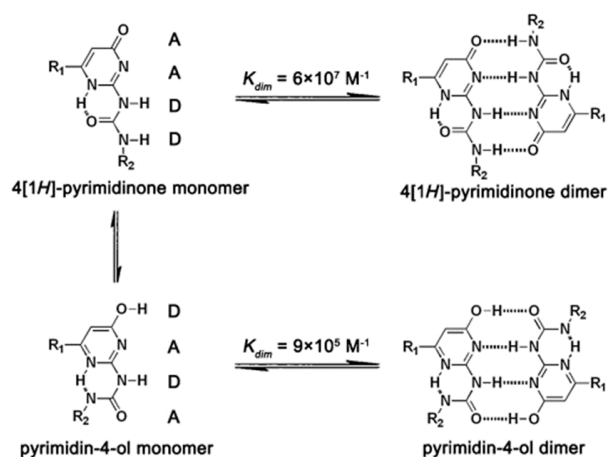


**Figure 1.5** Chemical structures of the keto (top) and enol (bottom) tautomers of UPy and their dimers<sup>10</sup>

### 1.3 Concepts in supramolecular chemistry

#### 1.3.1 Molecular self-assembly

This process, where precise organization takes place to produce aggregates that depend solely on the information stored in the functional units of a chemical building block, is an equilibrium between two or more molecular components, Figure 1.6. Though this process is usually spontaneous, it may be influenced by solvation effects or in the case of solids, by the nucleation and crystallization processes.<sup>11</sup>

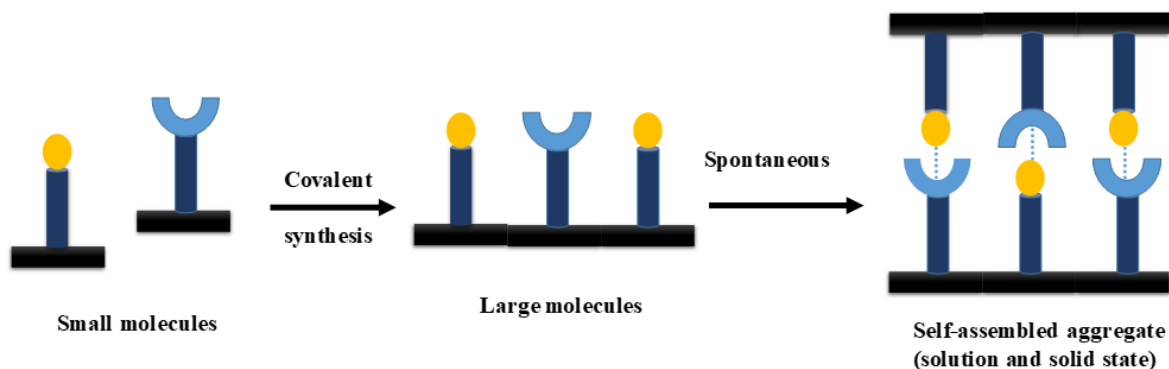


**Figure 1.6** Self-assembly between complementary molecules

Synthetic self-assembly systems depend on our capability to design molecules with complementary functionalities. The chemical system itself rearranges to the most thermodynamically stable product and we have no direct control over the assembly process.<sup>11</sup> Furthermore metastable forms can appear within a chemical system when their crystallization kinetics are faster (lower activation energy) than those of the stable form.<sup>12</sup> A metastable form, nonetheless, will eventually transform into a more stable form.<sup>12</sup> But like in the case of diamond a metastable form of crystalline carbon cannot under normal conditions reach the lower energy state of graphite due to a significant kinetic energy barrier.<sup>13</sup> However, it is possible to make intelligent and informed decisions as to which compounds may interact well together and thus develop versatile synthetic protocols. This is known as directed self-assembly; a process by which molecules adopt a defined arrangement with guidance or management from an outside source.<sup>14</sup>

### 1.3.2 Molecular recognition

“Molecular recognition” is a host molecule selectively binding to a certain type of guest molecule through non-covalent bonding, Figure 1.7. The fundamental basis for molecular



recognition is provided by the potential energy surface that represents the interaction energy of two or more molecules in a cluster as a function of their mutual separation and orientation.<sup>15</sup>

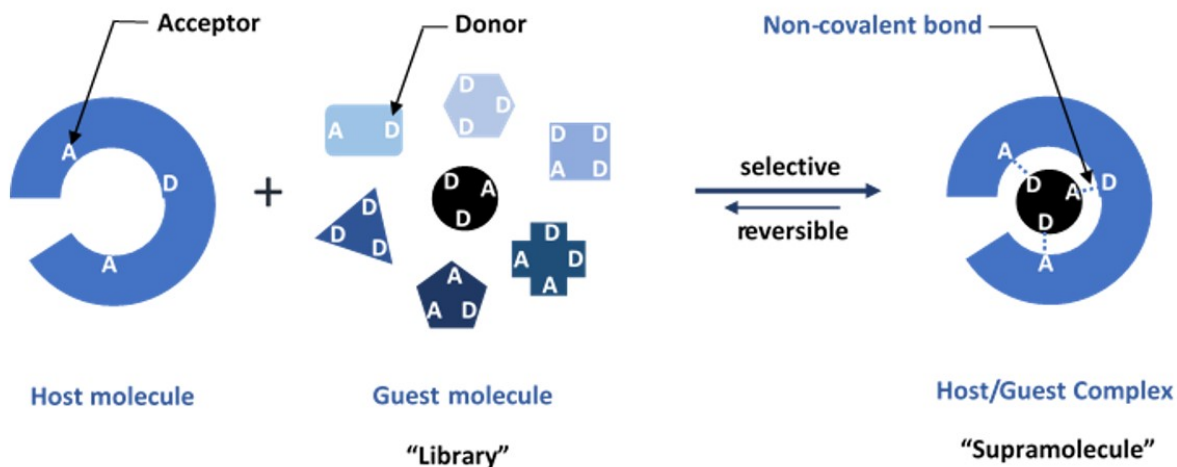


**Figure 1.7** Molecular recognition

## 1.4 Supramolecular interactions

Supramolecular chemistry involves reversible non-covalent interactions between molecules. These forces include hydrogen bonding, halogen bonding, metal ligand coordination, hydrophobic forces, van der Waals forces,  $\pi$ - $\pi$  interactions and electrostatic effects,<sup>16</sup> Table 1.1.

**Table 1.1** Strength scale of supramolecular interactions<sup>11</sup>

Interaction	Strength kJ mol <sup>-1</sup>
Ion-ion	200-300
Ion-dipole	50-200
Dipole-dipole	5-50
Halogen bonding <sup>17</sup>	10-150
Hydrogen bonding	4-120
Cation- $\pi$	5-80
$\pi$ - $\pi$	0-50

van der Waals	< 5 but variable depending on surface area
Hydrophobic	Related to solvent–solvent interaction energy

### 1.4.1 Hydrogen-bond

The hydrogen bond (HB) is defined as “an attractive interaction between a hydrogen atom from a molecule or a molecular fragment X–H in which X is more electronegative than H, and an atom or a group of atoms in the same or a different molecule, in which there is evidence of bond formation”,<sup>18</sup> Figure 1.8.

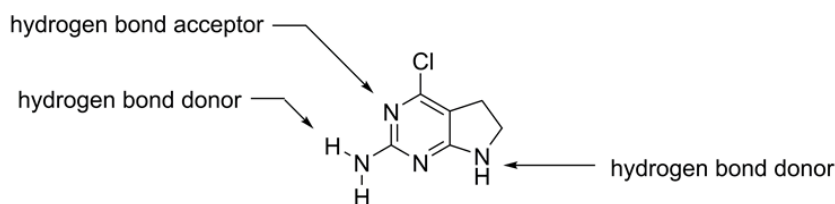


**Figure 1.8** Hydrogen bond donating and hydrogen bond accepting groups

The HB is directional and strong<sup>19</sup>, reflecting features of a covalent bond and it produces interatomic distances shorter than the sum of the van der Waals radii.<sup>20</sup> These have been instrumental in the preparation of distinctive structural aggregates, and the use of hydrogen bonding as a steering force is one of the most important tools in the context of supramolecular chemistry and crystal engineering.

### 1.4.2 Halogen bond

A halogen bond (XB) “occurs when there is evidence of a net attractive interaction between an electrophilic region associated with a halogen atom in a molecular entity and a nucleophilic region in another, or the same, molecular entity”,<sup>21</sup> Figure 1.19.

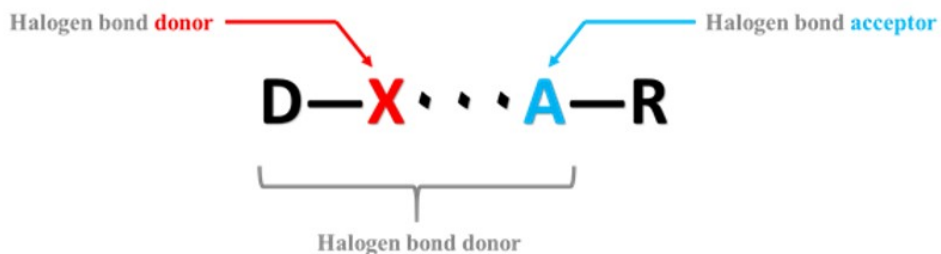


**Figure 1.9** Schematic diagram showing the formation of a halogen bond (R and D-molecular fragments or atoms; X-halogen atom; A-nucleophilic atom)

XBs are strong, specific, and directional interactions and can assist in generating well-defined structures. The strength of the XB allows it to compete with the HB.

In drawing parallels, an electron donor/ electron acceptor relationship exists in both XB and HB. What differentiates the two bonding types depends on the species that act as the electron donor/ acceptor.<sup>22</sup>

## 1.5 Solid-state supramolecular chemistry

Supramolecular interactions do not only occur within solution but also within solid-state systems. Ordered solids (except for giant covalent structures) are held together by non-covalent interactions.<sup>11</sup> Supramolecular chemistry in the solid state involves the study of crystals and all its applications in the fields of solid-state chemistry, crystal engineering, catalysis and material science, including organic, inorganic, bio-organic and bioinorganic chemistry etc.<sup>23</sup>

### 1.5.1 Crystal engineering

Crystal engineering, a sub-discipline of supramolecular chemistry, is the rational design and synthesis of novel crystalline solids through knowledge of intermolecular interactions and *supramolecular synthons* - recurring motifs / patterns of interactions between functional groups.<sup>11</sup> There are three pillars of crystal engineering, 1) determine the way molecules pack in the crystalline phase, 2) crystal design or supramolecular synthesis and 3) optimization of crystal properties to meet the desired application.<sup>24</sup> Crystal structure prediction (which is *not* the same as crystal engineering), a task that has yet to be accomplished reliably, is a theoretical route to determine crystal packing and symmetry (including space group) for a given molecule. It is also the focus of considerable current effort.<sup>25</sup> Furthermore symmetry-adapted perturbation theory (SAPT) of intermolecular forces can be utilized to provide both a theoretical framework for describing intermolecular interactions and a practical tool for calculating such interactions.<sup>26</sup>

A common synthetic procedure we employ in the process of crystal engineering is “grinding”,<sup>11</sup> Figure 1.10. This mechanochemical reaction involves taking two solids and directly mixing them in a solvent-free environment. Often times, drops or small amounts of solvent are added, which is then termed as ‘kneading reactions’ or ‘liquid assisted grinding’.<sup>27</sup> Due to the dissolution mediated co-crystal formation, whereby the solution becomes saturated with respect to reactants and supersaturated with respect to co-crystals, adding a drop of solvent becomes effective in the grinding process.<sup>28</sup>

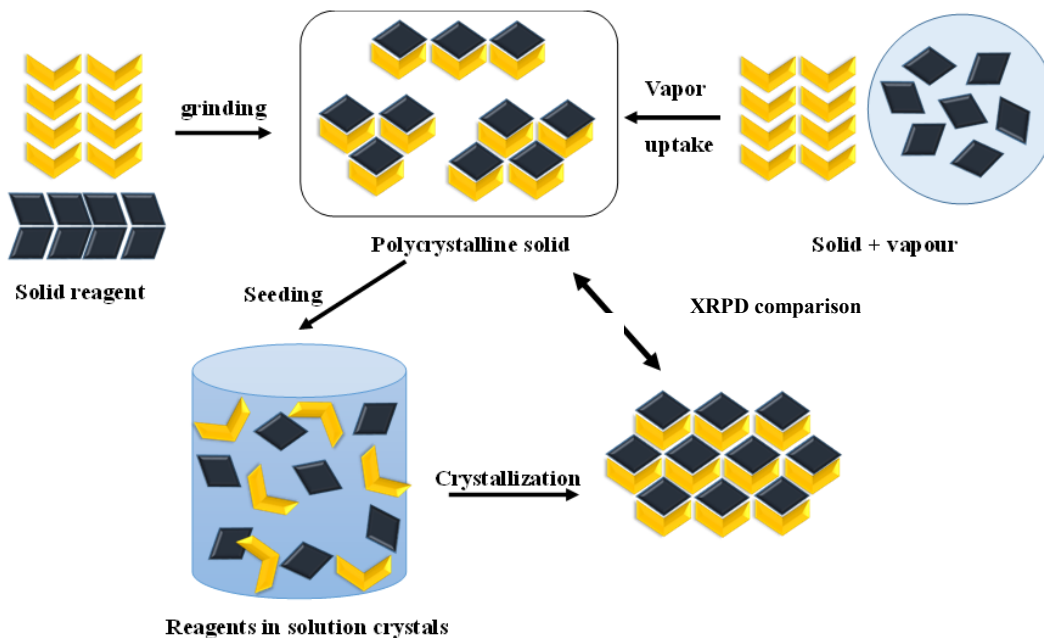


**Figure 1.10** Green route crystal engineering

While crystal engineering refers to a systematic study of the interactions within a crystal and attempts to design solids utilizing these forces, today crystal engineering has reached a new generation where crystal structure engineering is now transforming into crystal ‘property’ engineering,<sup>29</sup> Figure 1.11. One may target a property straightaway and derive the crystal structure or structures that are likely to yield this property by controlling aspects of the physical growth by utilizing the known chemical similarity of the systems.<sup>30</sup>

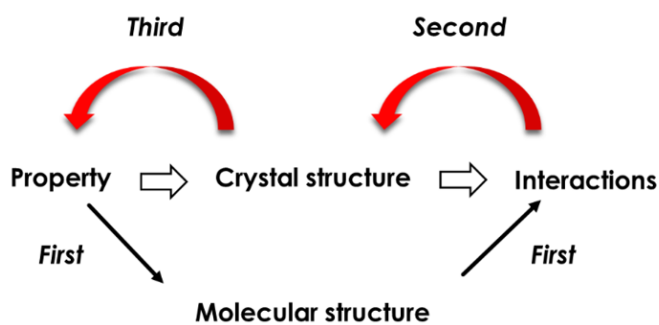


**Figure 1.11** Generations of crystal engineering<sup>29</sup>

Even though the first mention of the term “crystal engineering” was by R. Pepinsky in 1955<sup>31</sup>, it was G. M. J. Schmidt who correlated the solid-state reactivity of an array of photodimerizable compounds, particularly trans-cinnamic acids,<sup>2b</sup> Figure 1.12. The products formed were a result of proximity and parallel arrangement of the double bonds in the crystal lattice.

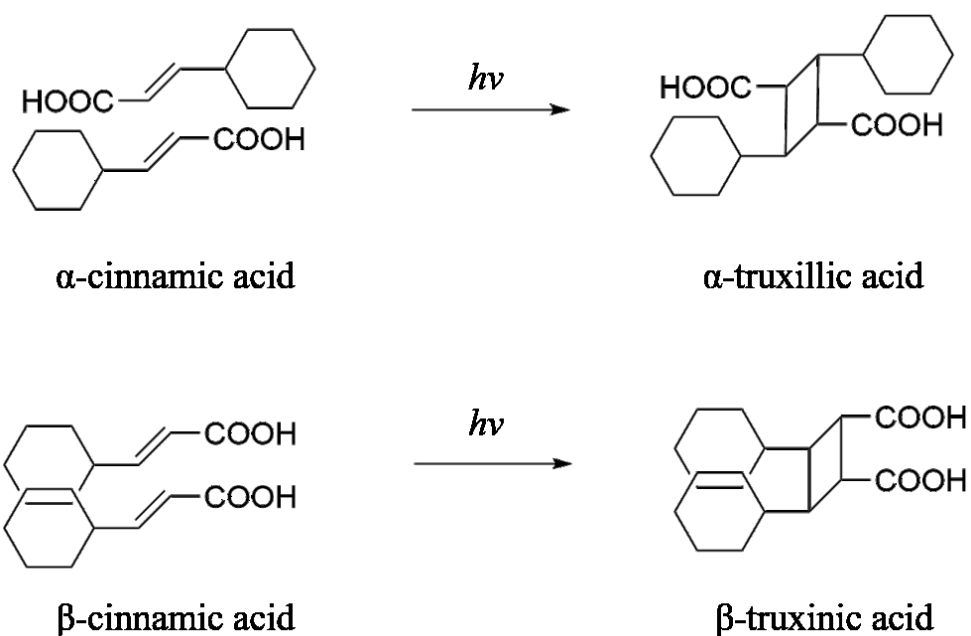


**Figure 1.12** Photodimerized products of trans-cinammic acid

## 1.6 Research overview

### 1.6.1 Overall challenge

By translating molecular function into predictable intermolecular recognition, we hope to gain control over the assembly of molecules that may create versatile pathways to improve performance of a wide range of specialty chemicals such as pharmaceuticals.

## 1.6.2 Goals

The goals of the thesis are as follows;

1. To determine whether supramolecular assemblies can be understood and guided by a quantitative thermodynamic assessment that integrates theoretical and experimental views of solution-based molecular recognition events. (Chapter 2)
2. To explore the effect of reliability and effectiveness of hydrogen bonding synthons on supramolecular architectures of flexible tritopic acceptors. This study will focus on co-crystallization of a series of tritopic acceptors with aliphatic and aromatic hydrogen bond donors. (Chapter 3)
3. To investigate the nature of halogen bonded supramolecular assemblies of flexible tritopic acceptors. This will be explored by co-crystalizing rigid perfluoroiodo arenes with above mentioned acceptors. (Chapter 4)
4. To apply crystal engineering for altering physiochemical properties. A systematic study will be carried out on a series of active pharmaceutical ingredients (API) with the goal of fine-tuning aqueous solubility. (Chapter 5)
5. To explore rigidity vs. flexibility to determine how well it allows the controlled assembly of molecular complexes by utilizing Tröger's base as core building block, which possess well-defined geometries. Design and synthesis of Tröger's base derivatives functionalized with halogen and hydrogen bond donor and acceptor groups. (Chapter 6)

## 1.7 References

1. Nobelprize.org. Jean-Marie Lehn - Nobel Lecture: Supramolecular Chemistry - Scope and Perspectives: Molecules - Supermolecules - Molecular Devices. (accessed 23 Mar 2018).
2. (a) Desiraju, G. R., *Crystal engineering: the design of organic solids*. Elsevier: Amsterdam; New York, 1989; p xiv, 312 p; (b) Schmidt, G. M. J., Photodimerization in the solid state. *Pure Appl. Chem.* 1971, 27 (4), 647-678.
3. Nangia, A., Supramolecular chemistry and crystal engineering. *J. Chem. Sci.* 2010, 122 (3), 295-310.
4. Hunter, C. A., Quantifying Intermolecular Interactions: Guidelines for the Molecular Recognition Toolbox. *Angew. Chem. Int. Ed.* 2004, 43 (40), 5310-5324.
5. Connors, K. A., Binding constants : the measurement of molecular complex stability. Wiley: New York, 1987; p xiv, 411 p.
6. Baron, R.; McCammon, J. A., Molecular Recognition and Ligand Association. *Annu. Rev. Phys. Chem.* 2013, 64 (1), 151-175.
7. You, L.-Y.; Chen, S.-G.; Zhao, X.; Liu, Y.; Lan, W.-X.; Zhang, Y.; Lu, H.-J.; Cao, C.-Y.; Li, Z.-T., C-H $\cdots$ O Hydrogen Bonding Induced Triazole Foldamers: Efficient Halogen Bonding Receptors for Organohalogenes. *Angew. Chem. Int. Ed.* 2012, 51 (7), 1657-1661.
8. Mele, A.; Metrangolo, P.; Neukirch, H.; Pilati, T.; Resnati, G., A Halogen-Bonding-Based Heteroditopic Receptor for Alkali Metal Halides. *J. Am. Chem. Soc.* 2005, 127 (43), 14972-14973.
9. Bolm, C.; Bruckmann, A.; Pena, M., Organocatalysis through Halogen-Bond Activation. *Synlett* 2008, 2008 (6), 900-902.
10. Beijer, F. H.; Sijbesma, R. P.; Kooijman, H.; Spek, A. L.; Meijer, E. W., Strong Dimerization of Ureidopyrimidones via Quadruple Hydrogen Bonding. *J. Am. Chem. Soc.* 1998, 120 (27), 6761-6769.
11. Steed, J. W.; Turner, D. R.; Wallace, K. J., *Core concepts in supramolecular chemistry and nanochemistry*. John Wiley: NJ, 2007; 307.
12. (a) Näther, C.; Jess, I.; Jones, P. G.; Taouss, C.; Teschmit, N., Structural, Thermodynamic, and Kinetic Aspects of the Polymorphism of Trimethylthiourea: The Influence of Kinetics on the Transformations between Polymorphs. *Cryst. Growth Des.* 2013, 13 (4), 1676-1684; (b) Jiang, S.; Jansens, P. J.; ter Horst, J. H., Mechanism and Kinetics of the Polymorphic Transformation of o-Aminobenzoic Acid. *Cryst. Growth Des.* 2010, 10 (5), 2123-2128.
13. Angus, J. C.; Wang, Y.; Sunkara, M., Metastable Growth of Diamond and Diamond-Like Phases. *Annu. Rev. Mater. Sci.* 1991, 21 (1), 221-248.



14. Comrie, J. P., *Molecular Self-Assembly: Advances in Chemistry, Biology and Nanotechnology*. Nova Science Publishers Inc: 2013.
15. Buckingham, A. D.; Legon, A. C.; Roberts, S. M., *Principles of Molecular Recognition*. 1993.
16. Biedermann, F.; Schneider, H.-J., Experimental Binding Energies in Supramolecular Complexes. *Chem. Rev.* 2016, 116 (9), 5216-5300.
17. Cavallo, G.; Metrangolo, P.; Milani, R.; Pilati, T.; Priimagi, A.; Resnati, G.; Terraneo, G., The Halogen Bond. *Chem. Rev.* 2016, 116 (4), 2478-2601.
18. Arunan, E.; Desiraju, G. R.; Klein, R. A.; Sadlej, J.; Scheiner, S.; Alkorta, I.; Clary, D. C.; Crabtree, R. H.; Dannenberg, J. J.; Hobza, P.; Kjaergaard, H. G.; Legon, A. C.; Mennucci, B.; Nesbitt, D. J., Definition of the hydrogen bond (IUPAC Recommendations 2011). *Pure Appl. Chem.* 2011, 83 (8).
19. Aakeröy, C. B.; Seddon, K. R., The hydrogen bond and crystal engineering. *Chem. Soc. Rev.* 1993, 22 (6), 397-407.
20. Palit, D. K., Ultrafast Dynamics of the Excited States of Hydrogen-Bonded Complexes and Solvation. 2010, 761-795.
21. Desiraju, G. R.; Ho, P. S.; Kloo, L.; Legon, A. C.; Marquardt, R.; Metrangolo, P.; Politzer, P.; Resnati, G.; Rissanen, K., Definition of the halogen bond (IUPAC Recommendations 2013). *Pure Appl. Chem.* 2013, 85 (8).
22. Metrangolo, P.; Resnati, G., Halogen Bonding: A Paradigm in Supramolecular Chemistry. *Chem. Eur. J.* 2001, 7 (12), 2511-2519.
23. (a) Resnati, G.; Boldyreva, E.; Bombicz, P.; Kawano, M., Supramolecular interactions in the solid state. *IUCrJ* 2015, 2 (6), 675-690; (b) Lehn, J.-M., Supramolecular Chemistry—Scope and Perspectives Molecules, Supermolecules, and Molecular Devices (Nobel Lecture). *Angew Chem Int* 1988, 27 (1), 89-112.
24. Tiekink, E. R. T., Crystal Engineering. *Supramol. Chem.* 2012.
25. Tiekink, E. R. T., Steric Control over Supramolecular Aggregation: A Design Element in Crystal Engineering? In *Frontiers in Crystal Engineering*, 2006; 117-134.
26. (a) Lao, K. U.; Herbert, J. M., Accurate and Efficient Quantum Chemistry Calculations for Noncovalent Interactions in Many-Body Systems: The XSAPT Family of Methods. *J. Phys. Chem. A* 2014, 119 (2), 235-252; (b) Szalewicz, K., Symmetry-adapted perturbation theory of intermolecular forces. *Wiley Interdiscip. Rev. Comput. Mol. Sci.* 2012, 2 (2), 254-272.
27. (a) Etter, M. C., Encoding and decoding hydrogen-bond patterns of organic compounds. *Acc. Chem. Res.* 1990, 23 (4), 120-126; (b) Etter, M. C., Hydrogen bonds as design

- elements in organic chemistry. *J. Phys. Chem.* 1991, 95 (12), 4601-4610; (c) Childs, S. L.; Rodriguez-Hornedo, N.; Reddy, L. S.; Jayasankar, A.; Maheshwari, C.; McCausland, L.; Shipplett, R.; Stahly, B. C., Screening strategies based on solubility and solution composition generate pharmaceutically acceptable cocrystals of carbamazepine. *CrystEngComm* 2008, 10 (7), 856-864.
28. Kuminek, G.; Cao, F.; Bahia de Oliveira da Rocha, A.; Gonçalves Cardoso, S.; Rodríguez-Hornedo, N., Cocrystals to facilitate delivery of poorly soluble compounds beyond-rule-of-5. *Adv. Drug Deliv. Rev.* 2016, 101, 143-166.
  29. Desiraju, G. R., Crystal engineering: structure, property and beyond. *IUCrJ* 2017, 4 (6), 710-711.
  30. Saha, S.; Desiraju, G. R., Crystal Engineering of Hand-Twisted Helical Crystals. *J. Am. Chem. Soc.* 2017, 139 (5), 1975-1983.
  31. Cohen, M. D.; Schmidt, G. M. J.; Sonntag, F. I., 384. Topochemistry. Part II. The photochemistry of trans-cinnamic acids. *J. Chem. Soc.* 1964, 2000.

# Chapter 2 - Molecular electrostatic potentials as a quantitative measure of hydrogen bonding preferences in solution<sup>1</sup>

## 2.1 Introduction

Molecular recognition is, “*selective binding with a purpose*”,<sup>2</sup> Figure 2.1. The recognition between molecules which are complementary in their geometry and electronic features, leads to an aggregation where the end result is an ensemble of two or more distinct units.<sup>3</sup>

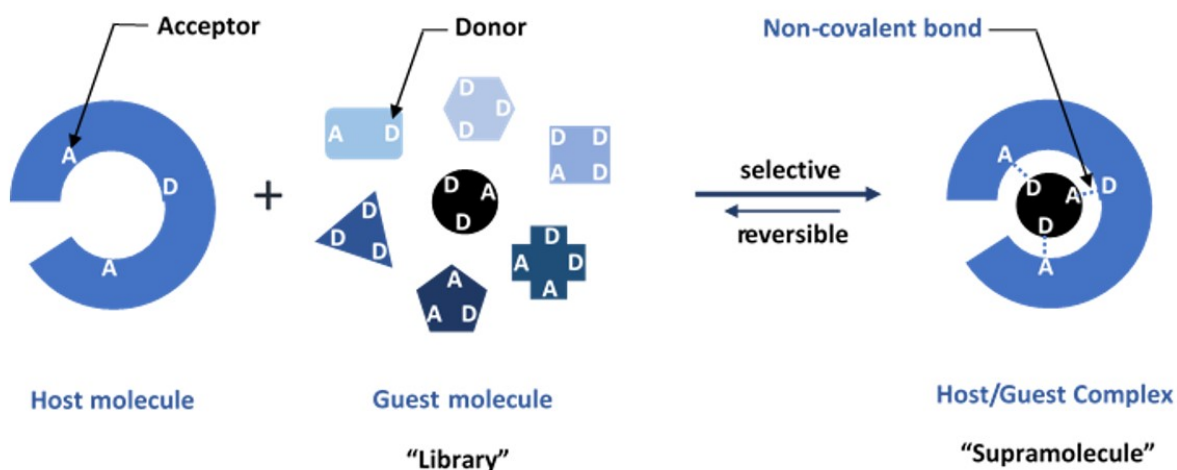
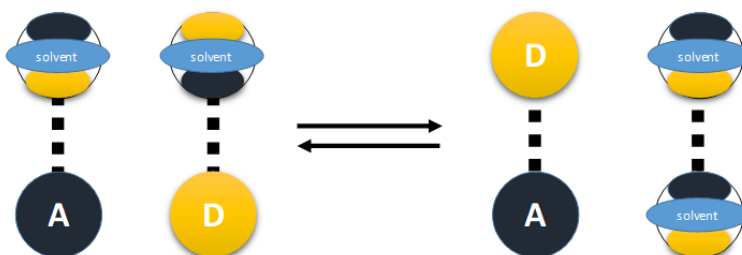


Figure 2.1 Molecular recognition

Solvents play an indirect but rather dominant role in driving molecular recognition in solution.<sup>4</sup> Computational and gas-phase data have shown the dominance of dispersion forces in molecular recognition, but solvent effects complicate the explicit quantification of these forces in solution. This is due to the competition between solute–solute, solvent–solvent, and solute–solvent interactions,<sup>5</sup> Figure 2.2. For molecules possessing simple groups, the primary mode of interaction is hydrogen-bond contacts between maxima in (yellow) and minima in (blue) in the electrostatic potential surfaces of the molecules. “A” represents a hydrogen acceptor solute and “D” a hydrogen

bond donor solute. In polar solvents like water, nonpolar solutes like hydrocarbons, interact in a way that minimizes solvent-solute interactions. Given the complexity and the solvent dependency of molecular recognition events, we have understood the importance of finding a simplified method that can offer reliable guidelines to predict molecular recognition in solution.<sup>6</sup>



**Figure 2.2** Schematic representation of the electrostatic solvent competition mode<sup>5</sup>

Molecular Electrostatic Potential Surface (MEPS) is a very useful descriptor for analyzing and predicting molecular behavior.<sup>7</sup> MEP is the result of a force acting on a positive test charge (a proton) located at a given point  $q(x,y,z)$  through the electrical charge cloud created in the space around a molecule by its nuclei and electrons,<sup>8</sup> Figure 2.3. MEPS has been widely used in many different areas such as a measure for estimating molecular acidity in different compounds,<sup>9</sup> for estimation of the reaction rate constant,<sup>10</sup> to analyze non-covalent interactions as well as in studies of hydrogen bonding.<sup>11</sup> In this study, it was intended to establish if MEPS values can offer a quantitative measure of solution binding.

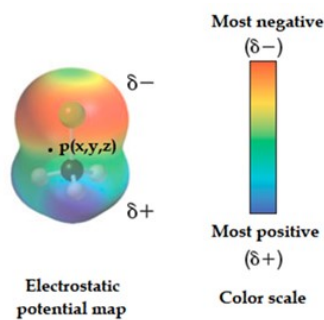


**Figure 2.3** Molecular electrostatic potential surface map on  $\text{CHCl}_3$

To synthesize more complex, multicomponent materials with the help of relatively weak interactions, it can be useful to implement a hierarchical view of different intermolecular forces within a synthetic protocol.<sup>12</sup> If such an approach is to be realized, we need a reliable method for ranking different intermolecular interactions in terms of strength and potential binding affinity. Therefore, employing molecular electrostatic potential surface (MEPS) values<sup>12-13</sup> to rank acceptor-donor sites, where a stronger acceptor has a higher negative value and the stronger donor has a higher positive value on the electrostatic surface, is a useful alternative among other reliable methods (i.e. using the relative strength based on the  $pK_a/pK_b$  values)<sup>13c</sup> used for ranking hydrogen-bond donors and acceptors. This will provide versatile guidelines for how best to combine hydrogen-bond interactions into succinct synthetic strategies and enable us to predict chemical composition and main structural features yielding from any supramolecular synthesis – the basis for successful and reproducible design of supramolecules.

It is assumed that electrostatic potentials play a particularly important role in molecular recognition in the initial stages as they are more long range and directional than dispersion. Since induced dipole-induced dipole interactions decrease more with increasing separation ( $E_{\text{dsp}} \propto (r^{-6})$ ) than electrostatic interactions ( $E_{\text{elc}} \propto (r^{-1})$ ). The foundation of molecular recognition events; ‘non-covalent interactions’,<sup>14</sup> are the primary tools used in the production of discrete<sup>15</sup> or extended<sup>16</sup> supramolecular architectures in crystal engineering. In this context, the hydrogen bond is, by far the most extensively studied intermolecular interaction.<sup>12, 14</sup> Even though many key factors like repulsion, induction, dispersion and electrostatics affect the interaction between two molecules, the recent definition on hydrogen bonding proposed by IUPAC in 2011, recognizes that electrostatics are at the very core of this interaction.<sup>17</sup>

The target molecule; a hydrogen-bond acceptor, 1,3,5-tris(imidazole-1-ylmethyl)-benzene, is conformationally flexible and contains three geometrically and electrostatically equivalent binding sites, Figure 2.4.

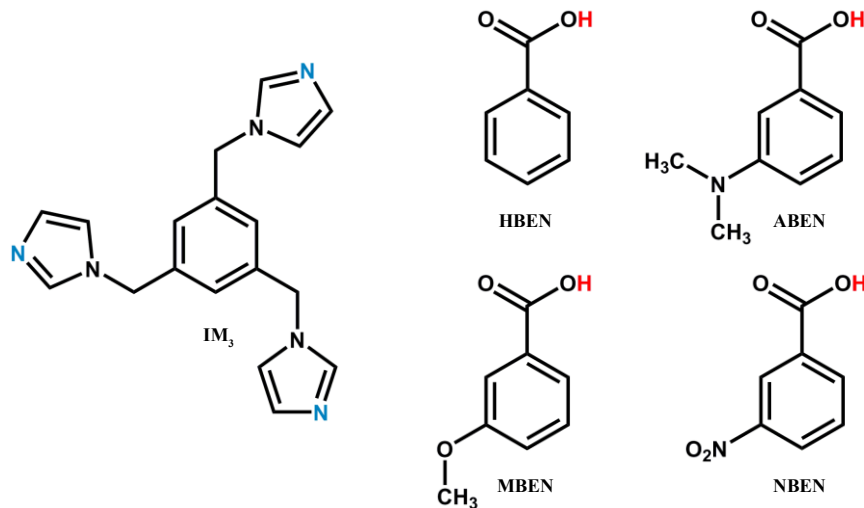


**Figure 2.4** Scheme representing tritopic acceptor and donors employed in this study

We intend to investigate binding to the tritopic acceptor purely by targeting its most prominent binding-sites regardless of shape, geometry or size with a selection of donors with similar chemical functionalities. Previously reported co-crystal for a similar multitopic acceptor 1,3,5-(5,6-dimethylbenzimidazol-1-yl)-2,4,6-trimethylbenzene shows a 1:1 binding with citramalic acid a tritopic donor in the solid-state.<sup>18</sup> Although we can observe solid state structures, they may or may not be reflecting solution phase behavior. This is where Isothermal titration calorimetry (ITC) is important. ITC has been proven as a universal technique that provides knowledge of affinity, thermodynamics, and stoichiometry of a binding interaction<sup>19</sup> which is not only of fundamental interest but also is key to the design and optimization of application-oriented supramolecular systems. To evaluate the binding stoichiometries and understand the intermolecular interactions, four benzoic acid derivatives with varying strengths were chosen.

Assuming that increased electrostatic stabilization will lead to notable differences in stability and equilibrium constants of supramolecular assemblies in solution, we aimed to correlate experimentally observed thermodynamic parameters with calculated electrostatic potential surfaces. We intended to explore calorimetry as a way of getting to stoichiometries as well as thermodynamic parameters in several supramolecular assembly events.

ITC is a tool that can be utilized to measure the relatively long-range interactions that take place in the initial stages and to identify and characterize stable supramolecular architectures in solution,<sup>17, 20</sup> Figure 2.5.

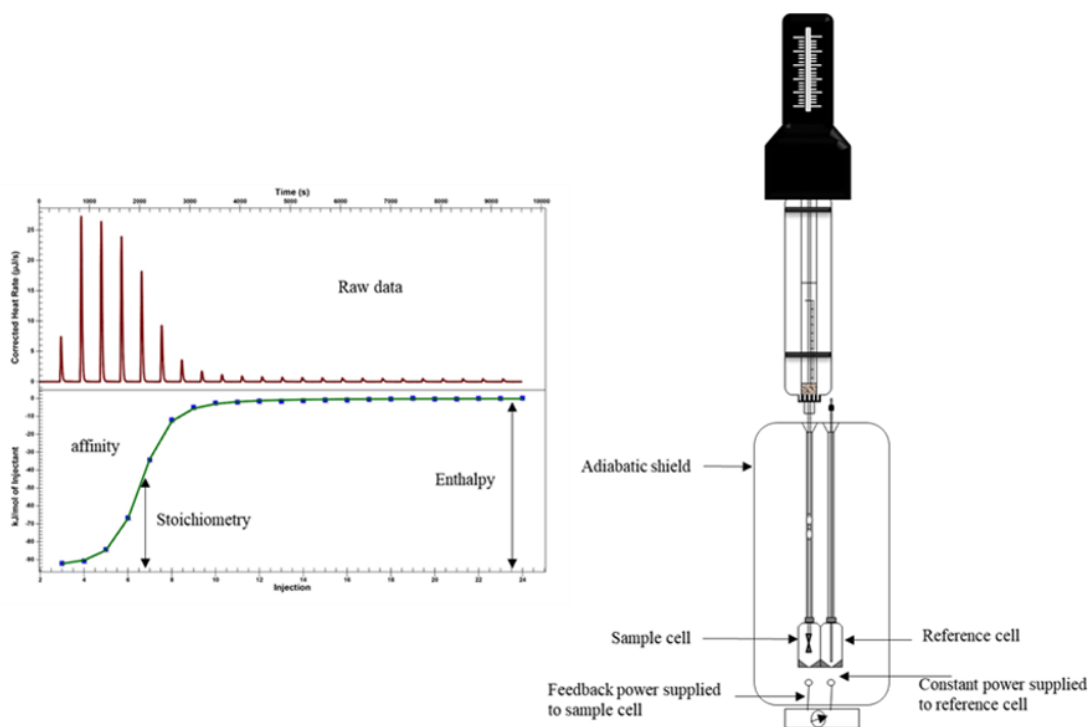


**Figure 2.5** A schematic of ITC cell and injection syringe and raw data from ITC experiment with binding isotherm<sup>21</sup>

With three binding sites being available, three structural outcomes are possible in the solution phase from intermolecular interactions with a monotopic donor as seen in Figure 2.6. In this context, we postulate the stronger acid to bind strongly to an acceptor in solution where

molecular recognition is governed mainly through molecular electrostatics, which can be modelled through electrostatic potential mapping of the respective acids. We aim to establish if a simple electrostatic depiction of hydrogen-bond interactions in solution is reflected in experimentally observed metrics that describe each supramolecular assembly in solution. The basic hypothesis is that by controlling and modulating the electrostatic component of these acceptor...donor hydrogen bonds we may be able to alter binding constant and the overall thermodynamic landscape of these systems.

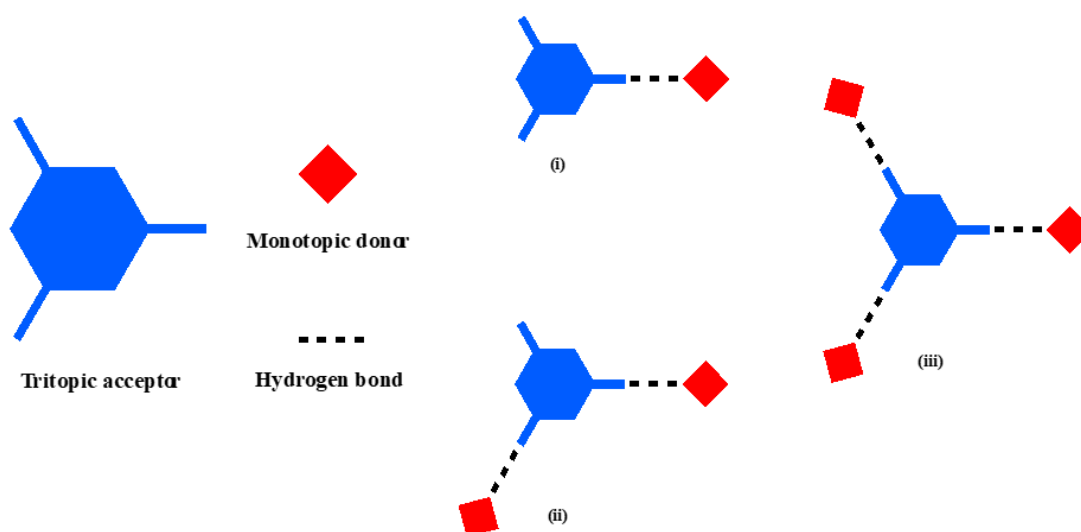


**Figure 2.6** Three possible outcomes when co-crystallizing monotopic donors with a tritopic acceptor

## 2.2 Experimental

### 2.2.1 Molecular electrostatic potential surface calculations

Molecular electrostatic potential surfaces on donor molecules were obtained with density functional theory (B3LYP), using 6-31G\* basis set in a vacuum. All molecules were geometry optimised with the maxima and minima in the electrostatic potential surface ( $0.002 \text{ e au}^{-1}$



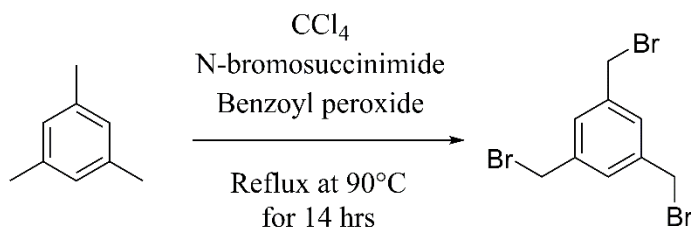
isosurface) determined using a positive point charge in the vacuum as a probe on the molecular surface. The numerical values specify the interaction energy ( $\text{kJ mol}^{-1}$ ) at a point between the surface of the molecule and the positive point probe. These numeric could be correlated to the electrostatic charges on the atoms with positive values corresponding to the positive charges and the negative values corresponding to the negative charges. All calculations were carried out using Spartan '10 software.

## 2.2.2 Materials and methods

All reagents, solvent, and donors (benzoic acid and derivatives) were purchased from commercial sources and used as received. 1,3,5-Tris(bromomethyl) benzene was synthesized according to a report by Wang and co-workers.<sup>19c</sup> 1,3,5-Tris(imidazole-1-yl-methyl) benzene was synthesized per a procedure reported.<sup>19a</sup> Titrations were performed on a NANO ITC standard volume isothermal titration calorimeter. Data analysis and data fit procedures were done using the software NanoAnalyze.

## 2.2.3 Synthesis

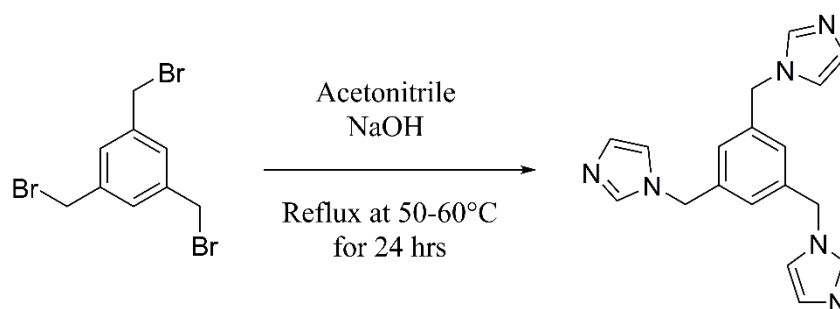
### 2.2.3.1 Synthesis of 1,3,5-tris(bromomethyl) benzene



A mixture of mesitylene (2.8 mL, 20 mmol), N-bromosuccinimide (10.62 g, 60 mmol), and benzoyl peroxide (0.11 g) in  $\text{CCl}_4$  (30 mL) was stirred and heated under  $\text{N}_2$  for 14 hours at  $90^\circ\text{C}$ . The reaction mixture was monitored with TLC and after completion, the solution was cooled in an

ice bath and the succinimide was filtered off and washed with carbon tetrachloride. The filtrate was washed with water and dried over anhydrous  $\text{MgSO}_4$ . Upon concentration of the  $\text{CCl}_4$  solution, a pale-yellow solid was obtained. Recrystallization in a 1:1 mixture of ethanol/hexane afforded colourless needle crystals. 81% Yield. mp 87-89 °C (Lit value 86-87 °C)<sup>19c</sup>;  $^1\text{H}$  NMR ( $\delta\text{H}$ ;  $\text{CDCl}_3$ , 400 MHz)  $\delta$  7.36 (s, 3H), 4.46 (s, 6H).

### 2.2.3.2 Synthesis of 1,3,5-tris(imidazole-1-yl-methyl) benzene



To a solution of imidazole (874 mg, 12.8 mmol) placed in a 100 mL round-bottomed flask with acetonitrile (50 mL) was added NaOH (1.029 g, 25.72 mmol) and stirred at room temperature for two hours. 1,3,5-Tris(bromomethyl) benzene (1.416 g, 4.000 mmol) in acetonitrile (20 mL) was added to the reaction mixture and refluxed for 24 hours at 50-60 °C. The reaction mixture was monitored with TLC and after completion, the solvent was removed by rotary evaporation, the residue was dissolved in water (100 mL) and extracted with methylene chloride (30 mL x 5). The organic layers were combined, dried over anhydrous  $\text{MgSO}_4$ , filtered and purified by flash column chromatography ( $\text{CH}_2\text{Cl}_2/\text{MeOH} = 5/1$ ) to give the desired product as a white solid. 54% Yield. mp 173-175 °C (Lit value 175-179 °C)<sup>19a</sup>;  $^1\text{H}$  NMR ( $\delta\text{H}$ ;  $\text{CDCl}_3$ , 400 MHz)  $\delta$  7.52 (s, 3H), 7.12 (s, 3H), 6.85 (m, 6H) 5.07 (s, 6H).

#### **2.2.4 Binding studies with ITC**

Stock solutions for the calorimetric studies were prepared using purified deionized water in volumetric flasks. All experiments were conducted at 25 °C. The sample cell was filled with 1.2 mL of the donor using a syringe with an elongated needle. The 250  $\mu$ L syringe was filled with the tritopic acceptor solution and an air gap roughly about the size of 5-10  $\mu$ L between the plunger tip and the liquid in the barrel (leaving an air gap is critical to prevent signal distortion). Fill the syringe to a slight excess, 2 or 3 mm beyond the highest gradation of the barrel. The instrument was left to equilibrate for about 30 mins, until the baseline was acceptable prior to data collection. The stir rate was set at 250 rpm and the instrument was left to equilibrate for about 30 minutes. The experiment was set to incremental titration with discrete injections every 250 seconds for 25 injections. For all titrations, the initial concentration of the tritopic acceptor was 1.20 mM and the concentrations of all the donors were 0.150 mM. Data analysis and data fitting were conducted using software NanoAnalyze.

#### ***2.2.4.1 Binding study of 1,3,5-tris(imidazole-1-yl-methyl) benzene and 3-nitrobenzoic acid***

1.2 mL of 0.150 mM aqueous 3-nitrobenzoic acid was filled into the sample cell. The instrument was allowed to stabilize and then 1.20 mM aqueous 1,3,5-tris(imidazole-1-yl-methyl) benzene solution was injected into it in aliquots of 8  $\mu$ L for a total of 25 injections using the automatic computerized instructions. The heat change patterns were recorded and analyzed.

#### ***2.2.4.2 Binding study of 1,3,5-tris(imidazole-1-yl-methyl) benzene and 3-methoxybenzoic acid***

1.2 mL of 0.150 mM aqueous 3-methoxybenzoic acid was filled into the sample cell. The instrument was allowed to stabilize and then 1.20 mM aqueous 1,3,5-tris(imidazole-1-yl-methyl) benzene solution was injected into it in aliquots of 8  $\mu$ L for a total of 25 injections using the automatic computerized instructions. The heat change patterns were recorded and analyzed.

#### ***2.2.4.3 Binding study of 1,3,5-tris(imidazole-1-yl-methyl) benzene and benzoic acid***

1.2 mL of 0.150 mM aqueous benzoic acid was filled into the sample cell. The instrument was allowed to stabilize and then 1.20 mM aqueous 1,3,5-tris(imidazole-1-yl-methyl) benzene solution was injected into it in aliquots of 8  $\mu$ L for a total of 25 injections using the automatic computerized instructions. The heat change patterns were recorded and analyzed.

#### ***2.2.4.4 Binding study of 1,3,5-tris(imidazole-1-yl-methyl) benzene and 3-dimethylaminobenzoic acid***

1.2 mL of 0.150 mM aqueous 3-dimethylaminobenzoic acid was filled into the sample cell. The instrument was allowed to stabilize and then 1.20 mM aqueous 1,3,5-tris(imidazole-1-yl

methyl) benzene solution was injected into it in aliquots of 8  $\mu\text{L}$  for a total of 25 injections using the automatic computerized instructions. The heat change patterns were recorded and analyzed.

## 2.3 Results

The acceptor molecule in this study has three geometrically and electrostatically equivalent imidazole nitrogen atoms that can act as hydrogen-bond acceptors in solution. The carboxylic acid sites (the hydrogen-bond donors) on the benzoic acids were ranked using calculated electrostatic potential surfaces, Figure 2.7.

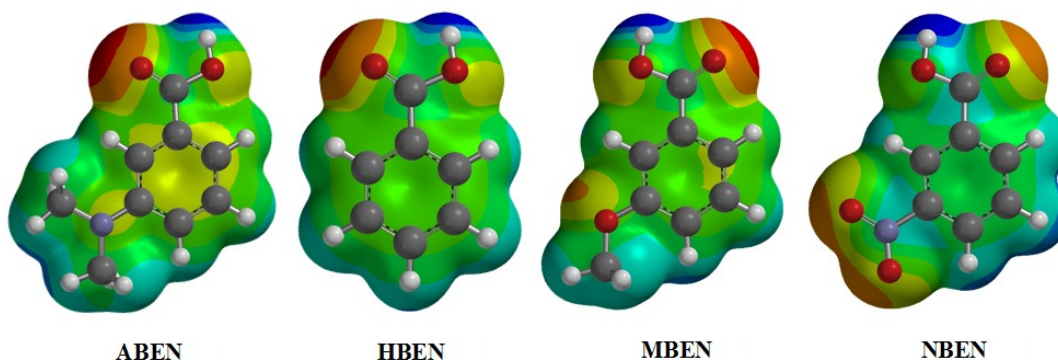


**Figure 2.7** Calculated molecular electrostatic potential surface maps; ABEN = 3-diamino benzoic acid; HBEN = benzoic acid; MBEN = 3-methoxybenzoic acid; and NBEN = 3-nitrobenzoic acid

With a higher positive potential on the carboxylic proton, the expectation is that the acid will engage in stronger and more prominent hydrogen bonds. Data analysis and data fitting conducted using NanoAnalyze is depicted in Table 2.3. The calculated values, together with the relevant  $\text{pK}_a$  values<sup>19b</sup> are shown in Table 2.2, and it is evident that a high electrostatic potential value largely reflect a trend inverse to that of  $\text{pK}_a$  values of the acid.

**Table 2.1** 95% confidence interval for association constants and thermodynamic parameters for benzoic acid derivatives and IM<sub>3</sub>

Molecule	K <sub>a</sub> [M <sup>-1</sup> ]		ΔH [kJmol <sup>-1</sup> ]		n <sup>1</sup>	
	95%		95%		95%	
	Value	Confidence interval (±)	Value	Confidence interval (±)	Value	Confidence interval (±)
NBEN	1.35×10 <sup>6</sup>	9.13×10 <sup>4</sup>	-94.3	0.72	0.394	0.002
MBEN	6.65×10 <sup>5</sup>	6.77×10 <sup>4</sup>	-88.4	1.45	0.377	0.003
HBEN	6.01×10 <sup>5</sup>	5.08×10 <sup>4</sup>	-111	2.8	0.298	0.004
ABEN	9.48×10 <sup>4</sup>	6.35×10 <sup>3</sup>	-98.1	4.02	0.291	0.008

**Table 2.2** Electrostatic potentials of donors (-COOH) and pK<sub>a</sub> values

Molecule	Atom	(kJ/mol)	pK <sub>a</sub>
3-Nitrobenzoic acid (NBEN)	Carboxyl H	287.9	3.45
3-Methoxybenzoic acid (MBEN)	Carboxyl H	250.0	4.09
Benzoic acid (HBEN)	Carboxyl H	252.0	4.21
3-Dimethylaminobenzoic acid (ABEN)	Carboxyl H	236.9	5.10

Liquid assisted grinding experiments were carried out in order to establish if co-crystals can be formed between IM<sub>3</sub> and the different carboxylic acids. The outcome of each reaction was characterized by IR spectroscopy and all four experiments resulted in co-crystal formation as indicated by broad bands in the 1,850 and 2,500 cm<sup>-1</sup> regions (a consequence of intermolecular N···H—O hydrogen bonds) and notable changes in the C=O stretch of the carboxylic acid, Table 2.3.

**Table 2.3** IR stretches for ground mixtures for respective acceptor and donors

Molecule	Carbonyl Stretch		O-H···N stretches (cm <sup>-1</sup> )	Co-crystal?
	Acid	Ground mixture		
NBEN	1683	1662	1936, 2432	Y
MBEN	1678	1690	1967, 2389	Y
HBEN	1677	1685	1916, 2463	Y
ABEN	1663	1682	1943, 2483	Y

With these data in hand, isothermal titration calorimetry (ITC) experiments were conducted to determine the binding strengths (binding preferences) between the tritopic acceptor and aromatic carboxylic acids in solution. All acids were titrated with the tritopic acceptor in an aqueous medium at 25 °C. The tritopic acceptor was eluted from the burette into the cell containing the benzoic acid derivatives and the results are listed in Table 2.4 and in Figures 2.6 – 2.9.

**Table 2.4** Association constants ( $K_a$ ) and thermodynamic binding parameters for benzoic acid derivatives and IM<sub>3</sub>

Molecule	$K_a$ [M <sup>-1</sup> ]	$\Delta G$ [kJmol <sup>-1</sup> ]	$\Delta H$ [kJmol <sup>-1</sup> ]	$-T\Delta S$ [kJmol <sup>-1</sup> ]	n
NBEN	$1.35 \times 10^6$	-34.9	-94.3	59.3	0.394
MBEN	$6.65 \times 10^5$	-33.2	-88.4	55.2	0.377
HBEN	$6.01 \times 10^5$	-32.9	-111	78.1	0.298
ABEN	$9.48 \times 10^4$	-28.4	-98.1	69.7	0.291

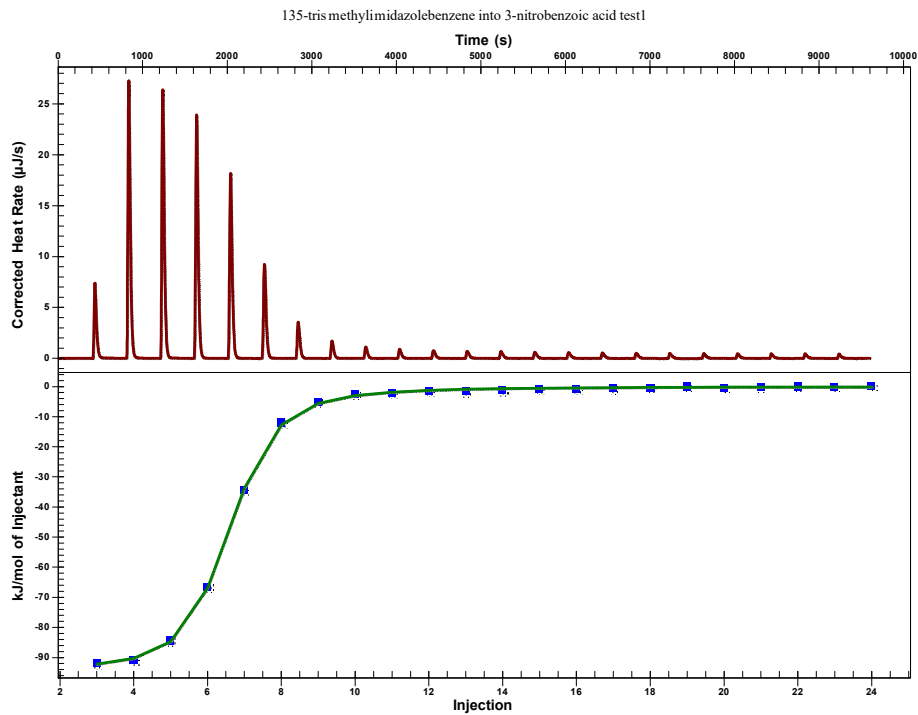


**Figure 2.8** ITC profile between IM<sub>3</sub> (1.20 mM) and NBEN (0.150 mM) at 25°C

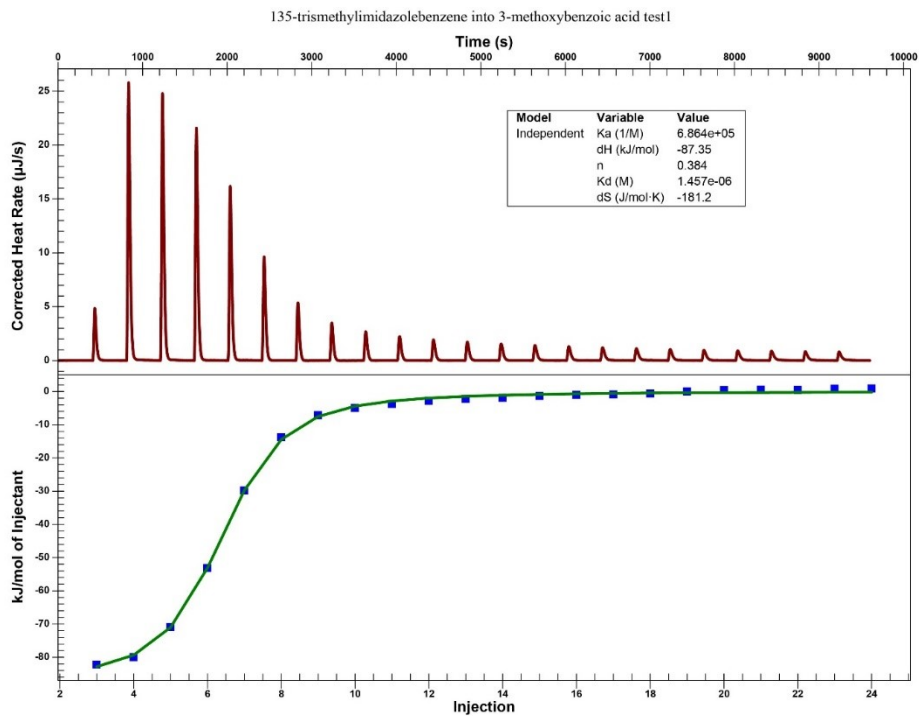


**Figure 2.9** ITC profile between IM<sub>3</sub> (1.20 mM) and MBEN (0.150 mM) at 25°C



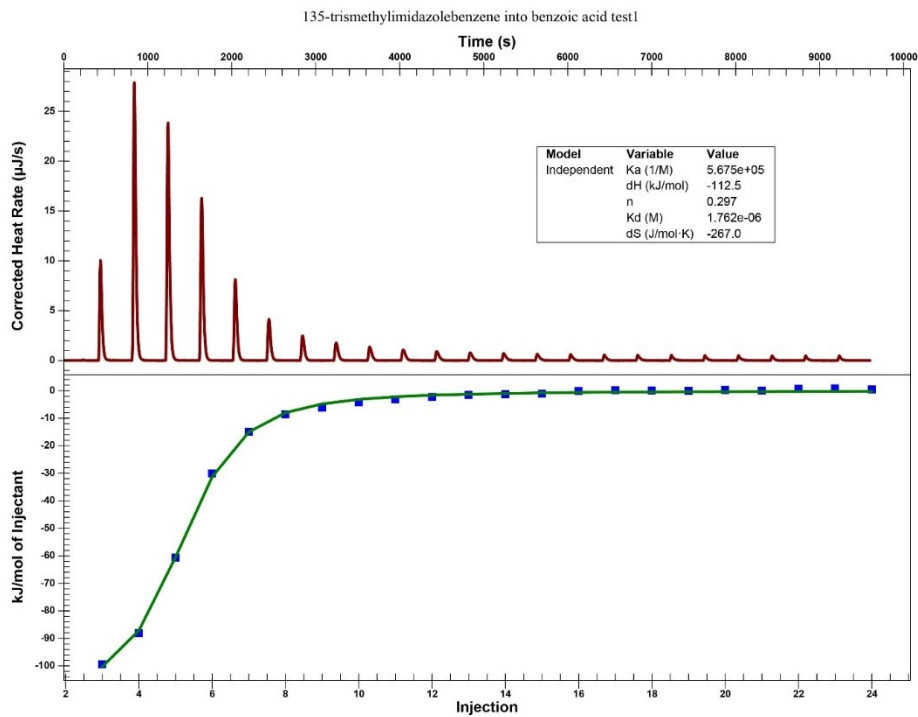


Figure 2.10 ITC profile between IM<sub>3</sub> (1.20 mM) and HBEN (0.150 mM) at 25°C

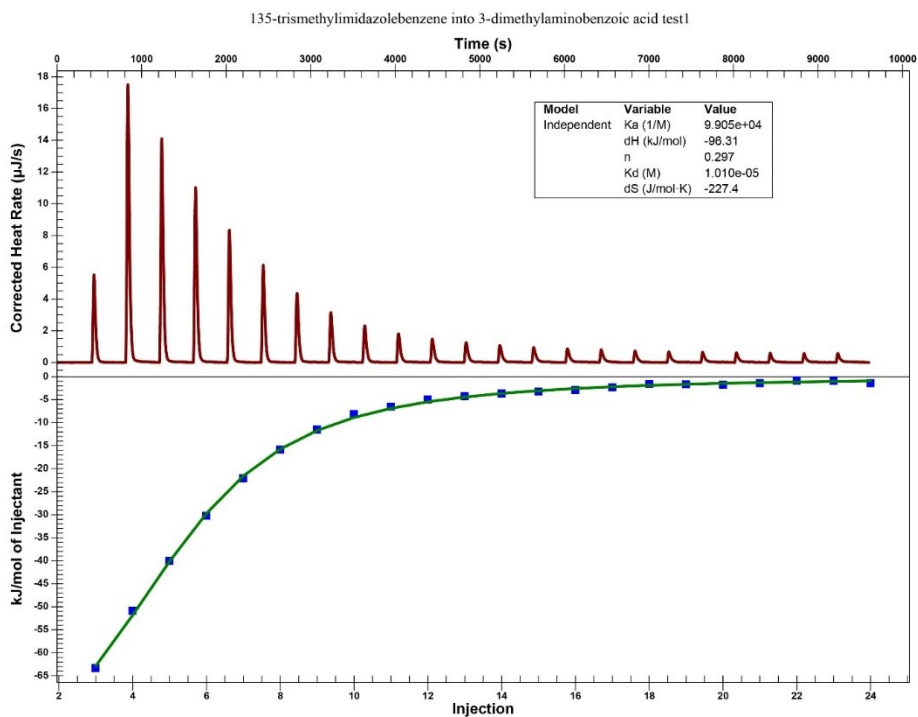


Figure 2.11 ITC profile between IM<sub>3</sub> (1.20 mM) and ABEN (0.150 mM) at 25°C

## 2.4 Discussion

The co-crystal screening that was done using infrared spectroscopy provided unambiguous conformation of co-crystal formation, but it does not reveal the stoichiometric ratio at which each acid binds with the tritopic acceptor and therefore to verify binding ratio ITC data are required.

ITC's widespread use is the characterization of enthalpies and equilibrium association constants of simple 1:1 interactions in solution. However, its use for more complex systems in which three or more binding sites is expanding. Reported work on multi-site binding models to ITC data specifically focuses on protein binding.<sup>22</sup> To the best of our knowledge, related research that has been done are, for a tetratopic cavitand and 4-nitrobenzoic acid that focuses on  $\text{COOH}\cdots\text{N}_{(\text{pyridine})}$  hydrogen bond interaction in the solution phase.<sup>13a</sup> With three binding sites available, three outcomes are possible. Expected  $n$  values = 0.33, 0.5, 1 means that either 3, 2 or 1 acids/ acid bind to the tritopic acceptor. Experimental data on both benzoic acid (HBEN) and 3-dimethylamino benzoic (ABEN) acid show stoichiometries of 0.298 and 0.291 where as NBEN and MBEN are 0.394 and 0.377 respectively. The calculated  $n$  values are higher and lower than the expected values, suggesting, the solution binding of the acceptor differs from its solid-state binding. For NBEN and MBEN, it can be assumed that a much weaker  $\text{O}-\text{H}\cdots\pi$  interaction,<sup>23</sup> could form a pentameric analogue of the tritopic acceptor. As per our understanding, there aren't many papers that report on simultaneous studies for matching solution- and solid- state data, for aromatic carboxylic acids with tritopic or multivalent acceptors, that could affirm the above assumption. The paucity of such literature on thermodynamic parameter estimation for a three or more binding site model is likely due to over-interpretation of multi-site ITC data and the lack of availability of macroscopic binding models and unavailability of microscopic models, in common

ITC software.<sup>22a, 22b, 22c</sup> Despite the experimental observations made here, which do not directly reflect the expected supramolecular stoichiometry, the values obtained for  $K_a$  and  $\Delta H^\circ$  are reasonable<sup>13a, 24</sup> since a substantive part of the isotherm displays a sufficiently large signal-to-noise ratio, and that stoichiometry is realistic and host/guest concentrations are known, ITC measurements can provide reliable data.

In a likely manner, when determining the association constants using ITC, it can be reliably measured if the value in question falls within the range of  $10^2 < K < 10^7$ ,<sup>25</sup> which is what we observed from the experimental data, Table 2.4. With larger electrostatic stabilization, increased stabilization of the supramolecular assemblies in solution can take place. This would be reflected by increased association between the tritopic acceptor and monotopic donor. The plot of association constant and the molecular electrostatic potentials on carboxylic protons reflect this hypothesis with a correlation coefficient of  $R^2=0.95$ , Figure 2.12.

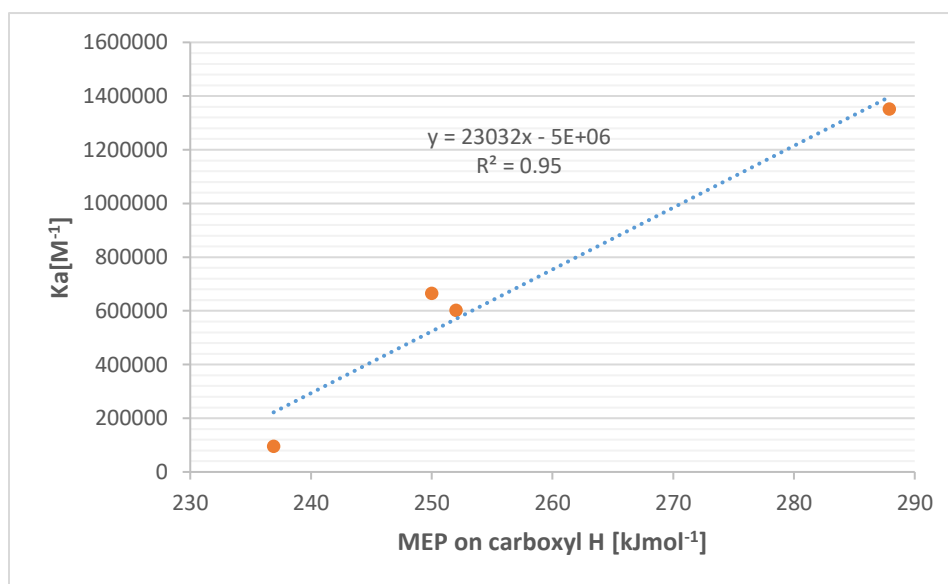


**Figure 2.12** Plot of the association constant versus electrostatic potential on carboxyl H for the binding of IM<sub>3</sub> with benzoic acid derivatives

The enthalpic contributions observed for the binding studies averages at  $98.02 \text{ kJmol}^{-1}$  with the highest being  $-111.2 \text{ kJmol}^{-1}$  and the lowest being  $-88.41 \text{ kJmol}^{-1}$ , Table 2.4. In each of the experiments, Table 2.4, a varying number of monotopic donors interact with the tritopic acceptor, to form a supramolecular assembly, which would yield an enthalpy, based on the intermolecular interactions taking place. Therefore, for a single experiment, assuming the interactions taking place are the same, between each donor with the tritopic acceptor, the averaging of the observed enthalpy (which would provide enthalpy per acid) should be made. Reported work on the binding of a trivalent system of receptor and ligand, derived from vancomycin and D-Ala-D-Ala, has a  $\Delta H$  value that is three times that for the monovalent vancomycin and D-Ala-D-Ala.<sup>26</sup> A similar study between multivalent analogues of carbohydrates with relatively high affinities possesses  $\Delta H$  per mole of the analogue for Concanavalin A and Dioclea grandiflora Lectin that reflect multiples of  $\Delta H$  for the corresponding monovalent binding epitopes.<sup>27</sup> When considering an averaged enthalpy (in other words, the enthalpy of formation per donor per site), Table 2.4, the observable enthalpies fall in the range of  $29 - 37 \text{ kJmol}^{-1}$  for a single  $\text{COOH} \cdots \text{N}_{(\text{imi})}$  hydrogen bond. A report on using IR spectroscopy to evaluate the hydrogen bond formation enthalpy ( $\text{COOH} \cdots \text{N}_{(\text{py})}$ ) between a pyridine and benzoic acid is found to be  $-44.52 \text{ kJmol}^{-1}$ . This is acceptable since pyridine acceptor sites  $\text{N}_{(\text{py})}$  are known to be more electronegative than imidazole acceptor sites  $\text{N}_{(\text{imi})}$ . This allows  $\text{N}_{(\text{py})}$  to be more competitive in hydrogen bond formation, which would result in greater electrostatic stabilization that would release more heat per bond formed. These values plotted against the molecular electrostatic potentials on carboxylic protons yielded a correlation coefficient of 0.87, Figure 2.13. As electrostatic stabilization increases, more heat is released when forming the intermolecular interactions that would formulate the supramolecular assemblies between  $\text{IM}_3$  and aromatic carboxylic acids.

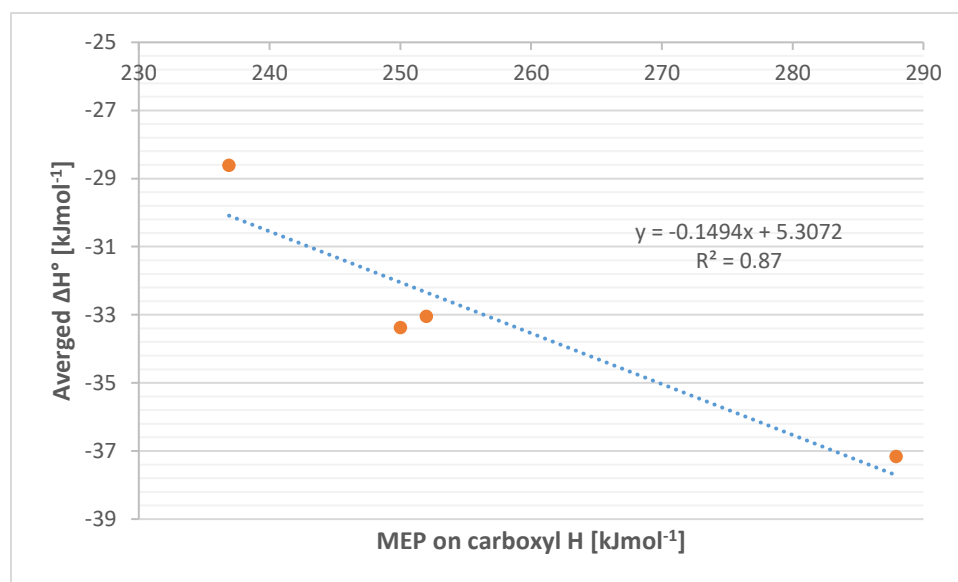


**Figure 2.13** Plots of average  $\Delta H$  versus electrostatic potential on carboxyl H for the binding of  $IM_3$  with benzoic acid derivatives

**Table 2.5** Averaged  $\Delta H$  values for benzoic acid derivatives and  $IM_3$

Molecule	$\Delta H$ [kJmol <sup>-1</sup> ]	n	Average $\Delta H$ [kJmol <sup>-1</sup> ]
NBEN	-94.32	0.394	-37.16
MBEN	-88.41	0.377	-33.37
HBEN	-111.2	0.298	-33.04
ABEN	-98.15	0.291	-28.61

The standard enthalpy  $\Delta H^\circ$  can be considered as a quantitative indicator of the changes in intermolecular bond energies such as hydrogen bonding and van der Waals interactions occurring during binding processes. The standard entropy  $\Delta S^\circ$ , on the other hand, an indicator of the rearrangement that undergoes by the solvent (which in this case study; water) molecules during the same process. For this study, we observe a correlation coefficient of 0.93 for the entropy-enthalpy compensation plot with a compensation temperature of 266.7 K as seen in Figure 2.14. For a true entropy-enthalpy compensation arising from chemical causality, Krug et al.<sup>28</sup> proposed

two conditions, (i) the compensation temperature  $\beta$  must be significantly different from the average experimental temperature  $\beta'$ ; (ii)  $\Delta H^\circ$  values should be linearly correlated with the corresponding  $\Delta G^\circ$  values, which as per Gilli et al.<sup>29</sup> would be too rigid a requisite to adhere to when the chemical nature of the ligands varies. And in our study, the chemical nature of the aromatic carboxylic acids is very different from each other, Figure 2.7. Furthermore, in drug receptor binding in aqueous solution, Gilli et al. have put forward that enthalpy-entropy compensation arises, based only on the intrinsic properties of the hydrogen bond, as a principal force controlling the intermolecular association in solution.<sup>29</sup> This is observed in Figure 2.13, where the standard enthalpy  $\Delta H^\circ$ ; an indicator of intermolecular interactions, such as hydrogen bond (an electrostatic force), is related to the electrostatic potential on carboxyl hydrogen. Furthermore, since a flexible tritopic acceptor has been used, when a weakly bound complex is formed, there is a possibility for an intermolecular motion to take place, in which case, on average the interacting functional groups are further apart than a strongly bound complex.<sup>30</sup> This structural tightening in bound complexes leads to entropy-enthalpy compensation, Figure 2.14. All the data points on the 3rd quadrant on the Cartesian plane indicates all reactions are enthalpically driven, Figure 2.14.

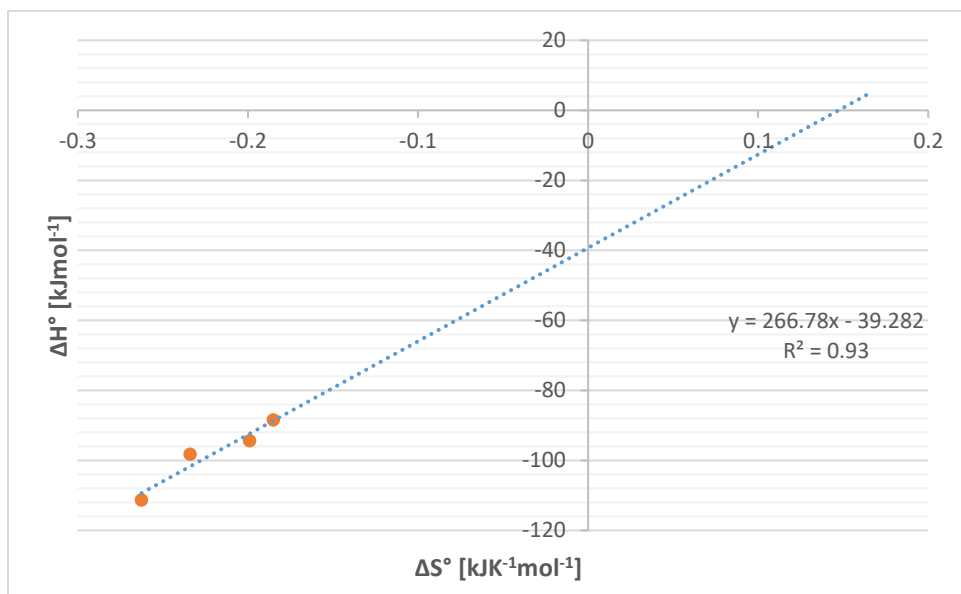


**Figure 2.14** Scatter plot of enthalpies  $\Delta H$  and entropies  $\Delta S$  for the binding of  $IM_3$  with benzoic acid derivatives

A similar analysis (ranking molecules using the relative strength of  $pK_a/pK_b$  values) was done to observe a relationship based on  $pK_a$  values of the donors and the observed association constants as well as averaged enthalpies, Figure 2.15 & Figure 2.16. Here, as expected, we observe a good correlation between  $pK_a$  values and experimentally observed association constants, which amounts to a correlation coefficient of 0.95, Figure 2.15. Similarly, an even better correlation is observed between  $pK_a$  values and averaged enthalpies, with a correlation coefficient of 0.99, Figure 2.16.

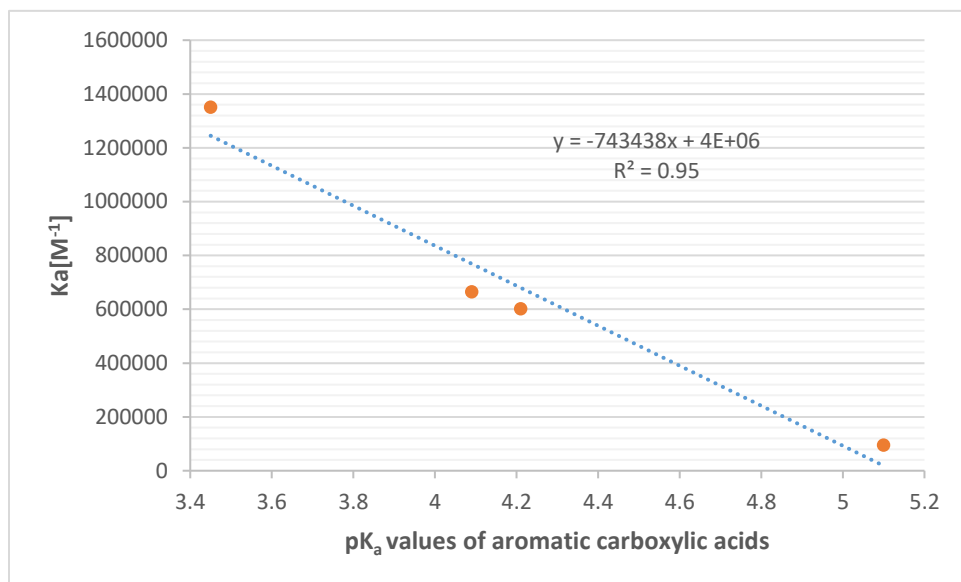


**Figure 2.15** Plot of the association constant versus  $pK_a$  values of aromatic carboxylic acids for the binding of  $IM_3$  with benzoic acid derivatives

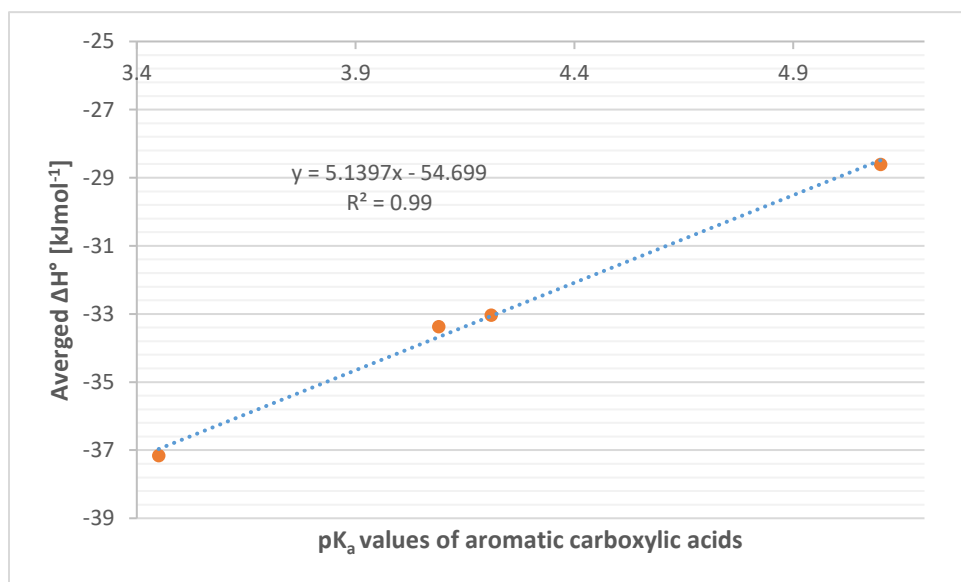


**Figure 2.16** Plots of average  $\Delta H$  versus  $pK_a$  values of aromatic carboxylic acids for the binding of  $IM_3$  with benzoic acid derivatives



## 2.5 Conclusions<sup>1</sup>

From this study, it is evident that molecular electrostatic potential surfaces play an important role in molecular recognition in the initial stages, which can provide quantitative measures of solution binding affinities. This was clearly illustrated when observing the plot between electrostatic potential on carboxyl H and the association constant. Consequently, this would further affirm that stronger stabilization and interaction is observed with increased electrostatic stabilization in solution. This also suggests that by controlling and modulating the electrostatic component of these acceptor···donor hydrogen bonds we can alter binding constant and the overall thermodynamic landscape of these systems. The linearity observed from this relationship provides good grounds for the use of MEPS as a ranking method that can offer quantitative measures of solution binding.

The intermolecular interactions of the reaction partners have taken place regardless of the size, geometry or the shape of the molecule, but purely focusing on the most prominent binding sites of the molecular partners. This study also stipulates the importance of ITC measurements in the determination of the functional valency for the tritopic analogue in the presence of a donor molecule in solution, which may differ from the structural valency of the acceptor.

Furthermore, according to the entropy-enthalpy compensation effect, it is evident that the principal force controlling the intermolecular association in solution is, predominantly hydrogen bonds. To observe the linearity and effectiveness of MEPS as a ranking method, it is important to consider the average binding per site of the tritopic acceptor for enthalpy to establish a correlation with MEPS values since the comparison is made between the electrostatic charge on the carboxyl hydrogen atom.

## 2.6 References

1. Andree, S. N. L.; Aakeröy, C. B., Molecular electrostatic potentials as a quantitative measure of hydrogen bonding preferences in solution. *Supramol. Chem.* **2017**, *30* (5-6), 455-463.
2. Lehn, J.-M., *Supramolecular Chemistry: Concepts and Perspectives*. **2006**.
3. (a) Lehn, J.-M., Supramolecular Chemistry—Scope and Perspectives Molecules, Supermolecules, and Molecular Devices (Nobel Lecture). *Angew Chem Int* **1988**, *27* (1), 89-112; (b) Lehn, J. M., Perspectives in chemistry: from supramolecular chemistry towards adaptive chemistry. *Febs Journal* **2013**, *280*, 1-2.
4. (a) Baron, R.; Setny, P.; McCammon, J. A., Water in Cavity–Ligand Recognition. *J. Am. Chem. Soc.* **2010**, *132* (34), 12091-12097; (b) Baron, R.; McCammon, J. A., Molecular Recognition and Ligand Association. *Annu. Rev. Phys. Chem.* **2013**, *64* (1), 151-175.
5. Hunter, C. A., Quantifying Intermolecular Interactions: Guidelines for the Molecular Recognition Toolbox. *Angew. Chem. Int. Ed.* **2004**, *43* (40), 5310-5324.
6. (a) Ariga, K.; Ito, H.; Hill, J. P.; Tsukube, H., Molecular recognition: from solution science to nano/materials technology. *Chem. Soc. Rev.* **2012**, *41* (17), 5800; (b) Yang, L.; Adam, C.; Nichol, G. S.; Cockroft, S. L., How much do van der Waals dispersion forces contribute to molecular recognition in solution? *Nat. Chem.* **2013**, *5*, 1006.
7. Politzer, P.; Laurence, P. R.; Jayasuriya, K., Molecular electrostatic potentials: an effective tool for the elucidation of biochemical phenomena. *Environ. Health Perspect.* **1985**, *61*, 191-202.
8. Zipse, H. *Molecular Electrostatic Potential (MEP)*. <http://www.cup.uni-muenchen.de/ch/compchem/pop/mep1.html>.
9. Liu, S.; Pedersen, L. G., Estimation of Molecular Acidity via Electrostatic Potential at the Nucleus and Valence Natural Atomic Orbitals. *J. Phys. Chem. A* **2009**, *113* (15), 3648-3655.
10. Alipour, M.; Mohajeri, A., Molecular Electrostatic Potential as a tool for Evaluating the Etherification Rate Constant. *J. Phys. Chem. A* **2010**, *114* (27), 7417-7422.
11. (a) Luque, F. J.; Orozco, M.; Illas, F.; Rubio, J., Effect of electron correlation on the electrostatic potential distribution of molecules. *J. Am. Chem. Soc.* **1991**, *113* (14), 5203-5211; (b) Sapse, A.-M., *Molecular orbital calculations for biological systems*. Oxford University Press: New York, **1998**; p xiv, 233 p.
12. Aakeroy, C. B.; Wijethunga, T. K.; Desper, J., *New J. Chem.* **2015**, *39* (2), 822-828.

13. (a) Aakeroy, C. B.; Chopade, P. D.; Quinn, C. F.; Desper, J., *CrystEngComm* **2014**, *16* (18), 3796-3801; (b) Aakeroy, C. B.; Spartz, C. L.; Dembowski, S.; Dwyre, S.; Desper, J., *IUCrJ* **2015**, *2* (Pt 5), 498-510; (c) Hunter, C. A., *Angew. Chem. Int. Ed.* **2004**, *43* (40), 5310-24; (d) Kenny, P. W., *J. Chem. Inf. Model* **2009**, *49* (5), 1234-44; (e) Musumeci, D.; Hunter, C. A.; Prohens, R.; Scuderi, S.; McCabe, J. F., *Chem. Science* **2011**, *2* (5), 883-890.
14. Aakeroy, C. B.; Wijethunga, T. K.; Haj, M. A.; Desper, J.; Moore, C., *CrystEngComm* **2014**, *16* (31), 7218-7225.
15. (a) Aakeroy, C. B.; Rajbanshi, A.; Desper, J., *Chem. Commun.* **2011**, *47* (41), 11411-11413; (b) Shin, D. M.; Chung, Y. K.; Lee, I. S., *Cryst. Growth Des.* **2002**, *2* (6), 493-496; (c) Stilinović, V.; Kaitner, B., *Cryst. Growth Des.* **2011**, *11* (9), 4110-4119.
16. (a) Atzori, M.; Marchiò, L.; Clérac, R.; Serpe, A.; Deplano, P.; Avarvari, N.; Mercuri, M. L., *Cryst. Growth Des.* **2014**, *14* (11), 5938-5948; (b) Hamdouni, M.; Walha, S.; Duhayon, C.; Kabadou, A.; Sutter, J.-P., *CrystEngComm* **2017**, *19* (12), 1633-1642; (c) Si, C.-D.; Hu, D.-C.; Fan, Y.; Dong, X.-Y.; Yao, X.-Q.; Yang, Y.-X.; Liu, J.-C., *Cryst. Growth Des.* **2015**, *15* (12), 5781-5793.
17. Aakeroy, C. B.; Wijethunga, T. K.; Desper, J., *J. Mol. Struct.* **2014**, *1072*, 20-27.
18. Aakeroy, C. B.; Smith, M.; Desper, J., *Can. J. Chem.* **2015**, *93* (8), 822-825.
19. (a) D'Anna, F.; Gunaratne, H. Q.; Lazzara, G.; Noto, R.; Rizzo, C.; Seddon, K. R., *Org. Biomol. Chem.* **2013**, *11* (35), 5836-46; (b) Davis, M. M.; Hetzer, H. B., *J Res Nat Bur Stand* **1958**, *60* (6), 569-592; (c) Wang, B. B.; Fang, J. F.; Li, B.; You, H.; Ma, D. G.; Hong, Z. R.; Li, W. L.; Su, Z. M., *Thin Solid Films* **2008**, *516* (10), 3123-3127.
20. (a) Corpinot, M. K.; Stratford, S. A.; Arhangelskis, M.; Anka-Lufford, J.; Halasz, I.; Judas, N.; Jones, W.; Bucar, D. K., *CrystEngComm* **2016**, *18* (29), 5434-5439; (b) Hathwar, V. R.; Chopra, D.; Panini, P.; Row, T. N. G., *Cryst. Growth Des.* **2014**, *14* (11), 5366-5369; (c) Shirman, T.; Lamere, J. F.; Shimon, L. J. W.; Gupta, T.; Martin, J. M. L.; van der Boom, M. E., *Cryst. Growth Des.* **2008**, *8* (8), 3066-3072.
21. . Nano Isothermal Titration Calorimeter (Nano ITC) *Getting Started Guide for Models 601000, 601001, 601002* [Online], 2014, p. 11-14.
22. (a) Brautigam, C. A., *Methods (San Diego, Calif.)* **2015**, *76*, 124-136; (b) Freire, E.; Schön, A.; Velazquez-Campoy, A., *Methods Enzymol.* **2009**, *455*, 127-155; (c) Freyer, M. W.; Lewis, E. A., *Methods Cell Biol.* **2008**, *84*, 79-113; (d) Gustchina, E.; Li, M.; Ghirlando, R.; Schuck, P.; Louis, J. M.; Pierson, J.; Rao, P.; Subramaniam, S.; Gustchina, A.; Clore, G. M.; Wlodawer, A., *PLoS ONE* **2013**, *8* (11), e78187; (e) Le, V. H.; Buscaglia, R.; Chaires, J. B.; Lewis, E. A., *Anal. Biochem.* **2013**, *434* (2), 233-241; (f) Zhao, H.; Schuck, P., *Anal. Chem.* **2012**, *84* (21), 9513-9519.

23. (a) Mohan, N.; Vijayalakshmi, K. P.; Koga, N.; Suresh, C. H., *J. Comput. Chem.* **2010**, *31* (16), 2874-82; (b) Steiner, T.; Schreurs, A. M. M.; Lutz, M.; Kroon, J., *New J. Chem.* **2001**, *25* (1), 174-178.
24. (a) Kaufmann, L.; Dzyuba, E. V.; Malberg, F.; Low, N. L.; Groschke, M.; Brusilowskij, B.; Huuskonen, J.; Rissanen, K.; Kirchner, B.; Schalley, C. A., *Org. Biomol. Chem.* **2012**, *10* (30), 5954-5964; (b) Turnbull, W. B.; Daranas, A. H., *J. Am. Chem. Soc.* **2003**, *125* (48), 14859-14866.
25. Sessler, J. L.; Gross, D. E.; Cho, W. S.; Lynch, V. M.; Schmidtchen, F. P.; Bates, G. W.; Light, M. E.; Gale, P. A., *J. Am. Chem. Soc.* **2006**, *128* (37), 12281-8.
26. Rao, J.; Lahiri, J.; Isaacs, L.; Weis, R. M.; Whitesides, G. M., *Science* **1998**, *280* (5364), 708-11.
27. Dam, T. K.; Roy, R.; Das, S. K.; Oscarson, S.; Brewer, C. F., *J. Biol. Chem.* **2000**, *275* (19), 14223-30.
28. Krug, R. R.; Hunter, W. G.; Grieger, R. A., *J Phys Chem-Us* **1976**, *80* (21), 2335-2341.
29. Gilli, P.; Ferretti, V.; Gilli, G.; Borea, P. A., *J Phys Chem-Us* **1994**, *98* (5), 1515-1518.
30. Hunter, C. A.; Tomas, S., *Chem. Biol.* **2003**, *10* (11), 1023-1032.

# **Chapter 3 - Guiding tritopic nitrogen heterocycles and multitopic carboxylic acids into co-crystals via selective O—H···N hydrogen bonds**

## **3.1 Introduction**

A necessity for non-covalent synthesis is the availability of reliable and effective supramolecular synthons<sup>1</sup>. The usefulness of such synthons in crystal engineering depends on the frequency of occurrence of a desired intermolecular interaction. Generally, the dependability of a supramolecular synthon is governed by its ability to withstand subtle changes in molecular shape, substituent groups as well as competing intermolecular interactions such as  $\pi \cdots \pi$  interactions<sup>2</sup> and solute··solvent interactions<sup>3</sup>.

Directed assembly of supramolecules with desired stoichiometries is of great importance due to the tunability of physiochemical properties of the resulting solids<sup>4</sup>. Tailored stoichiometries in the presence of monotopic, ditopic and tritopic acceptors rest upon the intermolecular interactions taking place between acceptor and donor molecules. To obtain a desired supramolecule with a suitable intermolecular interaction, an effective supramolecular synthon is needed.<sup>5</sup>

Supramolecular synthons are structural units within supramolecules that can form and/or assemble through known or conceivable synthetic operations involving intermolecular interactions,<sup>6</sup> Figure 3.1. In crystal engineering, to ensure generality and predictability, we aim to identify and design robust synthons that can be exchanged from one structure to another. In the context of supramolecular chemistry, given that many weaker interactions deform or get disrupted

in solution, a persistently recurring pattern effectuated by weak forces in crystals is an indication of the importance of a robust synthon.

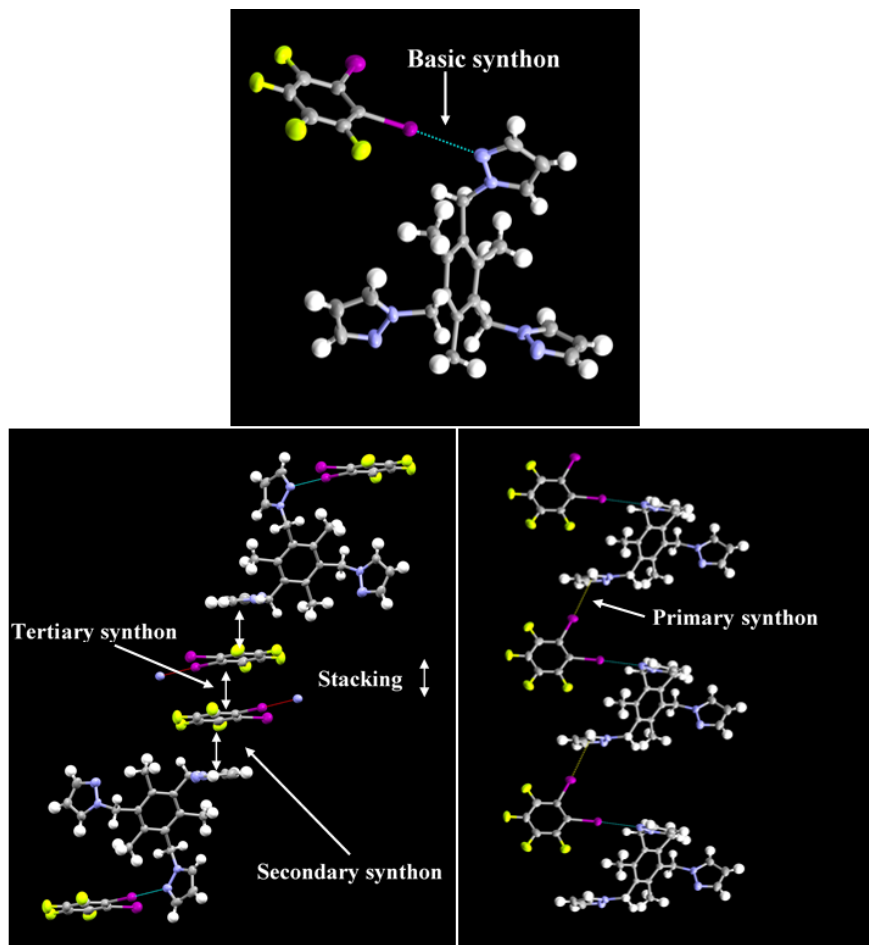


**Figure 3.1** Supramolecular synthons in a co-crystal

The significance of a certain synthon is a matter of crystal structure simplification. In Chapter 2, we examined the hydrogen bonding preferences, which employed carboxylic acid···imidazole synthon in the construction of extended architectures in solution. We saw that when changing the electrostatic component of the donor molecule in the acceptor···donor hydrogen bond, we could alter the binding constant which in turn would directly affect the hydrogen bond strength of a supramolecular synthon. It was also evident that the dominant supramolecular species is a tetrameric complex with 3:1 acid to acceptor stoichiometry. In this

chapter, we focus on COOH···imidazole, COOH···benzimidazole and COOH···pyrazole synthons, Figure 3.2, which are of biological relevance, and we aim to establish if ditopic and tritopic donors can formulate assemblies of 3:2 and 1:1 acid to acceptor stoichiometries with the use of both rigid and flexible multitopic donors.

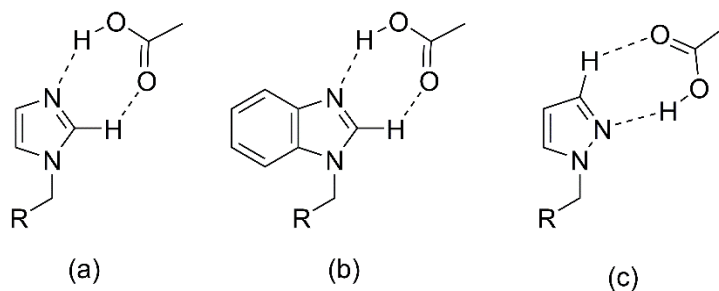


**Figure 3.2** Schematic showing some examples of observable synthons (a) COOH···imidazole (b) COOH···benzimidazole (c) COOH···pyrazole

The COOH···N-heterocyclic (imidazole, benzimidazole and pyrazole) synthons consist of a primary O—H···N hydrogen bond and an auxiliary C—H···O interaction which may not be present, Figure 3.3. When considering the O—H···N hydrogen bond in the COOH···Bzim synthon, it involves the best hydrogen bond donor - the hydroxyl group of the carboxylic acid and the best hydrogen bond acceptor - the heterocyclic nitrogen atom forming the primary intermolecular force.

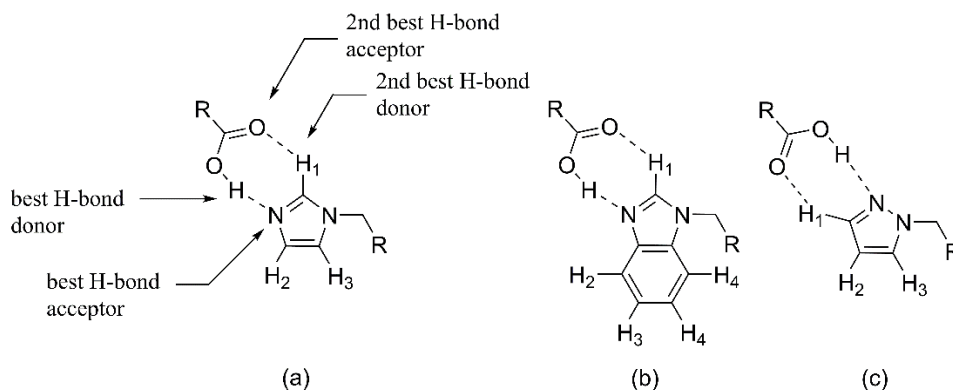


**Figure 3.3** The (a) COOH···imidazole and (b) COOH···benzimidazole synthons indicating the best and second-best hydrogen-bond donor/acceptor couples

The secondary intermolecular force  $C-H\cdots O$  arises from the  $C-H$  group on the carbon adjacent to the heterocyclic nitrogen atom. Unlike in pyrazole, both imidazole and benzimidazole possess two ortho-  $C-H$  groups with different positive electrostatics (acidities), Figure 3.3. Therefore, this study will also allow us to establish whether the carbonyl oxygen atom on the acid shows a preference for the more acidic of the two  $C-H$  options.

Herein we present the synthesis of ten closely related symmetric tritopic acceptors containing benzimidazole, imidazole and pyrazole moieties, Figure 3.5. The acceptors contain electrostatically and geometrically equivalent binding sites that are accessible and we can postulate several possible outcomes when a tritopic acceptor is combined with multitopic donors, Figure 3.4 and 3.6.

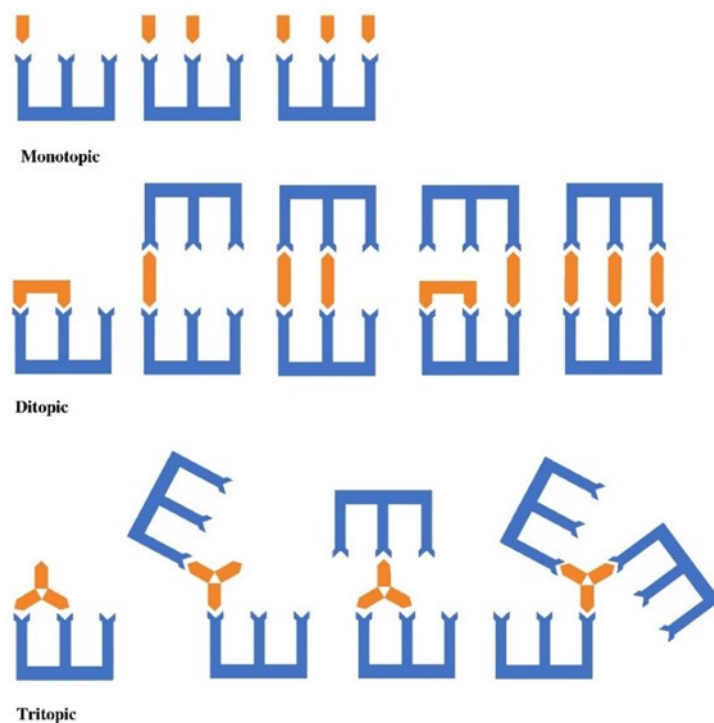


**Figure 3.4** Possible outcomes in this study in the presence of monotopic, flexible ditopic and rigid tritopic donors



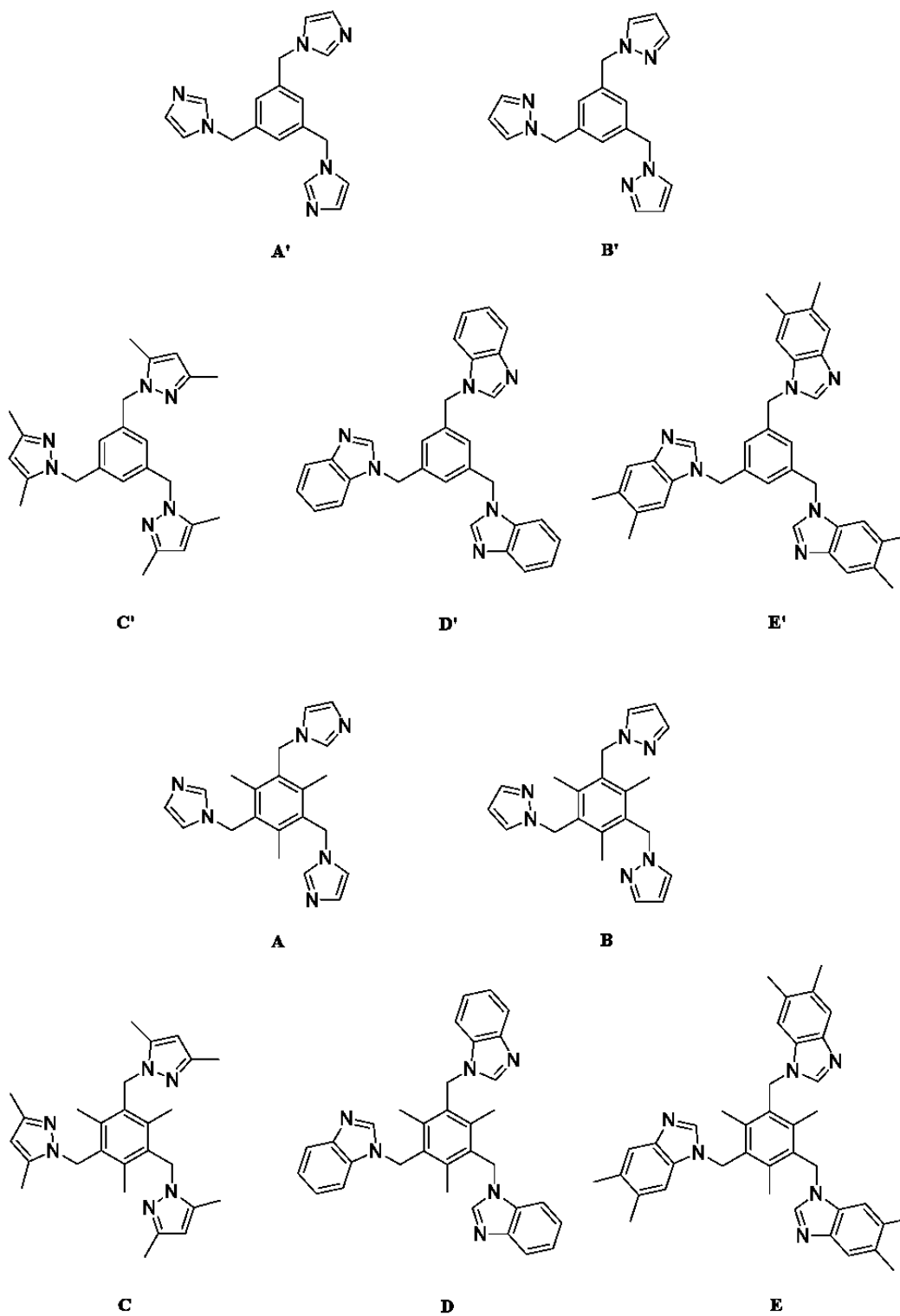


**Figure 3.5** Tritopic acceptors used in this study

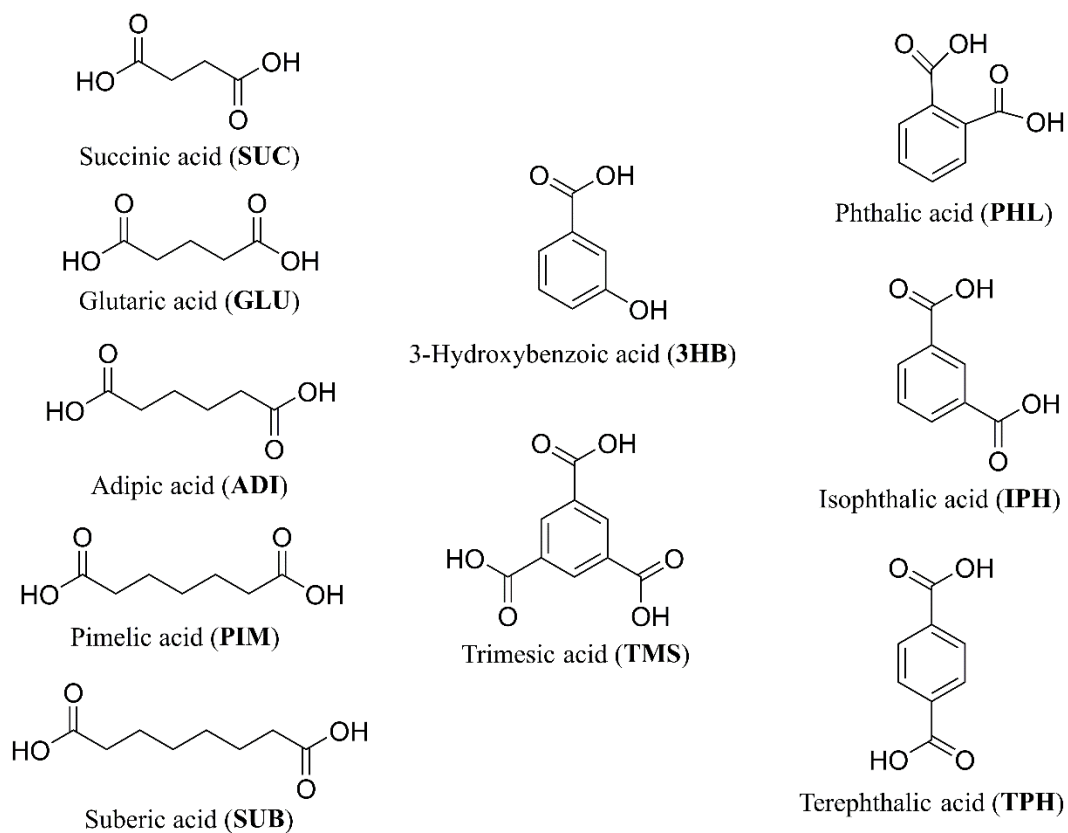


**Figure 3.6** Multitopic hydrogen bond donors used in this study

Overall specific goals of this chapter are as follows;

1. To investigate a correlation between the electrostatic potential surfaces on the heterocycle and the reliability of a supramolecular synthon.
2. To determine if an effective supramolecular synthon could promote desired co-crystal stoichiometry and connectivity.
3. To examine the usefulness of having an auxiliary interaction with the second-best donor to form C—H $\cdots$ O interactions. Is it structure directing or just a mere secondary interaction?

4. To determine if, having an additional “arm” can provide useful interactions with ditopic hydrogen bond donors.

## **3.2 Experimental**

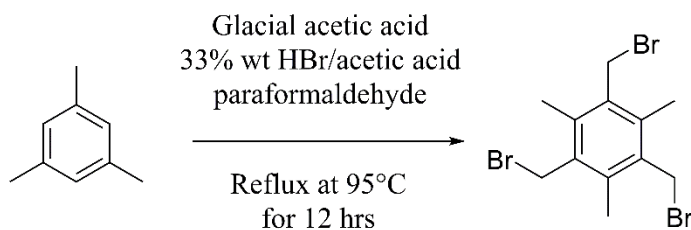
All reagents, solvents, precursors and hydrogen-bond donors were purchased from commercial sources and were used as received without further purification. A Fisher-Johns melting point apparatus (Vernon Hills, IL, USA) was used to determine melting points. A Varian Unity Plus (400 MHz) NMR spectrophotometer (Varian, Inc.) was used to record nuclear magnetic resonance spectra using the residual solvent signal as a reference. Infrared spectroscopic analyses were performed with a Nicolet 380 FT-IR instrument (Thermo Scientific, Madison, WI, USA).

### **3.2.1 Molecular electrostatic potential surface calculations**

To calculate the molecular electrostatic potential surface of the acceptor molecules, the geometries were optimized using hybrid density functional B3LYP level of theory with 6-31G\* basis set in vacuum. The geometry optimized molecules were then visualized through mapping its values, determined by a positive point charge in the vacuum as a probe, on the molecular surface with an outer contour of 0.002 a.u. electronic density. The surface potentials, which are the coulombic interaction energies (in  $\text{kJmol}^{-1}$ ) between the positive point probe and the surface of the molecule at that point. All calculations were done using Spartan 10 software, Wavefunction Inc.

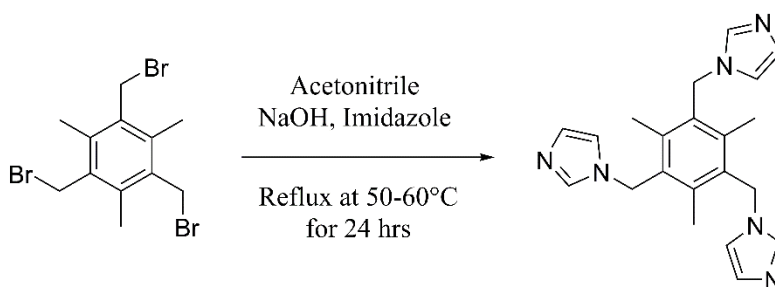
## 3.2.2 Synthesis of tritopic acceptors

### 3.2.2.1 Synthesis of 1,3,5-tris(bromomethyl)-2,4,6-trimethylbenzene<sup>7</sup> (α)



To a mixture of mesitylene (12.0 g; 0.10 mol), paraformaldehyde (10.26 g; 0.34 mol), and 75 mL of glacial acetic acid, 75 mL of a 33 wt% HBr/acetic acid solution was added rapidly. The mixture was kept for 12 h at 95 °C and then poured into 100 mL of water. The product was filtered off on a Buchner funnel and dried. Flash column chromatography (hexane: ethyl acetate = 98.5:1.5) gave the desired product as colorless needles. 90% yield. mp 184-186 °C (lit. mp 183–186 °C)<sup>7</sup>; <sup>1</sup>H-NMR (δH; CDCl<sub>3</sub>, 400 MHz) δ 4.58 (s, 6H), 2.46 (s, 9H).

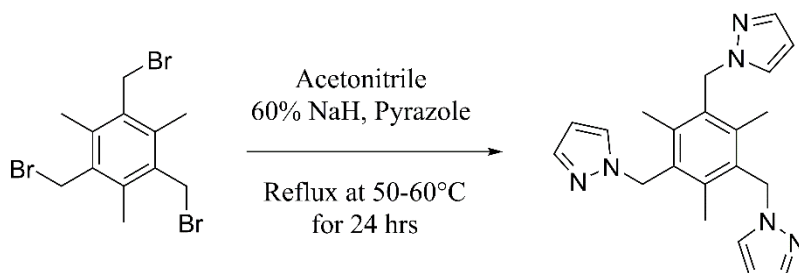
### 3.2.2.2 Synthesis of 1,3,5-tris(imidazole-1-yl-methyl)-2,4,6-trimethylbenzene<sup>8</sup> (A)



To a mixture of imidazole (874 mg, 12.8 mmol) in acetonitrile (50 mL), in a 100 mL round-bottomed flask, NaOH (1.029 g, 25.72 mmol) was added and stirred at room temperature for two hours. 1,3,5-Tris(bromomethyl)-2,4,6-trimethylbenzene (1.595 g, 4.000 mmol) in acetonitrile (20 mL) was added to the reaction mixture and refluxed for 24 h at 50–60 °C. The reaction mixture was monitored with TLC and after completion, the solvent was removed by rotary evaporation,

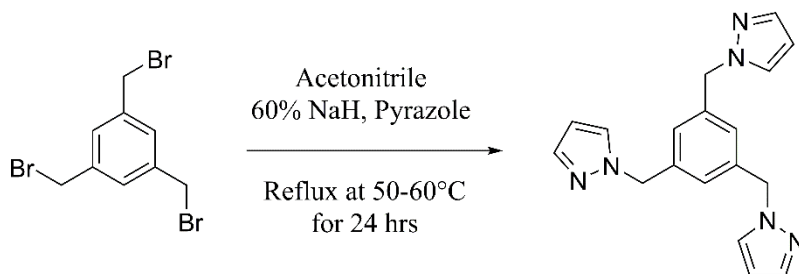
the residue was dissolved in water (100 mL) and extracted with methylene chloride (30 mL × 5). The organic layers were combined, dried over anhydrous MgSO<sub>4</sub>, filtered and purified by flash column chromatography (CH<sub>2</sub>Cl<sub>2</sub>/MeOH = 5/1) to give the desired product as a white solid. Recrystallization in ethyl acetate produced clear block like crystals 64% yield. mp 214–215 °C (Lit value 226–227 °C)<sup>8</sup>; <sup>1</sup>H-NMR (δH; CDCl<sub>3</sub>, 400 MHz) δ 7.31 (s, 3H), 7.07 (s, 3H), 6.75 (s, 3H), 5.24 (s, 6H) 2.32 (s, 9H).

### 3.2.2.3 Synthesis of 1,3,5-tris(pyrazole-1-yl-methyl)-2,4,6-trimethyl benzene<sup>9</sup> (B)



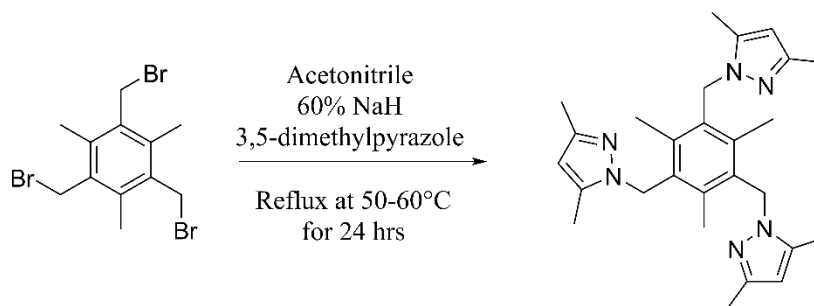
To a mixture of pyrazole (874 mg, 12.8 mmol) in acetonitrile (50 mL), in a 100 mL round-bottomed flask, 60% NaH (1.029 g, 25.72 mmol) was added and stirred at room temperature for two hours. 1,3,5-Tris(bromomethyl)-2,4,6-trimethyl benzene (1.595 g, 4.000 mmol) in acetonitrile (20 mL) was added to the reaction mixture and refluxed for 24 hours. The reaction mixture was monitored with TLC and after completion, the solvent was removed by rotary evaporation, the residue was dissolved in water (100 mL) and extracted with methylene chloride (30 mL x 5). The organic layers were combined, dried over anhydrous MgSO<sub>4</sub>, filtered and purified by flash column chromatography (CH<sub>2</sub>Cl<sub>2</sub>/MeOH = 10/1) to give the desired product as a white solid. 53% yield. mp 132-133 °C (Lit value 130-131 °C)<sup>9</sup>; <sup>1</sup>H NMR (δH; CDCl<sub>3</sub>, 400 MHz) δ 7.53 (d, 3H), 7.06 (d, 3H), 6.21 (t, 3H), 5.44 (s, 6H), 2.35 (s, 9H).

### 3.2.2.4 Synthesis of 1,3,5-tris(pyrazole-1-yl-methyl) benzene<sup>9</sup> (B')



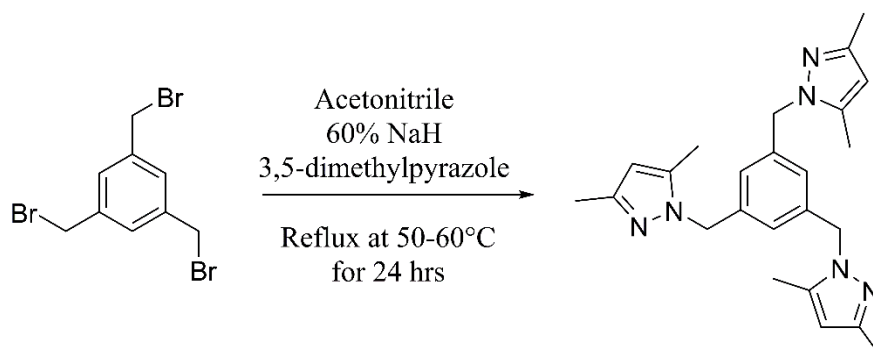
To a mixture of pyrazole (874 mg, 12.8 mmol) in acetonitrile (50 mL), in a 100 mL round-bottomed flask, 60% NaH (1.029 g, 25.72 mmol) was added and stirred at room temperature for two hours. 1,3,5-Tris(bromomethyl)-2,4,6-trimethyl benzene (1.427 g, 4.000 mmol) in acetonitrile (20 mL) was added to the reaction mixture and refluxed for 24 hours. The reaction mixture was monitored with TLC and after completion, the solvent was removed by rotary evaporation, the residue was dissolved in water (100 mL) and extracted with methylene chloride (30 mL x 5). The organic layers were combined, dried over anhydrous MgSO<sub>4</sub>, filtered and purified by flash column chromatography (CH<sub>2</sub>Cl<sub>2</sub>/MeOH = 10/1) The desired product was obtained as an off-white solid. 55% yield. mp 63-65 °C (Lit value 74-76 °C, 60-61 °C)<sup>9</sup>; <sup>1</sup>H NMR (δH; CDCl<sub>3</sub>, 400 MHz) δ 7.52 (d, 3H), 7.34 (d, 3H), 6.91 (s, 6H) 6.27 (t, 6H), 5.24 (s, 6H).433

### 3.2.2.5 Synthesis of 1,3,5-tris(3,5-dimethylpyrazole-1-yl-methyl)-2,4,6-trimethyl benzene<sup>9</sup> (C)



To a mixture of 3,5-dimethylpyrazole (1.230 g, 12.8 mmol) in acetonitrile (50 mL), in a 100 mL round-bottomed flask, 60% NaH (1.029 g, 25.72 mmol) was added and stirred at room temperature for two hours. 1,3,5-Tris(bromomethyl)-2,4,6-trimethyl benzene (1.595 g, 4.000 mmol) in acetonitrile (20 mL) was added to the reaction mixture and refluxed for 24 hours. The reaction mixture was monitored with TLC and after completion, the solvent was removed by rotary evaporation, the residue was dissolved in water (100 mL) and extracted with methylene chloride (30 mL x 5). The organic layers were combined, dried over anhydrous MgSO<sub>4</sub>, filtered and purified by flash column chromatography (CH<sub>2</sub>Cl<sub>2</sub>/MeOH = 10/1) to give the desired product as a white solid. 61% yield. mp 245-247 °C (Lit value 248-250 °C)<sup>9</sup>; <sup>1</sup>H NMR (δH; CDCl<sub>3</sub>, 400 MHz) δ 5.75 (s, 3H), 5.18 (s, 6H), 2.23 (s, 9H), 2.13 (s, 9H), 2.11 (s, 9H).

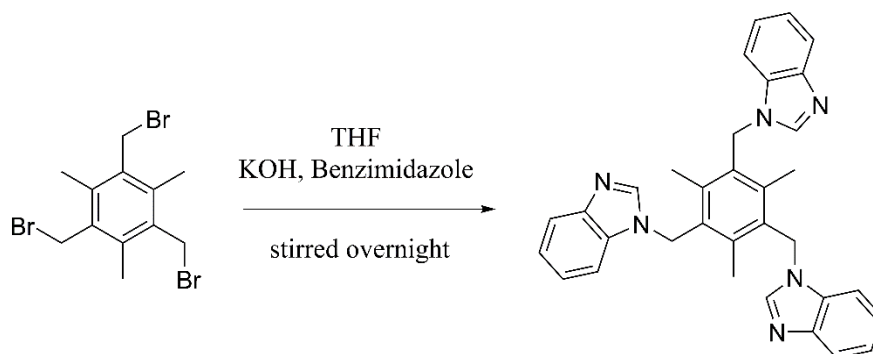
### 3.2.2.6 Synthesis of 1,3,5-tris(3,5-dimethylpyrazole -1-yl-methyl) benzene (C')



To a mixture of 3,5-dimethylpyrazole (1.230 g, 12.8 mmol) in acetonitrile (50 mL), in a 100 mL round-bottomed flask, 60% NaH (1.029 g, 25.72 mmol) was added and stirred at room temperature for two hours. 1,3,5-Tris(bromomethyl)-2,4,6-trimethyl benzene (1.427 g, 4.000 mmol) in acetonitrile (20 mL) was added to the reaction mixture and refluxed for 24 hours. The reaction mixture was monitored with TLC and after completion, the solvent was removed by rotary evaporation, the residue was dissolved in water (100 mL) and extracted with methylene chloride (30 mL x 5). The organic layers were combined, dried over anhydrous MgSO<sub>4</sub>, filtered and purified

by flash column chromatography ( $\text{CH}_2\text{Cl}_2/\text{MeOH} = 10/1$ ). The desired product was obtained as an off-white solid. 58% yield. mp  $94\text{--}96^\circ\text{C}$   $^1\text{H}$  NMR ( $\delta\text{H}$ ;  $\text{CDCl}_3$ , 400 MHz)  $\delta$  6.56 (s, 3H), 5.81 (s, 3H), 5.09 (s, 6H) 2.22 (s, 9H), 2.06 (s, 9H).

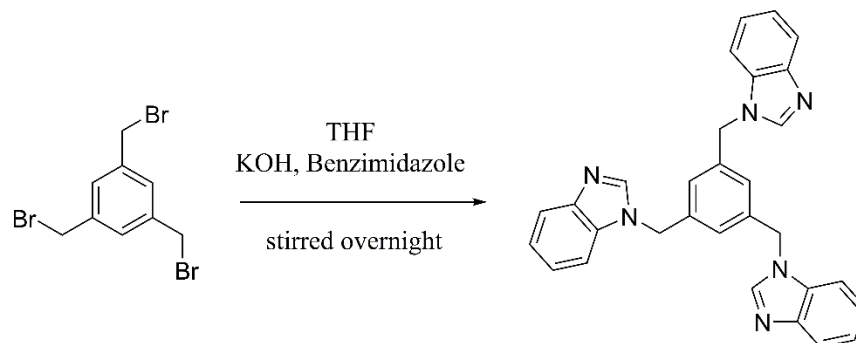
### 3.2.2.7 Synthesis of 1,3,5-tris(benzimidazole-1-yl-methyl)-2,4,6-trimethylbenzene<sup>8</sup> (D)



To a mixture of benzimidazole (1.512 g, 12.8 mmol) in THF (50 mL), in a 100 mL round-bottomed flask, KOH (1.029 g, 25.72 mmol) was slowly added and stirred at room temperature under  $\text{N}_2$  gas. After about 4 h, a solution of 1,3,5-tris(bromomethyl)-2,4,6-trimethyl benzene (1.595 g, 4.000 mmol) in 50 mL of THF was added dropwise, and the reaction mixture was stirred continuously overnight. The solvent was subsequently removed under reduced pressure, and the residue was poured into 100 mL of water and extracted 3 times with dichloromethane ( $3 \times 50$  mL). The combined organic extracts were washed with water, dried ( $\text{MgSO}_4$ ), and concentrated. The crude product was purified by recrystallization from hot ethanol to produce colorless plates. 78% Yield. mp  $> 300^\circ\text{C}$  (Lit value  $> 300^\circ\text{C}$ )<sup>8</sup>;  $^1\text{H}$ -NMR ( $\delta\text{H}$ ;  $\text{CDCl}_3$ , 400 MHz)  $\delta$  7.84 (m, 3H), 7.46 (s, 3H), 7.41 (m, 3H), 7.34 (m, 6H), 5.42 (s, 3H) 2.33 (s, 3H).

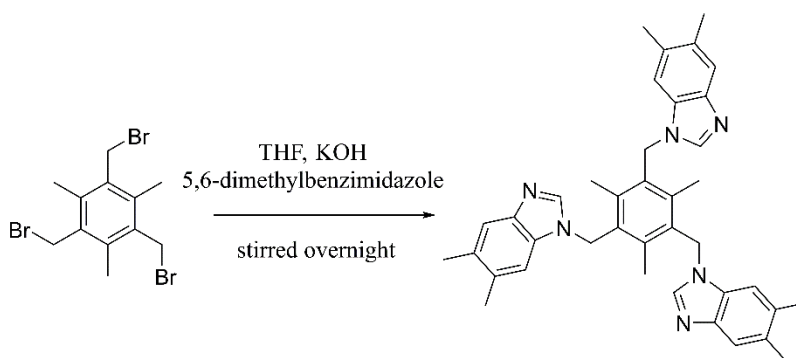


### 3.2.2.8 Synthesis of 1,3,5-tris(benzimidazole-1-yl-methyl)benzene<sup>10</sup> (D')



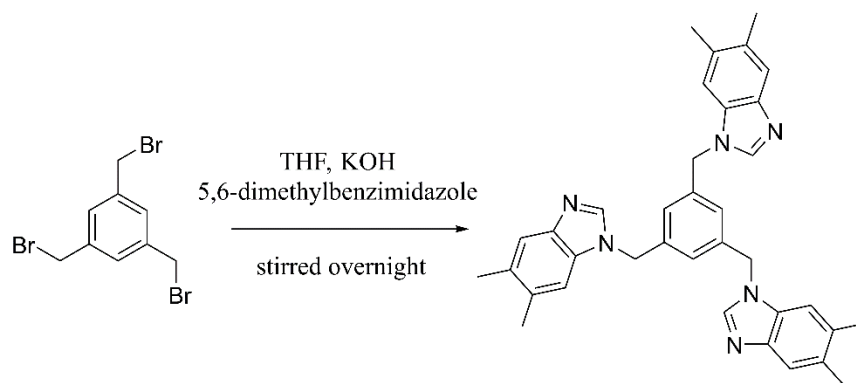
To a mixture of benzimidazole (1.512 g, 12.8 mmol) in THF (50 mL), in a 100 mL round-bottomed flask, KOH (1.029 g, 25.72 mmol) was slowly added and stirred at room temperature under N<sub>2</sub> gas. After about 4 h, a solution of 1,3,5-tris(bromomethyl) benzene (1.427 g, 4.000 mmol) in 50 mL of THF was added dropwise, and the reaction mixture was stirred continuously overnight. The solvent was subsequently removed under reduced pressure, and the residue was poured into 100 mL of water and extracted 3 times with dichloromethane (3 × 50 mL). The combined organic extracts were washed with water, dried (MgSO<sub>4</sub>), and concentrated. The desired product was obtained upon recrystallization in ethyl acetate to produce colorless rod-like crystals. 71% yield. mp 102–104 °C (Lit value 229–231 °C)<sup>10</sup> ; <sup>1</sup>H-NMR (δH; CDCl<sub>3</sub>, 400 MHz) δ 7.92 (s, 3H), 7.84 (d, 3H), 7.31 (t, 3H), 7.21 (t, 3H), 7.06 (d, 3H), 7.06 (d, 3H), 6.91 (s, 3H), 5.25 (s, 6H).

### 3.2.2.9 Synthesis of 1,3,5-tris(5,6-dimethylbenzimidazole-1-yl-methyl)-2,4,6-trimethylbenzene<sup>11</sup> (E)



To a mixture of 5,6-dimethylbenzimidazole (1.871 g, 12.8 mmol) in THF (50 mL), in a 100 mL round-bottomed flask, KOH (1.029 g, 25.72 mmol) was slowly added and stirred at room temperature under N<sub>2</sub> gas. After about 4 h, a solution of 1,3,5-tris(bromomethyl)-2,4,6-trimethyl benzene (1.595 g, 4.000 mmol) in 50 mL of THF was added dropwise, and the reaction mixture was stirred continuously overnight. The solvent was subsequently removed under reduced pressure, and the residue was poured into 100 mL of water and extracted 3 times with dichloromethane (3 × 50 mL). The combined organic extracts were washed with water, dried (MgSO<sub>4</sub>), and concentrated. The crude product was purified by recrystallization from hot ethanol which yielded pale yellowish-green pyramid-like crystals. 81% Yield. mp 285–290 °C (Lit value > 280 °C)<sup>11</sup>; <sup>1</sup>H-NMR (δH; CDCl<sub>3</sub>, 400 MHz) δ 7.58 (s, 3H), 7.33 (s, 3H), 7.20 (s, 3H) 5.33 (s, 6H), 2.42 (s, 9H), 2.39 (s, 9H), 2.30 (s, 9H).

### 3.2.2.10 Synthesis of 1,3,5-tris(5,6-dimethylbenzimidazole -1-yl-methyl)benzene (E')



To a mixture of 5,6-dimethylbenzimidazole (1.871 g, 12.8 mmol) in THF (50 mL), in a 100 mL round-bottomed flask, KOH (1.029 g, 25.72 mmol) was slowly added and stirred at room temperature under N<sub>2</sub> gas. After about 4 h, a solution of 1,3,5-tris(bromomethyl) benzene (1.427 g, 4.000 mmol) in 50 mL of THF was added dropwise, and the reaction mixture was stirred continuously overnight. The solvent was subsequently removed under reduced pressure, and the residue was poured into 100 mL of water and extracted 3 times with dichloromethane (3 × 50 mL).

The combined organic extracts were washed with water, dried (MgSO<sub>4</sub>), and concentrated. The desired product was obtained as a white solid. 76% yield. mp 295–296 °C <sup>1</sup>H-NMR (δH; CDCl<sub>3</sub>, 400 MHz) δ 7.78 (s, 3H), 7.58 (s, 3H), 6.87 (s, 3H), 6.85 (s, 3H) 5.18 (s, 6H), 2.37 (s, 9H), 2.28 (s, 9H).

### 3.2.3 Grinding experiments

Screenings for co-crystals were performed using solvent-assisted grinding technique. In a typical grinding experiment, the stoichiometric amounts of donor and acceptor were mixed in a microwell with the aid of a pestle and a drop of solvent (methylene chloride). The resulting solids from each reaction were subjected to IR analysis for characterization. A successful interaction will be characterized by specific peak shifts observed in the ground mixture compared to the starting compounds.

### 3.2.4 Synthesis of co-crystals

Tritopic acceptors were subjected to co-crystallization experiments with a series of aliphatic and aromatic hydrogen bond donors. After screenings for co-crystals of grounded mixtures using IR analysis, the samples were dissolved in a suitable solvent in borosilicate vials followed by slow evaporation.

#### *3.2.4.1 Synthesis of 1,3,5-tris(benzimidazole -1-yl-methyl) benzene suberic acid hydrate acetonitrile, D':SUB:ACN:H<sub>2</sub>O (1:1:1:1)*

1,3,5-Tris(benzimidazole -1-yl-methyl) benzene (0.0100 g, 0.0213 mmol) was dissolved in 1 mL of acetonitrile. To this solution was added suberic acid (0.0055 g, 0.032 mmol) in 1 mL of acetonitrile. The resulting solution was allowed for slow evaporation in a 2 dram borosilicate

vial at room temperature. Colorless block-shaped crystals were obtained after three weeks. Melting point 89-91 °C.

***3.2.4.2 Synthesis of 1,3,5-tris(5,6-dimethylbenzimidazole-1-yl-methyl)-2,4,6-trimethyl benzene succinic acid, E:SUC (1:1)***

1,3,5-Tris(5,6-dimethylbenzimidazole-1-yl-methyl)-2,4,6-trimethyl benzene (0.0100 g, 0.0168 mmol) was dissolved in 1 mL of acetonitrile. To this solution was added succinic acid (0.0038 g, 0.032 mmol) in 1 mL of acetonitrile. The resulting solution was allowed for slow evaporation in a 2 dram borosilicate vial at room temperature. Colorless block-shaped crystals were obtained after two weeks. Melting point 168-171 °C.

***3.2.4.3 Synthesis of 1,3,5-tris(5,6-dimethylbenzimidazole-1-yl-methyl)-2,4,6-trimethyl benzene terephthalic acid hydrate, E:TPH:H<sub>2</sub>O (1:1:1)***

1,3,5-Tris(5,6-dimethylbenzimidazole-1-yl-methyl)-2,4,6-trimethyl benzene (0.0100 g, 0.0168 mmol) was dissolved in 1 mL of ethanol. To this solution was added terephthalic acid (0.0042 g, 0.0252\* mmol) in 1 mL of ethanol. The resulting solution was allowed for slow evaporation in a 2 dram borosilicate vial at room temperature. Pale pink-orange colored hexagonal plate like crystals were obtained after two weeks. Melting point 257-259 °C.

***3.2.4.4 Synthesis of 1,3,5-tris(5,6-dimethylbenzimidazole-1-yl-methyl)-2,4,6-trimethyl benzene trimesic acid, E:TMS (1:1)***

1,3,5-Tris(5,6-dimethylbenzimidazole-1-yl-methyl)-2,4,6-trimethyl benzene (0.0100 g, 0.0168 mmol) was dissolved in 1 mL of ethanol. To this solution was added suberic acid (0.0035 g, 0.0168 mmol) in 1 mL of acetonitrile. The resulting solution was allowed for slow evaporation

in a 2 dram borosilicate vial at room temperature. Colorless block-shaped crystals were obtained after 12 days. Melting point 243-244 °C.

### 3.2.5 CSD search

A CSD search on the acceptor molecules **14IMI**, **13IMI**, **14PYZ**, **13PYZ**, **14BNZ**, and **13BNZ**, Figure 3.7, were performed using the following constraints: “not disordered”, “no errors”, “not polymeric”, “no ions”, “no powder structures”, “3D coordinates determined” and “only organics”. The search focused on recording stoichiometries and connectivity of donor and acceptor molecules. All the CSD search queries were run using ConQuest Version 1.19, CSD 5.38 November 2016 (CCDC, Cambridge, UK).

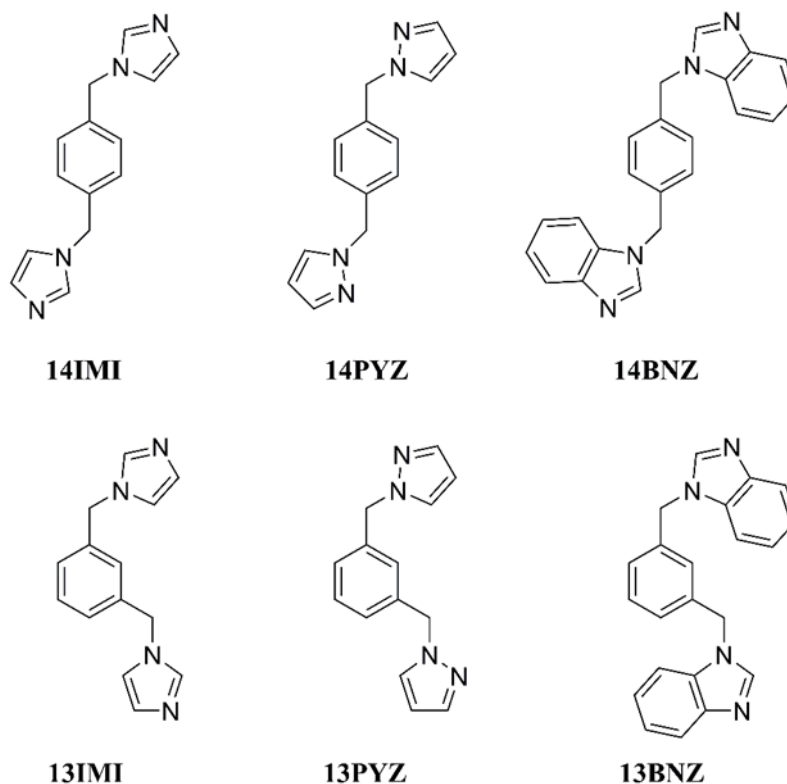


**Figure 3.7** Ditopic acceptors used in the CSD study

### 3.3 Results

Molecular electrostatic potentials were performed to rank the potential on the hydrogen atoms adjacent to the nitrogen on the heterocycles, Table 3.1. Initial co-crystal screening was conducted to evaluate the effectiveness of the O—H···N hydrogen bond synthon, Table 3.2 and Table 3.3. Four single crystals suitable for single crystal X-ray diffraction were obtained, **D':SUB**, **E:SUC**, **E:TPH**, **E:TMS**. Hydrogen-bond geometries of these co-crystals are listed in Table 3.4.

**Table 3.1** Molecular electrostatic potentials on hydrogen atoms adjacent to the nitrogen on the heterocyclic ring

Acceptor	A	A'	B	B'	C	C'	D	D'	E	E'
Potential on N	-229	-216	-187	-167	-174	-202	-204	-201	-212	-207
Potential on H <sub>1</sub>	+116	+107	+72	+70	n.a.	n.a.	+143	+142	+125	+128
Potential on H <sub>2</sub>	+58	+61	n.a.	n.a.	n.a.	n.a.	+50	+53	+33	+48

n.a. = not applicable

**Table 3.2** IR stretching frequencies (cm<sup>-1</sup>) of the solids produced by combining tritopic acceptors with aliphatic dicarboxylic acids

Mixture	Carbonyl stretch (cm <sup>-1</sup> )		O---H .... N Stretch (cm <sup>-1</sup> )	Co-crystal
	Di-acid	Ground mixture		
A':SUC	1685	1704	2455, 1923	Y
A':GLU	1683	1701	2467, 1932	Y
A':ADI	1684	1697	2446, 1920	Y
A':PIM	1685	1697	2467, 1923	Y
A':SUB	1685	1684	2482, 1929	Y
B':SUC	1685	1693	n/a	N
B':GLU	1683	1703	1917, 2528	Y

<b>B':ADI</b>	1684	1685	n/a	N
<b>B':PIM</b>	1685	1708	1932, 2568	Y
<b>B':SUB</b>	1685	1687	1865, 2525	Y
<b>C':SUC</b>	1685	1707	2525, 1892	Y
<b>C':GLU</b>	1683	1694	2528, 1907	Y
<b>C':ADI</b>	1684	1701	2513, 1926	Y
<b>C':PIM</b>	1685	1703	2531, 1880	Y
<b>C':SUB</b>	1685	1706	2525, 1935	Y
<b>D':SUC</b>	1685	1704	2476, 1914	Y
<b>D':GLU</b>	1683	1712	2507, 1920	Y
<b>D':ADI</b>	1684	1694	2464, 1910	Y
<b>D':PIM</b>	1685	1701	2498, 1921	Y
<b>D':SUB</b>	1685	1689	2525, 1907	Y
<b>E':SUC</b>	1685	1699	2476, 1929	Y
<b>E':GLU</b>	1683	1699	2495, 1910	Y
<b>E':ADI</b>	1684	1689	2492, 1907	Y
<b>E':PIM</b>	1685	1697	2519, 1935	Y
<b>E':SUB</b>	1685	1697	2479, 1907	Y
<b>A :SUC</b>	1685	1684	1932, 2544	Y
<b>A :GLU</b>	1683	1679	1971, 2553	Y
<b>A :ADI</b>	1684	1702	1938, 2519	Y
<b>A :PIM</b>	1685	1702	1944, 2495	Y
<b>A :SUB</b>	1685	1698	1939, 2448	Y
<b>B:SUC</b>	1685	1695	1828, 2517	Y
<b>B:GLU</b>	1683	1703	2528, 1907	Y
<b>B:ADI</b>	1684	1687	n/a	N
<b>B:PIM</b>	1685	1689	n/a	N
<b>B:SUB</b>	1685	1686	n/a	N
<b>C:SUC</b>	1685	1686	n/a	N
<b>C:GLU</b>	1683	1691	n/a	N
<b>C:ADI</b>	1684	1691	n/a	N
<b>C:PIM</b>	1685	1688	n/a	N
<b>C:SUB</b>	1685	1686	n/a	N
<b>D:SUC</b>	1685	1693	n/a	N
<b>D:GLU</b>	1683	1701	2492, 1938	Y

<b>D:ADI</b>	1684	1687	n/a	N
<b>D:PIM</b>	1685	1696	2580, 1929	Y
<b>D:SUB</b>	1685	1687	n/a	N
<b>E:SUC</b>	1685	1712	2522, 1926	Y
<b>E:GLU</b>	1683	1703	2555, 1909	Y
<b>E:ADI</b>	1684	1689	n/a	N
<b>E:PIM</b>	1685	1704	2516, 1929	Y
<b>E:SUB</b>	1685	1703	2470, 1917	Y

**Table 3.3** IR stretching frequencies ( $\text{cm}^{-1}$ ) of the solids produced by combining tritopic acceptors with aromatic carboxylic acids

Mixture	Carbonyl stretch ( $\text{cm}^{-1}$ )		O---H .... N Stretch ( $\text{cm}^{-1}$ )	Co-crystal
	Di-acid	Ground mixture		
<b>A':3HB</b>	1679	1696	2559, 1959	Y
<b>A':TPH</b>	1671	1675	2531, 1892	Y
<b>A':IPH</b>	1680	1688	2434, 1904	Y
<b>A':PHL</b>	1668	1687	1892, 2418	Y
<b>B':3HB</b>	1679	1692	1886, 2418	Y
<b>B':IPH</b>	1680	1696	1907, 2579	Y
<b>B':TPH</b>	1671	1675	n/a	N
<b>B':PHL</b>	1668	1700	1910, 2493	Y
<b>C':3HB</b>	1679	1694	2581, 1938	Y
<b>C':TPH</b>	1671	1678	1852, 2537	N
<b>C':IPH</b>	1680	1700	2461, 1883	Y
<b>C':PHL</b>	1668	1700	1905, 2470	Y
<b>D':3HB</b>	1679	1695	2477, 1912	Y
<b>D':TPH</b>	1671	1669	2525, 1895	Y
<b>D':IPH</b>	1680	1689	2519, 1935	Y
<b>D':PHL</b>	1668	1694	1910, 2517	Y
<b>E':3HB</b>	1679	1694	2481, 1916	Y
<b>E':TPH</b>	1671	1675	1929, 2519	Y
<b>E':IPH</b>	1680	1684	2513, 1895	Y
<b>E':PHL</b>	1668	1696	1920, 2592	Y
<b>A:3HB</b>	1679	1692	2573, 1943	Y



<b>A:TPH</b>	1671	1677	2453, 1950	Y
<b>A:IPH</b>	1680	1695, 1606	2492, 1915	Y
<b>A:PHL</b>	1668	1690	1923, 2450	Y
<b>B:3HB</b>	1679	1697, 1585	2586, 1935	Y
<b>B:TPH</b>	1671	1669	n/a	N
<b>B:IPH</b>	1680	1681	n/a	N
<b>B:PHL</b>	1668	1702	1903, 2511	Y
<b>C:3HB</b>	1679	1696, 1587	2562, 1895	Y
<b>C:TPH</b>	1671	1672	n/a	N
<b>C:IPH</b>	1680	1678	n/a	N
<b>C:PHL</b>	1668	1666	1905, 2505	Y
<b>D:3HB</b>	1679	1686	2419, 1893	Y
<b>D:TPH</b>	1671	1672	n/a	N
<b>D:IPH</b>	1680	1684	n/a	N
<b>D:PHL</b>	1668	1701	1893, 2382	Y
<b>E:3HB</b>	1679	1692	2568, 1925	Y
<b>E:TPH</b>	1671	1666	n/a	N
<b>E:IPH</b>	1680	1681	2470, 1898	Y
<b>E:PHL</b>	1668	1691	1885, 2459	Y

**Table 3.4** Hydrogen bond geometries

Compound	D—H···A	d(H···A)	d(D···A)	<(D—H···A)	Symmetry operation
<b>D': SUB</b>	O1—H10 <sub>u</sub> ···N2 <sub>v</sub>	1.77(3)	2.677(2)	176(3)	u= x,y,z v= x,y,z
<b>Co-crystal solvate</b>	O3—H30 <sub>u</sub> ···N6 <sub>v</sub>	1.66(6)	2.883(3)	178(4)	u= -x, 1-y, 1-z v= w,y,z
<b>E: SUC</b>	O2—H···N12		2.73(1)		u=x,y,z v= x,y,z
<b>Co-crystal</b>	O3—H···N8		2.70(1)		u=x,y,z v= x,y,z
	O7—H···N10		2.620(9)		u= 1-x, 1/2+y, 1.5-z v= x,y,z
	O5—H···N2		2.677		u= x, 1/2-y, -1/2-z v= x,y,z

<b>E:TPH</b>	O2—H10···N6	1.46(3)	2.531(2)	164(2)	$u=1/2-x, 1/2+y, 1/2-z,$ $v=x,y,z$
<b>Co-crystal</b>	O3—H20···N4	1.41(3)	2.536(2)	169(3)	$u=1/2+x, 1/2-y, 1/2+z,$ $v=x,y,z$
<b>hydrate</b>					
<b>E:TMS</b>	O(92)—H10···N21				$u= 1/2+x, 3/2-y, 1-z$ $v=x,y,z$
<b>Co-crystal</b>	O(102)—H10···N10				$u= 1-x, 1-y, 1+z$ $v=x,y,z$
	O(89)—H10···N49				$u= 1/2+x, 3/2-y, 1-z$ $v=x,y,z$
	O108—H10···N71				$u=1-x, 1-y, z$ $v=x,y,z$

### 3.3.1 Description of solid state architectures

#### 3.3.1.1 Crystal structure of 1,3,5-tris(benzimidazole -1-yl-methyl) benzene suberic acid<sub>0.5</sub> hydrate acetonitrile

The prime feature in the crystal structure of **D':SUB<sub>0.5</sub>:H<sub>2</sub>O:MeCN** is a 2:1 centrosymmetric termolecular aggregate, Figure 3.8. The primary intermolecular interaction is a hydrogen bond between the carboxylic hydrogen and benzimidazole nitrogen.

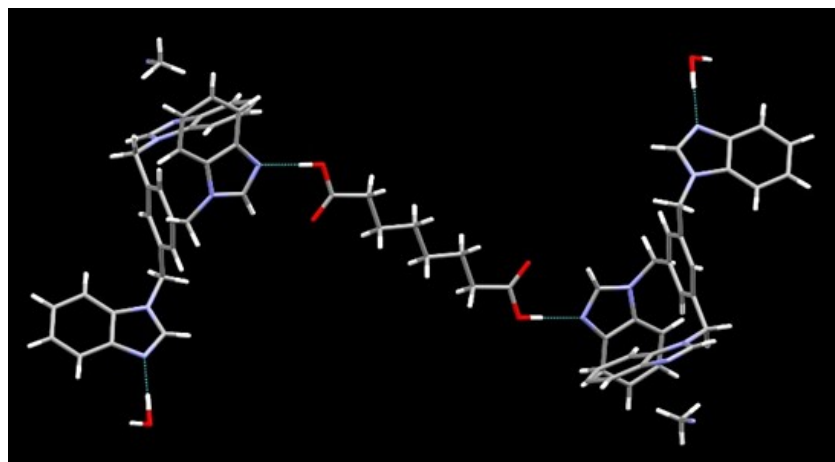


**Figure 3.8** Main interactions in the crystal structure of **D':SUB<sub>0.5</sub>:H<sub>2</sub>O:MeCN**

The tritopic acceptor has two arms on the same face of the benzene scaffold forming a chair like conformation. The two remaining acceptor sites are hydrogen bonded to two water molecules. The remaining acceptor site forms a close contact with another water molecule in a side on fashion. A secondary C—H···O interaction is seen between H8 of benzimidazole and carbonyl O2 of the COOH group. In this instance, the secondary interaction takes place between the second-best hydrogen bond donor, the more acidic of the C—H donors on the benzimidazole heterocycle.

### *3.3.1.2 Crystal structure of 1,3,5-tris(5,6-dimethylbenzimidazole-1-yl-methyl)-2,4,6-trimethyl benzene succinic acid*

The attempted co-crystallization of SUC acid and **E** has resulted in the formation of a 2:2 binary solid, Figure 3.9.

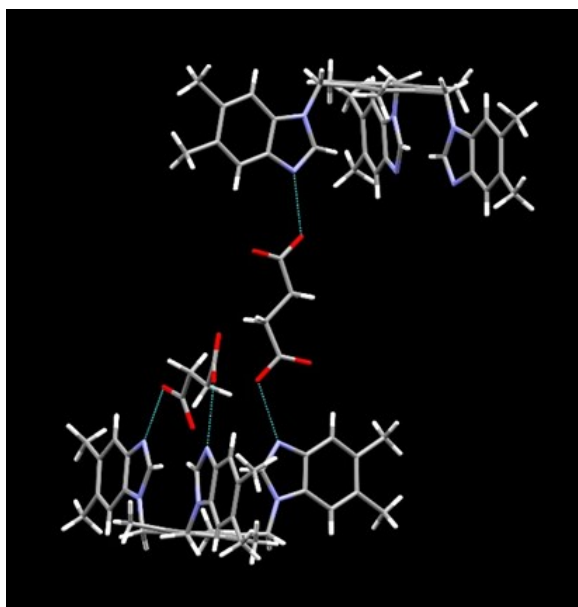


**Figure 3.9** Main interactions in the crystal structure of **E:SUC**

The two tritopic acceptors forming the discrete tetrameric architecture have the same crown-like conformation. One succinic acid molecule forms intermolecular hydrogen bonds connecting the two tritopic acceptors in a centrosymmetric manner. The other has formed

intramolecular hydrogen bonds which resulted in successful occupation of all the acceptor sites on one of the tritopic acceptors. The intermolecular O—H···N hydrogen bonds formed by the succinic acid molecule are accompanied by secondary C—H···O contacts involving H(13) and H(62) on Bzim and O(06) and O(03) (hydrogen atoms H(13) and H(62) are not the second-best donor on the benzimidazole). Likewise, the intramolecular O—H···N hydrogen bonds are backed by a C—H···O contacts from H(67) and on Bzim and O1 on COOH carbonyl oxygen atom (C(67)···O(01), 2.935). The above interaction between C(67)—H(67)···O(01) has taken place between the more acidic C—H which is the second-best donor.

### *3.3.1.3 Crystal structure of 1,3,5-tris(5,6-dimethylbenzimidazole-1-yl-methyl)-2,4,6-trimethyl benzene terephthalic acid hydrate*

The crystal structure of **E:TPH.H<sub>2</sub>O** reveals a discrete centrosymmetric tetramolecular aggregate, Figure 3.10. Within the formed tetramolecular species two water molecules interact with terephthalic acid molecules creating yet another centrosymmetric species.

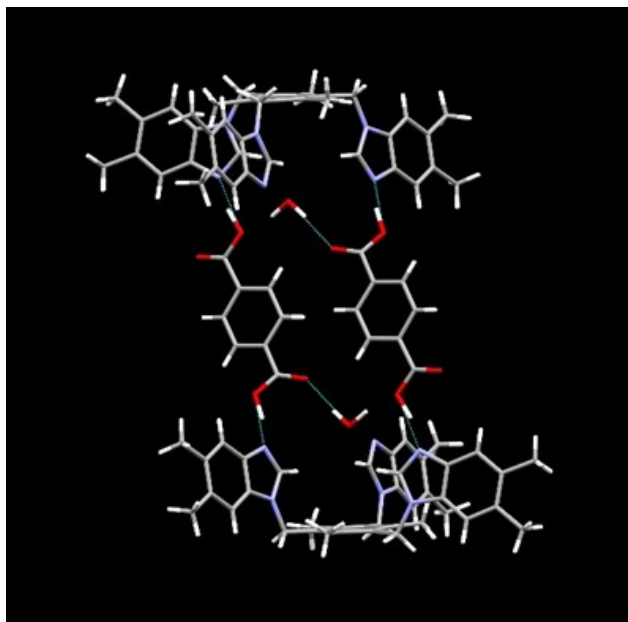


**Figure 3.10** Main interactions in the crystal structure of **E:TPH:H<sub>2</sub>O**

Two terephthalic acids interact via four O—H···N hydrogen bonds bring together two tritopic acceptor molecules (which are crown conformation) to create a capsule. There are no O—H···N interactions present in the primary motif, except a hydrogen bond taking place between an O—H of a water molecule and a carbonyl of a COOH moiety.

#### *3.3.1.4 Crystal structure of 1,3,5-tris(5,6-dimethylbenzimidazole-1-yl-methyl)-2,4,6-trimethyl benzene trimesic acid*

The acid and base in **TMS:E** interact primarily via O—H···N hydrogen bonds. Only two sites on both tritopic acceptor and donor participate in intermolecular interaction, Figure 3.11. The intrinsic binding pattern (much like a digital signal) extends into an infinite undulating 1-D chain like architecture. There are no C—H···O interactions present alongside O—H···N interactions, and no noteworthy interactions taking place with carbonyl oxygen on COOH moiety.

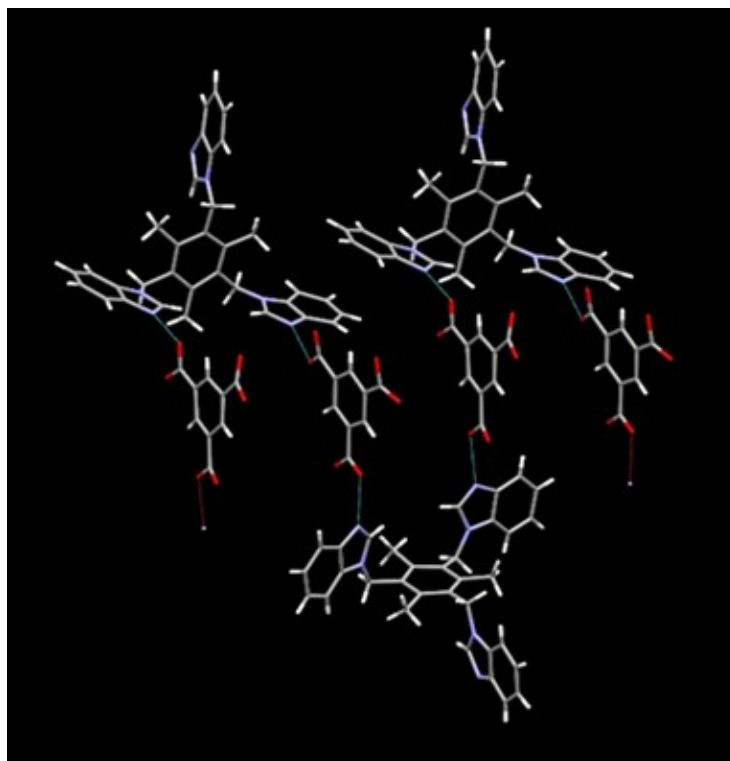


**Figure 3.11** Main interactions in the crystal structure of **E:TMS**

### 3.3.2 Crystal packing interactions observed in the crystal structures

#### 3.3.2.1 Crystal structure of *D'*:*SUB* and *E*:*SUC*

In both acceptors **D'** and **E**, C—H··· $\pi$  interactions between acceptor molecules are observed, Figure 3.12 and 3.13. Acceptor: acceptor interactions are only observed in co-crystals containing aliphatic dicarboxylic acids.

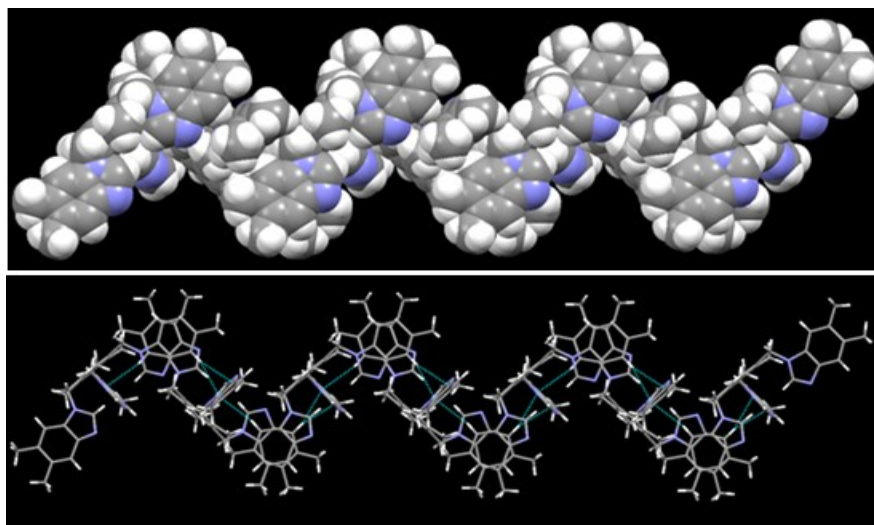


**Figure 3.12** Secondary C—H··· $\pi$  interactions observed for **E** in **E**:**SUC**

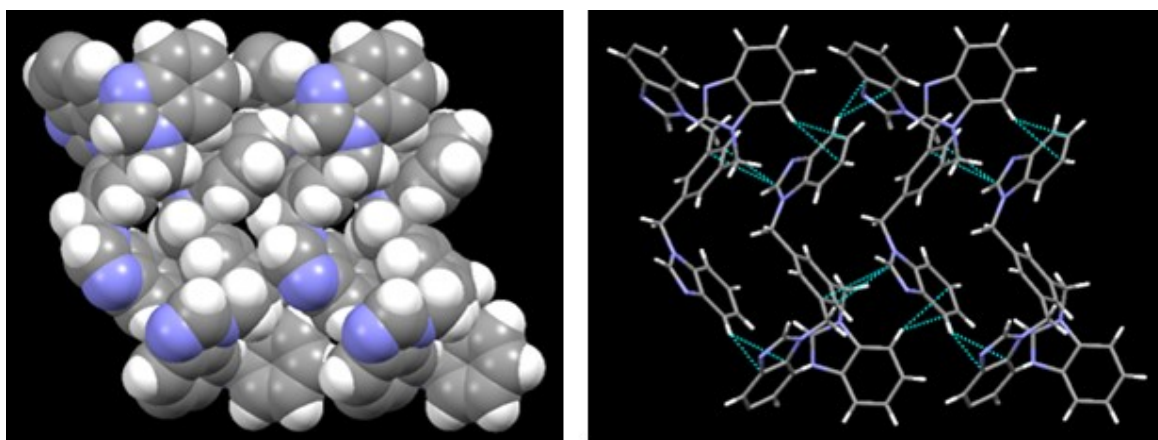


**Figure 3.13** Secondary C—H··· $\pi$  interactions observed for **D'** in **D'**:**SUB**

The structural frame in **E:SUC** and **D':SUB** are extended through the C—H $\cdots$  $\pi$  interactions that are observed in Figures 3.12 and 3.13 which are seen in the extended network of Figure 3.14, in (a) depicted in grey and dark blue and in (b) shown in grey, respectively.

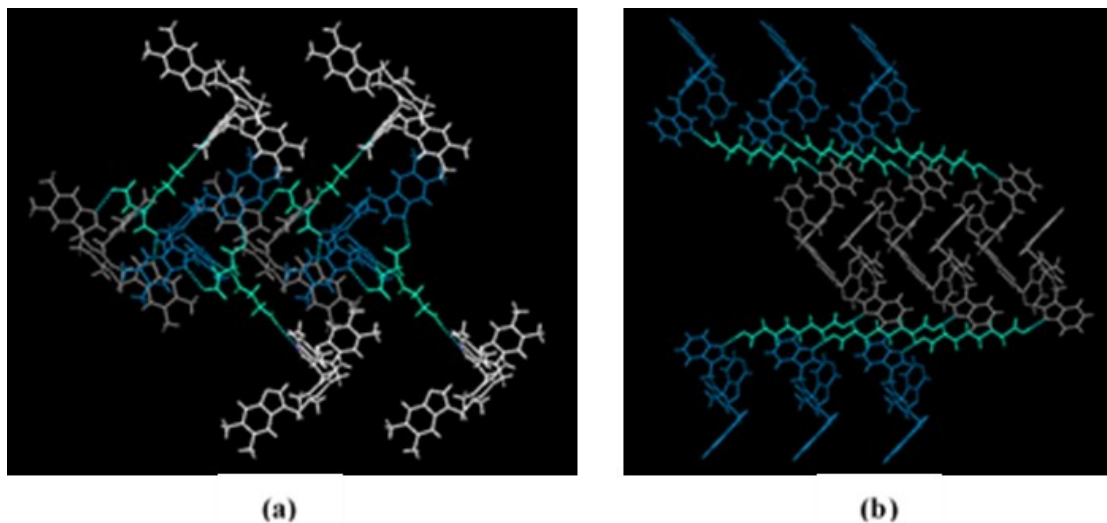


**Figure 3.14** Overall packing interactions of (a) **E:SUC** and (b) **D':SUB**

### 3.3.2.2 *Crystal structure of E:TPH and E:TMS*

Unlike in co-crystals resulting from aliphatic dicarboxylic acids, structures resulting with aromatic carboxylic acids do not possess C—H $\cdots$  $\pi$  interactions between acceptor molecules. But instead, both crystal structures **E:TPH** and **E:TMS** contain consecutive donor : acceptor stacking interactions, Figure 3.15 and Figure 3.16.

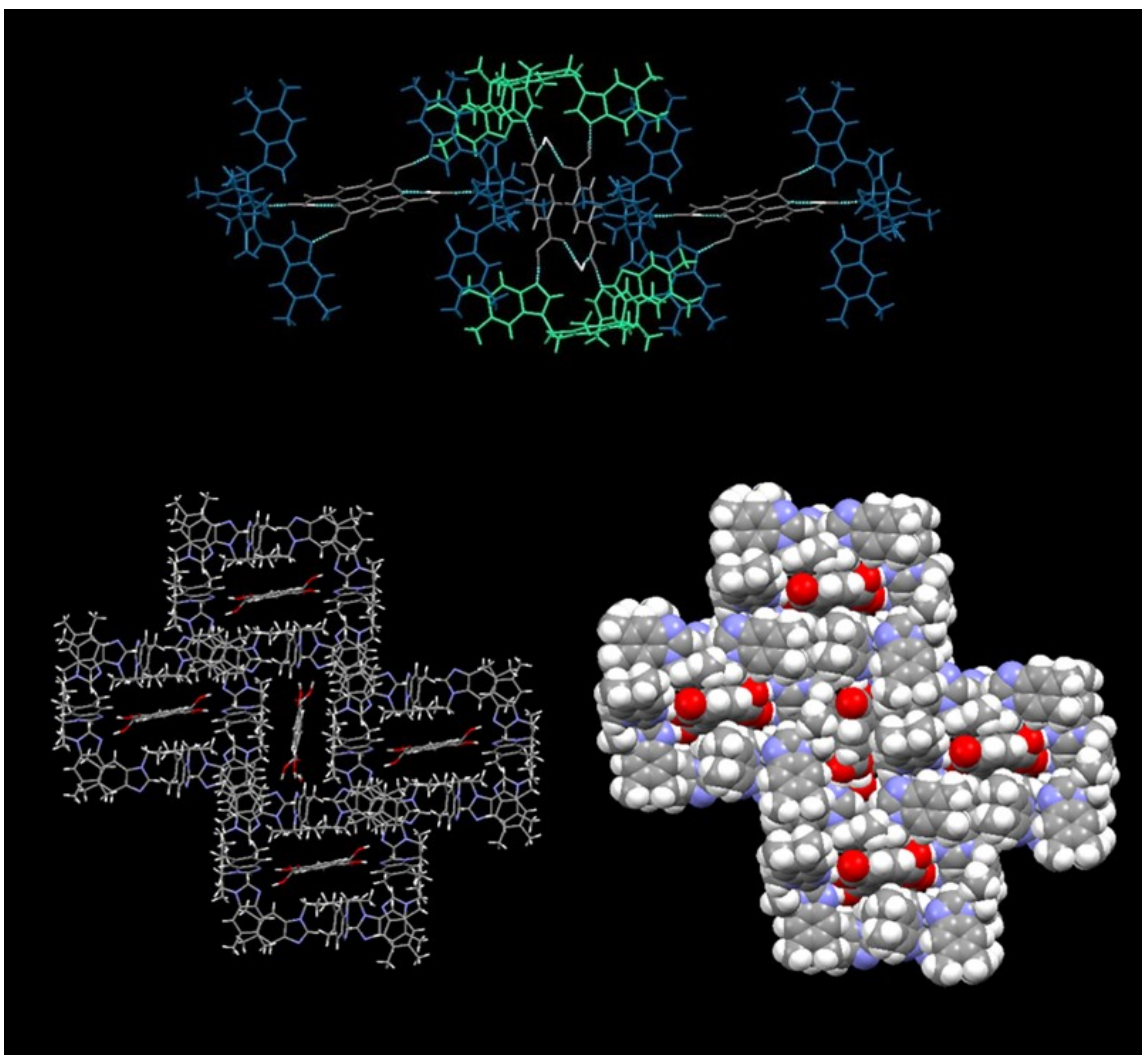


**Figure 3.15** Packing interactions of **E:TPH** (a) one dimensional (b) two dimensional (c) two dimensional space filling



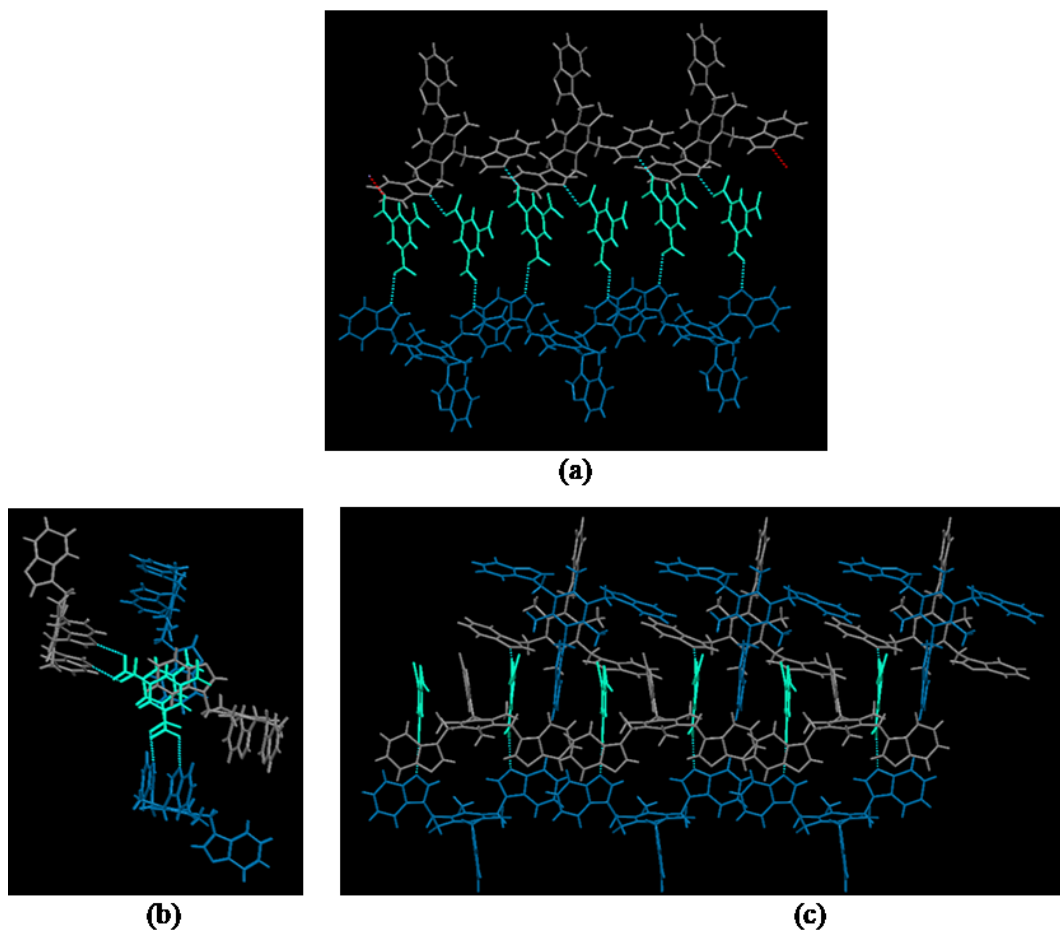


**Figure 3.16** Packing interactions of E:TMS (a) one dimensional (b) side view indicating acceptor donor stacking interactions (c) two dimensional

### 3.4 Discussion

The primary intermolecular interaction that governs the formation of these four co-crystals is a O—H $\cdots$ N hydrogen bond which stems between a carboxylic O—H group and benzimidazolic nitrogen, in which no protons have been transferred from the acid to the base. IR spectra of these compounds are indicative of co-crystal formation due to the presence of C=O stretches in correspondence to the carboxylic acid. Broad bands are around 2,500  $\text{cm}^{-1}$  and 1,900  $\text{cm}^{-1}$  due to acid—N-heterocyclic O—H stretch and hydrogen bonded O—H stretch, respectively<sup>12</sup>. These

characteristic O—H···N stretches reinforce the presence of the strong hydrogen bonds since these bands do not appear in any of the individual compounds.

**Table 3.5** Percentage of occurrence of O—H···N stretch in grinding experiments with aliphatic dicarboxylic acids

Acceptor	Potential on N (kJ/mol)	Grinding experiments with aliphatic dicarboxylic acids	
		Success rate	Supramolecular yield (%)
<b>A</b>	-229	5/5	100
<b>A'</b>	-216	5/5	100
<b>E</b>	-212	4/5	80
<b>C'</b>	-209	5/5	100
<b>E'</b>	-207	5/5	100
<b>D</b>	-204	2/5	40
<b>D'</b>	-201	5/5	100
<b>B</b>	-187	1/5	33.3
<b>C</b>	-173	0/5	0
<b>B'</b>	-167	3/5	60

The negative potential of the nitrogen atoms in these tritopic acceptors represents an attractive binding site for an approaching carboxylic acid. In an event where a O—H···N hydrogen bond is formed, if the strength would be a measure of how easily co-crystals could be obtained, one would expect imidazole containing tritopic acceptors to have the greatest success rate than benzimidazole and pyrazole containing acceptors.

Based on the spectroscopic data, the more basic imidazole containing acceptor produces more co-crystals than the corresponding benzimidazole and pyrazole containing acceptors, 18/18 (100%) vs 28/36 (77%) vs 19/36 (53%) Table 3.7. A considerable change in hydrogen bonding capability (due to an increase in the negative charge on a hydrogen-bond acceptor) can be observed in constitutional isomers containing imidazole compared to pyrazole acceptors. A subtle substitutional change to the molecular structure by incorporating an electron donating substituent

group (**B'**, **C'**) will allow us to fine tune the hydrogen bonding capability in a much more controlled manner.<sup>13</sup>

**Table 3.6** Percentage of occurrence of O—H···N stretch in grinding experiments with aromatic carboxylic acids

Acceptor	Potential on N (kJ/mol)	Grinding experiments with aromatic carboxylic acids	
		Success rate	Supramolecular yield (%)
<b>A</b>	-229	4/4	100
<b>A'</b>	-216	4/4	100
<b>E</b>	-212	3/4	75
<b>C'</b>	-209	3/4	75
<b>E'</b>	-207	3/4	75
<b>D</b>	-204	2/4	50
<b>D'</b>	-201	4/4	100
<b>B</b>	-187	2/4	50
<b>C</b>	-173	2/4	50
<b>B'</b>	-167	3/4	75

**Table 3.7** Overall percentage of occurrence of O—H···N stretch in grinding experiments with acids

Analogue	Acceptor	Potential on N (kJ/mol)	Grinding experiments with acids		Supramolecular yield by analogue
			Success rate	Supramolecular yield (%)	
<b>Imidazole</b>	<b>A</b>	-229	9/9	100	100%
	<b>A'</b>	-216	9/9	100	
<b>Benzimidazoles</b>	<b>E</b>	-212	7/9	77.7	77%
	<b>E'</b>	-207	8/9	88.8	
	<b>D</b>	-204	4/9	44.4	
	<b>D'</b>	-201	9/9	100	
<b>Pyrazole</b>	<b>C'</b>	-209	8/9	88.8	53%
	<b>B</b>	-187	3/9	33.3	
	<b>C</b>	-173	2/9	22.2	
	<b>B'</b>	-167	6/9	66.6	

Even though the synthon containing imidazole was clearly effective at forming desired O—H···N hydrogen bonds (in ground mixtures), we were unable to form diffraction quality single crystals to observe if it would promote the formation of three O—H···N hydrogen bonds to the acceptor. With four single crystal structures from benzimidazole containing tritopic acceptors, we observe that a desired stoichiometric outcome has not been met. In all the crystal structures, vacant acceptor sites are present regardless of the donor type being used. Furthermore, in **E:TMS**, we notice that the trimesic acid does not fully utilize its donor sites in forming hydrogen bonds. This does not comply with Etter's rule; "*all good proton donors and acceptors are used in hydrogen bonding*".<sup>14</sup> A part of the reason to this may be found in the synthon containing benzimidazole moiety (COOH··· benzimidazole), (with a supramolecular yield of 77%) which to an extent reflects that it might not be as effective at forming three O—H···N hydrogen bonds to a tritopic acceptor with benzimidazole sites, but possible steric consideration,<sup>15</sup> figure 3.17, and multiple sites for hydrogen bonding<sup>16</sup> might also play in the formation of such co-crystals.

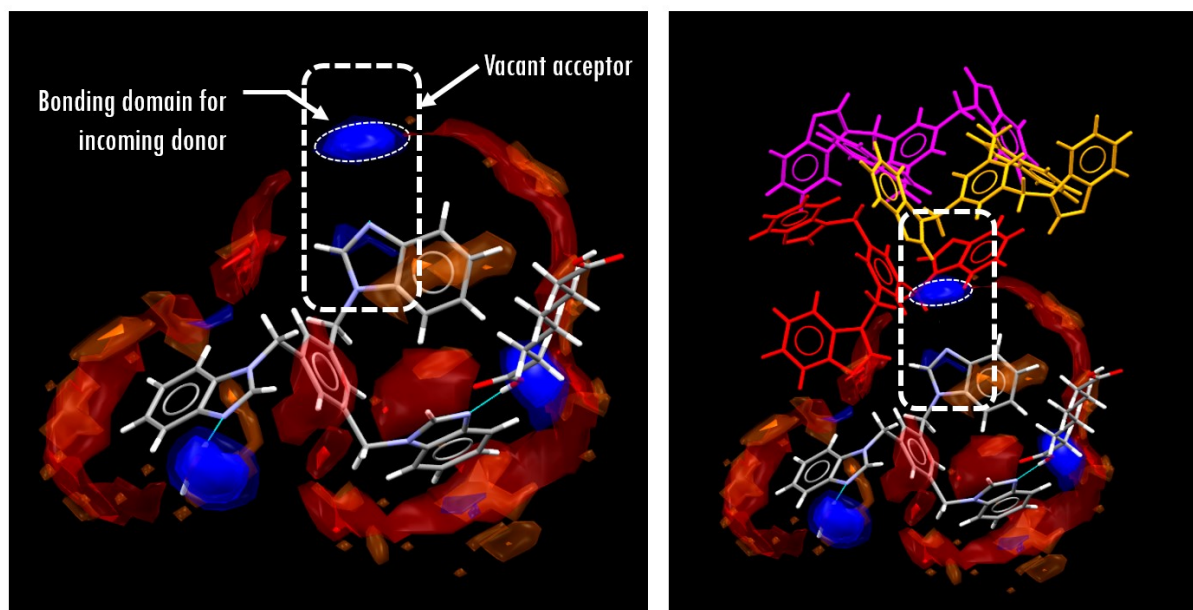
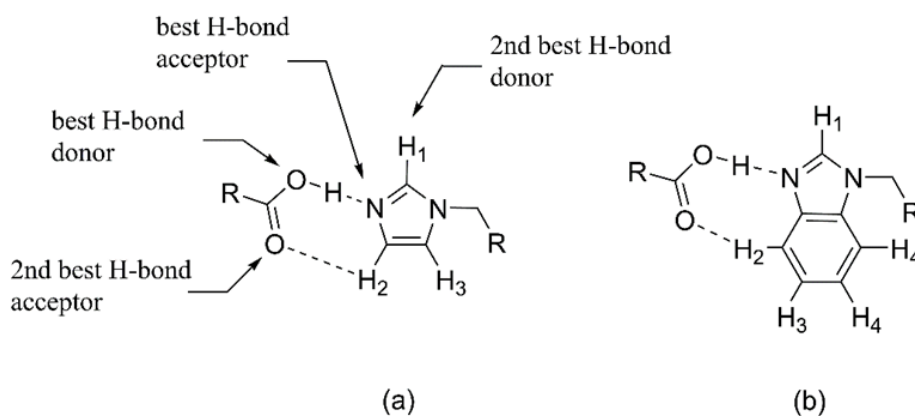


**Figure 3.17** Full interaction maps showing steric hindrance at the vacant acceptor site in **D':SUB**

The initial supramolecular reactions were subjected to polar-protic solvent methanol, which yielded no crystals leaving behind a sticky solid, and when subjected to IR spectroscopy, it indicates the presence of characteristic broad O—H···N bands around 2,500 cm<sup>-1</sup> and 1,900 cm<sup>-1</sup>. But, in the presence of a polar aprotic solvent acetonitrile, single crystals were obtained. This clearly indicates the potentially disruptive nature of solvent molecules in the formation of co-crystals, in which we clearly observe the reluctance to form single crystals from methanolic solutions.

It is interesting to note that the presence of solvent molecules; water and acetonitrile in the crystal lattices of **D':SUB** and **E:TPH** are not disrupting any intended O—H···N hydrogen bonds between acceptor and donor molecules, despite the fact that one is a good hydrogen bond donor while the other is a good acceptor. This further stress the importance of having reliable and robust supramolecular synthons as a way of eliminating unwanted synthon interference.

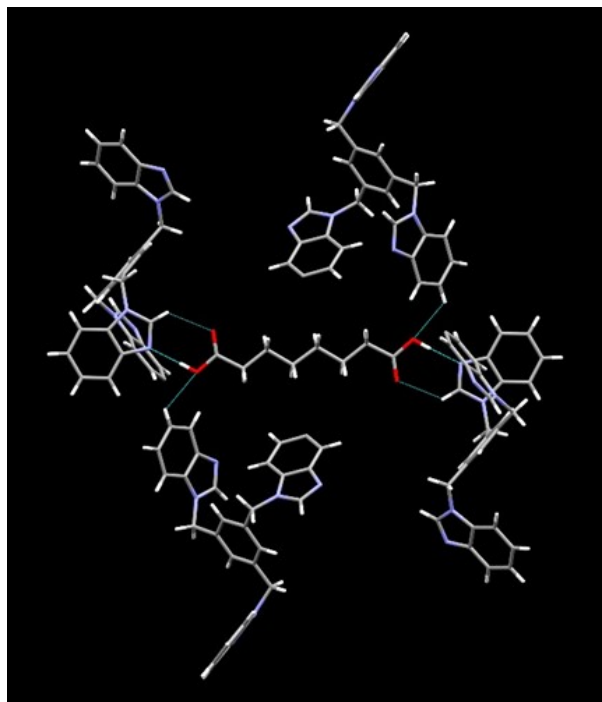
The O—H···N hydrogen bond forms between the best acceptor and best donor but the C—H···O interaction (electrostatic in nature<sup>17</sup>) does not necessarily utilize the most acidic C—H proton.



**Figure 3.18** Alternative heteromeric O—H···N/C—H···O motif in (a) COOH···imidazole and (b) COOH···benzimidazole interactions

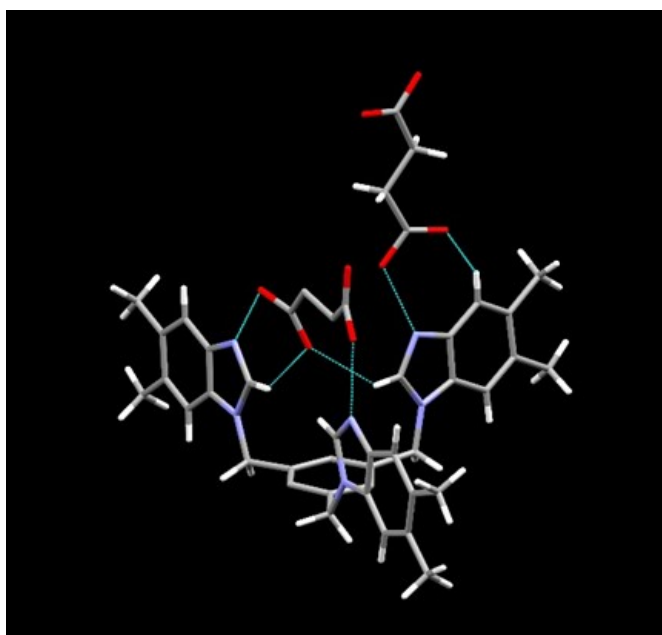
Furthermore, out of the four crystal structures, both containing aliphatic dicarboxylic acids employ C—H $\cdots$ O interactions while no interactions are observed in either of the aromatic acid containing crystal structures. The crystal structures possessing C—H $\cdots$ O contacts contain intrachain interactions, which utilizes either H1 or H2 protons on the Bzim moieties. Thus, one can formulate alternative heteromeric O—H $\cdots$ N/ C—H $\cdots$ O patterns compared to the suggestions shown in Figure 3.18 for the COOH $\cdots$ Bzim interactions shown in Figure 3.3. The chelating effect from presence of an auxiliary C—H $\cdots$ O interaction does not necessarily indicate it being useful in driving co-crystals with desired connectivity and stoichiometry.

In the structure of **D':SUB**, besides the intra-chain C—H $\cdots$ O interaction between the second best donor and acceptor, we notice another inter-chain C—H $\cdots$ O interaction formed between an aromatic C—H group and O—H acid group which directs further into a 3D structure, Figure 3.19.



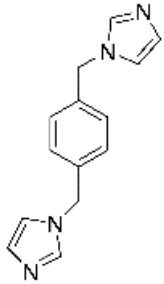
**Figure 3.19** Intra-chain and structure directing inter-chain C—H $\cdots$ O interactions observed in **D':SUB**

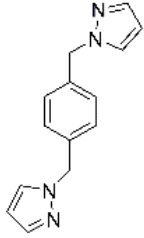
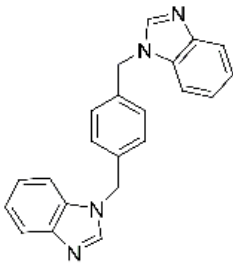
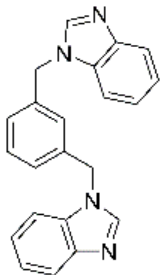
In **E:SUC**, we notice the importance of the auxiliary C—H···O interactions in aiding and directing the bowl like conformation in **E**, Figure 3.20. Therefore, we see that the presence of auxiliary C—H···O interactions are not merely passive bystanders but rather in most part act as “steering” or “tugboat” interactions in guiding structure directed assemblies.<sup>18</sup>



**Figure 3.20** Structure directing intramolecular chain C—H···O interactions observed in **E:SUC** (methyl substituent on benzene scaffold and hydrogens on succinic acid were removed for clarity)

**Table 3.8** Summary of CSD search on ditopic acceptors

Ditopic acceptor	Donor	Refcode	A: D	Connectivity*	
 <b>14IMI</b>	aliphatic	Monotopic	-	-	
		Ditopic	LATKUN	1:1	Y
			LATLAU LATLEY	1:1 1:1	Y Y
	Tritopic	-	-	-	
	Cyclic	Monotopic	-	-	-
		Ditopic	AMIVUO	1:1	Y

		Tritopic	-	-	-
	Aromatic	Monotopic	JEGBAZ	1:2	Y
			JEGBIH	1:2	Y
			JEGBON	1:2	Y
		Ditopic	LATLIC	1:1	Y
		Tritopic	-	-	-
 14PYZ	Aromatic	Monotopic	GENNIX	1:2	Y
			GENNET	1:2	Y
		Ditopic	-	-	-
		Tritopic	-	-	-
 14BNZ	aliphatic	Monotopic	-	-	-
		Ditopic	LATLOI	1:1	Y
			XAQPIP	1:1	Y
	Tritopic	-	-	-	
	Aromatic	Monotopic	JEFZUQ	1:2	Y
			JEGBED	1:2	Y
			JEGBUT	1:2	Y
NUJXAS			1:2	Y	
Ditopic	-	-	-		
Tritopic	-	-	-		
 13BNZ	aliphatic	Monotopic	-	-	-
		Ditopic	XAQPEL	1:1	Y
		Tritopic	-	-	-

\* Y on connectivity indicates sites on both donors and acceptors a stoichiometrically occupied



When comparing flexible ditopic acceptors with tritopic acceptors, from the CSD generated results, Table 3.8, we notice that in all cases, the expected two-point connectivity as well as expected stoichiometry are observed, which complies with Etter's rule we discussed earlier. In all the cases, ditopic acceptors have used either monotopic or ditopic acids which are more linearly related to stoichiometry (1:2 or 1:1 acceptor to donor stoichiometry). Tritopic acceptors crystalizing with ditopic donors were unable to attain a 2:3 stoichiometry between acceptor to donor, ended up having a lack of donors, leaving vacant sites on the acceptors. The only reported instance of a tritopic donor, citramalic acid, forming a complementary three-point interaction in a converging manner with **E** reveals a discrete dimeric cup in a face-to-face orientation<sup>11</sup>. This unforeseen rare occurrence of a perfectly desired connectivity cannot be fully satiated due to the presence of a "free" non-coordinating tritopic acceptor. There are four crystallographically unique molecules of **E** and two unique molecules of citramalic acid in the lattice leaving behind two acceptors completely vacant. This unshakable dark side of the tritopic acceptors remains to be an elusive mystery which we intend to pursue in the next chapter with the use of halogen bond donors.

### 3.5 Conclusions

IR data demonstrate that imidazolic tritopic acceptors, which had the highest electrostatic potential, are more reliable and effective, than benzimidazole and pyrazole, in making desired O—H···N interactions, suggesting that electrostatic potentials can be used as a tool to select a more reliable hydrogen-bond synthon.

However, co-crystals obtained contain the second best supramolecular synthon (ranked according to the electrostatic potential on the acceptor site): COOH···Bzim synthon. These interactions are responsible for the formation of supramolecular assemblies of tritopic

benzimidazoles and aliphatic/ aromatic carboxylic acids into co-crystals. In all the crystal structures, we observe vacant sites on the acceptor molecules. Though the exact reason for this is poorly understood just yet, we can assume that the availability of multiple hydrogen bonding sites and steric effects of methylated benzimidazole tritopic acceptors has influenced the cause, to some extent.

The auxiliary C—H···O interaction which is like the O—H···N, N—H···O and O—H···O hydrogen bonds, may not be as strong but is largely an electrostatic, attractive interaction with a long-range distance character. The weak intra-chain C—H···O hydrogen bonds within the chains are rather artefacts of the primary O—H···N interaction. Based on geometrical features and their role on the crystal structure, the C—H···O interaction could either be structure-directing or simply a supplemental interaction. As per what we observe, herein the C—H···O interactions actively engages in directing structural assemblies.

With evidence from the CSD, we see that the ditopic acceptors are clearly forming desired two-point supramolecular architectures regardless of using monotopic or ditopic hydrogen bond donors. Considering the final output of the connectivity of tritopic acceptors in the presence of hydrogen bond donors, we see that having an additional heterocyclic arm in most part does not provide any useful interactions, but rather hangs on as an “idle” arm.

### 3.6 References

1. Desiraju, G. R., Supramolecular Synthons in Crystal Engineering—A New Organic Synthesis. *Angew. Chem. Int. Ed. Engl.* **1995**, *34* (21), 2311-2327.
2. Barooah, N.; Sarma, R. J.; Baruah, J. B., Solid-state hydrogen bonded assembly of N,N'-bis(glycinyl)-pyromellitic diimide with aromatic guests. *CrystEngComm* **2006**, *8* (8), 608-615.

3. (a) Aakeröy, C. B.; Desper, J.; Leonard, B.; Urbina, J. F., Toward High-Yielding Supramolecular Synthesis: Directed Assembly of Ditopic Imidazoles/Benzimidazoles and Dicarboxylic Acids into Cocrystals via Selective O–H···N Hydrogen Bonds. *Cryst. Growth Des.* **2005**, *5* (3), 865-873; (b) Steed, J. W.; Atwood, J. L., *Supramolecular chemistry*. Wiley: Chichester ; New York, **2000**; p xxi, 745 p.
4. (a) Nauha, E.; Kolehmainen, E.; Nissinen, M., Packing incentives and a reliable N–H···N–pyridine synthon in co-crystallization of bipyridines with two agrochemical actives. *CrystEngComm* **2011**, *13* (21), 6531; (b) Aitipamula, S.; Wong, A. B. H.; Chow, P. S.; Tan, R. B. H., Pharmaceutical cocrystals of ethenzamide: structural, solubility and dissolution studies. *CrystEngComm* **2012**, *14* (24), 8515.
5. Reddy, D. S.; Ovchinnikov, Y. E.; Shishkin, O. V.; Struchkov, Y. T.; Desiraju, G. R., Supramolecular Synthons in Crystal Engineering. 3. Solid State Architecture and Synthon Robustness in Some 2,3-Dicyano-5,6-dichloro-1,4-dialkoxybenzenes. *J. Am. Chem. Soc.* **1996**, *118* (17), 4085-4089.
6. (a) Shishkin, O. V.; Zubatyuk, R. I.; Shishkina, S. V.; Dyakonenko, V. V.; Medvediev, V. V., Role of supramolecular synthons in the formation of the supramolecular architecture of molecular crystals revisited from an energetic viewpoint. *Phys. Chem. Chem. Phys.* **2014**, *16* (14), 6773; (b) Desiraju, G. R., Crystal Engineering: From Molecule to Crystal. *J. Am. Chem. Soc.* **2013**, *135* (27), 9952-9967.
7. Van der Made, A. W.; Van der Made, R. H., A convenient procedure for bromomethylation of aromatic compounds. Selective mono-, bis-, or trisbromomethylation. *J. Org. Chem.* **1993**, *58* (5), 1262-1263.
8. Yuan, Y.; Jiang, Z.-L.; Yan, J.-M.; Gao, G.; Chan, A. S. C.; Xie, R.-G., A Convenient and Effective Synthesis of Tris-Bridged Tricationic Azolophanes. *Synth. Commun.* **2007**, *30* (24), 4555-4561.
9. Hartshorn, C. M.; Steel, P. J., Poly(pyrazol-1-ylmethyl)Benzenes: New Multidentate Ligands. *Aust. J. Chem.* **1995**, *48* (9), 1587.
10. Yuan, Y.; Xiao, R.; Gao, G.; Su, X.-Y.; Yu, H.; You, J.; Xie, R.-G., A direct synthetic approach to tripodal imidazole compounds. *J. Chem. Res.* **2002**, *2002* (6), 267-269.
11. Aakeröy, C. B.; Smith, M.; Desper, J., Finding a single-molecule receptor for citramalic acid through supramolecular chelation. *Can. J. Chem.* **2015**, *93* (8), 822-825.
12. Mukherjee, A.; Tothadi, S.; Chakraborty, S.; Ganguly, S.; Desiraju, G. R., Synthon identification in co-crystals and polymorphs with IR spectroscopy. Primary amides as a case study. *CrystEngComm* **2013**, *15* (23), 4640.
13. Aakeröy, C. B.; Desper, J.; Fasulo, M. E., Improving success rate of hydrogen-bond driven synthesis of co-crystals. *CrystEngComm* **2006**, *8* (8), 586-588.

14. (a) Etter, M. C., Hydrogen bonds as design elements in organic chemistry. *J. Phys. Chem.* **1991**, *95* (12), 4601-4610; (b) Etter, M. C., Encoding and decoding hydrogen-bond patterns of organic compounds. *Acc. Chem. Res.* **2002**, *23* (4), 120-126.
15. Hart, H.; Lin, L.-T. W.; Goldberg, I., Can Solid Clathrates be Useful for Separating Molecular Species? A Systematic Approach to the Design of Novel Coordinato-Clathrates. *Mol. Cryst. Liq. Cryst.* **2006**, *137* (1), 277-286.
16. Goldberg, I.; Lin, L.-T. W.; Hart, H., Crystalline complexes of N,N'-ditritylurea (DTU) and N-tritylurea (NTU) hosts with molecular guests. *J. Inclusion Phenom.* **1984**, *2* (1-2), 377-389.
17. Taylor, R.; Kennard, O., Crystallographic evidence for the existence of C-H $\cdots$ O, C-H $\cdots$ N and C-H $\cdots$ Cl hydrogen bonds. *J. Am. Chem. Soc.* **1982**, *104* (19), 5063-5070.
18. (a) Desiraju, G. R., Hydrogen Bridges in Crystal Engineering: Interactions without Borders. *Acc. Chem. Res.* **2002**, *35* (7), 565-573; (b) Desiraju, G. R., The C-H $\cdots$ O Hydrogen Bond: Structural Implications and Supramolecular Design. *Acc. Chem. Res.* **1996**, *29* (9), 441-449; (c) Desiraju, G. R., The C-H $\cdots$ O hydrogen bond in crystals: what is it? *Acc. Chem. Res.* **2002**, *24* (10), 290-296.

# Chapter 4 - Structural examination of halogen-bonded co-crystals of tritopic acceptors<sup>1</sup>

## 4.1 Introduction

The halogen bond (D-X...A), an interaction that possesses many characteristics typical of the hydrogen bond, has gained considerable attention in recent years due to the anisotropic charge density distribution around the halogen atom,<sup>2</sup> Figure 4.1. The interesting phenomenon where negatively charged X-atom acts as the Lewis acid center interacting with A (a negatively charged Lewis base center) has been thoroughly investigated in the crystalline solid-state by Resnati,<sup>3</sup> Hanks<sup>4</sup> and others.<sup>5</sup>

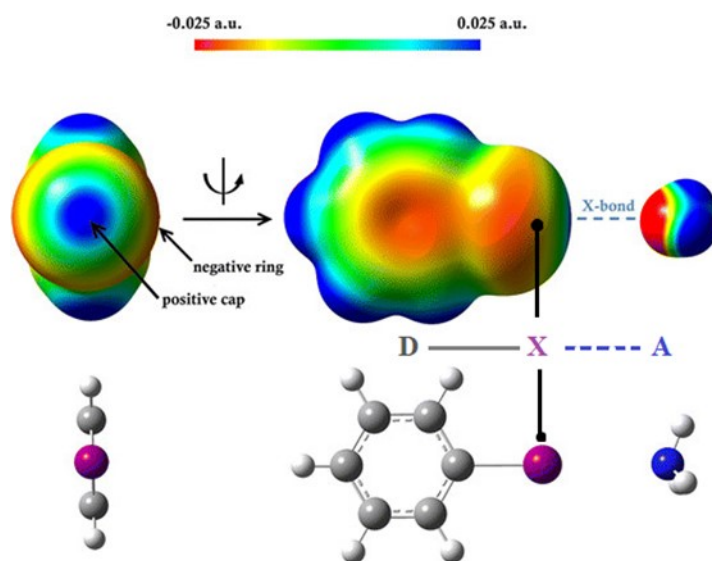


**Figure 4.1** Electrostatic potential surface representing a halogen bond<sup>6</sup>

Over the years, many attempts were made to define the halogen bond (XB) given its puzzling nature, and in 2013 a recommended definition was presented, which according to Desiraju et al., a halogen bond “occurs when there is evidence of a net attractive interaction between an electrophilic region associated with a halogen atom in a molecular entity and a

nucleophilic region in another, or the same, molecular entity".<sup>7</sup> Unique features of the XB, such as directionality,<sup>8</sup> strength,<sup>3,9</sup> tunability,<sup>2e,10</sup> hydrophobicity<sup>11</sup> and donor atom dimensions,<sup>11-12</sup> and the rapid growth of successful applications of XB in fields such as drug development<sup>13</sup> and materials design<sup>13-14</sup> have contributed to the recent advanced studies of the XB.

However, it is still uncertain how we can control chemical compositions and stoichiometries of targeted products when attempting to synthesize co-crystals of reactants that carry multiple donor- and acceptor sites. Given the interaction ability of activated halogen atoms in the solid state with neutral or ionic Lewis bases and its directionality, we intended to investigate if desired stoichiometries could be reached for the tritopic acceptors examined in Chapter 3. For this purpose, we have chosen ten tritopic acceptor analogues of imidazole, pyrazole and benzimidazole which possess a central methylated and nonmethylated aromatic scaffold, Figure 4.2.

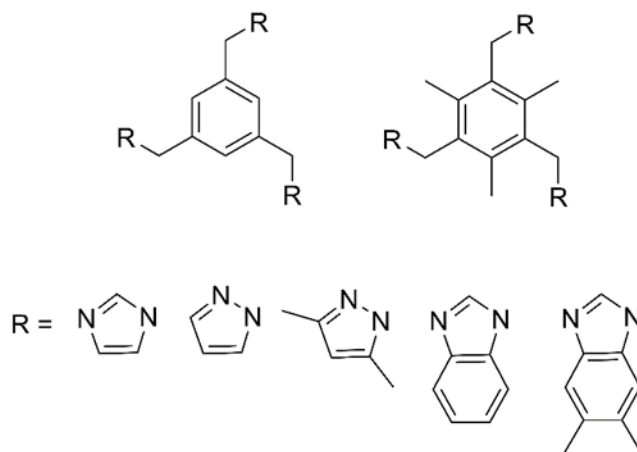


**Figure 4.2** Tritopic acceptors used in this study

The acceptor molecules are conformationally flexible halogen-bond acceptors, which contain three geometrically and electrostatically equivalent binding sites. There are no known halogen bonded crystal structures for these molecules, and organic co-crystals for these molecules

are rare. Previously reported co-crystal by van der Boom et al.<sup>15</sup> containing tripyridyl acceptor show a 1:2 and 1:0.5 with donors **14XB** and **135XB**, Figure 4.3.

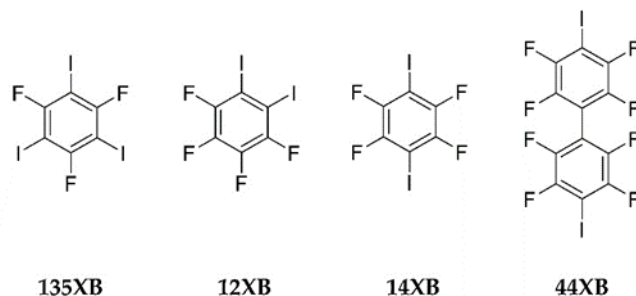


**Figure 4.3** Halogen bond donor molecules used in this study

The chosen donor molecules **14XB**, **12XB** and **135XB**, contain geometrically equivalent binding sites and are rigid unlike the tritopic acceptors. In terms of electrostatic surface potentials, all sites prior to binding are equivalent, but according to van der Boom et al.,<sup>15</sup> and Formigue et al.,<sup>16</sup> upon intermolecular interactions, a “deactivation” may take place at the remaining donor sites. Furthermore, compared to hydrogen atoms, halogen atoms are much bigger in size<sup>8a</sup> which causes differences in interactions of these atoms. Therefore, molecules containing halogen atoms such as these donor molecules are more likely to be sensitive to steric hindrance.<sup>11</sup> A study conducted by Schollhorn and co-workers<sup>12</sup> using 1,4-diiodotetrafluorobenzene (**14XB**) with 4,4'-, 2,2'- and 2,4'- bipyridine shows that the steric nature of 2,2'- and 2,4'- bipyridine affects the supramolecular coordination network by transforming from infinite 1D chains to well-defined termolecular complexes. In another study<sup>17</sup> to determine enthalpy–entropy compensation of DNA Holliday junctions containing halogenated uracil bases, it was found that, the most stable pairing was given by bromine where iodine’s greater polarizability was limited by the disadvantage resulting from its greater size. In light of this phenomenon, we have attempted to understand interactions present in these compounds.

Herein we report the synthesis of four co-crystals containing rigid perfluoroiodo arenes and flexible tritopic ligands using halogen bonding interactions to drive the formation of the co-crystals. We aim to utilize common concepts and simple models to rationalize what we observe in our co-crystals in terms of strength, directionality, and interaction geometry. An understanding of XB interactions is based upon a combination of X-ray crystal structure determination, calculated molecular electrostatic potential surfaces (MEPs).

## 4.2 Experimental

All reagents, solvents, precursors and halogen-bond donors were purchased from commercial sources and were used as received without further purification. A Fisher-Johns melting point apparatus (Vernon Hills, IL, USA) was used to determine melting points. A Varian Unity Plus (400 MHz) NMR spectrophotometer (Varian, Inc.) was used to record nuclear magnetic resonance spectra using the residual solvent signal as a reference. Infrared spectroscopic analyses were performed with a Nicolet 380 FT-IR instrument (Thermo Scientific, Madison, WI, USA).

### 4.2.1 Molecular electrostatic potential surface calculations

To calculate the molecular electrostatic potential surface of the donor molecules, the geometries were optimized using hybrid density functional B3LYP level of theory with 6-31G\* basis set in vacuum. All molecules were geometry optimized with the maxima and minima in the electrostatic potential surface ( $0.002 \text{ e au}^{-1}$  isosurface), determined using a positive point charge in the vacuum as a probe. These numbers, in other words, surface potentials, are the coulombic interaction energies (in  $\text{kJmol}^{-1}$ ) between the positive point probe and the surface of the molecule at that point. All calculations were done using Spartan 10 software (Wavefunction Inc., Irvine, CA, USA).



### 4.2.2 CSD search

A CSD search on **14XB**, **12XB** and **135XB** were performed using the following constraints: “not disordered”, “no errors”, “not polymeric”, “no ions”, “no powder structures”, “3D coordinates determined” and “only organics”. The search for halogen bonds of the above mention molecules was limited to acceptors with sp<sup>2</sup>-hybridized nitrogen atoms. All the CSD search queries were run using ConQuest Version 1.19, CSD 5.38 November 2016 (CCDC, Cambridge, UK).

### 4.2.3 Grinding experiments

Screenings for co-crystals were performed using solvent-assisted grinding. In a typical experiment, stoichiometric amounts of donor and acceptor were mixed in a microwell with the aid of a pestle and a drop of solvent (methylene chloride). The resulting solids from each reaction were subjected to IR analysis for characterization. A successful interaction would be characterized by specific peak shifts observed in the ground mixture compared to the starting compounds.

### 4.2.4 Synthesis of co-crystals

All crystal growth experiments were carried out from the resulting solid mixtures used in the grinding experiments via slow evaporation of a 1:1 mixture of methylene chloride: ethyl acetate. A typical experiment would entail transferring the ground mixture into a 2-dram glass vial, which was then fully dissolved in a minimal amount of solvent. The loosely capped vial was left undisturbed at ambient conditions to allow the solvent to evaporate slowly. Out of 40 experiments, four produced crystals suitable for single-crystal X-ray diffraction.

#### 4.2.5 X-ray crystallography

Upon preliminary IR and melting point analysis, crystals were subjected to single crystal X-ray diffraction.

Datasets were collected on a Bruker Kappa APEX II system using MoK $\alpha$  radiation. Data were collected using APEX2 software. Initial cell constants were found by small widely separated “matrix” runs. Data collection strategies were determined using COSMO. Scan speed and scan widths were chosen based on scattering power and peak rocking curves. Datasets were collected at 23 °C (**135XB:A**), -73 °C (**12XB:B**), -93 °C (**135XB:E:EtOAc**), and -143 °C (**14XB:E**) using an Oxford Cryostream low-temperature device.

The unit cell constants and orientation matrix were improved by least-squares refinement of reflections thresholded from the entire dataset. Integration was performed with SAINT, using this improved unit cell as a starting point. Precise unit cell constants were calculated in SAINT from the final merged dataset. Lorenz and polarization corrections were applied. Multi-scan absorption corrections were performed with SADABS.

The data were reduced with SHELXTL. The structures were solved in all cases by direct methods without incident. All hydrogen atoms were located in idealized positions and were treated with a riding model. All non-hydrogen atoms were assigned anisotropic thermal parameters. Refinements continued to convergence, using the recommended weighting schemes.

### 4.3 Results

Molecular electrostatic potential surface calculations were performed on the halogen bond donors as a means of ranking the expected capability of each donor site, Table 4.1. With an initial

co-crystal screening Table 4.2, four crystals suitable for single crystal X-ray diffraction were obtained **14XB:E**, **135XB:E:EtOAc**, **12XB:B**, **135XB:A**. IR results of grounded mixtures with halogen-bond donors are given in Table 4.3. A summary of the crystallographic data is included in Table 4.4, and halogen-bond geometries are listed in Table 4.5.

**Table 4.1** 1 CSD-based summary of frequency of interactions to available halogen-bond donors and MEPs values

<b>Halogen Bond Donor</b>	<b>135XB:E:EtOAc</b>		<b>12XB</b>		<b>14XB</b>	
MEP	158 kJ/mol		163 kJ/mol		169 kJ/mol	
No. Hits in the CSD	30 hits		19 hits		100 hits	
Coordination*	2 out of 3	3 out of 3	1 out of 2	2 out of 2	1 out of 2	2 out of 2
Result	16	14	2	17	3	97
% outcome	53%	47%	10.5%	89.5%	3%	97%

\*Coordination: number of donor sites occupied in a molecule

**Table 4.2** Grinding results

	<b>Acceptors</b>										<b>%Success</b>
	<b>A</b>	<b>A'</b>	<b>B</b>	<b>B'</b>	<b>C</b>	<b>C'</b>	<b>D</b>	<b>D'</b>	<b>E</b>	<b>E'</b>	
<b>135XB</b>	√	√	√	√	√	√	√	√	√	√	100
<b>12XB</b>	-	√	√	√	√	√	-	√	√	√	80
<b>14XB</b>	√	√	√	√	-	-	-	-	√	√	60
<b>44XB</b>	-	-	√	-	√	-	√	√	√	-	50
<b>%Success</b>	50	75	100	75	75	50	50	75	100	75	

**Table 4.3** IR results between tritopic acceptors and halogen bond donors

Ground mixture ID	Stoichiometry	IR results (cm <sup>-1</sup> )	
		Halogen bond donor	Grinding mixture
14XB:A	3:2	1456, 938	1453, 936
14XB:B	3:2	1456, 938	1460, 940
14XB:C	3:2	1456, 938	1457, 940
14XB:D	3:2	1456, 938	1456, 940
14XB:E	3:2	1456, 938	1461, 941
14XB:A'	3:2	1456, 938	1452, 938
14XB:B'	3:2	1456, 938	1459, 942
14XB:C'	3:2	1456, 938	1456, 939
14XB:D'	3:2	1456, 938	1456, 939
14XB:E'	3:2	1456, 938	1459, 941
12XB:A	3:2	1487, 1436	1486, 1436
12XB:B	3:2	1487, 1436	1485, 1438
12XB:C	3:2	1487, 1436	1484, 1436
12XB:D	3:2	1487, 1436	1485, 1436
12XB:E	3:2	1487, 1436	1482, 1433
12XB:A'	3:2	1487, 1436	1485, 1433
12XB:B'	3:2	1487, 1436	1484, 1435
12XB:C'	3:2	1487, 1436	1484, 1436
12XB:D'	3:2	1487, 1436	1485, 1434
12XB:E'	3:2	1487, 1436	1484, 1433
135XB:A	1:1	1563, 1403, 1049	1561, 1397, 1041
135XB:B	1:1	1563, 1403, 1049	1562, 1392, 1037
135XB:C	1:1	1563, 1403, 1049	1551, 1397, 1042
135XB:D	1:1	1563, 1403, 1049	1560, 1403, 1050
135XB:E	1:1	1563, 1403, 1049	1566, 1398, 1049
135XB:A'	1:1	1563, 1403, 1049	1562, 1399, 1048
135XB:B'	1:1	1563, 1403, 1049	1562, 1392, 1037
135XB:C'	1:1	1563, 1403, 1049	1551, 1397, 1042
135XB:D'	1:1	1563, 1403, 1049	1559, 1400, 1039
135XB:E'	1:1	1563, 1403, 1049	1562, 1398, 1037
44XB:A	3:2	1460, 950	1458, 949
44XB:B	3:2	1460, 950	1466, 957
44XB:C	3:2	1460, 950	1467, 956
44XB:D	3:2	1460, 950	1469, 956
44XB:E	3:2	1460, 950	1469, 957
44XB:A'	3:2	1460, 950	1459, 952
44XB:B'	3:2	1460, 950	1459, 950
44XB:C'	3:2	1460, 950	1458, 951
44XB:D'	3:2	1460, 950	1458, 953
44XB:E'	3:2	1460, 950	1459, 949

**Table 4.4** Crystallographic data

<b>Code</b>	<b>14XB:E</b>	<b>135XB:E:EtOAc</b>	<b>12XB:B</b>	<b>135XB:A</b>
Formula moiety	(C <sub>39</sub> H <sub>42</sub> N <sub>6</sub> ), (C <sub>6</sub> F <sub>4</sub> I <sub>2</sub> )	(C <sub>39</sub> H <sub>42</sub> N <sub>6</sub> ), (C <sub>6</sub> F <sub>3</sub> I <sub>3</sub> ), (C <sub>4</sub> H <sub>8</sub> O <sub>2</sub> )	(C <sub>21</sub> H <sub>24</sub> N <sub>6</sub> ), (C <sub>6</sub> F <sub>4</sub> I <sub>2</sub> )	(C <sub>21</sub> H <sub>24</sub> N <sub>6</sub> ), (C <sub>6</sub> F <sub>3</sub> I <sub>3</sub> )
Empirical formula	C <sub>45</sub> H <sub>42</sub> N <sub>6</sub> F <sub>4</sub> I <sub>2</sub>	C <sub>49</sub> H <sub>50</sub> F <sub>3</sub> I <sub>3</sub> N <sub>6</sub> O <sub>2</sub>	C <sub>27</sub> H <sub>24</sub> N <sub>6</sub> F <sub>4</sub> I <sub>2</sub>	C <sub>27</sub> H <sub>24</sub> F <sub>3</sub> I <sub>3</sub> N <sub>6</sub>
Molecular weight	996.65	1192.65	762.32	870.22
Crystal system	Monoclinic	Triclinic	Triclinic	Orthorhombic
Space group	<i>P2</i> <sub>1</sub> / <i>c</i>	<i>P</i> $\bar{1}$	<i>P</i> $\bar{1}$	<i>Pbca</i>
<i>a</i> , Å	16.337(6)	9.764(4)	9.255(3)	7.931(2)
<i>b</i> , Å	16.340(5)	11.594(4)	11.995(4)	20.310(5)
<i>c</i> , Å	15.642(5)	22.901(9)	13.507(5)	37.342(10)
$\alpha$ , °	90	101.90(2)	78.82(2)	90
$\beta$ , °	102.862(13)	97.56(3)	84.15(2)	90
$\gamma$ , °	90	99.98(2)	68.959(19)	90
Volume, Å <sup>3</sup>	4071(2)	2460.4(16)	1372.1(8)	296(2)
<i>Z</i>	4	2	2	8
Density, g/cm <sup>3</sup>	1.626	1.610	1.845	1.922
<i>T</i> , K	130	180	200	296(2)
X-ray wavelength, Å	0.71073	0.71073	0.71073	0.71073
$\mu$ , mm <sup>-1</sup>	1.604	1.961	2.348	3.164
R <sub>1</sub> (observed)	0.0442	0.0338	0.0497	0.0638
wR <sub>2</sub> (all)	0.1198	0.1100	0.1773	0.1740

**Table 4.5** Halogen-bond geometries

Compound	D—I⋯A	d(I⋯A)	d(D⋯A)	<(D–I⋯A)	Symmetry Operation
<b>12XB:B</b> Co-crystal	C(29)–I(35)u⋯N(9)v	2.934(7)	5.03(1)	177.0(2)	u = x,y,z; v = x,y,z
<b>14XB:E</b> Co-crystal	C(46)– I(52)u⋯N(10)v	2.922(4)	5.024(6)	171.3(2)	u = x,y,z; v = x,y,z
<b>135XB:E:EtOAc</b> Co-crystal	C(48)– I(54)u⋯N(23)v	2.936(5)	5.063(7)	171.8(1)	u = x,y,z; v = -x, l - y, 2 - z
Co-crystal Solvate	C(50)– I(56)u⋯N(10)v	2.864(4)	4.991(6)	175.7(1)	u = x,y,z; v = -l + x, l + y, z
<b>135XB:A</b> Co-crystal	C(32)– I(38)u⋯N(17)v	2.869(9)	4.95(1)	175.9(3)	u = x,y,z; v = l + x,y,z
Co-crystal	C(28)– I(34)u⋯N(17)v	3.206(9)	5.23(1)	162.7(3)	u = x,y,z; v = -l/2 + x, 3/2 - y, l - z
	C(30)– I(36)u⋯N(24)v	3.093(2)	5.15(2)	170.9(4)	u = x,y,z; v = 1/2 - x, -l/2 + y, z

u / v – symmetry operation on donor / acceptor

### 4.3.1 Description of solid state architectures

The attempted co-crystallization of **12XB** and **B** resulted in the formation of a 1:1 binary solid, Figure 4.4. The primary halogen bond in the structure of **12XB:B** takes place between one of the iodine atoms and N<sub>(pyz)</sub> forming a C—I⋯N conventional halogen bond and the second iodine atom engages in a C—I⋯π<sub>(pyz)</sub> interaction with an adjacent pyrazole moiety. These two interactions result in 1D infinite chains. Two remaining pyrazole acceptor sites do not form

interactions via halogen bonds but rather form identical short contacts with a methyl C–H on the benzene scaffold of another overlapping tritopic acceptor.

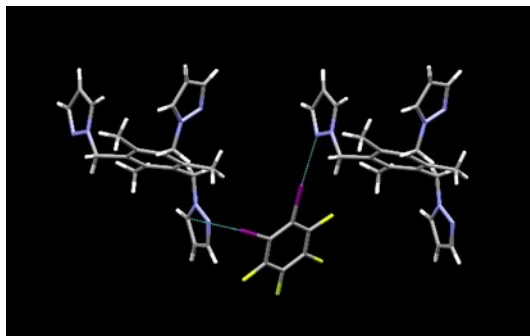


**Figure 4.4** Main interactions in the crystal structure of **12XB:B**

The primary feature in the 1:1 co-crystal **14XB:E** is a discrete tetramer built around a centrosymmetric (central) (bzim)C–H $\cdots$ N/N $\cdots$ H–C(bzim) hydrogen bonded homo-synthon, which is then extended via two symmetry-related C–I $\cdots$ N(bzim) halogen bonds, Figure 4.5. Only one of the two iodine atoms in **14XB** participates in a halogen bond. The remaining heterocyclic nitrogen atom on the tritopic acceptor forms a short contact with an aromatic C–H moiety of a neighboring benzimidazole group.

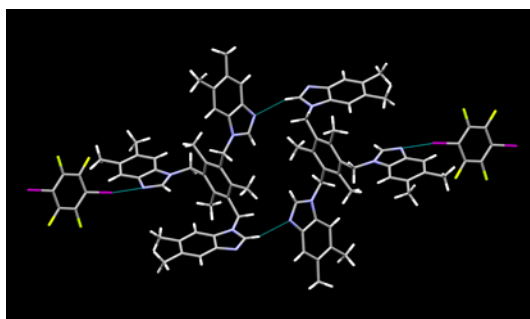


**Figure 4.5** Tetramer in the structure of **14XB:E**

The structure determination of the product resulting from the reaction between **135XB** and **E** revealed that an ethyl acetate solvate had formed (the overall stoichiometry is 1:1:1), Figure 4.6. The solvent does not participate in any noteworthy interactions, but rather is lodged within the

hydrophobic cavity created by the two benzimidazole arms. The three arms are on the same face of the benzene scaffold. Two of the three halogen atoms on **135XB** participate in C–I···N halogen bonds leading to a centrosymmetric tetrameric aggregate. The shorter I···N bond takes place with the (N) atom in a perpendicular benzimidazole site, whereas the longer I···N contact is formed with the acceptor site pointing away from the central scaffold, rotated along the C–N axis.

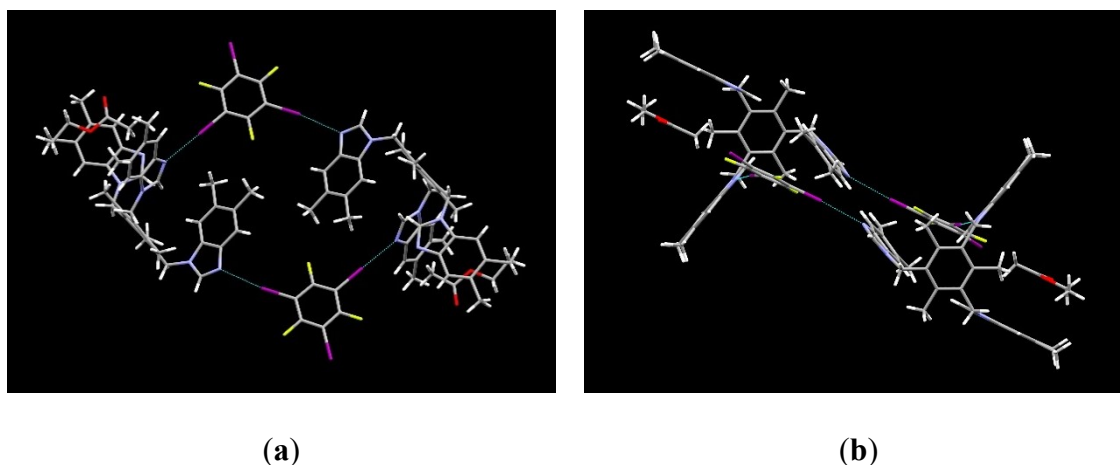


**Figure 4.6** (a) Tetramer in the crystal structure of **135XB:E:EtOAc** (b) Ethyl acetate wedged between benzimidazole arms

Finally, in the 1:1 crystal structure of **135XB:A** all three iodine atoms of the donor participate in conventional C–I···N halogen bonds, Figure 4.7.

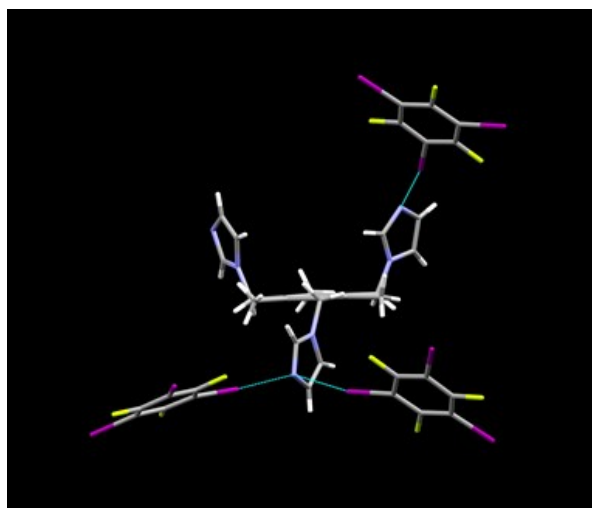


**Figure 4.7** Primary halogen bond interactions in the structure of **135XB:A**



The 1D chains propagate via C–I $\cdots$ N bifurcated interactions and is also further extended into 3D molecular networks through a conventional C–I $\cdots$ N interaction. The molecular network is further stabilized by bifurcated C–H $\cdots$ N interactions.

### 4.3.2 Aromatic stacking

In the crystal structure of **12XB:B**, a stacked dimer of donors is sandwiched between two symmetry related arms of acceptor molecules, Figure 4.8.

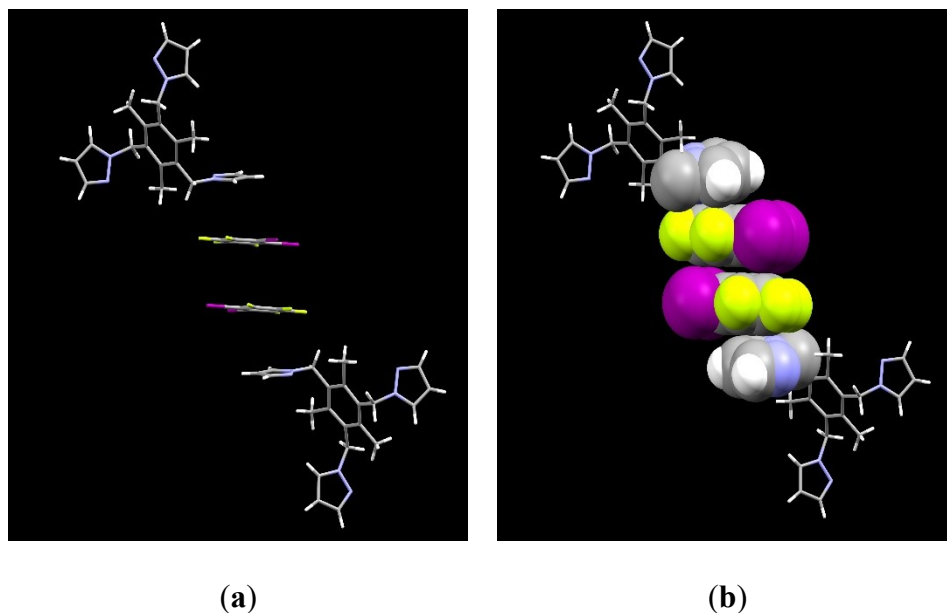
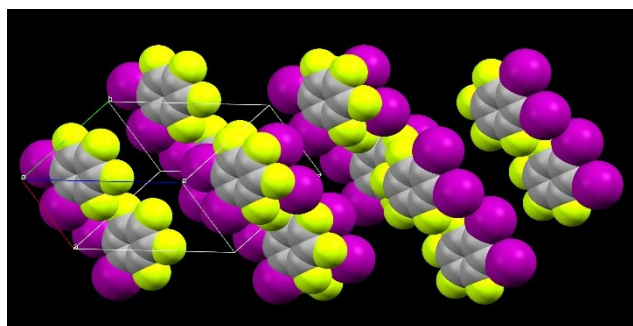
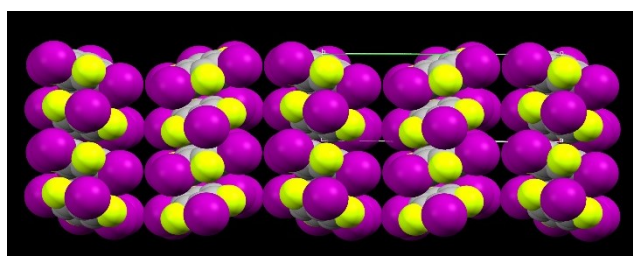


**Figure 4.8** (a) Stacking interactions between the two components in the structure of **12XB:B**; (b) Space filling representation of the packing showed in (a)

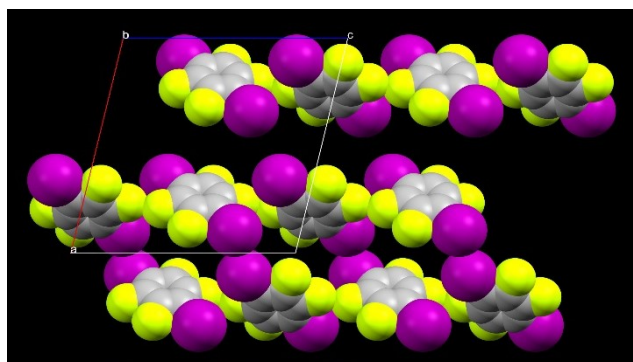
An off-set packing mode or rather a parallel-displaced geometry can be noted between donor molecules **12XB** and **135XB** in co-crystals **12XB:B** and **135XB:A**, respectively, Figure 4.9. **14XB** in the crystal structure of **14XB:E** display several C $\cdots$ F close contacts, which probably arise due to close packing of the donor molecules, Figure 4.9.



(a)



(b)

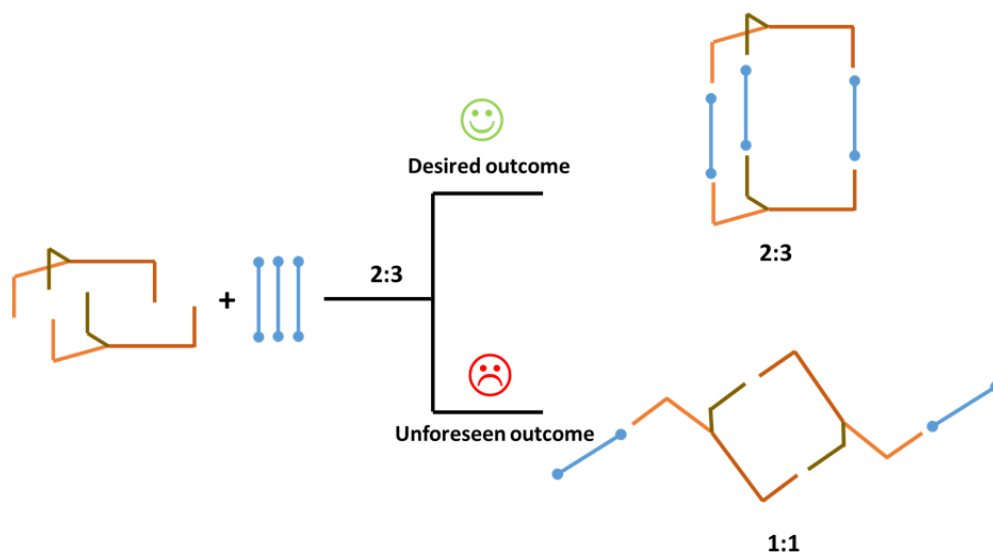


(c)

**Figure 4.9** (a) Stacking of donors in **12XB:B** (b) Stacking of donors in **135XB:A**; (c) Close packing of donor molecules in **14XB:E**

## 4.4 Discussion

It has been noted in previous studies that it is difficult to maintain stoichiometric control in co-crystals that contain multi-topic halogen bond donors.<sup>15, 18</sup> Similarly, co-crystals obtained in this study did not afford the desired stoichiometries, Figure 4.10, regardless of using stoichiometric amounts of both donor and acceptor. For both co-crystals **12XB:B** and **14XB:E** the targeted stoichiometry was 3:2, however, the observed stoichiometry was 1:1 in both instances. Only one out of the two iodine atoms in **14XB:E** participated in halogen bonding. For both **135XB:E:EtOAc** and **135XB:A**, a 1:1 stoichiometry was observed as expected, but with rather unforeseen coordination. For co-crystal **135XB:E:EtOAc**, only two out of the three halogen atoms form interactions and in co-crystal **135XB:A**, a bifurcated halogen bond and a conventional halogen bond interact with two imidazole sites of the tritopic acceptor. These results clearly demonstrate the difficulty in controlling the delicate balance between intermolecular interactions at the event of nucleation. And thus, we are in pursuit to understand the challenge; the inability of multi-topic XB donors to simultaneously engage all donor sites in the solid state.



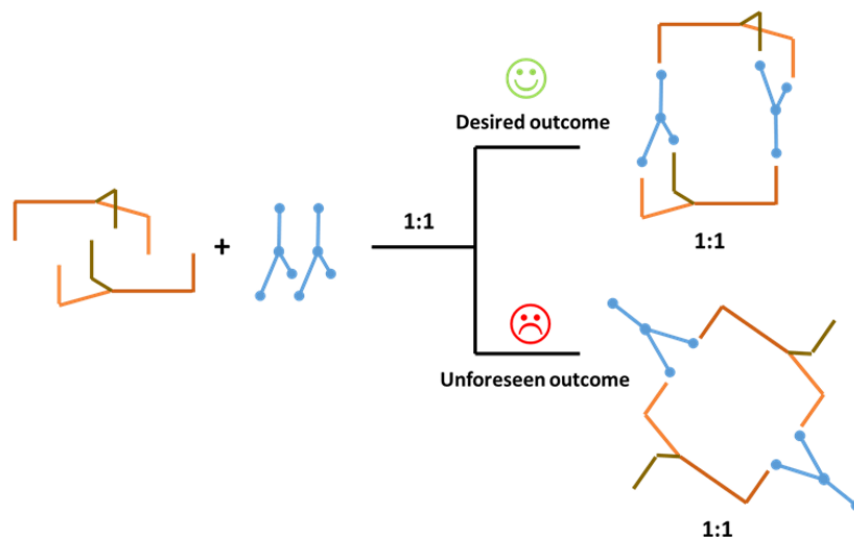


**Figure 4.10** Expected vs unexpected connectivity

A CSD study was implemented to extract more structural information, considering the nature of halogen bonding observed in these co-crystals and the reluctance of reaching a full coordination via C—I $\cdots$ N interactions. Geometric data on C—I $\cdots$ N bond lengths, bond angles and coordination about halogen bond donors (**12XB**, **14XB** and **135XB**) were gathered to draw a generalized overview of halogen bonds formed with sp<sup>2</sup> hybridized N. The data gathered in Table 4.1, 17/19 and 97/100 for **12XB** and **14XB** respectively, indicate that ditopic donors are typically more like to engage all their sites in halogen bonding, whereas for tritopic donors, the likelihood of having a full complement of halogen bonds has dropped to 47% (14/30). It is possible that the number of available acceptor sites, possible steric considerations, and step-wise deactivation of the donor sites probably were the main contributors to this, while the slightly higher electrostatic potentials of the ditopic donors (163 kJ/mol for **12XB**, 169 kJ/mol for **14XB**, and 158 for **135XB**, respectively) may also have played a part.

In these **14XB** structures, where the failure to reach a full coordination, relevant literature does not reveal as to why a full coordination has not been achieved for all three structures

TOJBOK, TAWFEF and VABNUJ, Figure 4.11. It can be conjectured that a disproportionate ratio of donors to acceptors has led to a reluctance in forming a full coordination. For structures TOJBOK and TAWFEF the number of donor sites are greater than acceptor sites (a methanol molecule causes the disproportion in TOJBOK) and otherwise for VABNUJ, Table 4.6. Given that structure VABNUJ has more acceptor sites, it is presumable that the spatial arrangements of the acceptor sites are positioned in a way that could not effectively accommodate an incoming donor molecule.

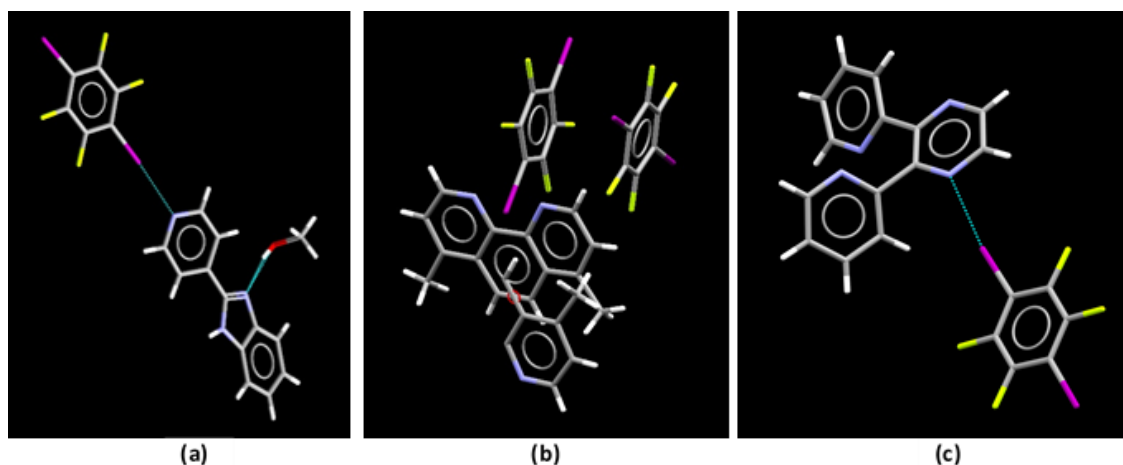
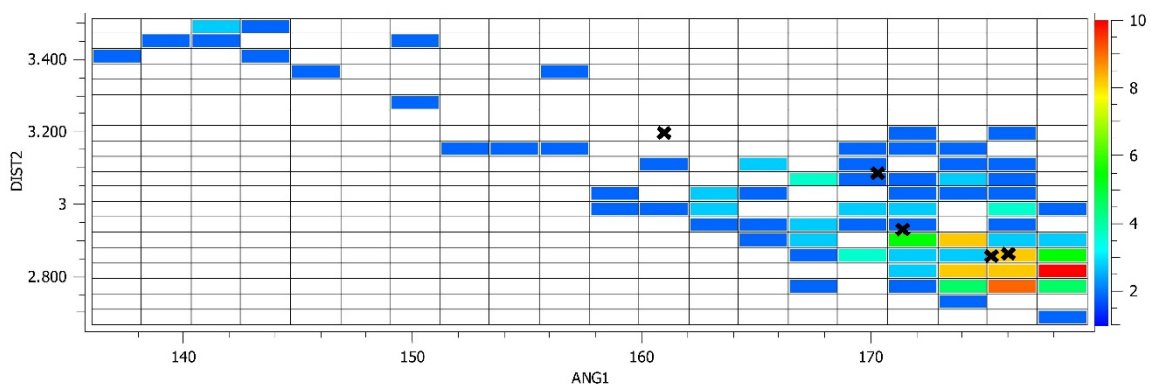


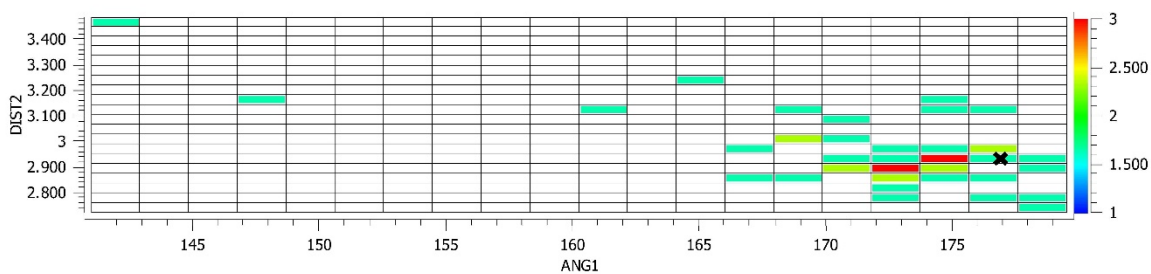
**Figure 4.11** 14XB structures that failed to reach a full coordination. (a) TOJBOK, (b) TAWFEF, (c) VABNUJ

There is obviously a difference between the probability that ditopic and tritopic donors will engage in a maximum number of halogen-bonds, which triggered the question as to whether there are any notable differences in halogen-bond metrics between the two types of molecules. To address this issue, we constructed three separate graphs where the I $\cdots$ N bond length was plotted against the C-I $\cdots$ N bond angle for all halogen bonds in crystal structures containing either of the three donors, **12XB**, **14XB**, or **135XB**, Figure 4.12. The heat distribution plots between bond angle and bond length for the three donor molecules have a considerable fraction of shorter bond

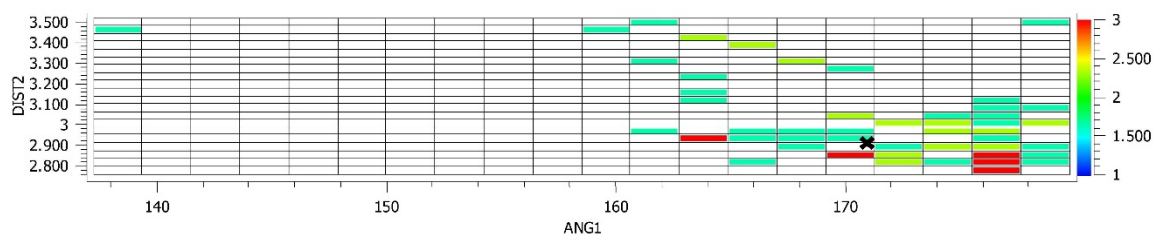
lengths with more linear bond angles. A trend is noticeable: longer the I⋯N distance, shorter the C—I⋯N bond angle, implying that a stronger interaction would have a near linear interaction with a shorter bond distance.



(a)



(b)



(c)

**Figure 4.12** Halogen-bond distances and angles extracted from a CSD search on crystal containing sp<sup>2</sup>-hybridized nitrogen atoms as acceptors and (a) **135XB**, (b) **12XB** and (c) **14XB**, respectively. The colors indicate number of hits in each cell

The dotted notations on the plots indicate the co-crystals obtained in this study. It is quite notable that the overall appearance of the graphs for the ditopic acceptors are quite different to the way in which the analogous data for **135XB** comes out. First, the I $\cdots$ N bond-lengths for tritopic structures cover a much broader range, and the expected positive correlation between larger (more linear) angles and shorter I $\cdots$ N distances is also readily apparent, Figure 4.9(a). For the ditopic donors, the angular dependence has a much more narrow distribution and the vast majority of C-I $\cdots$ N bond angles are greater than 160°. This underscores that in order for **135XB** to simultaneously form three halogen bonds, the molecule is often forced to make a structural compromise (resulting in considerable deviations from linearity), whereas ditopic halogen-bond donors are more likely to be able to find two suitable donors that are both oriented in such a way that a near-linear bond is produced.

It is notable the last iodine atom of each donor molecule in co-crystals **135XB:E:EtOAc** and **14XB:E** is not participating in any considerable interaction. Even though this incident is not so uncommon for **135XB**, to our surprise, in a rare occurrence, **14XB** also participates via single C—I $\cdots$ N interaction. C—I bond lengths of co-crystals **135XB:E:EtOAc** and **14XB:E**, Table 4.6, delineates this.

**Table 4.6** C—I bond lengths of co-crystals **135XB:E:EtOAc** and **14XB:E**

Compound	D—I	d(D $\cdots$ I)
<b>135XB:E</b>	C(48)—I(54)	2.140
	C(50)—I(56)	2.131
	C(46)—I(52)	2.110
<b>14XB:E</b>	C(46)—I(52)	2.116
	C(49)—I(55)	2.080

Part of the reason for using flexible tritopic acceptor molecules was to maximize the opportunities for formation of geometrically near-linear C-I $\cdots$ N halogen bonds to ditopic and tritopic donors. The tritopic acceptors used in this study contain several rotatable bonds but the molecular geometries can be simplified into one of two classes, a “crown” conformation with all three arms on the same side of the aromatic core, or a “chair” conformation with two arms on one side and the third arm on the opposite side of the aromatic core. As it turns out, both types of conformations were observed in these crystal structures with the chair appearing in the structures of **14XB:E**, **12XB:B**, **135XB:A** and the crown in the crystal structure of **135XB:E:EtOAc**, Figure 4.13.

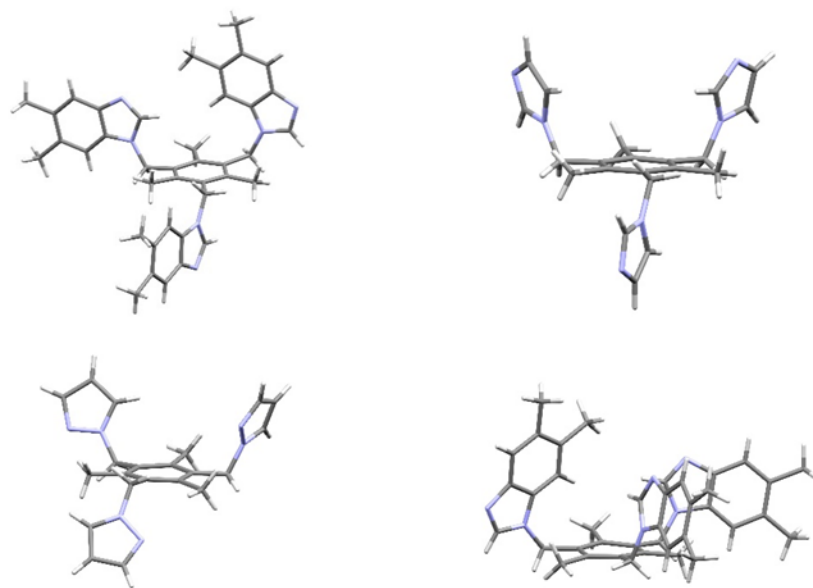


**Figure 4.13** Molecular geometries of the tritopic acceptor molecules in the crystal structures of **14XB:E** (top left), **12XB:B** (bottom left), **135XB:A** (top right), and **135XB:E:EtOAc** (bottom right). The crown conformation is only observed in the crystal structure of **135XB:E:EtOAc**, whereas the chair is present in the other three structures

In the two co-crystals **14XB:E** and **135XB:E:EtOAc**, acceptor **E** has two different conformations, exhibiting its flexible nature to change the conformation as per the need of the



donor molecules, meaning that, these molecules are not strongly predisposed to one arrangement over another. Despite this flexibility, it was not possible to realize a perfect match between donors and acceptor in these structures simply by controlling the reaction stoichiometry. A key explanation for this behavior can, undoubtedly, be found by evoking the sequential  $\sigma$ -hole deactivation that takes place in multi-topic halogen bond donors upon binding, as shown by van der Boom<sup>15</sup> and Formigue<sup>16</sup>.  $\sigma$ -hole on the iodine atoms is formed as a result of electron withdrawing fluorine atoms creating a positive potential in the benzene core. Upon binding of a nucleophile with a  $\sigma$ -hole in an iodine atom, an elongation is observed with the weakening of the C—I bond. This is due to interaction of the nitrogen lone pair with the lowest vacant  $\sigma^*$  orbital of C-I, Figure 4.14. This as a result decreases the positive potential of the benzene core which deactivates the remaining  $\sigma$ -holes to an extent. In the co-crystals presented herein, it is likely that when C—I $\cdots$ N binding interactions takes place, the magnitude of the  $\sigma$ -hole on the non-bonded halogen atom(s) diminish to a point where C—H hydrogen-bond donors suddenly become competitive, resulting in C—H $\cdots$ N interactions (as observed in the crystal structure of **14XB:E**, Figure 4.7)

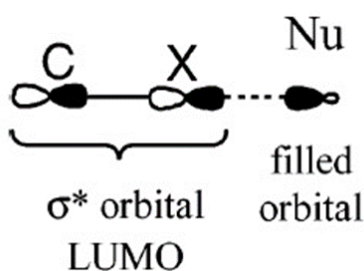


**Figure 4.14**  $\sigma$ -hole bonding

However, this concept cannot be generalized and applied to **14XB**, given the following circumstances. First, **14XB** has a more pronounced  $\sigma$ -hole with a higher positive potential than **12XB** and **135XB**, (both in which all iodine atoms have participated in interactions) in co-crystals

**12XB:B** and **135XB:A** respectively, and thus, is expected to have both iodine atoms in **14XB** to partake in intermolecular interactions (as per the CSD search; 99% from 100 hits). Secondly, out of the two donors **135XB** and **14XB**, where **E** is the common acceptor, **135XB** being the weaker donor, was still capable of making a two-point interaction as seen in co-crystal **135XB:E:EtOAc**. Therefore, it can be suggested that the reason the second iodine atom in **14XB:E** did not participate in halogen bonding due to the sterically hindering bulky groups of acceptor **E**. Co-crystal structures **12XB:B** and **135XB:A** which contain much less bulky imidazole and pyrazole acceptors and much weaker donors (**12XB** and **135XB**), having all the iodine atoms participate in intermolecular interactions, give further grounds for this suggestion.

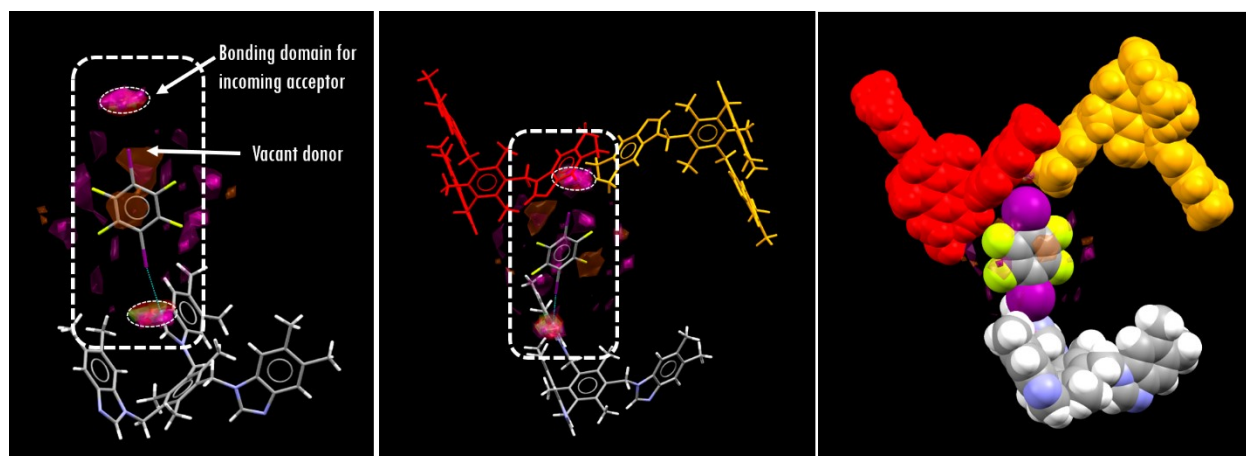


**Figure 4.15** Full interaction maps showing steric hinderance at the vacant donor site in **E:14XB**

## 4.5 Conclusions<sup>1</sup>

Halogen bonding was successfully employed in synthesizing co-crystals of a series of ten tritopic N-heterocyclic compounds using four multi-topic halogen-bond donors. IR data showed that 70% of the experiments produced halogen-bonded co-crystals and four structures were obtained which are driven by C—I $\cdots$ N halogen bonds.

However, the structures obtained show two different architectures: discrete tetrameric aggregates and 1D chains. A comparison with data from a systematic CSD analysis shows that the halogen-bond distances and angles in the four structures presented herein are consistent with commonly observed parameters. In addition, a variety of  $\pi$ -stacking and C–H $\cdots\pi$  interactions were also seen in two co-crystals.

Our results underscore the difficulty of controlling stoichiometries and chemical compositions of targeted products when attempting to synthesize co-crystals with reactants that carry multiple donor- and acceptor sites. Only two of the four co-crystals met the expected stoichiometric ratios, even though they also displayed unexpected connectivities. A key factor that contributes to the synthetic challenges is the fact that upon deactivation of  $\sigma$ -hole and halogen-bond donor capability, other interactions, such as C–H hydrogen-bond donors become competitive, which subsequently leads to a preference for C–H $\cdots$ N hydrogen bonds over C–I $\cdots$ N halogen bonds. Even though the halogen bond can deliver selectivity, strength and directionality, much more work is still required before we can fully realize its potential as a reliable synthetic vector capable of delivering supramolecular assemblies with desired chemical composition, stoichiometry, and topology.

## 4.6 References

1. Andree, S. N. L.; Sinha, A. S.; Aakeröy, C. B., Structural Examination of Halogen-Bonded Co-Crystals of Tritopic Acceptors. *Molecules* **2018**, *23* (2), 163.
2. (a) Auffinger, P.; Hays, F. A.; Westhof, E.; Ho, P. S., Halogen bonds in biological molecules. *Proc. Natl. Acad. Sci. U.S.A.* **2004**, *101* (48), 16789-16794; (b) Brinck, T.; Murray, J. S.; Politzer, P., Surface Electrostatic Potentials of Halogenated Methanes as Indicators of Directional Intermolecular Interactions. *Int. J. Quantum Chem.* **1992**, 57-64; (c) Kolář, M. H.; Hobza, P., Computer Modeling of Halogen Bonds and Other  $\sigma$ -Hole Interactions. *Chem. Rev.* **2016**, *116* (9), 5155-5187; (d) Murray, J. S.; Paulsen, K.; Politzer, P., Molecular surface electrostatic potentials in the analysis of non-hydrogen-bonding

- noncovalent interactions. *Proc.-Indian Acad. Sci., Chem. Sci.* **1994**, *106* (2), 267-275; (e) Politzer, P.; Lane, P.; Concha, M. C.; Ma, Y.; Murray, J. S., An overview of halogen bonding. *J. Mol. Model.* **2007**, *13* (2), 305-311.
3. Metrangolo, P.; Neukirch, H.; Pilati, T.; Resnati, G., Halogen Bonding Based Recognition Processes: A World Parallel to Hydrogen Bonding. *Acc. Chem. Res.* **2005**, *38* (5), 386-395.
  4. Crihfield, A.; Hartwell, J.; Phelps, D.; Walsh, R. B.; Harris, J. L.; Payne, J. F.; Pennington, W. T.; Hanks, T. W., Crystal engineering through halogen bonding. 2. Complexes of diacetylene-linked heterocycles with organic iodides. *Cryst. Growth Des.* **2003**, *3* (3), 313-320.
  5. Zordan, F.; Brammer, L.; Sherwood, P., Supramolecular Chemistry of Halogens: Complementary Features of Inorganic (M-X) and Organic (C-X) Halogens Applied to M-X...X'-C Halogen Bond Formation. *J. Am. Chem. Soc.* **2005**, *127* (16), 5979-5989.
  6. Yang, Z.; Liu, Y.; Chen, Z.; Xu, Z.; Shi, J.; Chen, K.; Zhu, W., A quantum mechanics-based halogen bonding scoring function for protein-ligand interactions. *J. Mol. Model.* **2015**, *21* (6).
  7. Desiraju, G. R.; Ho, P. S.; Kloo, L.; Legon, A. C.; Marquardt, R.; Metrangolo, P.; Politzer, P.; Resnati, G.; Rissanen, K., Definition of the halogen bond (IUPAC Recommendations 2013). *Pure Appl. Chem.* **2013**, *85* (8).
  8. (a) Kolář, M.; Hostaš, J.; Hobza, P., The strength and directionality of a halogen bond are co-determined by the magnitude and size of the  $\sigma$ -hole. *Phys. Chem. Chem. Phys.* **2014**, *16* (21), 9987-9996; (b) Politzer, P.; Murray, J. S.; Clark, T., Halogen bonding: an electrostatically-driven highly directional noncovalent interaction. *Phys. Chem. Chem. Phys.* **2010**, *12* (28), 7748 - 7757; (c) Tsuzuki, S.; Wakisaka, A.; Ono, T.; Sonoda, T., Magnitude and Origin of the Attraction and Directionality of the Halogen Bonds of the Complexes of C<sub>6</sub>F<sub>5</sub>X and C<sub>6</sub>H<sub>5</sub>X (X=I, Br, Cl and F) with Pyridine. *Chem. Eur. J.* **2012**, *18* (3), 951-960.
  9. (a) Alkorta, I.; Sánchez-Sanz, G.; Elguero, J., Linear free energy relationships in halogen bonds. *CrystEngComm* **2013**, *15* (16), 3178; (b) Bauzá, A.; Quiñero, D.; Frontera, A.; Deyà, P. M., Substituent effects in halogen bonding complexes between aromatic donors and acceptors: a comprehensive ab initio study. *Phys. Chem. Chem. Phys.* **2011**, *13* (45), 20371; (c) Politzer, P.; Murray, J. S., Halogen Bonding: An Interim Discussion. *ChemPhysChem* **2013**, *14* (2), 278-294.
  10. (a) Riley, K. E.; Murray, J. S.; Fanfrlík, J.; Řezáč, J.; Solá, R. J.; Concha, M. C.; Ramos, F. M.; Politzer, P., Halogen bond tunability II: the varying roles of electrostatic and dispersion contributions to attraction in halogen bonds. *J. Mol. Model.* **2012**, *19* (11), 4651-4659; (b) Riley, K. E.; Murray, J. S.; Fanfrlík, J.; Řezáč, J.; Solá, R. J.; Concha, M. C.; Ramos, F. M.; Politzer, P., Halogen bond tunability I: the effects of aromatic fluorine

- substitution on the strengths of halogen-bonding interactions involving chlorine, bromine, and iodine. *J. Mol. Model.* **2011**, *17* (12), 3309-3318.
11. Cavallo, G.; Metrangolo, P.; Milani, R.; Pilati, T.; Priimagi, A.; Resnati, G.; Terraneo, G., The Halogen Bond. *Chem. Rev.* **2016**, *116* (4), 2478-2601.
  12. Syssa-Magale, J. L.; Boubekour, K.; Palvadeau, P.; Meerschaut, A.; Schollhorn, B., The tailoring of crystal structures via the self-assembly of organic coordination compounds by N center dot center dot center dot I non-covalent halogen bonds: co-crystals of sterically hindered N-heterocycles and 1,4-diiodo-tetrafluorobenzene. *CrystEngComm* **2005**, *7*, 302-308.
  13. Hirst, A. R.; Escuder, B.; Miravet, J. F.; Smith, D. K., High-Tech Applications of Self-Assembling Supramolecular Nanostructured Gel-Phase Materials: From Regenerative Medicine to Electronic Devices. *Angew. Chem. Int. Ed.* **2008**, *47* (42), 8002-8018.
  14. Piepenbrock, M.-O. M.; Lloyd, G. O.; Clarke, N.; Steed, J. W., Metal- and Anion-Binding Supramolecular Gels. *Chem. Rev.* **2010**, *110* (4), 1960-2004.
  15. Lucassen, A. C. B.; Karton, A.; Leitus, G.; Shimon, L. J. W.; Martin, J. M. L.; van der Boom, M. E., Co-Crystallization of Sym-Triiodo-Trifluorobenzene with Bipyridyl Donors: Consistent Formation of Two Instead of Anticipated Three N···I Halogen Bonds. *Cryst. Growth & Des.* **2007**, *7* (2), 386-392.
  16. Nicolas, I.; Barrière, F.; Jeannin, O.; Fourmigué, M., Sequential Halogen Bonding with Ditopic Donors:  $\sigma$ -Hole Evolutions upon Halogen Bond Formation. *Cryst. Growth & Des.* **2016**, *16* (5), 2963-2971.
  17. Carter, M.; Voth, A. R.; Scholfield, M. R.; Rummel, B.; Sowers, L. C.; Ho, P. S., Enthalpy–Entropy Compensation in Biomolecular Halogen Bonds Measured in DNA Junctions. *Biochemistry* **2013**, *52* (29), 4891-4903.
  18. Vartanian, M.; Lucassen, A. C. B.; Shimon, L. J. W.; van der Boom, M. E., Cocrystallization of a Tripyridyl Donor with Perfluorinated Iodobenzene Derivatives: Formation of Different N···I Halogen Bonds Determining Network vs Plain Packing Crystals. *Cryst. Growth & Des.* **2008**, *8* (3), 786-790.

## Chapter 5 - Co-crystal technology for drug development via

### O—H···N hydrogen bonds

#### 5.1 Introduction

The process of discovery and formulation of drugs is a costly and time-consuming process. Poor biopharmaceutical properties such as oral bioavailability, unlike toxicity or lack of efficacy, contribute to the fact that less than one percent of active compounds make it onto the market<sup>1</sup>, and, solubility<sup>2</sup> is a key physicochemical parameter that needs to be addressed at an early stage in the drug development process.

The vast majority of active pharmaceutical ingredients (API's), such as painkillers, exist as solids at room temperature. The particular solid form defines the APIs physical properties such as solubility, thermal and mechanical stability, and particle morphology which affects downstream processability and formulation.<sup>3</sup> The physical properties of the APIs also control pharmacokinetic properties such as bioavailability, absorption and dissolution.<sup>4</sup> One big hurdle in this field is the lack of versatile technologies that can alter or improve key physical properties of API's.

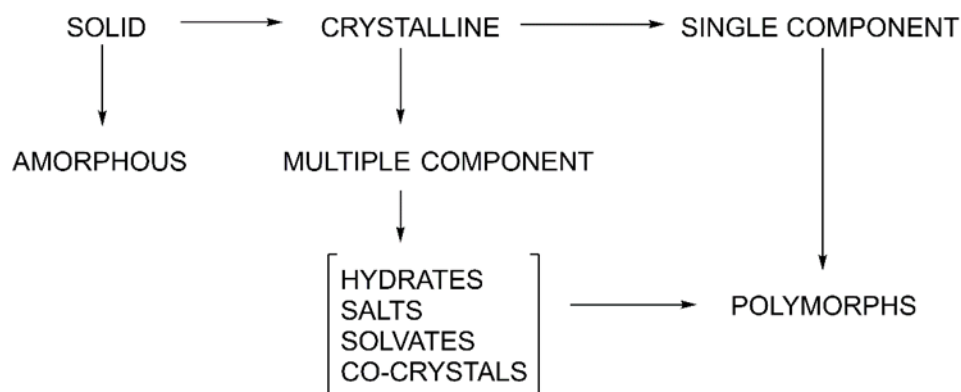


**Figure 5.1** API solid form classification according to the structure and composition

APIs can exist in many distinct solid forms, including polymorphs, solvates, hydrates, salts, co-crystals and amorphous solids,<sup>5</sup> Figure 5.1. Even though these solid forms display unique physiochemical properties they do not alter the drugs pharmacological behavior. The preferred solid form is generally the thermodynamically most stable crystalline form of the compound. Inadequate solubility or dissolution rate of the stable crystal form of the parent compound may result in poor oral absorption, Table 5.1.

**Table 5.1** Solubility according to the US Pharmacopoeia<sup>6</sup>

<b>Descriptive term</b>	<b>Part of solvent required per part of solute</b>
Very soluble	Less than 1
Freely soluble	From 1 to 10
Soluble	From 10 to 30
Sparingly soluble	From 30 to 100
Slightly soluble	From 100 to 1000
Very slightly soluble	From 1000 to 10,000
Practically insoluble	10,000 and over

According to the Biopharmaceutical classification (BCS),<sup>7</sup> active pharmaceutical ingredients can be divided into four classes. Class I drugs possess both good membrane permeability and solubility; Class II drugs have good permeability but poor solubility; Class III drugs poorly permeable but higher in solubility; Class IV drugs are poorly permeable and poorly soluble Figure 5.2.

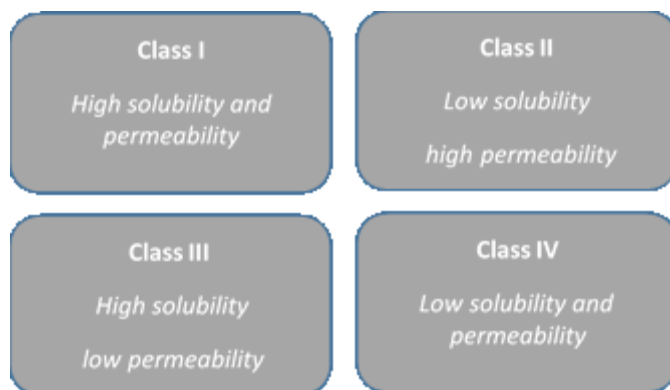
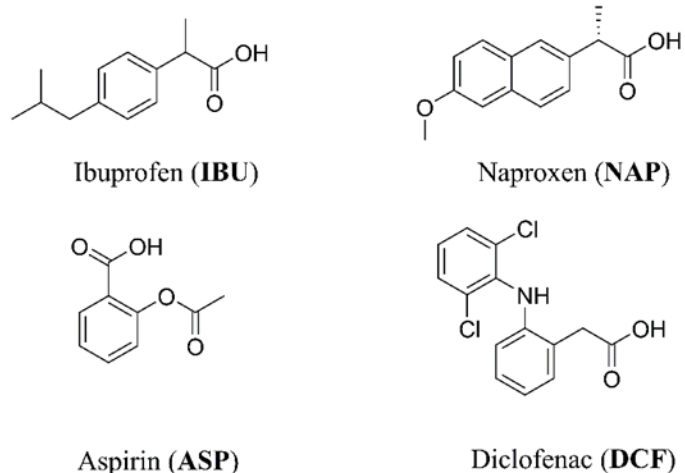


**Figure 5.2** BCS classification of API's

Pharmaceutical co-crystals, which recently gained attention as a means of modifying physiochemical properties of APIs are singular crystalline solids that incorporate two neutral molecules, one being an API and the other a co-crystal former.<sup>5</sup> Co-crystal former may be an excipient or another drug. Pharmaceutical co-crystal technology is used to identify and develop new solid forms and offer a chance to increase the number of forms of an API.

In Chapter 3, we saw that with multitopic carboxylic acids,  $\text{COOH} \cdots \text{N}$ -heterocyclic (imidazole, benzimidazole and pyrazole) synthons were used to construct supramolecular architectures with tritopic acceptors. The reliability and effectiveness of the synthon were determined by the supramolecular yield. Herein, we have chosen four nonsteroidal anti-inflammatory (NSAID) drugs; Ibuprofen, Naproxen, Aspirin and Diclofenac, Figure 5.3, due to the presence of their  $\text{COOH}$  moiety, that can be utilized to synthesize co-crystals using the above mentioned supramolecular synthons with the use of tritopic acceptors, Figure 5.4.

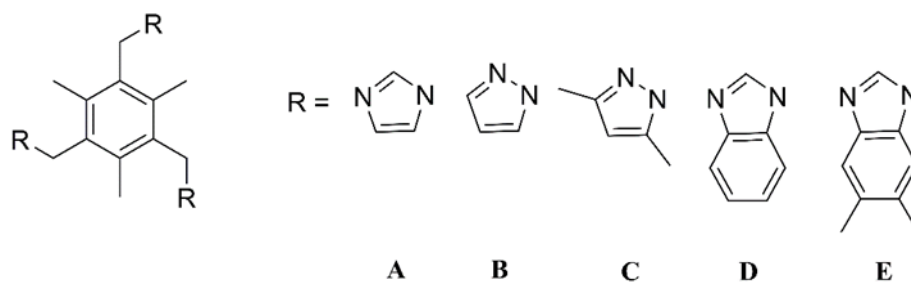




**Figure 5.3** Non-steroidal anti-inflammatory drugs

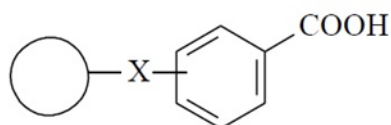
The NSAIDs can be sub-classified on the basis of chemical structure as follows:

- Salicylates
- Propionic acids (Profens)
- Anthranilates (Fenamates)



**Figure 5.4** Schematic of tritopic acceptors used in the study

In general, these molecules structurally consist of an acidic moiety (carboxylic acid) attached to a planar, aromatic functionality, Figure 5.5. Some analgesics also contain a polar linkage group, attached to an additional lipophilic group.

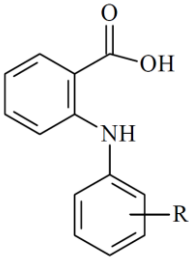


**Figure 5.5** NSAID general structure

The major mechanism by which the NSAIDs work is by inhibition of the prostaglandin synthesis.<sup>8</sup> Furthermore, NSAIDs for the most part competitively inhibit cyclooxygenases (COXs),<sup>9</sup> the enzyme that catalyzes the synthesis of cyclic endo peroxides from arachidonic acid to form prostaglandins. There are two types of cyclooxygenases namely COX-1 which is responsible for the baseline levels of prostaglandins while COX-2 produces prostaglandins through stimulation.

**Table 5.2** Sub-class structures of NSAID and type of COX being inhibited

NSAID general structure	NSAID sub-class structure	Type of COX inhibited
	<p><b><i>Salicylates</i></b></p>	Selective COX-1
	<i>Aspirin</i>	
	<p><b><i>Propionic acids (Profens)</i></b></p>	Slightly selective COX-1
	<i>Ibuprofen, Naproxen</i>	

	 <p><i>Anthranilates (Fenamates)</i></p>	Slightly selective COX-2
	<p><i>Diclofenac</i></p>	

Although shape, geometry and size of the NSAIDs, Table 5.2, are of great significance for an effective and competitive inhibition of cyclooxygenases from arachidonic acid, formation of co-crystals primarily depend on the chemical functionality on NSAIDs; the COOH moiety.

The goals of this chapter are as follows;

1. Co-crystallization targeting COOH moiety of the NSAIDs with tritopic acceptors, to evaluate the formation of co-crystals. We also want to establish whether there is a correlation between the type of NSAID used with the supramolecular yield.
2. Does the supramolecular yields for the NSAIDs depend on the type of tritopic acceptor used?
3. Is the supramolecular assembly in solution reflected in the solid state?
4. Is bulk synthesis and characterization of the co-crystals possible?
5. Could we expect a change in solubility for the bulk co-crystals with respect to the NSAID?

## 5.2 Experimental

All reagents, solvents, precursors and hydrogen-bond donors were purchased from commercial sources and were used as received without further purification. A Varian Unity Plus (400 MHz) NMR spectrophotometer (Varian, Inc.) was used to record nuclear magnetic resonance spectra using the residual solvent signal as a reference. The  $^1\text{H}$  NMR spectra are reported as follows: chemical shift  $\delta$  in ppm relative to TMS ( $\delta = 0$  ppm), multiplicity, coupling constant (J in Hz), number of protons. The resonance multiplicity is described as s (singlet), d (doublet), t (triplet), q (quartet) or m (multiplet). A Fisher-Johns melting point apparatus (Vernon Hills, IL, USA) was used to determine melting points. Infrared spectroscopic analyses were performed with a Nicolet 380 FT-IR instrument (Thermo Scientific, Madison, WI, USA).

### 5.2.1 Synthesis

#### 5.2.1.1 Synthesis of diclofenac<sup>10</sup>

To a 100 mL beaker 70 mL of water and 3.00 g sodium salt of the diclofenac was added. The suspension was stirred until it completely dissolved with minimum heating. Once dissolved, a few drops of concentrated HCl was added dropwise. With the addition of HCl, neutral diclofenac precipitated as a white solid. The resultant solid was vacuum filtered and air dried on a watch glass. Mp 156 - 158 °C (lit value Mp 157 °C)<sup>11</sup>  $\delta\text{H}$  (400 MHz, DMSO-d<sub>6</sub>) 3.88 (2H, s, COCH<sub>2</sub>), 6.56 (1H, d, Ar-H), 6.81 (1H, NH), 6.98 (2H, m, Ar-H), 7.15 (1H, t, Ar-H), 7.24 (1H, d, Ar-H), 7.34 (2H, dd, Ar-H).

### ***5.2.1.2 Co-crystal synthesis via solvent assisted grinding experiments***

Co-crystal screening was performed between NSAIDs and tritopic acceptors using solvent assisted grinding method. A typical experiment entailed, grinding stoichiometric amounts of donor and acceptor in a microwell with a pestle and a drop of solvent. The solids resulting from grinding experiments are characterized using IR spectroscopy. The success of a grinding experiment is revealed by peak shifts observed in the ground mixture compared to the starting components.

## **5.2.2 Co-crystal experiments**

Four nonsteroidal anti-inflammatory drugs were subjected to co-crystallization experiments with five flexible tritopic acceptors. After screenings for co-crystals of ground mixtures using IR analysis, the samples were dissolved in a suitable solvent in borosilicate vials and carried out slow evaporation.

### ***5.2.2.1 Synthesis of 1,3,5-tris(5,6-dimethylbenzimidazole-1-yl-methyl)-2,4,6-trimethyl benzene tri aspirin, E:(ASP)<sub>3</sub>***

1,3,5-Tris(5,6-dimethylbenzimidazole-1-yl-methyl)-2,4,6-trimethyl benzene (0.0100 g, 0.0168 mmol) was dissolved in 1 mL of ethanol. To this solution was added aspirin (0.0035 g, 0.0168 mmol) in 1 mL of acetonitrile. The resulting solution was allowed for slow evaporation in a 2 dram borosilicate vial at room temperature. Orange colored column-shaped crystals were obtained after three weeks. Melting point 209-211 °C.

### ***5.2.2.2 Synthesis of 1,3,5-tris(5,6-dimethylbenzimidazole-1-yl-methyl)-2,4,6-trimethyl benzene aspirin, E:ASP***

1,3,5-Tris(5,6-dimethylbenzimidazole-1-yl-methyl)-2,4,6-trimethyl benzene (0.0100 g, 0.0168 mmol) was dissolved in 1 mL of ethanol. To this solution was added aspirin (0.0035 g, 0.0168 mmol) in 1 mL of acetonitrile. The resulting solution was allowed for slow evaporation in a 2 dram borosilicate vial at room temperature. Colorless column-shaped crystals were obtained after one week. Melting point 213-215 °C.

## **5.2.3 Solubility studies**

### ***5.2.3.1 Preparation of co-crystals for solubility studies<sup>12</sup>***

Bulk synthesis of **E:ASP** was done using solvothermal methods. Supersaturation of **E** and aspirin were created by cooling a solution of **E** (500 mg, 0.84 mmol) and aspirin (453 mg, 2.5 mmol) in 20 mL of acetonitrile from 40 to 5 °C using an ice bath. The precipitate was harvested by filtration and dried over a filter paper to remove loosely bound solvent. The solid was characterized using FT-IR spectroscopy and was confirmed to be a co-crystal and the obtained IR matched the previous IR of the single crystal submitted for X-ray analysis. PXRD pattern of the bulk sample indicated the presence of a new crystalline material.

### ***5.2.3.2 Preparation of standard series of salicylic acid for solubility studies of E:ASP***

A stock solution was prepared by dissolving 19.2 mg of salicylic acid and 0.1g citric acid in a minimum amount of purified water. This solution was diluted to 100.0 mL with methanol. Working standards were prepared by pipetting 5, 10 ,15, 20 and 25 mL aliquots of the stock

standard solution into separate 100.0 ml volumetric flasks, adding 25 mL of 0.2 M NaOH and diluting to volume with 0.2 M HCl.

#### ***5.2.3.3 Time dependent study of aspirin hydrolysis***

A stock solution was prepared by dissolving 25 mg of aspirin in a 50.0mL volumetric flask. 30 mL of methanol was added and after agitation the sample was diluted to volume with methanol. Three 5.0 mL aliquots of each sample were pipetted into separate 100.0 mL volumetric flasks and 25.0 mL of 0.2 M NaOH was added to each. At intervals of 5, 10 and 20 minutes the volumetric flasks were diluted to volume to stop the reaction by adding 0.2 M HCl. The absorbance of the solutions was measured using UV-Vis Varian and plotted against time of digestion.

#### ***5.2.3.4 Aqueous solubility of E:ASP***

A suspension of the **E:ASP** (172 mg) was stirred in 1.0 mL of distilled water in a sealed vial and placed in a water bath to maintain constant temperature. After stirring for 72 hrs, the remaining solid was filtered off. A 0.8 mL aliquot of the filtrate was diluted to 8.0 mL using methanol. After hydrolysis and quenching with HCl, absorbance of this solution was measured at 303 nm using UV-Visible spectroscopy and required dilutions were carried out to obtain a suitable absorbance value. The absorbance values were used to calculate the corresponding concentration from the equation of the calibration curve and thus the solubility of the co-crystals.

#### **5.2.4 Binding study of aspirin and 1,3,5-tris(imidazole-1-yl-methyl) benzene (A') using isothermal titration calorimetry**

Stock solutions for the calorimetric studies were prepared using purified deionized water in volumetric flasks. All experiments were conducted at 25 °C. The stir rate was set at 250 rpm

and the instrument was left to equilibrate for about 30 min. The experiment was set to incremental titration with discrete injections every 300 s for 25 injections. For titrations, the initial concentration of the tritopic acceptor **A'** was 1.20 mM and the concentration of aspirin were 0.150 mM. Data analysis and data fitting were conducted using NanoAnalyze,

## 5.3 Results and discussion

### 5.3.1 IR screening of solids resulting from solvent assisted grinding method

Attempted reactions between five acceptors and NSAIDs aspirin, ibuprofen, naproxen and diclofenac were characterized by analyzing solids resulting from solvent assisted ground mixtures, Table 5.3. In chapter 3, we observed that the effectiveness of a supramolecular synthon is directly related to the potential on the nitrogen of the acceptor site, where both imidazole and benzimidazole containing analogues had higher supramolecular yields. We observe the same trend in the ground mixtures with painkillers, where, imidazole and benzimidazole containing analogues possessing the characteristic peak pattern in the region of 1,900 and 2,500  $\text{cm}^{-1}$ , indicative of co-crystal formation. The O—H $\cdots$ N hydrogen bond formed between the acceptor and donor is further confirmed by the shift in the carbonyl stretch which appears in the 1,650-1,700  $\text{cm}^{-1}$  regions.

In the percentage success rate for acceptors, we observe the following trend where **A, E, D** >> **C, B**, Table 5.4, which is due to the higher electrostatic potential difference between acceptors containing imidazole and benzimidazole when compared with acceptors containing pyrazoles. When considering the drugs, we see that there is no significant difference in supramolecular yield for ibuprofen and diclofenac (4/5, 80%) and naproxen and aspirin (3/5, 60%); as drugs being weakly acidic ( $\text{pK}_a$  for ibuprofen 4.91, diclofenac 4.15, naproxen 4.15 and aspirin 3.49).



**Table 5.3** IR stretching frequencies ( $\text{cm}^{-1}$ ) of the solids produced by combining tritopic acceptors with ibuprofen, naproxen, aspirin, diclofenac

Mixture	Carbonyl stretch ( $\text{cm}^{-1}$ )		O---H .... N Stretch ( $\text{cm}^{-1}$ )	Co-crystal
	Drug	Ground mixture		
<b>A-IBU</b>	1708	1706	1905, 2435	Y
<b>A-NAP</b>	1724	1709	1929, 2440	Y
<b>A-ASP</b>	1680	1700	1940, 2466	Y
<b>A-DCF</b>	1689	1688	1932, 2559	Y
<b>B-IBU</b>	1708	1711	1907, 2562	Y
<b>B-NAP</b>	1724	1724	-	N
<b>B-ASP</b>	1680	1677	-	N
<b>B-DCF</b>	1689	1689	-	N
<b>C-IBU</b>	1708	1714	-	N
<b>C-NAP</b>	1724	1724	-	N
<b>C-ASP</b>	1680	1683	-	N
<b>C-DCF</b>	1689	1690	1886, 2596	Y
<b>D-IBU</b>	1708	1702	1895, 2485	Y
<b>D-NAP</b>	1724	1724	1922, 2443	Y
<b>D-ASP</b>	1680	1692	1914, 2485	Y
<b>D-DCF</b>	1689	1690	1907, 2553	Y
<b>E-IBU</b>	1708	1705	1909, 2479	Y
<b>E-NAP</b>	1724	1730	1919, 2461	Y
<b>E-ASP</b>	1680	1703	1914, 2469	Y
<b>E-DCF</b>	1689	1691	1929, 2510	Y

**Table 5.4** Co-crystal formation with ibuprofen, naproxen, aspirin, diclofenac and A-E

Acceptor	Potential on N (kJ/mol)	Grinding experiments with NSAIDs	
		Success rate	Supramolecular yield (%)
<b>A</b>	-229	4/4	100
<b>E</b>	-212	4/4	100
<b>D</b>	-204	4/4	100
<b>B</b>	-187	1/4	25
<b>C</b>	-173	1/4	25

When subjected to slow evaporation in acetonitrile, out of the 20 combinations, only **E** and **ASP** produced two different crystal morphologies one of which was suitable for X-ray diffraction, Figure 5.6.

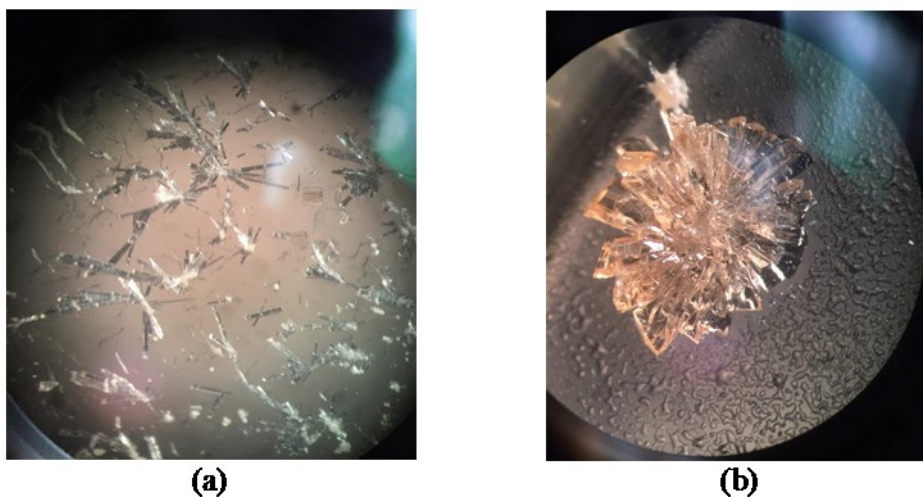


**Figure 5.6** Two unique morphologies of **E** and **ASP** (a) ribbon-like and (b) columnar-like crystals

### 5.3.2 Crystal structure of $\text{EH}^+:\text{ASP}^-:(\text{ASP})_2$

X-ray diffraction data were obtained on the orangish columnar like crystal, Figure 5.6 (b). The asymmetric unit of the attempted co-crystallization of **ASP** and **E** contains one monocation of **E**, 2-carboxyphenolate and two neutral molecules of salicylic acid, Figure 5.7.

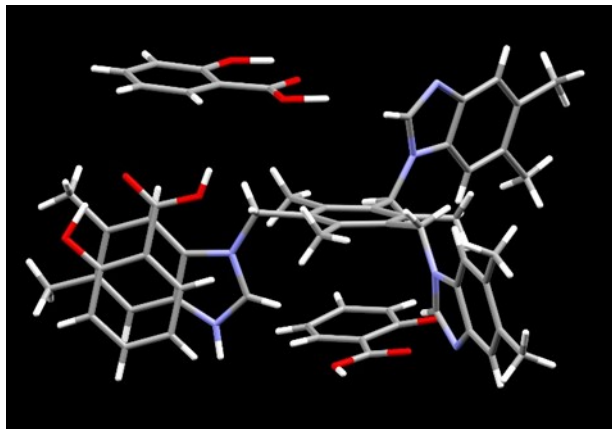


**Figure 5.7** Asymmetric unit of the crystal resulting from  $\text{EH}^+:\text{ASP}^-:(\text{ASP})_2$

The main feature observed in the assembly is a discrete tetramer built around a centrosymmetric  $(\text{bzim})\text{N}-\text{H}^+\cdots\text{N}/\text{N}\cdots+\text{H}-\text{N}(\text{bzim})$  hydrogen bonded homo-synthon, which is then extended via two symmetry related  $\text{O}-\text{H}\cdots\text{N}(\text{bzim})$  hydrogen bonds, Figure 5.8.

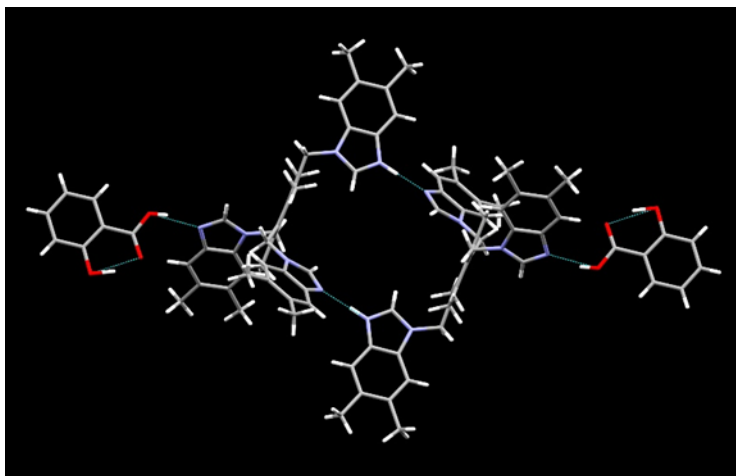


**Figure 5.8** Tetramer in the crystal structure of  $\text{EH}^+:\text{ASP}^-:(\text{ASP})_2$

Furthermore, in the crystal structure there are two types of dimers that are formed. The first dimer is observed between two 2-carboxyphenolate ions which are encapsulated within the centrosymmetric cavity formed by the two acceptor molecules, Figure 5.9 (a). The second dimer is observed between two salicylic acid molecules which is stacked between two discrete tetramers, Figure 5.9 (b).

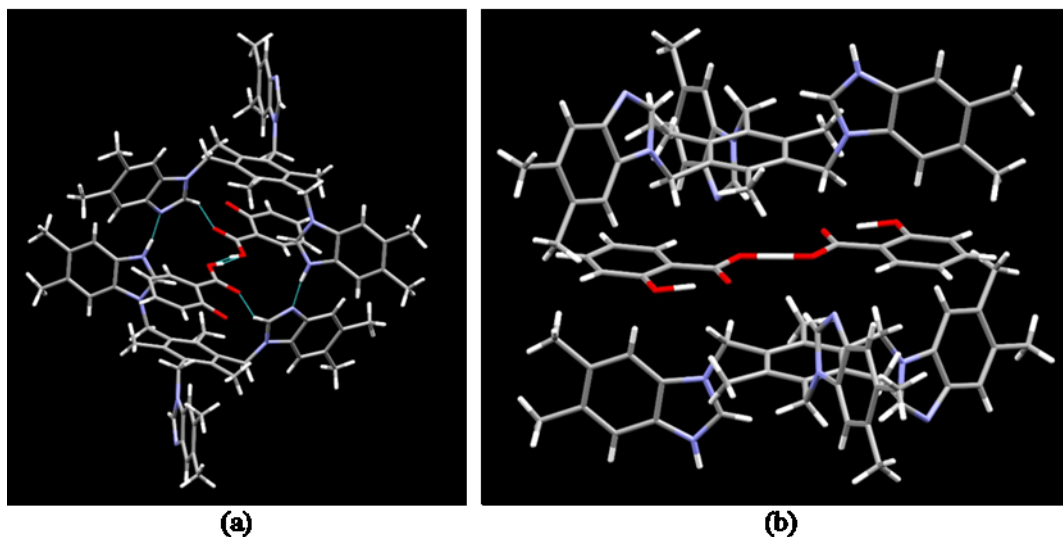


**Figure 5.9** Dimers formed between (a) 2-carboxyphenolate ions (b) salicylic acids

From the crystallographic data it is evident that the column like crystals are of a 3:1 stoichiometric ratio between aspirin and **E**.

### 5.3.3 $^1\text{H}$ NMR of solid resulting from slow evaporation

To determine the composition of the ribbon-like crystal, Figure 5.6 (a), we subjected a portion of the crystal to  $^1\text{H}$  NMR. The NMR of the crystals was found to be a 1:1 stoichiometry between aspirin and acceptor **E**, Figure 5.10. This cannot confirm the formation of a co-crystal between aspirin and acceptor **E** since a 1:1 physical mixture of the two compounds would produce

the same result. Therefore, to confirm the formation of a O—H···N hydrogen bond between aspirin and **E**, IR of the crystals is required.

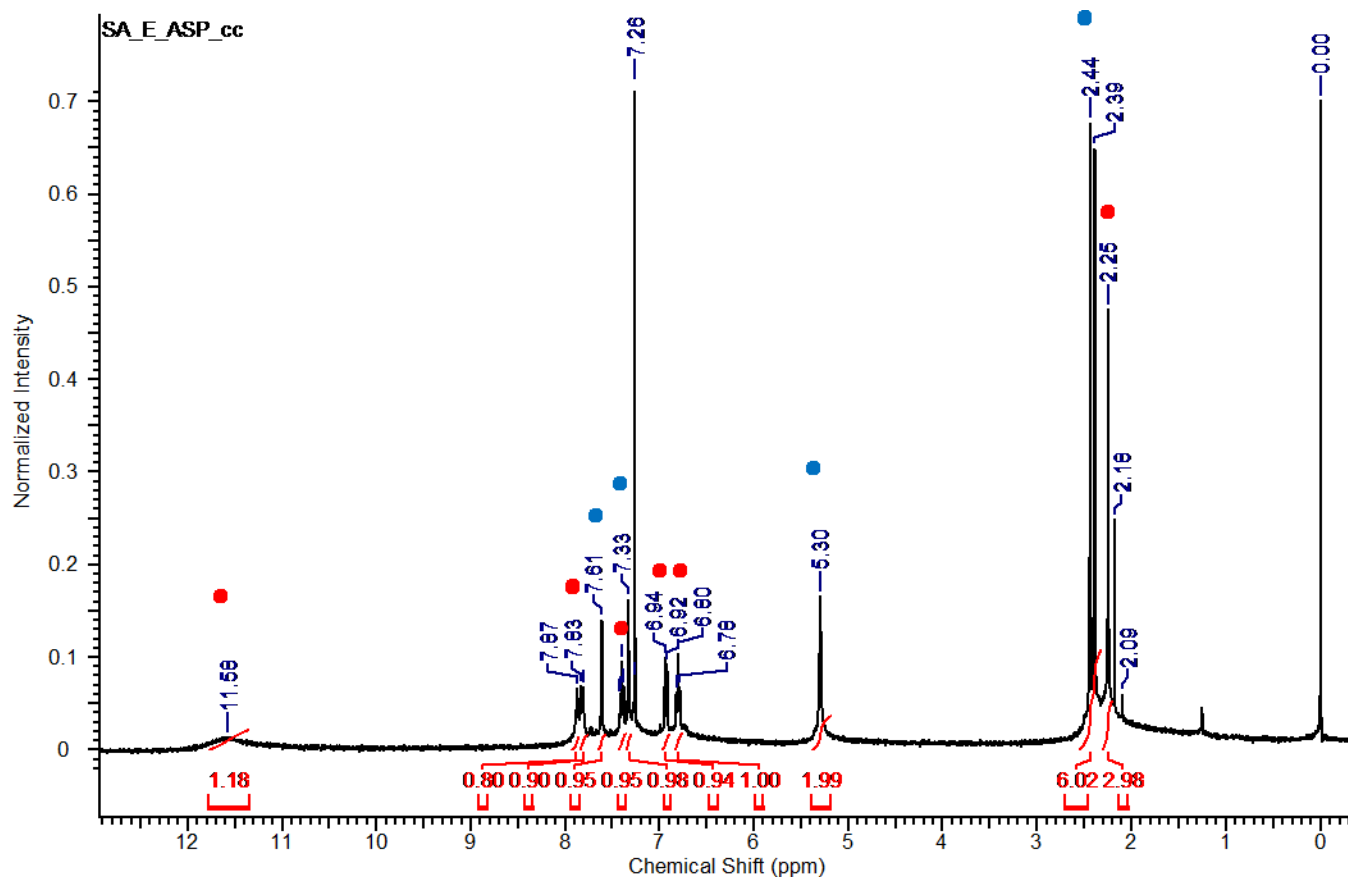


**Figure 5.10**  $^1\text{H}$  NMR of ribbon-like crystal, where peaks denoted in red correspond to aspirin and peaks in cyan correspond to acceptor **E**

### 5.3.4 IR and PXRD data analysis of solids resulting from solvothermal method and slow evaporation method

IR spectroscopy was used in the initial screening phase of co-crystals synthesized using solvothermal technique. Herein the IR spectrum of the resulting solid was compared with the IR spectrum of the co-crystal **E**:ASP, Figure 5.11. The following, Figure 5.12, depicts the overlaid IR spectra of **E**:ASP and **EH**<sup>+</sup>:ASP·:(ASP)<sub>2</sub>.

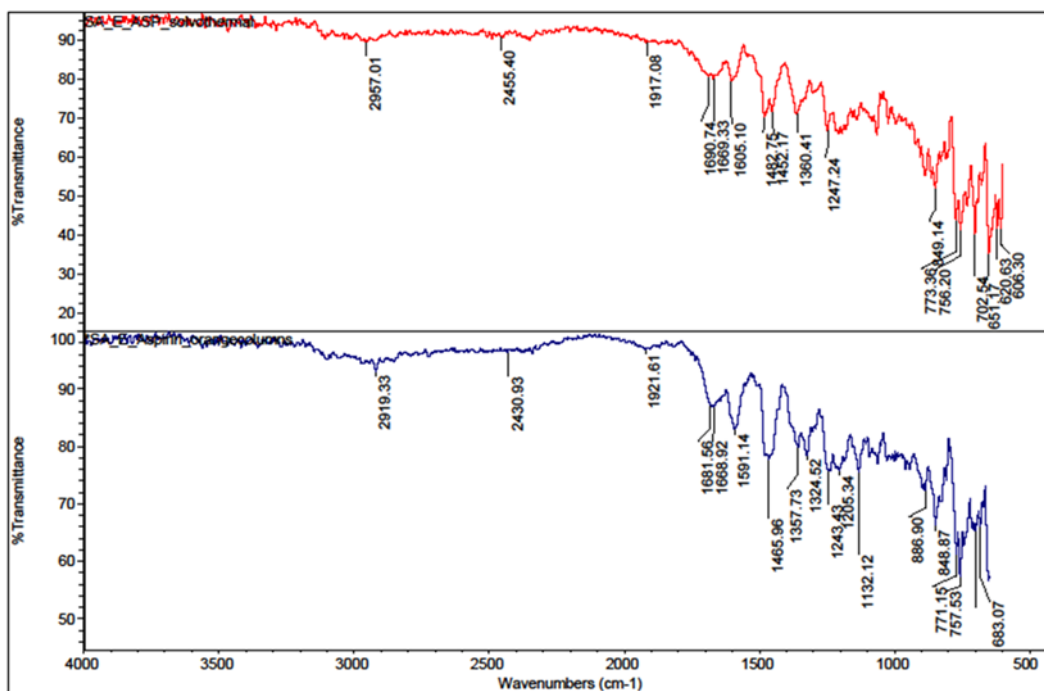


Figure 5.11 Top is the IR spectrum of **E:ASP** prepared from a solvothermal method and the bottom is the IR spectrum for single crystal of **E:ASP**

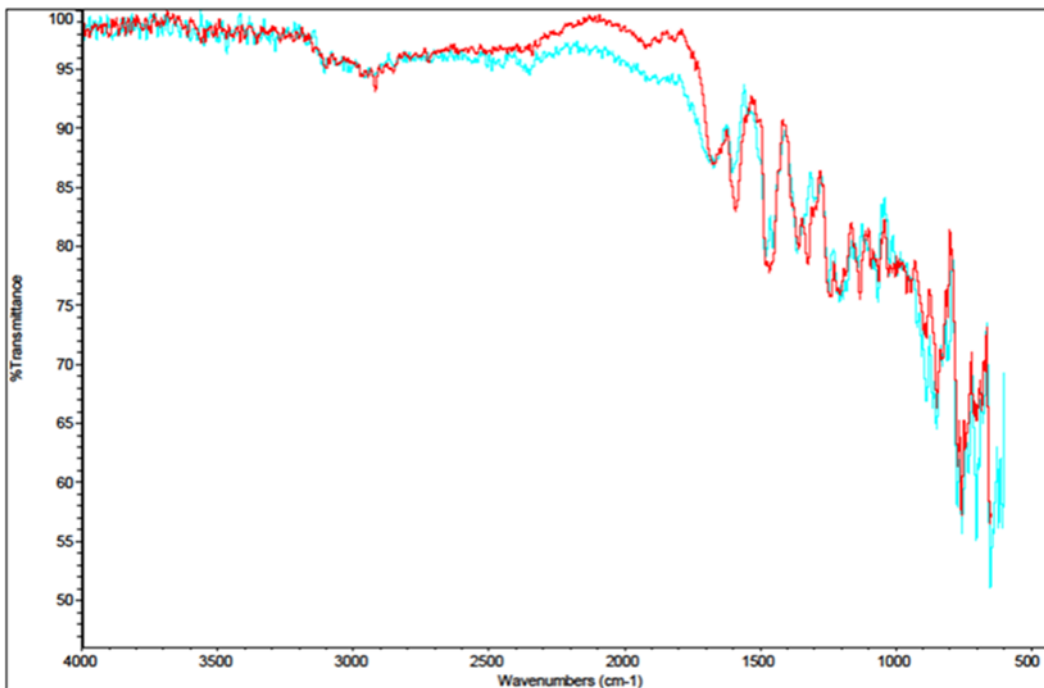
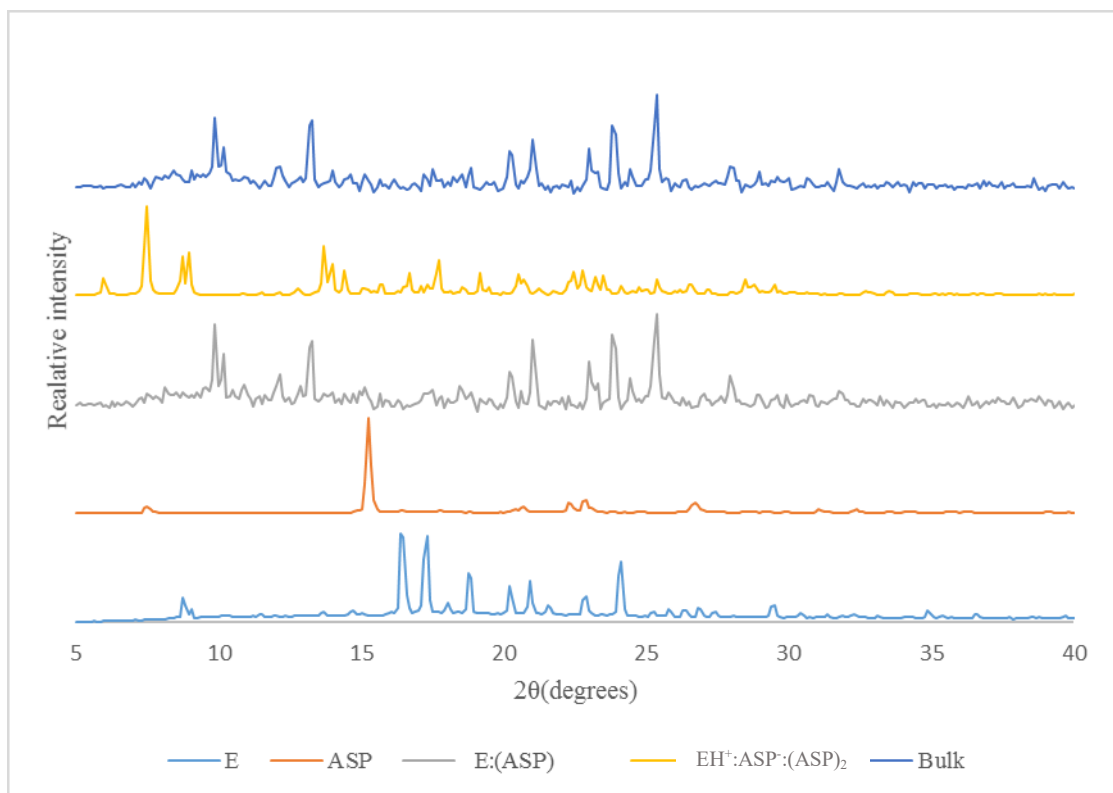


Figure 5.12 Overlaid IR spectra of crystals resulting from slow evaporation of **E:ASP** in red and **EH<sup>+</sup>:ASP:(ASP)<sub>2</sub>** in cyan

IR spectrums of bulk resulting from solvothermal method, **E:ASP** and **EH<sup>+</sup>:ASP<sup>-</sup>:(ASP)<sub>2</sub>** contain the characteristic double hump in the region of 1,900 and 2,500 cm<sup>-1</sup> indicative of O—H···N hydrogen bond formation. This affirms the formation of two unique compounds containing aspirin and **E**.

In Figure 5.11, we would expect to see the presence of a C—O- stretching at around 1,280 cm<sup>-1</sup> corresponding to the 2-carboxyphenolate ion in **EH<sup>+</sup>:ASP<sup>-</sup>:(ASP)<sub>2</sub>**, Figure 5.7, but instead, what we see is two peaks present at 1,247 and 1,243 cm<sup>-1</sup> for prepared bulk and **EH<sup>+</sup>:ASP<sup>-</sup>:(ASP)<sub>2</sub>** which are indicative of the presence of C—OH stretching (phenolic C—OH stretch 1,249 cm<sup>-1</sup>).<sup>13</sup> What we also observe in the IR is symmetric and antisymmetric carboxylate stretching modes which are typically found in the 1,400 and 1,600 cm<sup>-1</sup> ranges.<sup>14</sup>

Despite IR spectrometry being useful for establishing formation of a co-crystal, it does not provide sufficient evidence for homogeneity of the co-crystal solid which is imperative when carrying out solubility experiments. Therefore, to affirm structural homogeneity in the solid prepared using a solvothermal method, a PXRD was obtained of the resulting solid. It was then compared to the PXRD patterns of both aspirin and **E** to verify the absence of pure **E** and aspirin in the solid, Figure 5.13. It is evident from the powder patterns that the solid prepared using a solvothermal method is in fact **E:ASP**.



**Figure 5.13** Overlaid powder patterns of **E**, **ASP**, **E:ASP**, simulated **EH<sup>+</sup>:ASP<sup>-</sup>:(ASP)<sub>2</sub>** and bulk (resulting from solvothermal method)

### 5.3.5 <sup>1</sup>H NMR and DSC data analysis of solid resulting from solvothermal method

IR spectra and PXRD patterns provide evidence of formation of co-crystals and the homogeneity of the resulting bulk material, but none of the characterization methods discussed above provide evidence of stoichiometric ratio between acceptor and donor.

To accurately measure the solubility of **E:ASP**, the stoichiometry of the resulting bulk material is essential. Therefore, an NMR of the product resulting from solvothermal method was obtained and found to be a 1:1 stoichiometry between aspirin and acceptor **E**, Figure 5.14. The same was true for the single crystal **E:ASP** which is a 1:1 stoichiometry based on <sup>1</sup>H NMR.



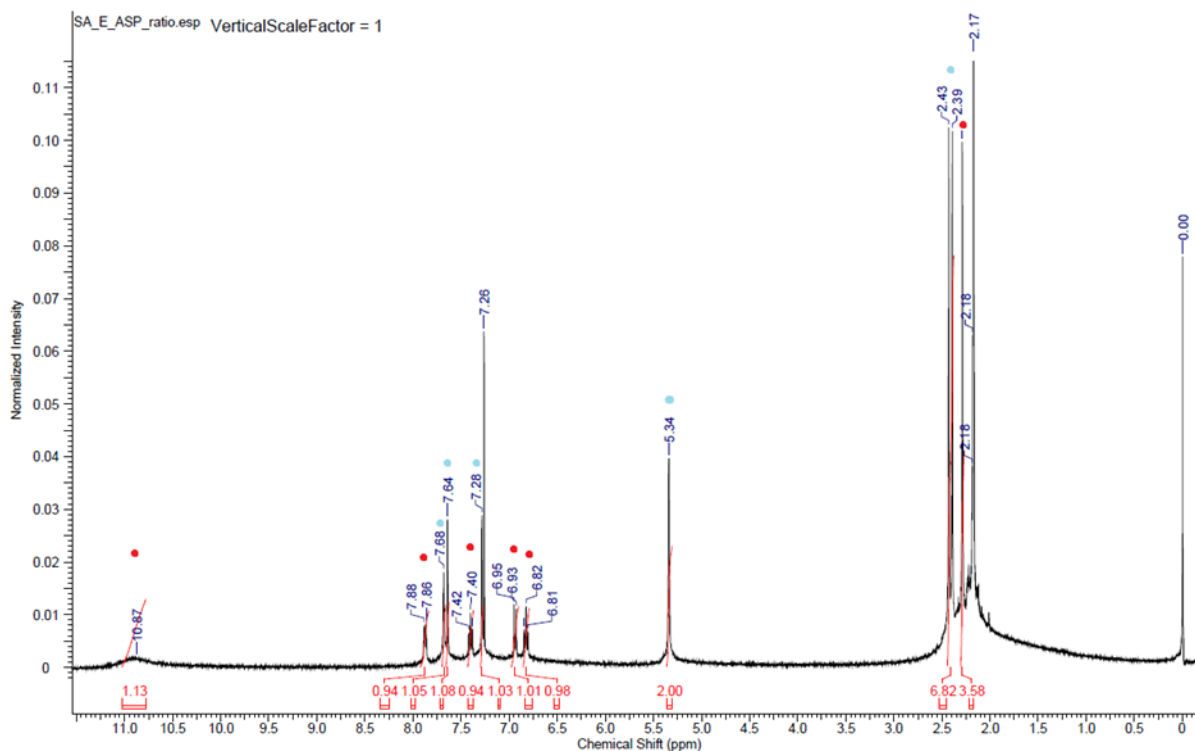


**Figure 5.14**  $^1\text{H}$  NMR of bulk **E:ASP**, where peaks denoted in red correspond to aspirin and peaks in cyan correspond to acceptor **E**

Differential scanning calorimetric studies were performed on acceptor **E**, aspirin and the resulting bulk material to further affirm the formation of a co-crystal. Acceptor **E** melts at a temperature of 292-294 °C (Lit value > 285 °C)<sup>15</sup> when subjected to a heating rate 5 °C/min while aspirin melts at 130-132 °C at a heating rate of heating rate of 0.2 °C/min (Lit value > 135.5 °C)<sup>16</sup>. The solid resulting from the solvothermal method possess melts at temperature of 217-219 °C, Figure 5.15.

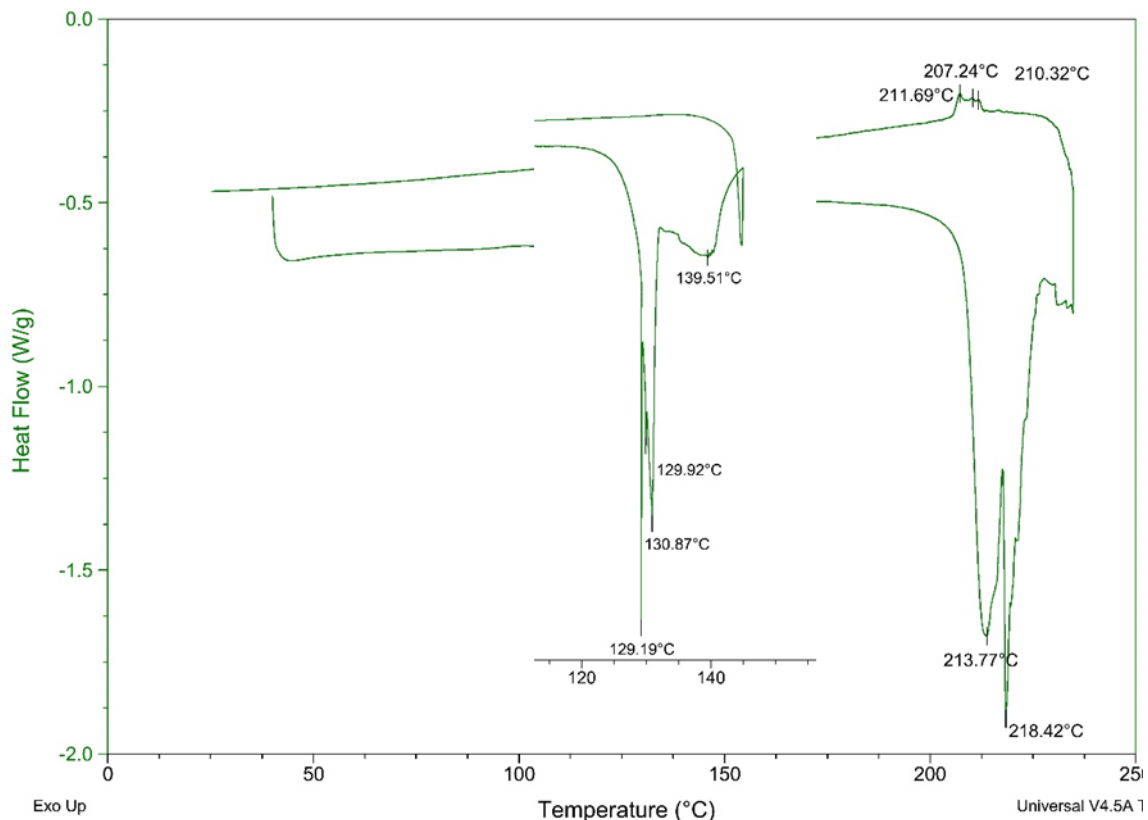


**Figure 5.15** DSC thermograms for bulk solid **E:ASP** and aspirin by itself

### 5.3.6 Isothermal calorimetry

To analyze thermodynamic parameters like enthalpy change ( $\Delta H$ ), entropy change ( $\Delta S$ ), which can be further resolved into Gibb free energy change ( $\Delta G$ ) of the system, water soluble tritopic acceptor 1,3,5-tris(imidazole-1-yl-methyl) benzene (**A'**) was titrated into aspirin, Figure 5.16.

Unlike **A'**, acceptor **E** is very poorly soluble in water. To evaluate thermodynamic properties and binding ability to aspirin, a more soluble analogue containing imidazole was used. The binding resulted in a stoichiometry of 1:3 between **E** and **ASP**.

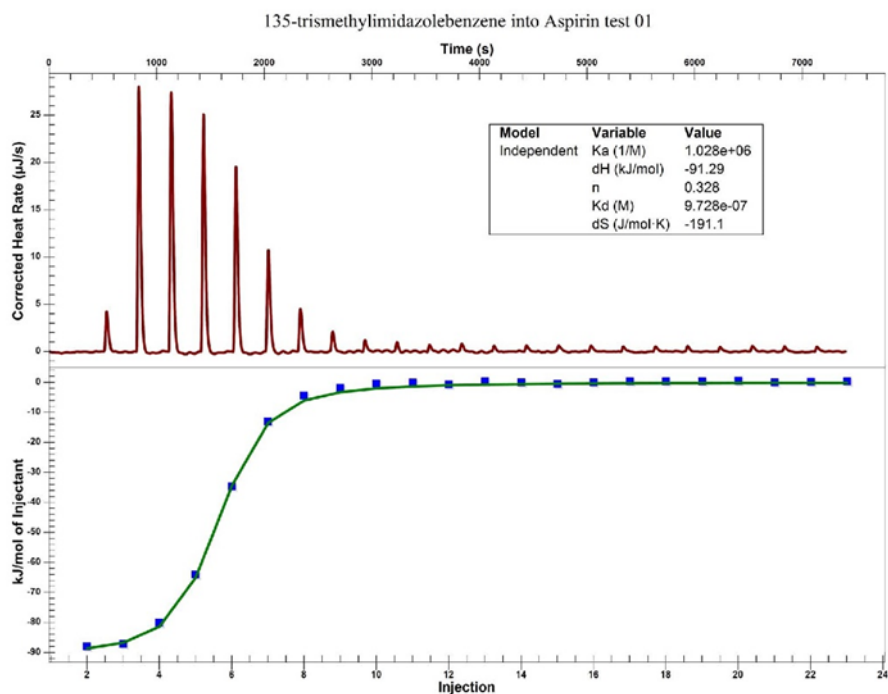


**Figure 5.16** ITC profile between **A'** (1.20 mM) and aspirin (0.150 mM) at 25°C

In the solid state, we observed that **E** and **ASP** could be present in two distinct solid compositions. The two solid constitutes a 1:1 and a 1:3 stoichiometry between **E** and **ASP**. Even though  $\text{EH}^+:\text{ASP}:(\text{ASP})_2$  has an anticipated ratio between acceptor and donor, the much-desired  $\text{O—H}\cdots\text{N}$  hydrogen bond connectivity between acceptor and donor is not observed. This observation is also seen in Chapter 3, where the attempts made to engineer desired connectivity between acceptor and donor were hampered by the conformational freedom of **E**.

### 5.3.7 Aqueous solubility of co-crystal

Official method described in the British Pharmacopeia for analysis of aspirin in tablet formulations are based on direct titration of salicylic acid formed during hydrolysis of the drug. But, a new method was developed by Dutta and co-workers<sup>17</sup> using UV spectrophotometric assay of aspirin, based on the marked increase in absorbance at 303 nm that takes place during alkaline

hydrolysis of aspirin, Figure 5.17. The increase in absorbance is due to the formation of salicylic acid, which has an absorption maximum at 303 nm, Figure 5.18.

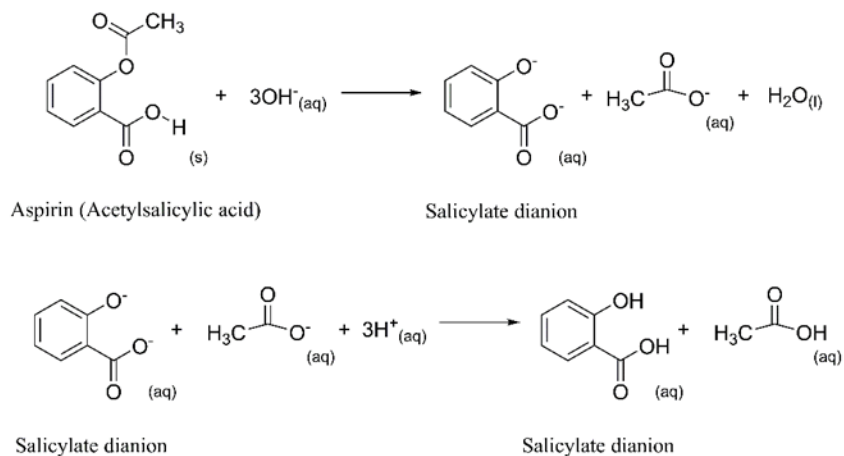


**Figure 5.17** Alkaline hydrolysis of aspirin followed by acidification resulting in salicylic acid

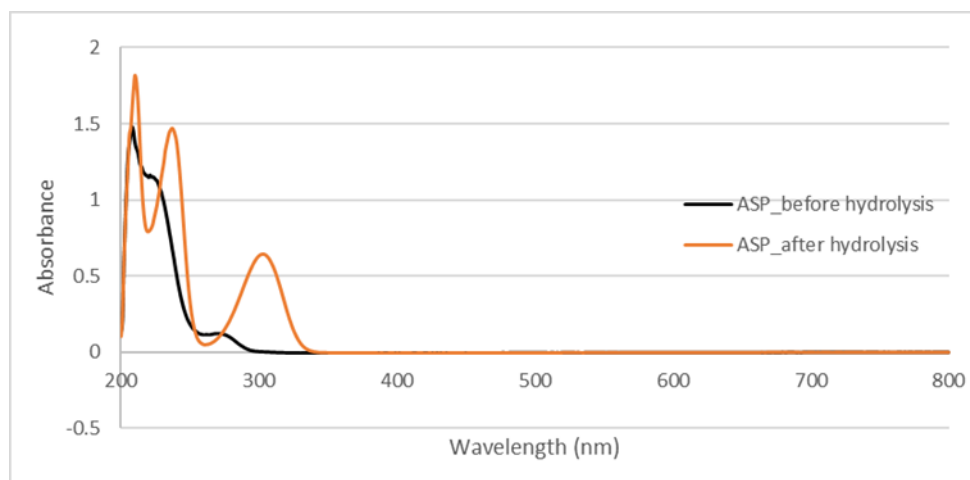


**Figure 5.18** Ultraviolet absorption spectra of aspirin in acidic solution before (black) and after (orange) hydrolysis

To evaluate the time taken to fully hydrolyze aspirin into salicylic acid, a time dependent study was performed. At different time intervals, aspirin samples in alkaline solutions were quenched by acidification. Effect of time on aspirin hydrolysis was monitored by observing change

in absorbance at 303 nm. Throughout the selected time interval, absorbance remained at 303 nm indicating the hydrolysis was quick, Figure 5.19.

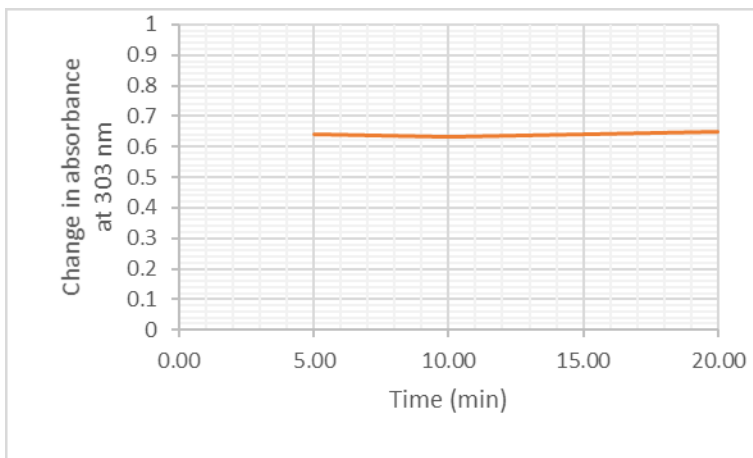


**Figure 5.19** Effect of time on aspirin hydrolysis

Data obtained from the standard series prepared using salicylic acid was measured at 303 nm using UV-Vis spectrophotometer, to determine the unknown concentration of aspirin in the co-crystal, Figure 5.20.

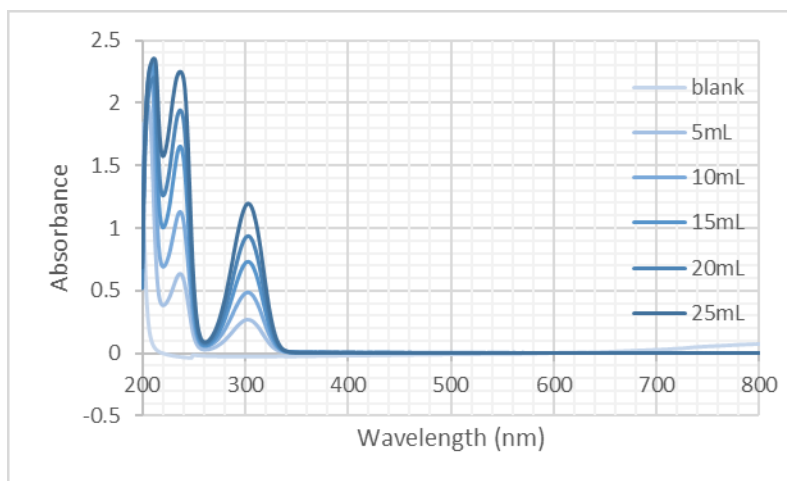


**Figure 5.20** Absorption maxima at 303 nm for salicylic acid at different concentrations

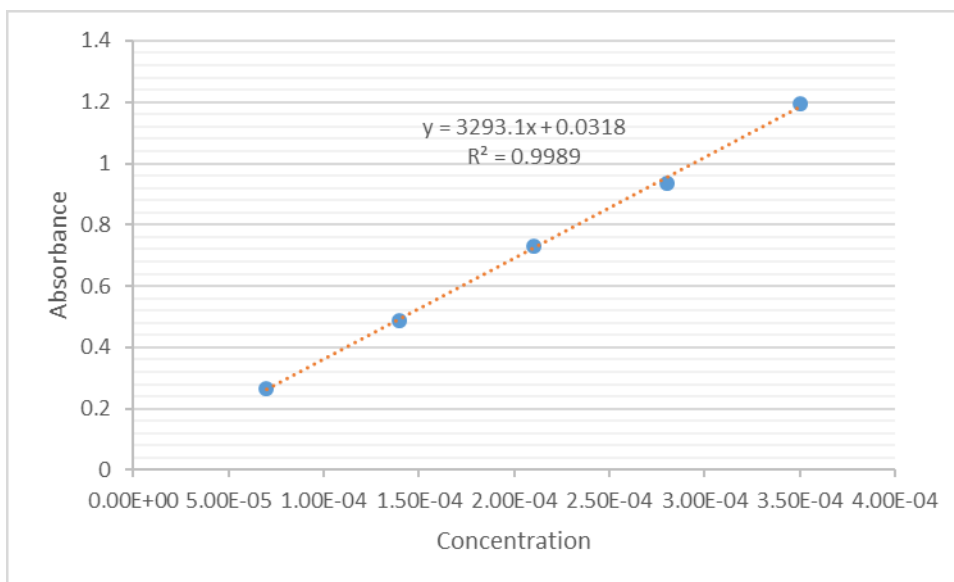


**Figure 5.21** Absorption vs concentration plot of salicylic acid

With the equation of the best fit line using the calibration curve, Figure 5.21, data was used to calculate the concentration (solubility) of the co-crystal. The solubility measurements of co-crystals were carried out for 72 hrs. The solubility of aspirin in the co-crystal was 0.246 mg/mL ( $\pm 0.010$  mL). This is a 12-time reduction of aqueous solubility of aspirin at room temperature which is 3 mg/mL. According to Table 5.1, aspirin falls under very soluble category. Upon co-crystal formation, the solubility descriptor changes to freely soluble.

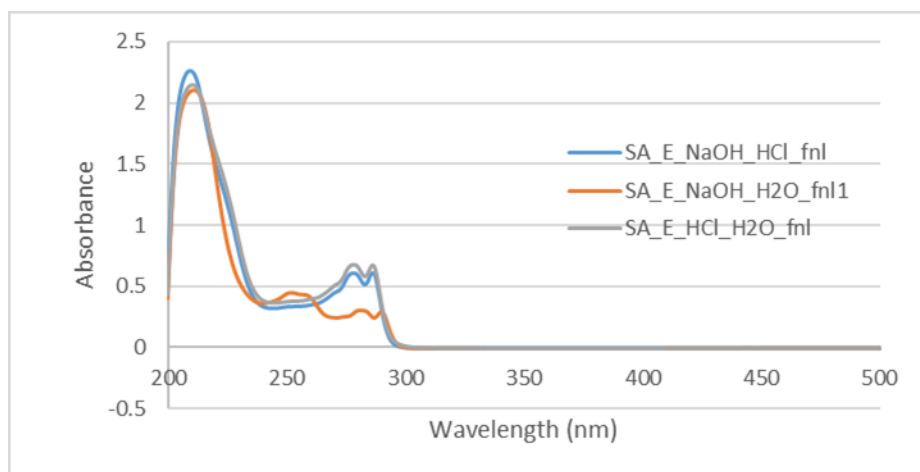


**Figure 5.22** Control experiment of acceptor E

To further confirm that the tritopic acceptor **E** posed no discrepancies to the absorption maxima of salicylic acid, several control experiments were done, Figure 5.22. Initially, **E** was subjected alkaline hydrolysis followed by quenching with acid. Second control experiment subjecting **E** to alkaline hydrolysis followed by diluting with water. Third control experiment included acidifying **E** followed by diluting with water. When comparing these spectrums with before and after hydrolysis of aspirin, it is clear that the regions do not overlap and the maxima at 302 nm can easily be distinguished, Figure 5.23. Furthermore, acceptor **E** is poorly soluble in water and the absence of absorption peak in the region of 281 – 290 nm suggests only aspirin dissolves in water.

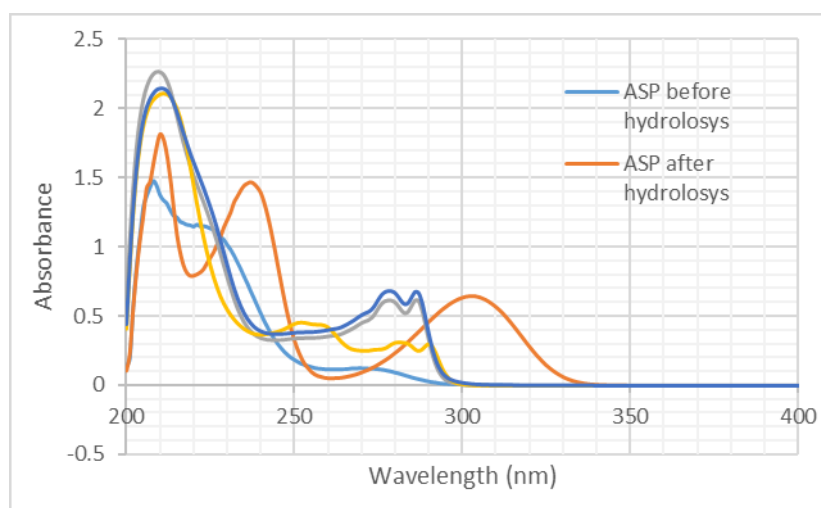


**Figure 5.23** Control experiment of acceptor **E** compared with before and after hydrolysis of aspirin

## 5.4 Conclusions

We have demonstrated that by targeting the COOH moiety of the NSAIDs, we were able to synthesis co-crystals with five tritopic acceptors. It was evident that electrostatically more prominent imidazole and benzimidazole could react with higher supramolecular yield. There seems to be such a disparity between imidazolic family and pyrazoles, when a hydrogen bond is

formed with the nitrogen site. Pyrazole, unlike imidazole or benzimidazole, cannot stabilize through inductive effects. On the other hand, there is no noticeable difference in supramolecular yield for the NASIDs due to their weak acidic character ( $pK_a$  ranging from 3.49 – 4.91).

Slow evaporation yielded two different solids, which constituted **E** and aspirin in a 1:1 and a 1:3 stoichiometry, respectively. When a solution phase study was conducted using **A'**, a similar analogue of **E**, a 1:3 binding between **E** and aspirin was noted which reflects what is discerned in the solid state.

The bulk synthesis of **E** and **ASP** delivered a stoichiometry of 1:1 between acceptor and donor. The bulk material was characterized using IR, PXRD,  $^1\text{H}$  NMR and DSC, in order to confirm the formation of a co-crystal, its homogeneity and composition.

The solubility of the 1:1 co-crystal decreased by 12-fold compared to pure aspirin (3mg/mL at 20 °C), which would be beneficial to use as an extended release drug. Such a low solubility in the co-crystal may be attributed to the low aqueous solubility of the co-former **E**.

## 5.5 References

1. (a) *Biopharmaceutical Research Industry Profile*; 2016; (b) Qiao, N.; Li, M.; Schlindwein, W.; Malek, N.; Davies, A.; Trappitt, G., Pharmaceutical cocrystals: An overview. *Int. J. Pharm.* **2011**, *419* (1-2), 1-11; (c) Aakeröy, C. B.; Forbes, S.; Desper, J., Using Cocrystals To Systematically Modulate Aqueous Solubility and Melting Behavior of an Anticancer Drug. *J. Am. Chem. Soc.* **2009**, *131* (47), 17048-17049.
2. Blagden, N.; de Matas, M.; Gavan, P. T.; York, P., Crystal engineering of active pharmaceutical ingredients to improve solubility and dissolution rates. *Adv. Drug Deliv. Rev.* **2007**, *59* (7), 617-630.
3. Aakeröy, C. B. From molecular sociology via structural chemistry to functional materials 2016, p. 1-7.



4. Lu, J.; Rohani, S., Preparation and Characterization of Theophylline–Nicotinamide Cocrystal. *Org. Process Res. Dev.* **2009**, *13* (6), 1269-1275.
5. Schultheiss, N.; Newman, A., Pharmaceutical Cocrystals and Their Physicochemical Properties. *Cryst. Growth Des.* **2009**, *9* (6), 2950-2967.
6. Friedman, D.; Besonov, A.; Tamarkin, D.; Eini, M., Vasoactive kit and composition and uses thereof. Google Patents: 2008.
7. Wu, C.-Y.; Benet, L. Z., Predicting Drug Disposition via Application of BCS: Transport/Absorption/ Elimination Interplay and Development of a Biopharmaceutics Drug Disposition Classification System. *Pharm. Res.* **2005**, *22* (1), 11-23.
8. Ricciotti, E.; FitzGerald, G. A., Prostaglandins and Inflammation. *Arterioscler. Thromb. Vasc. Biol.* **2011**, *31* (5), 986-1000.
9. Meek, I. L.; Van de Laar, M. A. F. J.; E. Vonkeman, H., Non-Steroidal Anti-Inflammatory Drugs: An Overview of Cardiovascular Risks. *Pharmaceuticals* **2010**, *3* (7), 2146-2162.
10. Bua, S.; Di Cesare Mannelli, L.; Vullo, D.; Ghelardini, C.; Bartolucci, G.; Scozzafava, A.; Supuran, C. T.; Carta, F., Design and Synthesis of Novel Nonsteroidal Anti-Inflammatory Drugs and Carbonic Anhydrase Inhibitors Hybrids (NSAIDs–CAIs) for the Treatment of Rheumatoid Arthritis. *J. Med. Chem.* **2017**, *60* (3), 1159-1170.
11. Abraham, M. H.; Acree, W. E., The solubility of liquid and solid compounds in dry octan-1-ol. *Chemosphere* **2014**, *103*, 26-34.
12. Nehm, S. J.; Rodríguez-Spong, B.; Rodríguez-Hornedo, N., Phase Solubility Diagrams of Cocrystals Are Explained by Solubility Product and Solution Complexation. *Cryst. Growth Des.* **2006**, *6* (2), 592-600.
13. Pinchas, S., The C-O stretching frequency of hydrated isotopic phenolate ions. *Spectrochim. Acta A.* **1972**, *28* (4), 801-802.
14. Oomens, J.; Steill, J. D., Free Carboxylate Stretching Modes. *J. Phys. Chem. A* **2008**, *112* (15), 3281-3283.
15. Aakeröy, C. B.; Smith, M.; Desper, J., Finding a single-molecule receptor for citramalic acid through supramolecular chelation. *Can. J. Chem.* **2015**, *93* (8), 822-825.
16. Hughes, L. D.; Palmer, D. S.; Nigsch, F.; Mitchell, J. B. O., Why Are Some Properties More Difficult To Predict than Others? A Study of QSPR Models of Solubility, Melting Point, and Log P. *J. Chem. Inf. Model.* **2008**, *48* (1), 220-232.
17. A.K. Sanyal, A. D., Rapid and Selective Ultraviolet Spectrophotometric Assay of Aspirin in Complex Tablet Formulations. *Journal of AOAC International* **1992**, 1303-1306.

# Chapter 6 - A take on Tröger's base as a potential hydrogen and halogen bond acceptors and donors

## 6.1 Introduction

The stoichiometry of two components forming a co-crystal depends on the delicate balance between shape, size, and functional complementarities. An understanding of molecular recognition and self-assembly is vital in the development of new strategies for crystal growth with tailored stoichiometries. With a flexible tritopic acceptor, we saw in Chapters 3 and 4 that not all acceptor sites were occupied in the resulting supramolecules. Therefore, an additional arm does not necessarily provide useful intermolecular interactions for multi-topic hydrogen and halogen bond donors, and here we intend to look into a new molecule which is much less flexible and has fewer potential binding sites, in order to better control stoichiometry.

Tröger's base, 2,8-dimethyl-6H-12H-5,11-methanodibenzo[b,f][1,5]diazocine, was originally prepared in 1887 using p-toluidine,<sup>1</sup> Figure 6.1. Spielman<sup>2</sup> deduced the structure of this molecule in 1935, while Wagner<sup>3</sup> proposed a mechanism of formation. Prelog<sup>4</sup> recognized the chiral nature of Tröger's base and was able to chromatographically separate its enantiomers using lactose as the chiral stationary phase. Nearly a century after the synthesis of the molecule, the structure was confirmed by single crystal X-ray crystallography.<sup>5</sup> Until 1980s, Tröger's base was mainly used for the evaluation of new separation techniques. The revival of Tröger's bases started in 1985 by Wilcox with a series of publications which included a “torsion balance”<sup>6</sup> that can measure the strength of intermolecular interactions.

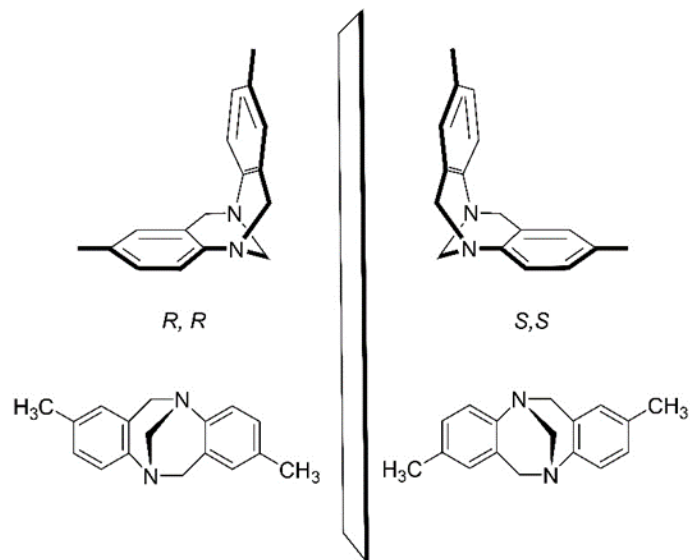


**Figure 6.1** Tröger's base showing its two enantiomers

Tröger's base consists of a bicyclic aliphatic unit, a diazocine ring fused with two aromatic rings, Figure 6.2. The centrosymmetric methanodiazocine ring extends the aromatic rings in a near perpendicular manner. As a result, this creates a hydrophobic v-shaped cavity. Due to the rigidity of the molecule, both N-atoms (stereogenic centers) are sterically fixed. This makes the molecule dissymmetric and therefore chiral. This conformational rigidity makes it almost an ideal building block to introduce curvature into larger molecules. Therefore, this is of great importance in supramolecular chemistry to achieve concave structures in molecular assemblies such as receptors.

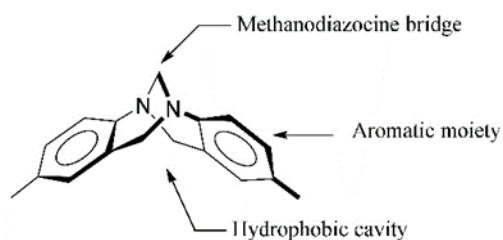


**Figure 6.2** Tröger's base depicting its main moieties and possible adaptable locations

Tröger's base derivatives are usually formed by reaction of an aniline, formaldehyde and a strong acid.<sup>7</sup> The formation of the methano[1,5]diazocine skeleton of Tröger's base involves an electrophilic substitution reaction. Aromatic amines with various electrophilic reactive centers can promote polymerization. To inhibit polymerization, it is necessary for the aniline derivative to have the para position blocked, Figure 6.3. In principle, the starting aniline can be fully substituted except for one ortho position which is required for the desired cyclization reaction of Tröger's base. The electronic and steric effects of the ring substituents are known to influence the regiochemistry<sup>8</sup> and yield.

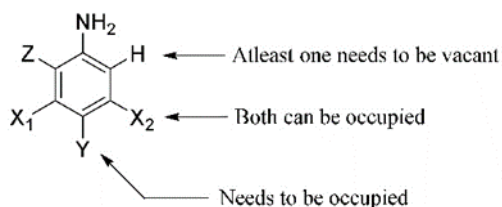


**Figure 6.3** Aniline substitution for Tröger's base synthesis

In this chapter, we are focusing on synthesizing a precursor for the 2,8-disubstituted analogues of Tröger's bases: the 2,8-diiodo-substituted derivative, Figure 6.4. It has been argued that the Tröger's bases condensation reaction is hampered by the electronic requirement of the aniline and that reactions work best with electron rich anilines.

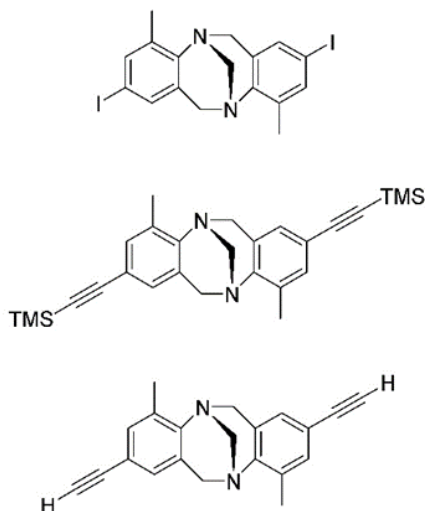


**Figure 6.4** Main precursors of 2,8-disubstituted analogues of Tröger's bases

However, Wärnmark and co-workers were able to synthesize halo substituted analogues of Tröger's base using paraformaldehyde, trifluoroacetic acid and a corresponding aniline,<sup>8</sup> Figure 6.5. Although the synthesis was successful, it is very sensitive to reaction conditions, especially the scale. The reaction generally works best with 4-halo-2-methylanilines due to the electron donating character of the substituted methyl group facilitating the electrophilic aromatic substitution, which is a part of the formation mechanism.

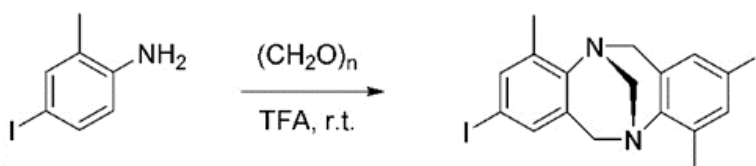


**Figure 6.5** 2,8-Diiodo substituted Tröger's base analogue synthesized by Wärnmark and co-workers

Having 2,8-diiodo substituted Tröger's base as a starting point, a whole new spectrum of transition-metal catalyzed cross coupling reactions are available, from which we will use Sonogoshira type coupling reactions for the synthesis of the following analogues, Figure 6.6.

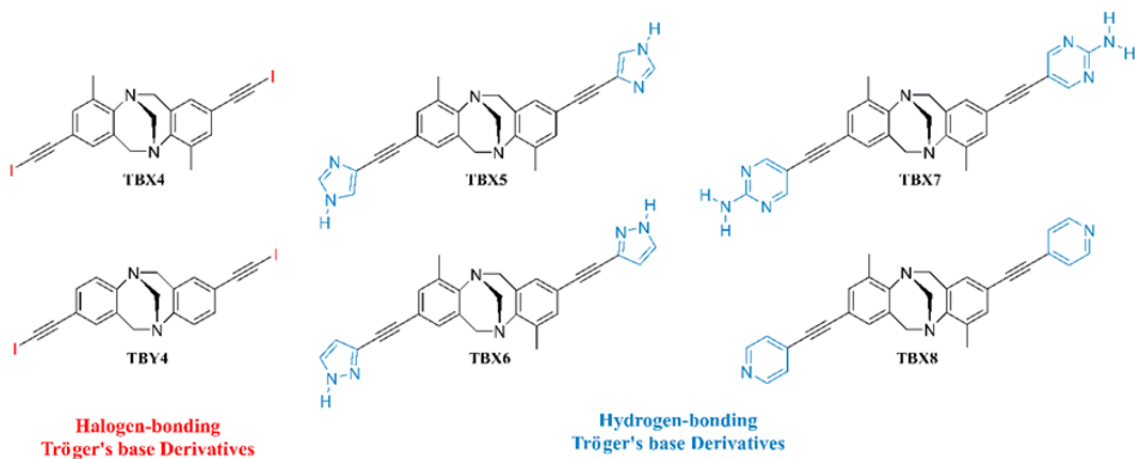


**Figure 6.6** Targeted Tröger's base halogen bond donors and hydrogen bond acceptors

In the previous chapters, aliphatic dicarboxylic acids were used as co-formers with tritopic scaffolds that contain imidazolic, benzimidazolic and pyrazolic arms and they did not produce desired supramolecular architectures. Thus, we wanted to see if the same imidazolic, benzimidazolic and pyrazolic arms could be utilized with a different scaffold, the Tröger's base, using the same aliphatic dicarboxylic acids as co-formers. We also wanted to explore the complementarity of halogen-bonding Tröger's bases by using symmetric ditopic heterocycles, Figure 6.7.

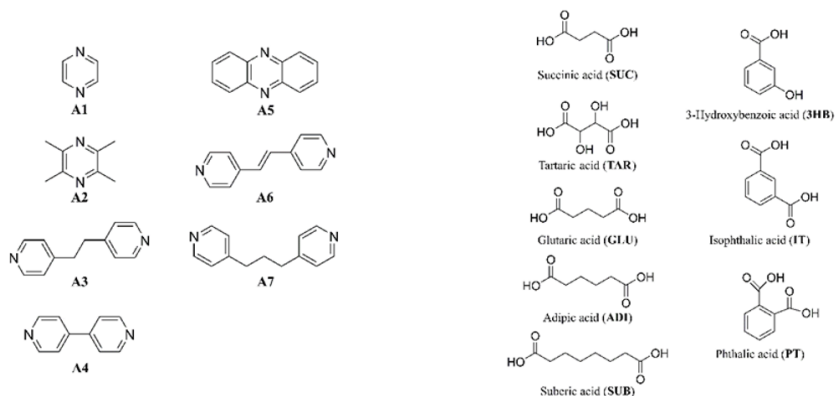


**Figure 6.7** Co-formers used in the study; symmetric ditopic acceptors and aliphatic dicarboxylic acids

Considering the spatial arrangement of the functional groups in halogen and hydrogen bonding Tröger's bases, we hope to predict their main structural features.

The structural outcome of these analogues depends on; 1) the highly directional halogen bond, 2) co-formers used, and 3) the dihedral angle between the aromatic rings, Figure 6.8. A CSD search shows that the dihedral angle  $\Theta$  is usually is in the range of  $88^\circ$ - $105^\circ$  for Tröger's base analogues. The measurements were done in Mercury, by constructing planes on the aromatic rings and measuring the angle between the constructed planes.

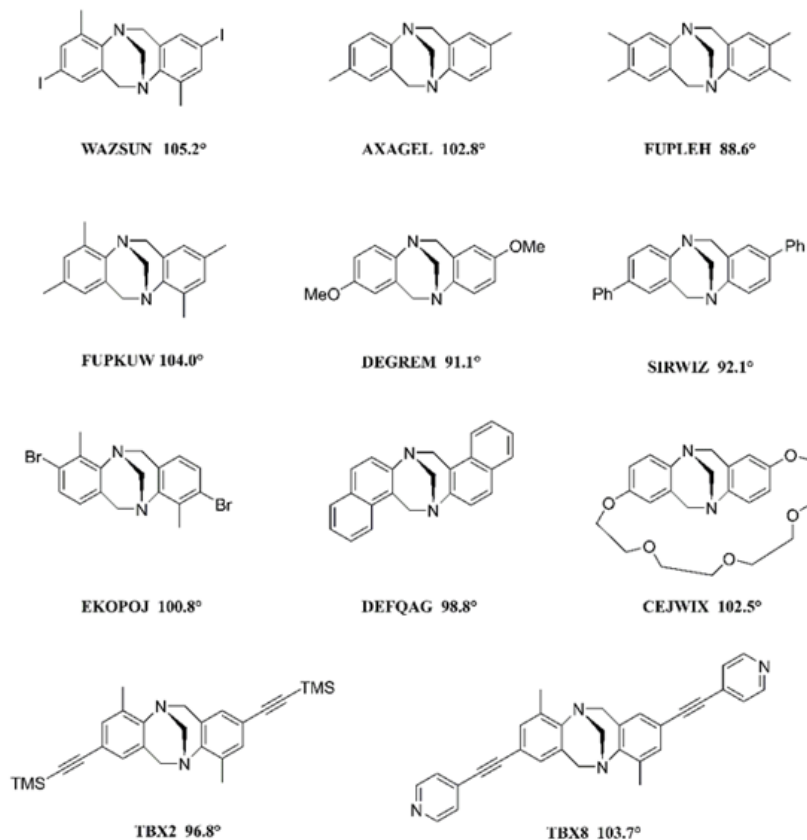


**Figure 6.8** Scheme of dihedral angles between aromatic rings of some structures reported in the CSD

Taking all these into consideration, we anticipate the resulting structure to be a 1-D zig-zag chain like architecture, Figure 6.9.



**Figure 6.9** Expected halogen-bonded supramolecular architecture

The goals of this chapter are as follows:

1. To synthesize a series of hydrogen bond acceptor Tröger's base analogues using N containing heterocycles.
2. To study the binding ability of these Tröger's base analogues with a series of aliphatic and aromatic dicarboxylic acids.
3. To synthesize iodoethynyl functionalized Tröger's base analogues, and to study binding ability with a series of symmetric ditopic acceptors.
4. To establish if nitrogen atoms on the diazocine ring act as potential binding sites which compete with suitable ditopic acceptors.
5. To determine if decreasing the number of binding sites is beneficial in tailoring the stoichiometry of supramolecules.
6. To establish how geometric flexibility, affect the solid-state landscape.



## 6.2 Experimental

### 6.2.1 General

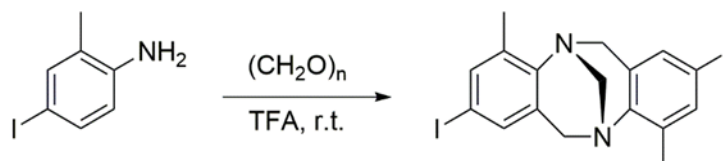
All reagents, solvents, precursors and hydrogen-bond donors were purchased from commercial sources and were used as received without further purification. A Varian Unity Plus (400 MHz) NMR spectrophotometer (Varian, Inc.) was used to record nuclear magnetic resonance spectra using the residual solvent signal as a reference. The  $^1\text{H}$  NMR spectra are reported as follows: chemical shift  $\delta$  in ppm relative to TMS ( $\delta = 0$  ppm), multiplicity, coupling constant (J in Hz), number of protons. The resonance multiplicity is described as s (singlet), d (doublet), t (triplet), q (quartet) or m (multiplet). A Fisher-Johns melting point apparatus (Vernon Hills, IL, USA) was used to determine melting points. Infrared spectroscopic analyses were performed with a Nicolet 380 FT-IR instrument (Thermo Scientific, Madison, WI, USA).

### 6.2.2 Electrostatic potential calculations

To calculate the molecular electrostatic potential surface of the acceptor molecules **TBX5-TBX8**, and donor molecules **TBX4** and **TBY4** the geometries were optimized using hybrid density functional B3LYP level of theory with 6-31G\* basis set in vacuum. The geometry optimized molecules were then visualized through mapping its values, determined by a positive point charge in the vacuum as a probe, on the molecular surface with an outer contour of 0.002 a.u. electronic density. The surface potentials, which are the coulombic interaction energies (in  $\text{kJmol}^{-1}$ ) between the positive point probe and the surface of the molecule at that point. All calculations were done using Spartan 10 software, Wavefunction Inc.

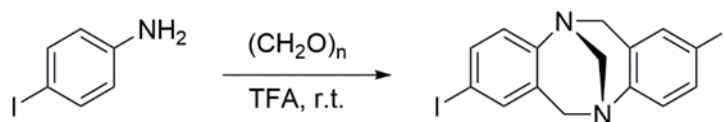
## 6.2.3 Synthesis

### 6.2.3.1 2,8-Diiodo-4,10-dimethyl-6H,12H-5,11-methanodibenzo[b,f]-diazocine TBX1<sup>8</sup>



4-Iodo-2-methylaniline (18.00 g, 77.25 mmol) was dissolved gradually in 75 mL of trifluoroacetic acid (TFA) batch-wise. In a separate 100 mL beaker, paraformaldehyde (4.64 g, 154 mmol) was mixed with TFA 50 mL batch-wise until clumps were dissolved. This was transferred portion wise into aniline in TFA. Stirring was continued for 17 h at r.t. TFA was removed in vacuo, water (75 mL) was added followed by addition of a saturated aqueous solution of NH<sub>3</sub> (75 mL) diluted in 25 mL water. The aqueous layer was extracted with dichloromethane (3 × 150 mL). The combined organic layers were dried (MgSO<sub>4</sub>), filtered, concentrated in vacuo and purified by column chromatography (EtOAc: Hexane 1:49) gave 8.671 g (59%). Pale yellow crystals were obtained. mp 235-236 °C. <sup>1</sup>H NMR (400 MHz, CDCl<sub>3</sub>): δ = 2.33 (s, 6 H, 2 × CH<sub>3</sub>), 3.89 (d, 2H, J = 16.9 Hz, H-6<sub>endo</sub> and H-12<sub>endo</sub>), 4.24 (s, 2 H, H-13), 4.50(d, 2 H, J = 16.9 Hz, H-6<sub>exo</sub> and H-12<sub>exo</sub>), 7.10 (s, 2 H, H-1 and H-7), 7.38 (s, 2 H, H-3 and H-9).

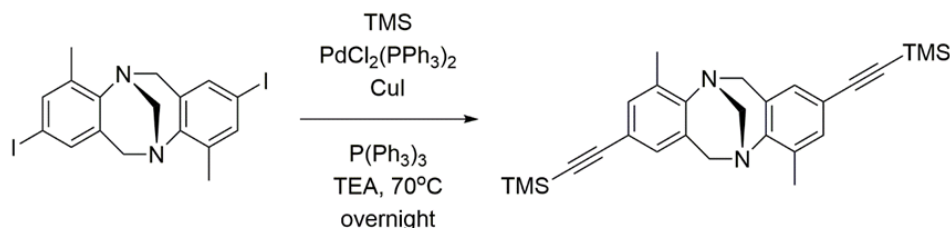
### 6.2.3.2 2,8-Diiodo-6H,12H-5,11-methanodibenzo[b,f]-diazocine TBY1<sup>8</sup>



4-Iodoaniline (2.95 g, 13.47 mmol) was dissolved gradually in 15 mL of TFA acid batch-wise. In a separate 100 mL beaker, paraformaldehyde (0.82 g, 20.20 mmol) was mixed with TFA 10 mL batch-wise until clumps were dissolved. This was transferred portion wise into aniline in TFA. Stirring was continued for 17 h at r.t. TFA was removed in vacuo, water (15 mL) was added

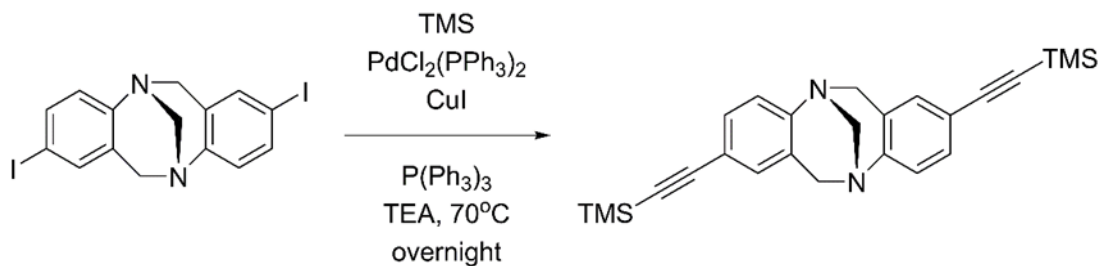
followed by addition of a saturated aqueous solution of  $\text{NH}_3$  (15 mL) diluted in 5 mL water. The aqueous layer was extracted with dichloromethane ( $3 \times 50$  mL). The combined organic layers were dried ( $\text{MgSO}_4$ ), filtered, concentrated in vacuo and purified by column chromatography (EtOAc: Hexane 1:49) gave 0.99 g (31%). Pale yellow crystals were obtained. mp 180-181 °C.  $^1\text{H}$  NMR (400 MHz,  $\text{CDCl}_3$ ):  $\delta$  = 4.08 (d, 2 H,  $J$  = 16.8 Hz, H-6endo and H-12endo), 4.24 (s, 2 H, H-13), 4.62 (d, 2 H,  $J$  = 16.8 Hz, H-6exo and H-12exo), 6.87 (d, 2 H,  $J$  = 8.5 Hz, H-4 and H-10), 7.23 (s, 2 H,  $J$  = 1.5 Hz, H-1 and H-7), 7.45 (dd, 2 H,  $J$  = 8.5 Hz,  $J$  = 1.5 Hz, H-3 and H-9).

**6.2.3.3**      **4,10-Dimethyl-2,8-bis[(trimethylsilyl)ethynyl]-6H,12H-5,1methanodibenzo[b,f]-diazocine TBX2<sup>9</sup>**



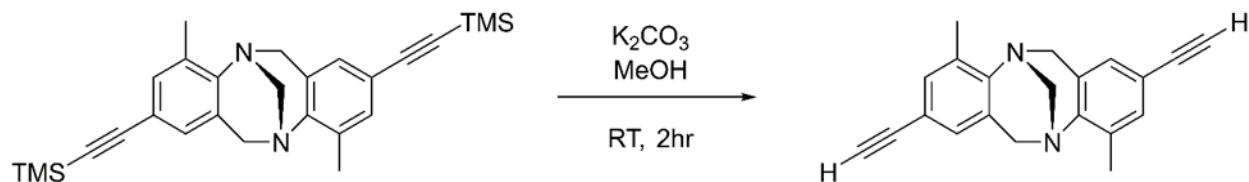
**TBX1** (8.51 g, 16.8 mmol), was dissolved in triethylamine (100 mL) and degassed by bubbling  $\text{N}_2$  through the reaction mixture for 20 mins. To this solution were added trimethylsilylacetylene (6.80 mL, 47.8 mmol) [ $\text{PdCl}_2(\text{PPh}_3)_2$ ] (639.0 mg, 0.9104 mmol),  $\text{P}(\text{Ph}_3)_3$  (477.5 mg, 1.820 mmol) and  $\text{CuI}$  (1.7337 g, 9.104 mmol). After 20 h, the reaction mixture was quenched with sat. aq  $\text{NaCl}$  (30 mL) and filtered over Celite. The residue was extracted with  $\text{CH}_2\text{Cl}_2$ . The filtrate was washed with aq sat.  $\text{NaHCO}_3$  (50 mL), dried ( $\text{MgSO}_4$ ), and concentrated in vacuo. Purification by column chromatography (EtOAc: Hexane 1:49) gave 6.45 g (86%) of **TBX2** as a yellow solid; mp 67–69 °C.  $^1\text{H}$  NMR (400 MHz,  $\text{CDCl}_3$ ):  $\delta$  = 0.19 [s, 18 H,  $\text{Si}(\text{CH}_3)_3$ ], 2.33 (s, 6 H,  $2 \times \text{CH}_3$ ), 3.91 (d, 2 H, H-6endo and H-12endo,  $2J = -17.0$  Hz), 4.27 (s, 2 H, H-13), 4.50 (d, 2 H, H-6exo and H-12exo,  $2J = -17.0$  Hz), 6.89 (s, 2 H, H-1, H-7,  $4J = 1.1$  Hz), 7.15 (s, 2 H, H-3, H-9).

#### 6.2.3.4 2,8-Bis[(trimethylsilyl)ethynyl]-6H,12H-5,11-methanodibenzo[b,f]-diazocine **TBY2**<sup>9</sup>



**TBY1** (0.43 g, 0.91 mmol), was dissolved in triethylamine (15 mL) and degassed by bubbling N<sub>2</sub> through the reaction mixture for 20 mins. To this solution were added trimethylsilylacetylene (0.27 mL, 1.91 mmol) [PdCl<sub>2</sub>(PPh<sub>3</sub>)<sub>2</sub>] (25.6 mg, 0.0365 mmol), P(Ph<sub>3</sub>)<sub>3</sub> (0.0191 mg, 0.0730 mmol) and CuI (69.5 mg, 0.365 mmol). After 20 h, the reaction mixture was quenched with sat. aq NaCl (30 mL) and filtered over Celite. The residue was extracted with CH<sub>2</sub>Cl<sub>2</sub>. The filtrate was washed with aq sat. NaHCO<sub>3</sub> (50 mL), dried (MgSO<sub>4</sub>), and concentrated in vacuo. Purification by column chromatography (EtOAc: Hexane 1:49) gave 0.20 g (55%) of **TBY2** as a yellow solid; mp 42–44 °C. <sup>1</sup>H NMR (400 MHz, CDCl<sub>3</sub>): δ = 0.21 [s, 18 H, Si(CH<sub>3</sub>)<sub>3</sub>], 4.10 (d, 2 H, H-6endo and H-12endo, 2J = -17.0 Hz), 4.26 (s, 2 H, H-13), 4.61 (d, 2 H, H-6exo and H-12exo, 2J = -17.0 Hz), 7.00 (d, 2 H, J = 8.5 Hz, H-4 and H-10), 7.02 (s, 2 H, J = 1.5 Hz, H-1 and H-7), 7.24 (dd, 2 H, J = 8.5 Hz, J = 1.5 Hz, H-3 and H-9).

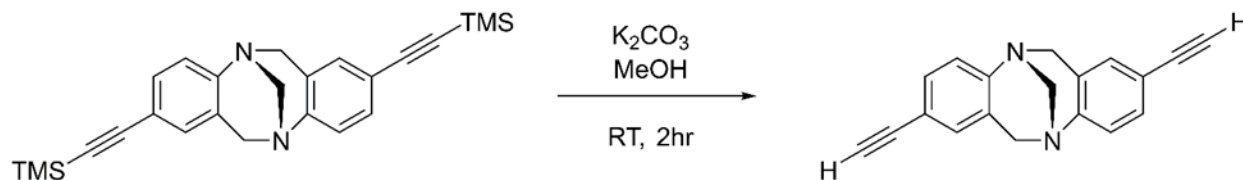
#### 6.2.3.5 4,10-Dimethyl-2,8-bisethynyl-6H,12H-5,11-methanodibenzo[b,f]-diazocine **TBX3**<sup>10</sup>



**TBX2** (1.20 g, 2.71 mmol) and potassium carbonate (0.41 g, 2.98 mmol) were stirred in methanol at room temperature for 2 hrs. Upon completion, the solvent was removed by rotary

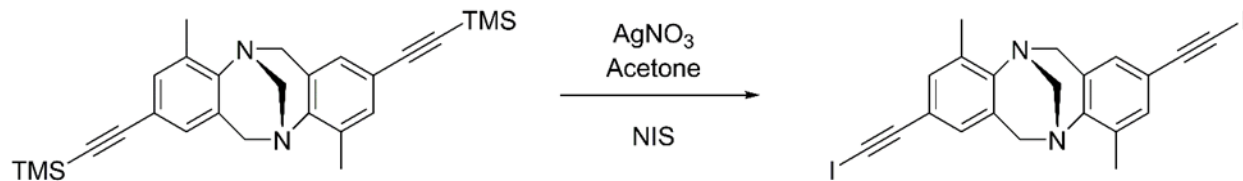
evaporation and the residue was dissolved in diethyl ether and washed with water (2 x 50 mL). The combined organic layers were dried over anhydrous MgSO<sub>4</sub> and concentrated via rotary evaporation to obtain the product. Purification by column chromatography (EtOAc: Hexane 1:49) gave 0.73 g (91%) of **TBX3** as colorless needlelike crystals. m. p. 173 - 175 °C; <sup>1</sup>H NMR (400 MHz, CDCl<sub>3</sub>): δ = 2.37 (s, 6 H, 2 × CH<sub>3</sub>), 2.96 (s, 2 H, 2 × ethynyl-H), 3.94 (d, 2 H, J = 16.9 Hz, H-6<sub>endo</sub> and H-12<sub>endo</sub>), 4.27 (s, 2 H, H-13), 4.54 (d, 2 H, J = 16.9 Hz, H-6<sub>exo</sub> and H-12<sub>exo</sub>), 6.92 (d, 2 H, J = 1.0 Hz, H-1 and H-7), 7.19 (d, 2 H, J = 1.0 Hz, H-3 and H-9).

#### 6.2.3.6 2,8-Bisethynyl-6H,12H-5,11-methanodibenzo[b,f]-diazocine **TBY3**<sup>10</sup>



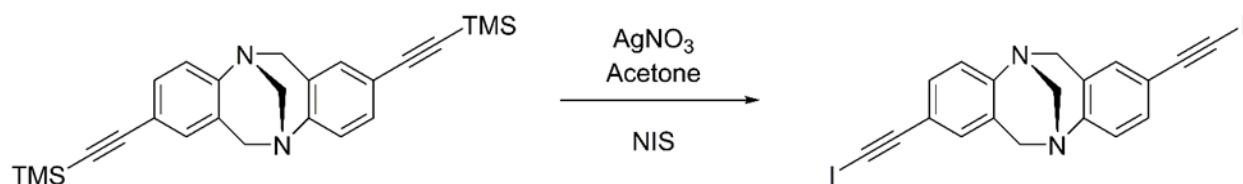
**TBY2** (0.18 g, 0.43 mmol) and potassium carbonate (0.07 g, 0.50 mmol) were stirred in methanol at room temperature for 2 hrs. Upon completion, the solvent was removed by rotary evaporation and the residue was dissolved in diethyl ether and washed with water (2 x 50 mL). The combined organic layers were dried over anhydrous MgSO<sub>4</sub> and concentrated via rotary evaporation to obtain the product. Purification by column chromatography (EtOAc: Hexane 1:49) gave 0.10 g (91%) of **TBY3** as a yellow solid. m. p. 136-138 °C; <sup>1</sup>H NMR (400 MHz, CDCl<sub>3</sub>): δ = 2.97 (s, 2 H, 2 × ethynyl-H), 4.13 (d, 2 H, J = 16.9 Hz, H-6<sub>endo</sub> and H-12<sub>endo</sub>), 4.28 (s, 2 H, H-13), 4.64 (d, 2 H, J = 16.9 Hz, H-6<sub>exo</sub> and H-12<sub>exo</sub>), 7.00 (d, 2 H, J = 8.5 Hz, H-4 and H-10), 7.02 (s, 2 H, J = 1.5 Hz, H-1 and H-7), 7.24 (dd, 2 H, J = 8.5 Hz, J = 1.5 Hz, H-3 and H-9).

### 6.2.3.7 4,10-Dimethyl-2,8-diiodoethynyl-6H,12H-5,11-methanodibenzo[b,f]-diazocine TBX4<sup>11</sup>



**TBX2** (2.21 g, 4.97 mmol) and AgNO<sub>3</sub> (1.69 g, 9.95 mmol) was placed in round-bottomed flask and CH<sub>3</sub>CN (200 mL) was added. The mixture was stirred under purging nitrogen for 20 min. The flask was wrapped in aluminum foil and under dark conditions, NIS (2.24 g, 9.95 mmol) was added. The mixture was stirred overnight at room temperature after which, it was passed through a 2 cm plug of silica gel. The solvent was removed by rotary evaporation. The resulting residue was dissolved in CH<sub>2</sub>Cl<sub>2</sub> and washed with H<sub>2</sub>O (100 mL). The organic part was separated, dried over anhydrous MgSO<sub>4</sub> and solvent was removed under vacuum. Purification by column chromatography (EtOAc: Hexane 1:49) gave 1.88 g (69%) of **TBX4** as an off-white solid. m. p. 215-217 °C; <sup>1</sup>H NMR (400 MHz, CDCl<sub>3</sub>): δ = 2.34 (s, 6 H, 2 × CH<sub>3</sub>), 3.91 (d, 2 H, J = 16.9 Hz, H-6endo and H-12endo), 4.26 (s, 2 H, H-13), 4.50 (d, 2 H, J = 16.9 Hz, H-6exo and H-12exo), 6.86 (d, 2 H, J = 1.0 Hz, H-1 and H-7), 7.13 (d, 2 H, J = 1.0 Hz, H-3 and H-9). <sup>13</sup>C NMR (400 MHz, CDCl<sub>3</sub>): δ = 4.97 (C – ethynyl) 17.19 (2 C, 2 × CH<sub>3</sub>), 54.94 (2 C, C- 6 and C-12), 67.55 (1 C, C- 13), 94.17 (C – ethynyl), 118.82 (2 C, C-2 and C-8), 128.1 (2 C, C-4 and C-10), 128.70 (2 C), 133.0 (2 C, C-3 and C-9), 133.25 (2 C, C-1 and C-7), 135.9 (2 C), 146.93 (2 C).

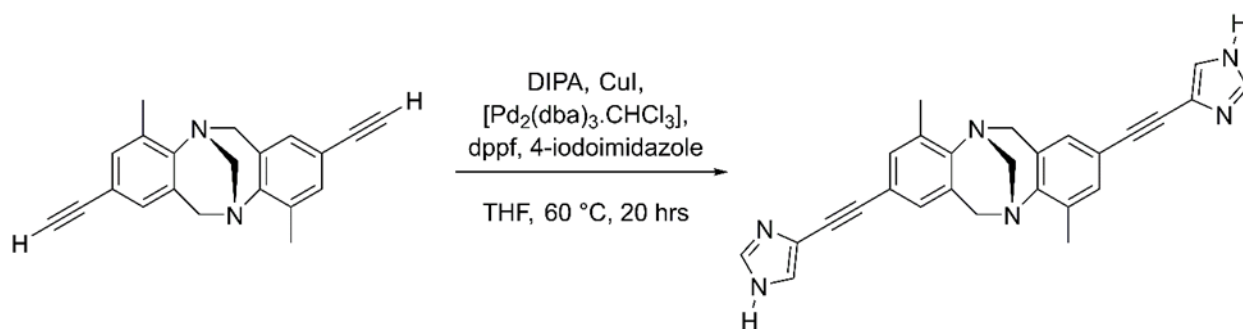
### 6.2.3.8 2,8-Diiodoethynyl-6H,12H-5,11-methanodibenzo[b,f]-diazocine TBY4<sup>11</sup>



**TBY2** (0.18 g, 0.43 mmol) and AgNO<sub>3</sub> (0.15 g, 0.86 mmol) was placed in round-bottomed flask and CH<sub>3</sub>CN (200 mL) was added. The mixture was stirred under purging nitrogen for 20 min. The flask was wrapped in aluminum foil and under dark conditions, NIS (0.19 g, 0.14 mmol) was added. The mixture was stirred for overnight at room temperature after which time it was passed through a 2 cm plug of silica gel. The solvent was removed by rotary evaporation. The resulting residue was dissolved in CH<sub>2</sub>Cl<sub>2</sub> and washed with H<sub>2</sub>O (100 mL). The organic part was separated, dried over anhydrous MgSO<sub>4</sub> and solvent was removed under vacuum. Purification by column chromatography (EtOAc: Hexane 1:49) gave 0.16 g (72%) of **TBY4** as a pale orange colored solid. m. p. 191-192 °C; <sup>1</sup>H NMR (400 MHz, CDCl<sub>3</sub>): δ = 4.10 (d, 2 H, J = 16.9 Hz, H-6endo and H-12endo), 4.27 (s, 2 H, H-13), 4.62 (d, 2 H, J = 16.9 Hz, H-6exo and H-12exo), 7.01 (d, 2 H, J = 8.5 Hz, H-4 and H-10), 7.05 (s, 2 H, J = 1.5 Hz, H-1 and H-7), 7.22 (dd, 2 H, J = 8.5 Hz, J = 1.5 Hz, H-3 and H-9).

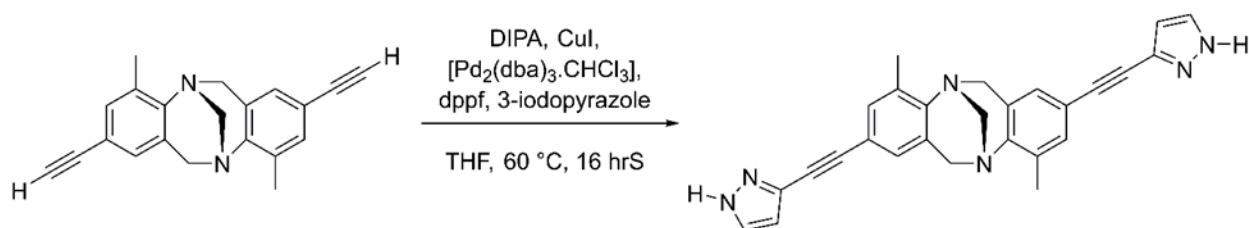
As a precursor to these Tröger's base derivatives, **TBX1** was chosen over **TBY1** due to the ease of synthesis, ease of scaling the reaction and the time scale (1/5th that of **TBY1**, 82 hr). The inclusion of a moderately electron donating methyl substituent on the 4-iodoaniline which made the iodoaniline more reactive towards the Tröger's base condensation reaction facilitated **TBX1** synthesis.

#### 6.2.3.10 2,8-Bis-4-ethynylimidazole -6H,12H-5,11-methanodibenzo[b,f]-diazocine **TBX5**<sup>12</sup>



10 mL THF and 163 mg diisopropylamine (1.61 mmol, 2.4 equiv) were added to 200 mg (0.670 mmol) **TBX3**, 5 mg ( $26.8 \times 10^{-3}$  mmol, 4 mol %) CuI, 21 mg ( $20.1 \times 10^{-3}$  mmol, 6 mol % Pd)  $[\text{Pd}_2(\text{dba})_3 \cdot \text{CHCl}_3]$ , 22 mg ( $40.2 \times 10^{-3}$  mmol, 6 mol %) 1,1'-bis(diphenylphosphino)ferrocene (dppf) 286 mg (1.47 mmol, 2.2 equiv) 4-iodoimidazole and the resulting mixture was stirred at 60 °C for 16 hours. Sat. aq NaCl and  $\text{CH}_2\text{Cl}_2$  were added and the mixture was filtered over Celite and the residue was washed with  $\text{CH}_2\text{Cl}_2$ . The filtrate was washed with sat. aq  $\text{NaHCO}_3$  and the organic layer was dried over  $\text{MgSO}_4$ . The crude product was purified by column chromatography (methanol/EtOAc 1:9) and could be obtained as a yellow solid. Yield: 0.118 g (41 %), mp 180-181 °C.  $^1\text{H}$  NMR (400 MHz,  $\text{CDCl}_3$ ):  $\delta$  = 2.33 (s, 6 H,  $2 \times \text{CH}_3$ ), 4.01 (d, 2 H, H-6*endo* and H-12*endo*), 4.24 (s, 2 H, H-13), 4.49 (d, 2 H, H-6*exo* and H-12*exo*), 6.96 (d, 2 H, H-1 and H-7), 7.18 (d, 2 H, H-3 and H-9), 7.41, 7.73, 8.10.

#### 6.2.3.11 2,8-Bis-3-ethynylpyrazole-6H,12H-5,11-methanodibenzo[b,f]-diazocine **TBX6**<sup>12</sup>

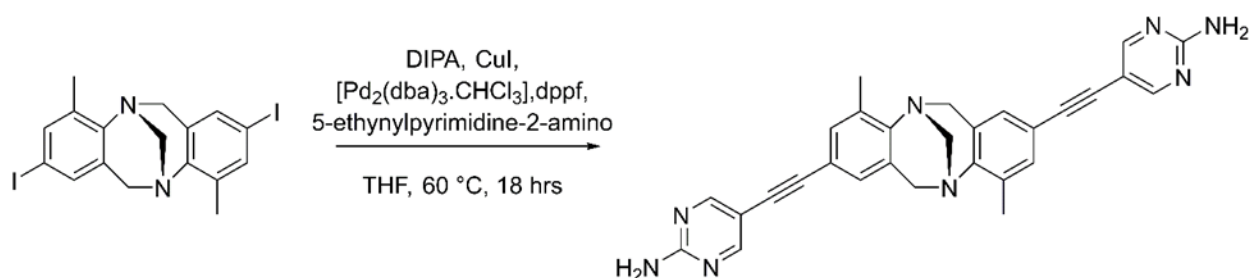


8 mL THF and 108 mg diisopropylamine (1.07 mmol, 2.4 equiv) were added to 133 mg (0.446 mmol) **TBX3**, 3 mg ( $17.8 \times 10^{-3}$  mmol, 4 mol %) CuI, 14 mg ( $13.3 \times 10^{-3}$  mmol, 6 mol % Pd)  $[\text{Pd}_2(\text{dba})_3 \cdot \text{CHCl}_3]$ , 15 mg ( $26.7 \times 10^{-3}$  mmol, 6 mol %) 1,1'-bis(diphenylphosphino)ferrocene (dppf) 191 mg (0.98 mmol, 2.2 equiv) 3-iodopyrazole and the resulting mixture was stirred at 60 °C for 16 hours. Sat. aq NaCl and  $\text{CH}_2\text{Cl}_2$  were added and the mixture was filtered over Celite and the residue was washed with  $\text{CH}_2\text{Cl}_2$ . The filtrate was washed with sat. aq  $\text{NaHCO}_3$  and the organic layer was dried over  $\text{MgSO}_4$ . The crude product was purified by column chromatography



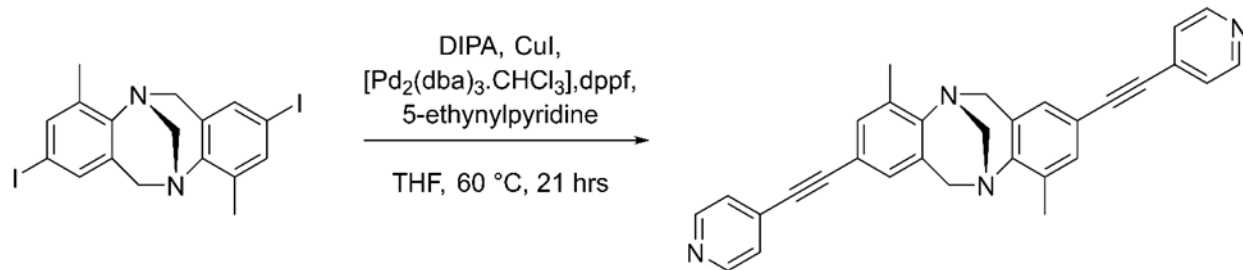
(EtOAc/hexane 1:9) and could be obtained as a yellow solid. Yield: 42 mg (0.092 mmol, 13 %), mp 146-148 °C. <sup>1</sup>H NMR (400 MHz, CDCl<sub>3</sub>): δ = 2.39 (s, 6 H, 2 × CH<sub>3</sub>), 3.98 (d, 2 H, H-6<sub>endo</sub> and H-12<sub>endo</sub>), 4.30 (s, 2 H, H-13), 4.57 (d, 2 H, H-6<sub>exo</sub> and H-12<sub>exo</sub>), 6.48 (d, 2 H, H-1 and H-7), 6.98 (d, 2 H, H-3 and H-9), 7.25, 7.57, 10.23.

**6.2.3.12 2,8-Bis-5-ethynylpyrimidine-2-amino -6H,12H-5,11-methanodibenzo[b,f]-diazocine TBX7<sup>12</sup>**



10 mL THF and 169 mg diisopropylamine (1.68 mmol, 2.4 equiv) were added to 351 mg (0.700 mmol) **TBX1**, 5 mg (28×10<sup>-3</sup> mmol, 4 mol %) CuI, 22 mg (21×10<sup>-3</sup> mmol, 6 mol % Pd [Pd<sub>2</sub>(dba)<sub>3</sub> · CHCl<sub>3</sub>], 23 mg (42×10<sup>-3</sup> mmol, 6 mol %) 1,1'-bis(diphenylphosphino)ferrocene (dppf) 183 mg (1.54 mmol, 2.2 equiv) 5-ethynylpyrimidine-2-amino and the resulting mixture was stirred at 60 °C for 16 hours. Sat. aq NaCl and CH<sub>2</sub>Cl<sub>2</sub> were added and the mixture was filtered over Celite and the residue was washed with CH<sub>2</sub>Cl<sub>2</sub>. The filtrate was washed with sat. aq NaHCO<sub>3</sub> and the organic layer was dried over MgSO<sub>4</sub>. The crude product was purified by column chromatography (EtOAc/hexane 1:9) and could be obtained as a yellow solid. Yield: 0.179 g (53%), mp 281-283 °C. <sup>1</sup>H NMR (400 MHz, CDCl<sub>3</sub>): δ = 2.39 (s, 6 H, 2 × CH<sub>3</sub>), 3.98 (d, 2 H, H-6<sub>endo</sub> and H-12<sub>endo</sub>), 4.31 (s, 2 H, H-13), 4.57 (d, 2 H, H-6<sub>exo</sub> and H-12<sub>exo</sub>), 5.15, 6.94 (d, 2 H, H-1 and H-7), 7.21 (d, 2 H, H-3 and H-9), 8.39.

### 6.2.3.13 2,8-Bis-5-ethynylpyridine-6H,12H-5,11-methanodibenzo[b,f]-diazocine TBX8<sup>12</sup>



10 mL THF and 169 mg diisopropylamine (1.68 mmol, 2.4 equiv) were added to 351 mg (0.700 mmol) **TBX1**, 5 mg ( $28 \times 10^{-3}$  mmol, 4 mol %) CuI, 22 mg ( $21 \times 10^{-3}$  mmol, 6 mol % Pd) [Pd<sub>2</sub>(dba)<sub>3</sub>.CHCl<sub>3</sub>], 23 mg ( $42 \times 10^{-3}$  mmol, 6 mol %) 1,1'-bis(diphenylphosphino)ferrocene (dppf) 158 mg (1.54 mmol, 2.2 equiv) 5-ethynylpyridine and the resulting mixture was stirred at 60 °C for 16 hours. Sat. aq NaCl and CH<sub>2</sub>Cl<sub>2</sub> were added and the mixture was filtered over Celite and the residue was washed with CH<sub>2</sub>Cl<sub>2</sub>. The filtrate was washed with sat. aq NaHCO<sub>3</sub> and the organic layer was dried over MgSO<sub>4</sub>. The crude product was purified by column chromatography (EtOAc/hexane 4:1) and could be obtained as a yellow solid. Yield: 0.148 g (47 %), mp 219-220 °C. <sup>1</sup>H NMR (400 MHz, CDCl<sub>3</sub>):  $\delta$  = 2.41 (s, 6 H, 2  $\times$  CH<sub>3</sub>), 4.00 (d, 2 H, H-6<sub>endo</sub> and H-12<sub>endo</sub>), 4.32 (s, 2 H, H-13), 4.59 (d, 2 H, H-6<sub>exo</sub> and H-12<sub>exo</sub>), 7.01 (d, 2 H, H-1 and H-7), 7.27 (d, 2 H, H-3 and H-9), 7.31(d, 2 H), 8.57 (d, 2 H).

### 6.2.4 Grinding experiments

Screenings for co-crystals were performed using solvent-assisted grinding technique. In a typical grinding experiment, the stoichiometric amounts of donor and acceptor were mixed in a microwell with the aid of a pestle and a drop of solvent (methylene chloride). The resulting solids from each reaction were subjected to IR analysis for characterization. A successful interaction would be characterized by specific peak shifts observed in the ground mixture compared to the starting compounds.

## 6.3 Results

### 6.3.1 MEP surface calculations

In order to attain a broader view of the relative strengths of the hydrogen-bond acceptor sites of **TBX5-TBX8** and halogen bond donor sites of **TBX4, TBY4** of the Tröger's base derivatives and symmetric ditopic acceptors, molecular electrostatic potential (MEP) surface calculations were performed. The values are used to rank the relative strengths of the nitrogens on the diazocine rings and potential acceptor sites on the heterocyclic arms on the Tröger's base molecules **TBX5-TBX8**. These values are further used to establish whether the acceptor sites of the diazocine ring on the halogen bond donor Tröger's base derivatives **TBX4** and **TBY4** are competitive enough for the symmetric ditopic acceptors. The MEP surface energies are shown in Table 6.1 Table 6.2 and Table 6.3.

**Table 6.1** Electrostatic surface potential energies for hydrogen bond acceptor and halogen bond donor Tröger's base derivatives

Tröger's base derivative	E(N <sub>HET</sub> ) kJ/mol	E(I) kJ/mol	E(N <sub>AZC</sub> ) kJ/mol	E(N—H) kJ/mol
<b>TBX5</b>	-220	-	-119	+275
<b>TBX6</b>	-189	-	-113	+254
<b>TBX7</b>	-158	-	-107	+207
<b>TBX8</b>	-192	-	-82	-
<b>TBX4</b>	-	+163	-93	-
<b>TBY4</b>	-	+166	-116	-

**Table 6.2** Electrostatic surface potential energies for symmetric ditopic acceptors

Ditopic acceptor	Potential on acceptor site kJ/mol
Pyrazine ( <b>A1</b> )	-153
Tetramethyl pyrazine ( <b>A2</b> )	-162
1,2-bis(4-pyridyl)ethane ( <b>A3</b> )	-186
4,4'-dipyridyl ( <b>A4</b> )	-172
Phenazine ( <b>A5</b> )	-149
1,2-di(4-pyridyl)ethylene ( <b>A6</b> )	-182
4,4'-trimethylene dipyridine ( <b>A7</b> )	-191

### 6.3.2 Covalent synthesis

#### 6.3.2.1 Synthesis of **TBX1**

The scale up synthesis of **TBX1** is very sensitive to the reaction conditions. Using the same procedure indicated as for a small-scale did not produce the desired product. A simple modification of the procedure where both paraformaldehyde and respective aniline were mixed separately in TFA and introducing the solutions dropwise increased the yield to 59%.

#### 6.3.2.2 Synthesis of **TBX4**

The synthesis of **TBX4** was sought after using the following routes after Sonogoshira coupling reaction on **TBX1** to synthesize **TBX2**, Figure 6.10. The first route which used concentrated I<sub>2</sub> in methanol did not give the desired product. Similarly (route 2) under the following conditions AgF, N-iodosuccinimide in acetonitrile produced the same result. Route 3, which used one step less to synthesize the desired product through direct TMS to iodo conversion using AgNO<sub>3</sub>, N-iodosuccinimide in acetonitrile, resulted in good yield.

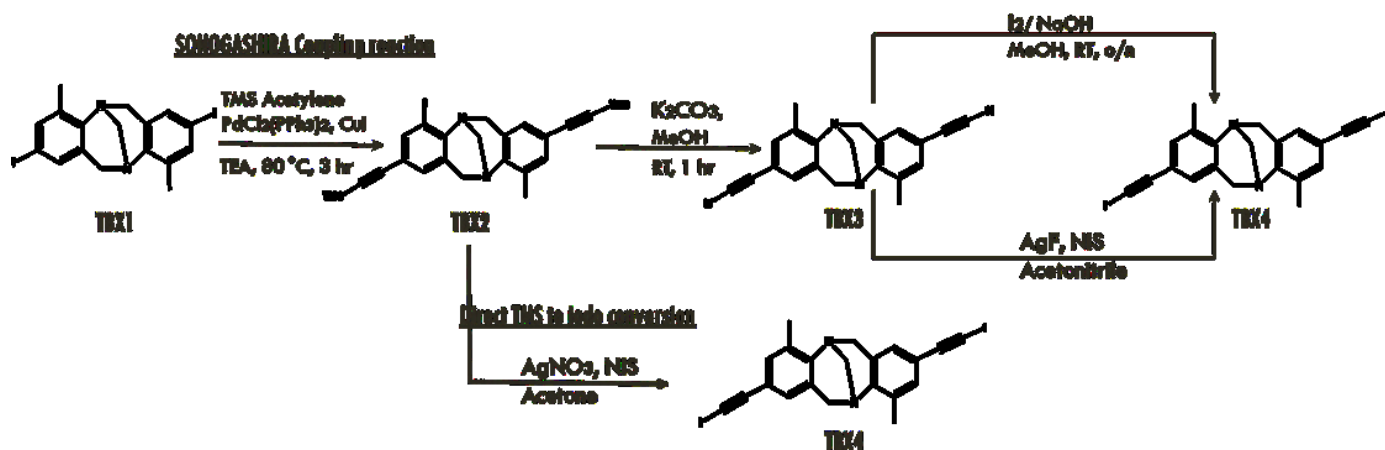


Figure 6.10 Synthetic route to TBX4

### 6.3.3 IR stretching frequencies of ground mixtures

Tröger's base derivatives **TBX5-TBX8** were subjected to solvent assisted grinding experiments with aliphatic dicarboxylic acids and aromatic dicarboxylic acids and were analyzed through IR spectroscopy. Out of these experiments, all 28 of the ground mixtures resulted a successful co-crystal formation. All co-crystals displayed broad bands near the 1,850 and 2,500  $\text{cm}^{-1}$  regions (as a result of O-H $\cdots$ N hydrogen bonds) and significant changes in the C=O stretch of the carboxylic acid indicating co-crystal formation, Table 6.3.

Halogen bond donor Tröger's base derivatives **TBX4** and **TBY4** were subjected to solvent assisted grinding experiments with symmetric ditopic acceptors and were analyzed through IR spectroscopy. Formation of a co-crystal was established by comparing the IR spectrum of the ground solid mixture with the IR spectra of the pure donor and the acceptor. A successful co-crystal event is then further determined by observing shifts of other stretches corresponding to either donor or the acceptor, Table 6.4.

**Table 6.3** IR stretching frequencies ( $\text{cm}^{-1}$ ) of the solids produced by combining Tröger's base derivatives **TBX5-TBX8** acceptors with aliphatic dicarboxylic acids

Mixture	Carbonyl stretch ( $\text{cm}^{-1}$ )		O---H .... N Stretch ( $\text{cm}^{-1}$ )	Co-crystal
	Di-acid	Ground mixture		
TBX5:SUC	1685	1685	1953, 2528	Y
TBX5:GLU	1683	1717	1916, 2525	Y
TBX5:ADI	1684	1688	1927, 2562	Y
TBX5:TAR	1685	1700	1950, 2559	Y
TBX5:SUB	1685	1691	1933, 2596	Y
TBX5:3HB	1679	1694	1920, 2513	Y
TBX5:IT	1680	1681	1895, 2525	Y
TBX5:PT	1668	1696	1923, 2516	Y
TBX6:SUC	1685	1699	1978, 2516	Y
TBX6:GLU	1683	1690	1913, 2568	Y
TBX6:ADI	1684	1689	1944, 2548	Y
TBX6:TAR	1685	1717	1893, 2508	Y
TBX6:SUB	1685	1690	1919, 2562	Y
TBX7:SUC	1685	x	1882, 2544	Y
TBX7:GLU	1683	1698	1911, 2493	Y
TBX7:ADI	1684	1689	1916, 2558	Y
TBX7:TAR	1685	1720	1907, 2491	Y
TBX7:SUB	1685	x	1925, 2639	Y
TBX7:3HB	1679	x	1883, 2479	Y
TBX7:IT	1680	x	1898, 2541	Y
TBX8:SUC	1685	1688	1903, 2553	Y
TBX8:GLU	1683	1700	1927, 2554	Y
TBX8:ADI	1684	1687	1905, 2559	Y
TBX8:TAR	1685	1717	1922, 2517	Y
TBX8:SUB	1685	1688	1919, 2531	Y
TBX8:3HB	1679	1687	1914, 2461	Y
TBX8:IT	1680	1684	1926, 2534	Y
TBX8:PT	1668	1700	1919, 2457	Y

**Table 6.4** IR stretching frequencies (cm<sup>-1</sup>) of the solids produced by combining Tröger's base derivatives **TBX4** and **TBY4** donors with symmetric ditopic acceptors

	A1	A2	A3	A4	A5	A6	A7
	1416, 1491	1406, 1438	1412, 1556, 1593	1404, 1486, 1530, 1586	1357, 1428, 1467, 1510	1411, 1592	1412, 1501, 1555, 1602
<b>TBX4</b> 1435, 1469, 2152	1431, 1468, 2155	1407, 1433, 1469, 2180	1413, 1431, 1469, 1557, 1595, 2155	1404, 1430, 1468, 1531, 1590, 2148	1359, 1430, 1469, 1514, 2145	1413, 1435, 1468, 1596, 2148	1414, 1429, 1468, 1556, 1599, 2158
<b>TBY4</b> 1396, 1488, 1709	1401, 1432, 1488, 1714	1373, 1407, 1432, 1488, 1598, 1706	1412, 1487, 1557, 1596, 1709	1403, 1432, 1487, 1596, 1712	1358, 1402, 1430, 1489, 1511, 1709	1412, 1488, 1555, 1595, 1705	1413, 1431, 1487, 1557, 1599, 1710

### 6.3.4 Description of solid state architectures

#### 6.3.4.1 Crystal structure of 2, 8-diiodo-4,10-dimethyl-6H,12H-5,11-methanodibenzo [b,f]-diazocine (**TBX1**)

No noteworthy interactions are observed for **TBX1** due to the inactive iodine, Figure 6.11. Two interactions, C—I $\cdots$  $\pi$  with a distance of 3.432 Å and aromatic stacking may have been due to close packing. The crystal packing of **TBX1** leads to the formation of discrete void spaces in the crystal lattice, Figure 6.12.

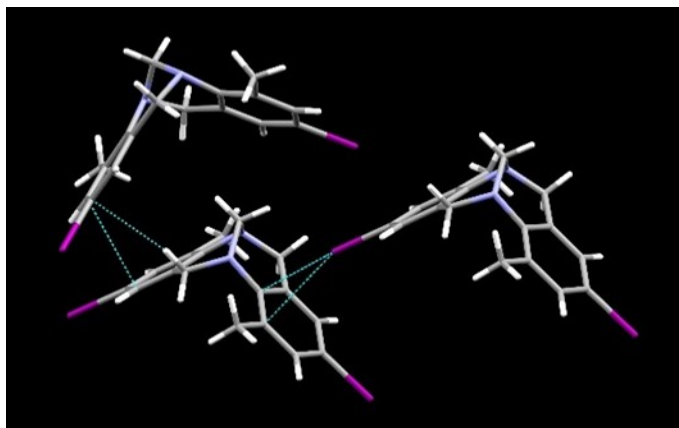


**Figure 6.11** C—I··· $\pi$  and aromatic stacking interaction observed in **TBX1**

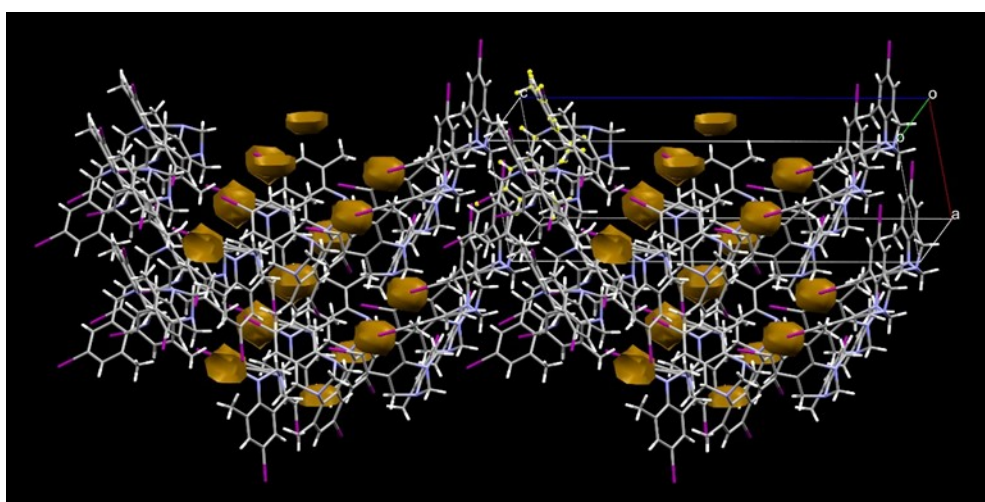


**Figure 6.12** Discrete void space observed in overall packing of **TBX1**

#### 6.3.4.2 *Crystal structure of 4,10-dimethyl-2,8-bis[(trimethylsilyl)ethynyl]-6H,12H-5,11-methanodibenzo[b,f]-diazocine (TBX2)*

The crystal structure of **TBX2** possess two distinct interaction motifs. The ethynyl group acts as a hydrogen bond acceptor to a C—H group on TMS, Figure 6.13. This interaction is accompanied via C—H··· $\pi$  (2.816 Å with aromatic core and 2.719 Å with ethynyl group) interaction on the phenyl group of the Tröger's base. The TMS group is situated well within the hydrophobic cavity of the Tröger's base, where the cavity created by the two aromatic rings has a dihedral angle of 96.2°. Besides these interactions, another C—H···N (2.688 Å) type interaction is observed between the nitrogen on the diazocine ring and C—H group on TMS, Figure 6.14.



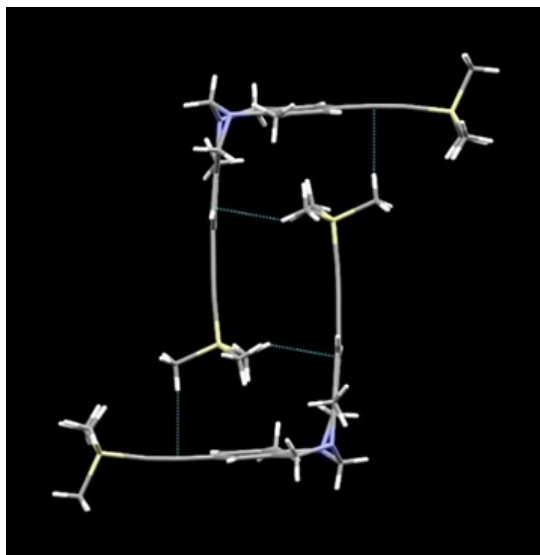


**Figure 6.13** C—H $\cdots$  $\pi$  with ethynyl group and aromatic ring in **TBX2**

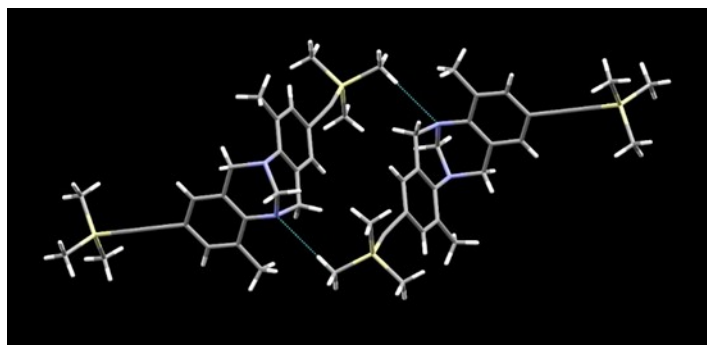


**Figure 6.14** C—H $\cdots$ N interactions observed between methyl C—H and diazocine N in **TBX2**

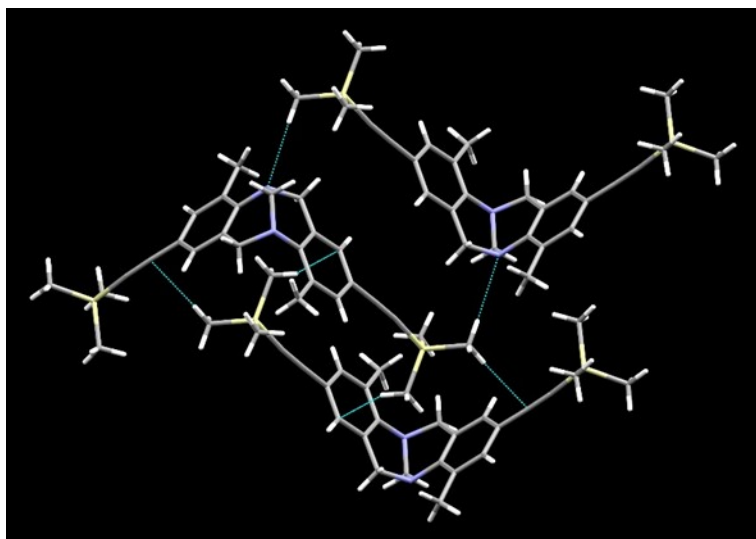


**Figure 6.15** Overall packing observed in **TBX2**

### 6.3.4.3 Crystal structure of 4,10-dimethyl-2,8-dipyridinethynyl-6H,12H-5,11-methanodibenzo[b,f]-diazocine (TBX8)

There are several different interactions that are taking place in **TBX8**. The C—H $\cdots$  $\pi$  (2.872 Å) interaction is observed between C—H of a methyl group and the phenyl group within the hydrophobic cavity, Figure 6.16.

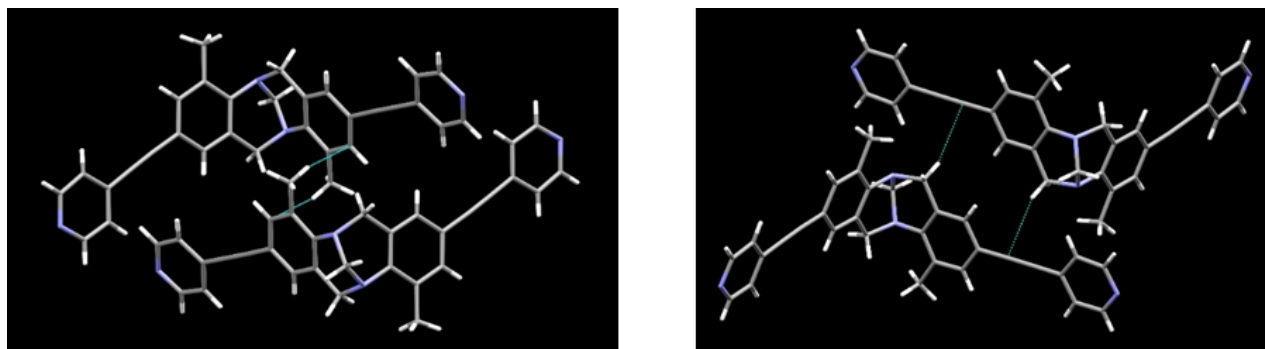


**Figure 6.16** C—H $\cdots$  $\pi$  and aromatic stacking interaction observed in **TBX8**

The dihedral angle between the two aromatic ring results in 103.7°. These interactions are further accompanied via C—H $\cdots$  $\pi$  (2.853 Å) interactions with the ethynyl group. The pyridine acceptor site on the molecule interacts via bifurcated hydrogen bonds forming C—H $\cdots$ N (2.704 Å) type interactions, Figure 6.17.

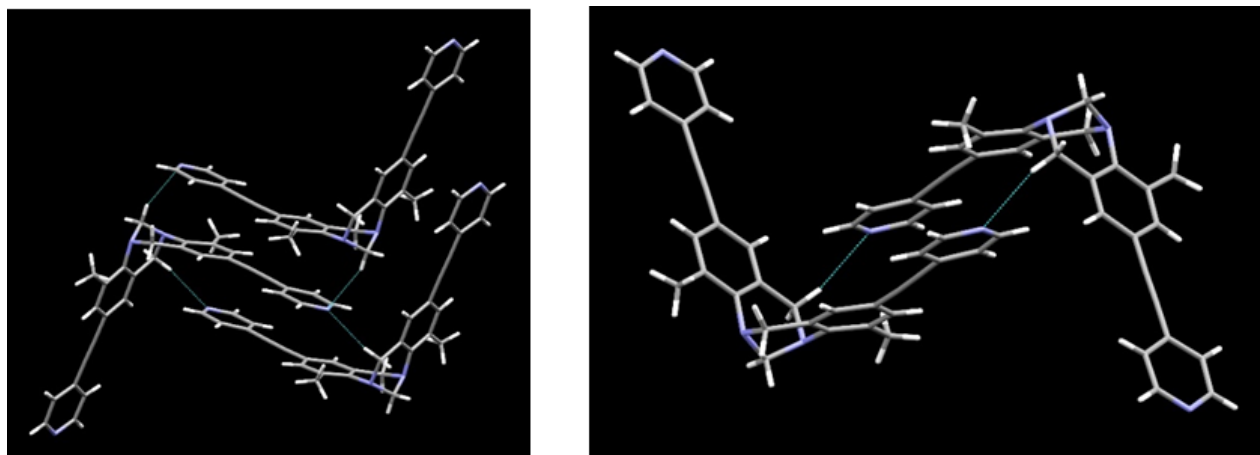


**Figure 6.17** Bifurcated C—H $\cdots$ N type interactions in **TBX8**

#### 6.3.4.4 Crystal structure of 4,10-dimethyl-2,8-diiodoethynyl-6H,12H-5,11-methanodibenzo[*b,f*]-diazocine tetramethylpyrazine (TBX4:A2)

The primary feature in the crystal structure of **TBX4:A2** is a 1D infinite zig-zag chain, Figure 6.18. The desired C—I···N halogen bond is formed by the C≡C—I group on the Tröger's base and the nitrogen on the tetramethylpyrazine (I50···N54, 3.147 Å, I25···N51, 3.051 Å, I10···N64, 3.153 Å, I35···N61, 3.057 Å). The respective bond angle are as follows; (C49—I50···N54, 171.65°, C24—I25···N51, 171.35°, C9—I10···N64, 171.22°, C34—I35···N61, 171.33°).

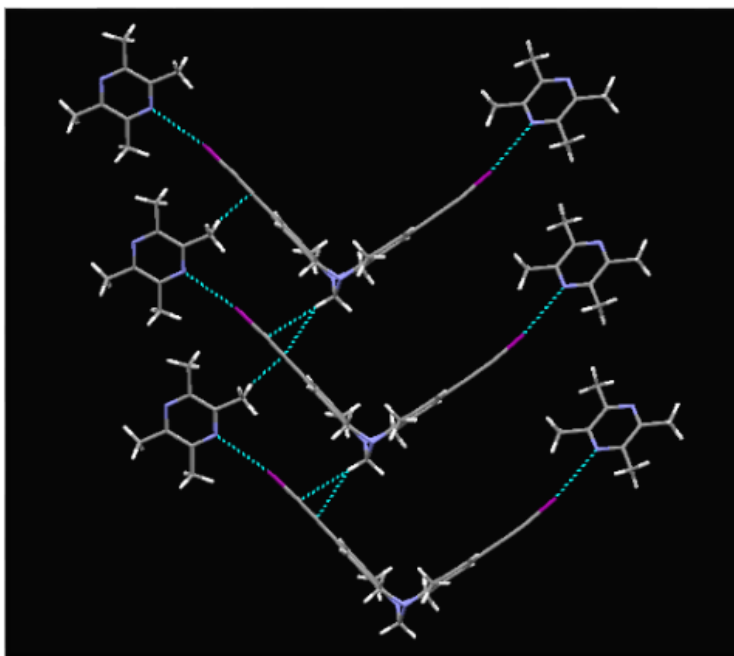


**Figure 6.18** Main interactions in the crystal structure of **TBX4:A2**

The halogen bond is accompanied by C—H··· $\pi$  interactions that stems forth from methyl substituent groups on pyrazine and on the methanodiazocine bridge which interacts with the ethynyl group on the Tröger's base extended arms, forming a 2D structure. The 2D frameworks are extended into 3D architectures via C—H··· $\pi$  interactions that take place between aromatic C—H groups and C≡C group on the Tröger's base.

#### 6.3.4.4 Crystal structure of 4,10-dimethyl-2,8-diiodoethynyl-6H,12H-5,11-methanodibenzo[b,f]-diazocine 1,2-di(4-pyridyl)ethylene (TBX4:A6)

The attempted co-crystallization of **TBX4** and **A6** resulted in the formation of a 1:1 binary solid, Figure 6.19. The primary interaction takes place between C≡C—I group on the Tröger's base and the nitrogen on the 1,2-di(4-pyridyl)ethylene, forming a 1-D infinite zig-zag chain with bond distances of (I21⋯N37, 2.821 Å, I25⋯N30, 2.809 Å) and bond angles of (C20—I21⋯N37, 178.63°, C24—I25⋯N30, 166.76°).

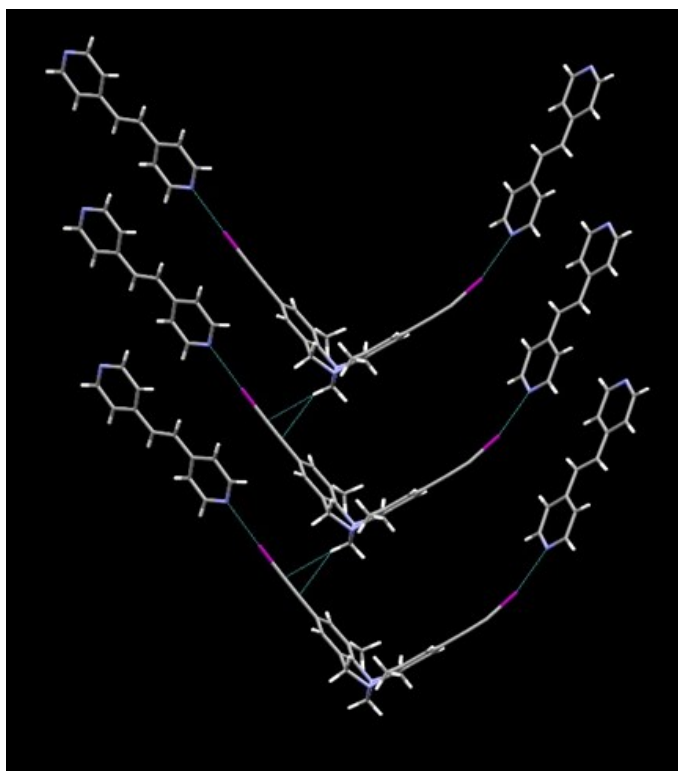


**Figure 6.19** Main interactions in the crystal structure of **TBX4:A6**

The halogen bond is accompanied by C—H⋯ $\pi$  interactions that form between the methyl substituent groups on the methanodiazocine bridge and the ethynyl group on the Tröger's base, forming a 2D structure.

## 6.4 Discussion

Five novel Tröger's base derivatives were synthesized, out of which, three contained nitrogen containing heterocycles as arms, extending outward from the Tröger's base scaffold that can act as hydrogen bond acceptors, and two, possessing an iodoethynyl functionality that can act as halogen bond donors. In the synthesis of **TBX1**, the substitution of a methyl group in the ortho position, on 4-iodoaniline, ensures only one regioisomer; the linear symmetric derivative, is formed. The linear regioisomer is probably the most useful precursor for applications of supramolecular chemistry. This also provides a sizable hydrophobic cavity for the synthesized analogues of Tröger's base.

The ground mixtures of hydrogen bond acceptor Tröger's base derivatives were tested using IR spectroscopy to reveal the formation of co-crystals. Among the grounded mixtures, all 28 grinding experiments formed co-crystals which is indicated by broad stretches that appear near 2,500 and 1,900  $\text{cm}^{-1}$  as well as considerable shifts in the carbonyl peaks, Figure 6.20.

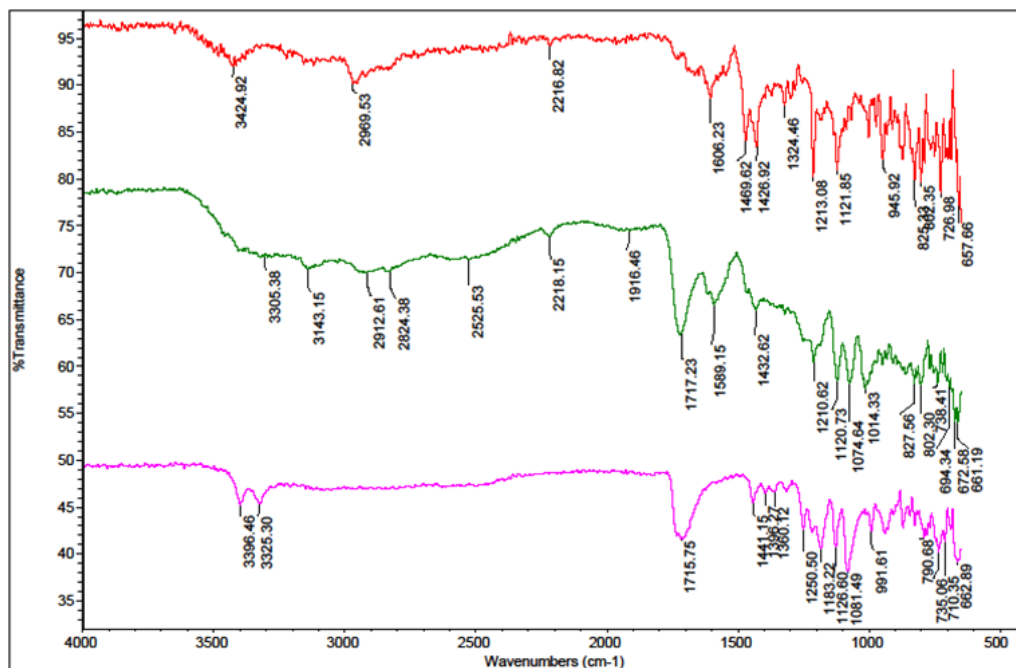
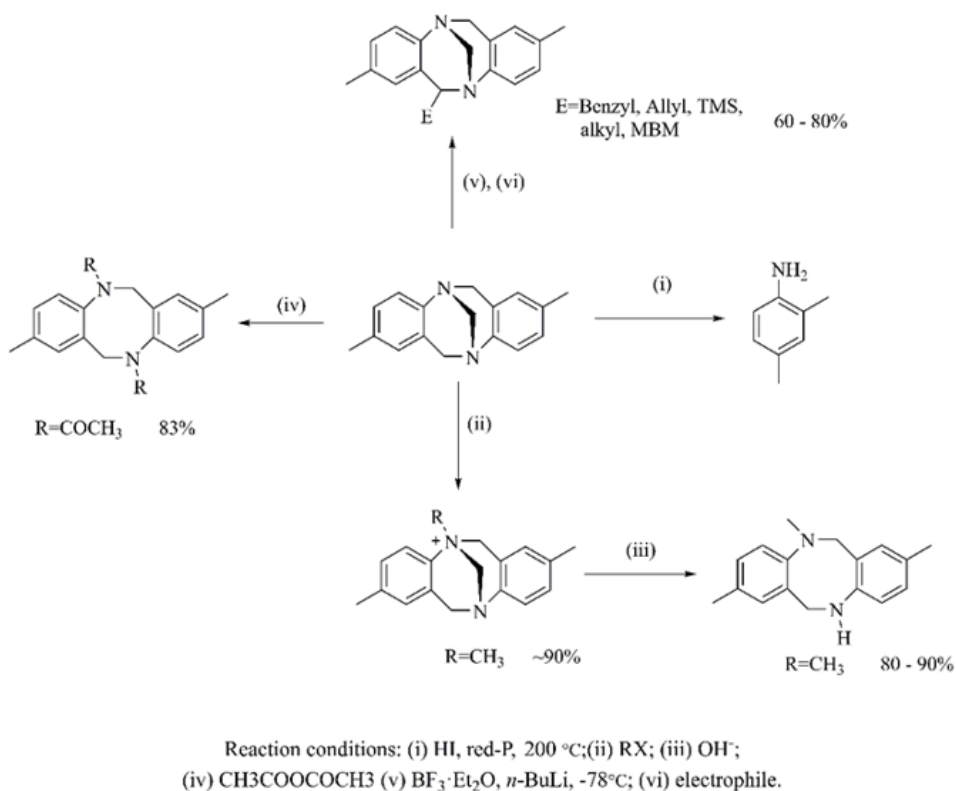


Figure 6.20 IR spectra of **TBX5** and Tartaric acid and the co-crystal thereof

Similarly, the ground mixtures of iodoethynyl Tröger's bases with symmetric ditopic acceptor produced co-crystals for all 14 experiments. A productive outcome is characterized in peak shifts corresponding to the C≡C in the iodoethynyl on the Tröger's base derivative and in the peaks in the range of 1,600 – 1,460 cm<sup>-1</sup> which are indicative of C=N stretch on the symmetric acceptors.

The Tröger's base despite its name, has a very low basicity. The methanodiazocine bridge is known to be unaffected by sodium and boiling ethanol. To date, only a few reactions involving the modification of the methanodiazocine bridge have been reported, Figure 6.21.



**Figure 6.21** Scheme representing the reactivity of the methanodiazocine of the Tröger's base

Given the low reactivity of the diazocine bridge, as a result of low basicity, implies that, the diazocine nitrogen's participating in any intermolecular interactions is considerably low. If a C—H···N type interaction is present, given the population of the antibonding orbital between the

nitrogen and the CH<sub>2</sub> bridge upon formation of a hydrogen bond at the nitrogen, we expect to observe an elongated bond length between the hydrogen-bonded nitrogen and CH<sub>2</sub> bridge.<sup>13</sup> But rather, we see that the bond length between the remaining nitrogen and CH<sub>2</sub> bridge approximately the same length (1.462 Å and 1.468 Å), Figure 6.22. Therefore, what is observed in Figure 6.14 is a close contact. Thus, we can see that the nitrogen atoms on the diazocine ring have not acted as potential binding sites.

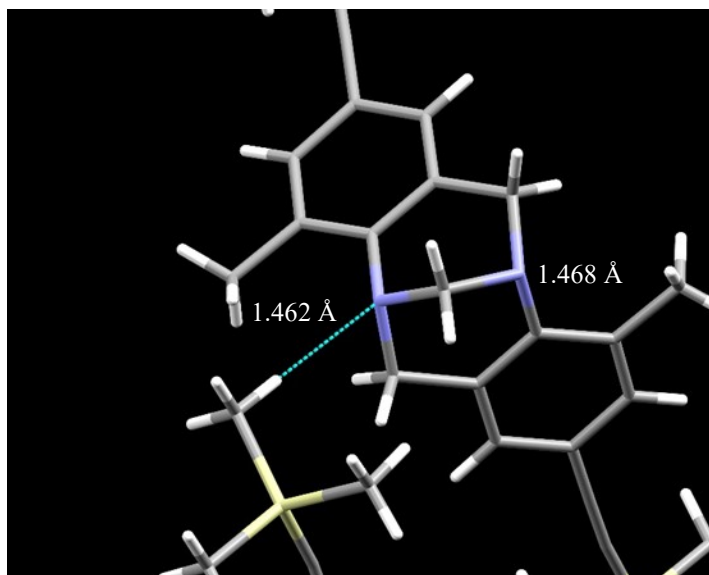


**Figure 6.22** Bond distance between diazocine nitrogens and CH<sub>2</sub> bridge

Calculated molecular electrostatic potential surfaces for **TBX4** and **TBY4** indicate lower electrostatic potentials for nitrogens on the diazocine ring than that for nitrogens on the symmetric ditopic acceptors. The resulting intermolecular interaction thus would form between; the best donor in the iodoethynyl Tröger's base and the N on the symmetric ditopic acceptor.

As expected, we observed that the best donor and best acceptor interact forming C—I⋯N type halogen bonds in structures **TBX4:A2** and **TBX4:A6**. In these supramolecular architectures, we observe the predicted 1-D chain propagating in a zig-zag pattern, Figure 6.23. Therefore,

reflecting upon the reasoning of such an outcome, it is clear, with guided synthetic protocols, a well-defined supramolecular synthon coupled with suitable supramolecular reagents which are conformationally rigid, desirable outcomes are a possibility. This further affirms the fact that with a fixed molecular shape, the structure can easily be predicted for rigid molecules, like Tröger's base derivatives.

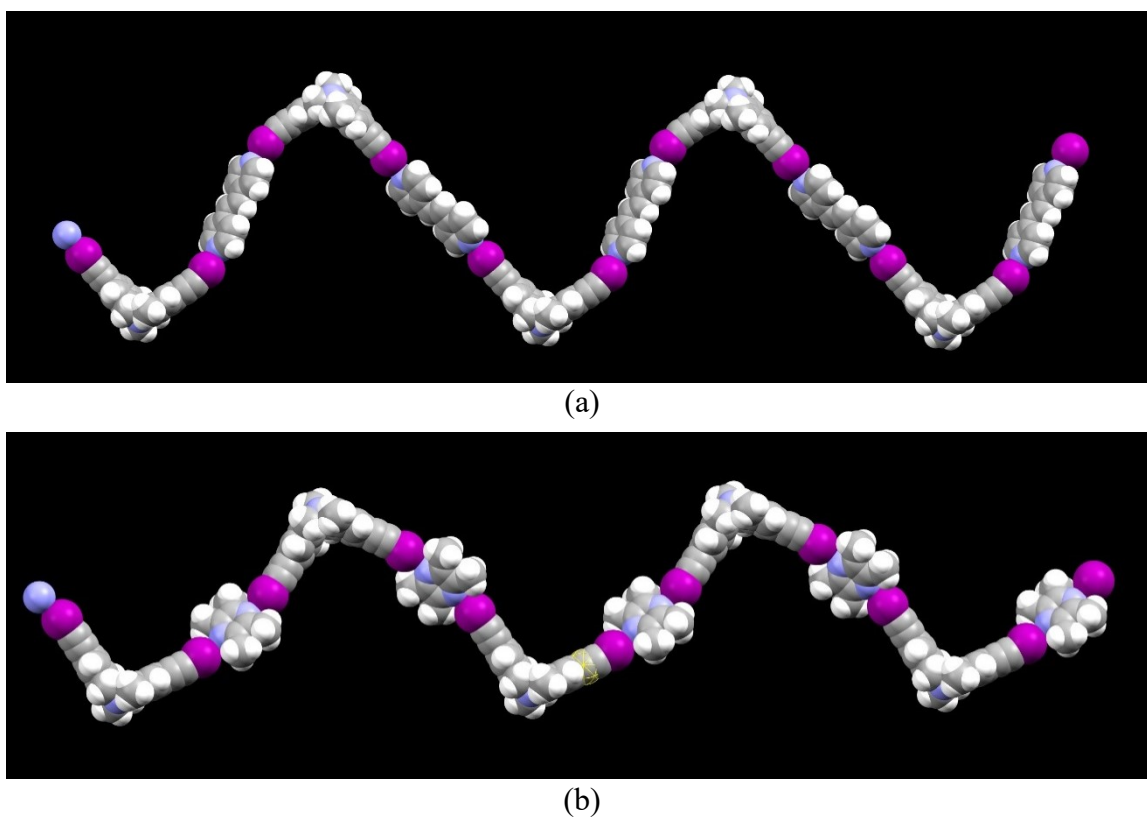


**Figure 6.23** Expected 1-D zig-zag chains of (a) **TBX4:A2** and (b) **TBX4:A6**

From a sample size of 43, and total count of 61 interactions of  $C\equiv C \cdots I \cdots N$  derived from the CSD we observe an average bond distance of 2.782 Å and bond angle of 175.645°. Bond distances are significantly longer (goes beyond population maximum of 3.073 Å) and bond angle are close to 171° for **TBX4:A2**, whereas, for **TBX4:A6** it falls within an acceptable range. Such a high deviation in the case of **TBX4:A2** can be attributed to the low negative potential on the



pyrazine compared to the acceptors sites considered in the CSD search which were predominantly pyridines which possess a higher negative potential as seen in Table 6.2. (*The CSD search was carried out between an  $sp^2$  nitrogen and  $C\equiv C$  —I checking all filter on the CSD search setup menu*)

The structure directing zigzag pattern observed herein is mainly due to the angle between the two aromatic cores. As for the **TBX4** in crystal structures **TBX4:A2** and **TBX4:A6**, the dihedral angle was  $99.41^\circ$  and  $99.95^\circ$ , respectively. These numbers fall closer towards the larger dihedral angles from a range of  $88^\circ - 105^\circ$  obtained from the CSD. The dihedral angle of **TBX1**, **TBX2** and **TBX8** fall within the range mentioned above.

It is a challenge to foresee the molecular geometry for a supramolecular reagent that is flexible, as also seen in chapters 3 and 4, given that it can possess different conformations. The fact that a change in the positioning of the function groups and the overall shape with respect to the molecular conformation, can lead to different crystal packing arrangements that ultimately influence the properties of the co-crystal. Therefore, an inherent flexibility in a supramolecule can be viewed as an obstacle for the successful construction of desired molecular architectures in crystal engineering. In view of this, it is clear that, reducing the number of binding sites and introducing rigidity to the molecule, we were successful in formulating co-crystals with both desired stoichiometry as well as expected connectivity occupying all donor and acceptor sites.

## 6.5 Conclusions

We were able to successfully synthesize hydrogen-bonding and halogen-bonding Tröger's base derivatives, which were used as building blocks to study the structural outcome of

conformationally rigid molecules. IR of the ground mixtures suggest a 100% supramolecular indicative of the robustness of both halogen bonded and hydrogen bonded synthons.

We observed that the diazocine nitrogen atoms are inert in the context of non-covalent interactions and even a remote possibility that they would compete with symmetric ditopic acceptors is improbable.

Reducing the number of binding sites to two, decreases the complexity of the molecular assembly, and we observed a 1:1 stoichiometry between **TBX4:A2** and **TBX4:A6**.

The solid-state landscapes resulting in 1-D zig-zag chains are a consequence of restricted geometric flexibility of the Tröger's base derivatives and thus, it affirms that formulating directed structures can be achieved relatively easily when the molecular building blocks are conformationally rigid.

## 6.6 References

1. Tröger, J., Ueber einige mittelst nascirenden Formaldehydes entstehende Basen. *J. Prakt. Chem.* **1887**, 36 (1), 225-245.
2. Spielman, M. A., The Structure of Troeger's Base. *J. Am. Chem. Soc.* **1935**, 57 (3), 583-585.
3. Wagner, E. C., Condensations of Aromatic Amines with Formaldehyde in Media Containing Acid. III. The Formation of Tröger's Base. *J. Am. Chem. Soc.* **1935**, 57 (7), 1296-1298.
4. Prelog, V.; Wieland, P., Über die Spaltung der Tröger'schen Base in optische Antipoden, ein Beitrag zur Stereochemie des dreiwertigen Stickstoffs. *Helv. Chim. Acta.* **1944**, 27 (1), 1127-1134.
5. Larson, S. B.; Wilcox, C. S., Structure of 5,11-methano-2,8-dimethyl-5,6,11,12-tetrahydrodibenzo[b,f][1,5]diazocine (Tröger's base) at 163 K. *Acta Crystallogr., Sect. C: Cryst. Struct. Commun.* **1986**, 42 (2), 224-227.

6. Kim, E.-i.; Paliwal, S.; Wilcox, C. S., Measurements of Molecular Electrostatic Field Effects in Edge-to-Face Aromatic Interactions and CH- $\pi$  Interactions with Implications for Protein Folding and Molecular Recognition. *J. Am. Chem. Soc.* **1998**, *120* (43), 11192-11193.
7. Smith, L. I.; Schubert, W. M., Polyalkylbenzenes. XXXIV.1The Reaction between Polymethyl-p-methoxyanilines and Formaldehyde. *J. Am. Chem. Soc.* **1948**, *70* (8), 2656-2661.
8. Jensen, J.; Wärnmark, K., Synthesis of Halogen Substituted Analogues of Tröger's Base. *Synthesis* **2001**, *2001* (12), 1873-1877.
9. Kiehne, U.; Luetzen, A., Synthesis of 2,8-Disubstituted Analogues of Troeger's Base. *ChemInform* **2004**, *35* (46).
10. Rajbanshi, A. Supramolecular interactions from small-molecule selectivity to molecular capsules. Kansas State University, 2010.
11. Osowska, K.; Lis, T.; Szafert, S., Protection/Deprotection-Free Syntheses and Structural Analysis of (Keto-aryl)diynes. *Eur. J. Org. Chem.* **2008**, *2008* (27), 4598-4606.
12. (a) Kiehne, U.; Weilandt, T.; Lützen, A., Diastereoselective Self-Assembly of Double-Stranded Helicates from Tröger's Base Derivatives. *Org. Lett.* **2007**, *9* (7), 1283-1286; (b) Kiehne, U.; Lützen, A., Synthesis of Bis(catechol) Ligands Derived from Tröger's Base and Their Dinuclear Triple-Stranded Complexes with Titanium(IV) Ions. *Eur. J. Org. Chem.* **2007**, *2007* (34), 5703-5711.
13. Dolenský, B.; Elguero, J.; Král, V.; Pardo, C.; Valík, M., Current Tröger's Base Chemistry. **2007**, *93*, 1-56.

## Chapter 7 - Conclusions and future work

The main focus of this thesis is to gain knowledge and understanding of intermolecular forces in molecular recognition events of flexible molecules both in solution and solid-state and to emphasize the importance of molecular rigidity in driving desired supramolecular solid forms with predictability.

To address this, a solution phase study using isothermal titration calorimetry (ITC) was conducted between an imidazolic tritopic acceptor and a series of monotopic benzoic acid derivatives, to evaluate hydrogen-bond preferences and binding affinities in solution. By changing the electrostatic component of the donor molecule in the hydrogen-bond formed between acceptor···donor both binding constant and thermodynamic landscape can be modulated, Figure 7.1.

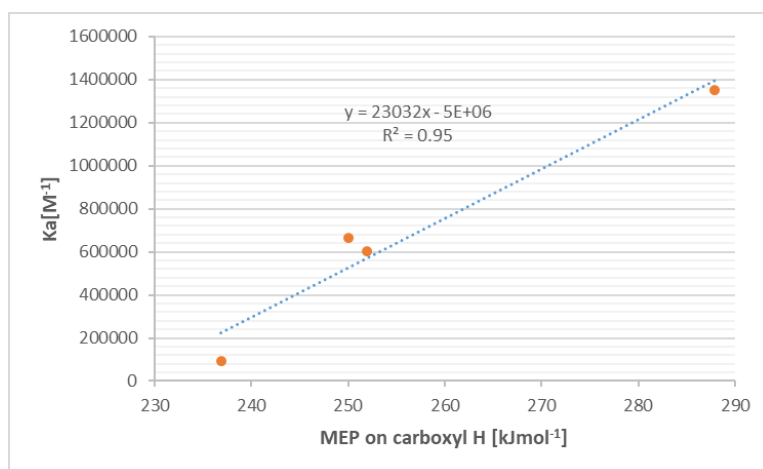


**Figure 7.1** Binding constant dependence on MEPS

Further, it was evident that to achieve desired supramolecular connectivity and stoichiometry, the reliability of a supramolecular synthon is important. In the case of hydrogen- and halogen-bond donors, we observed that desired connectivity was achieved with respect to the

hydrogen-bond donors even though vacant binding sites were observed in the tritopic acceptors. When considering the halogen-bond donors, the observations were different due to the deactivation of the  $\sigma$ -holes in the remaining binding site with consecutive binding, Figure 7.2. The presence of vacant sites on tritopic acceptors in both hydrogen- and halogen-bond complexes can also be attributed to possible steric hindrance and multiple sites for hydrogen bonding. When compared to similar flexible ditopic acceptors, having an additional arm does not provide any useful interactions. Unlike in biological systems where we observe multiple binding sites with expected connectivity, tritopic acceptors cannot pre-organize in solution to form a stable conformation prior to binding.

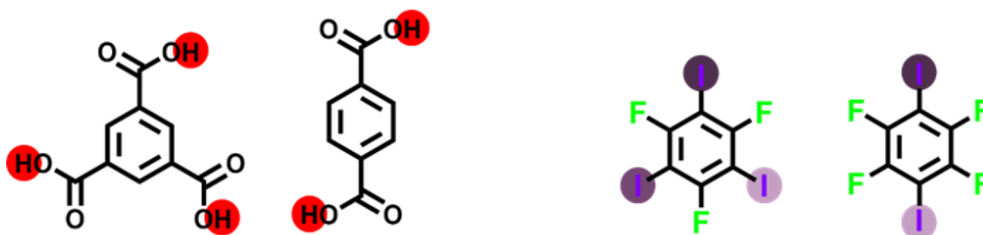


**Figure 7.2** Deactivated halogen bond donors compared to hydrogen bond donors

But, when the complexity of the tritopic acceptor is reduced by changing from three-binding sites to two-binding sites and introducing a conformationally restricted frame work, Figure 7.3, desired supramolecular outcomes are a possibility. To achieve this, a Tröger's base molecular scaffold was used with iodoethynyl functionality along with symmetric ditopic acceptors. The structural outcome of these analogues depended on; 1) the highly directional halogen bond, 2) conformers used, and 3) the dihedral angle between the aromatic rings which afforded 1-D zig zag chains as predicted.

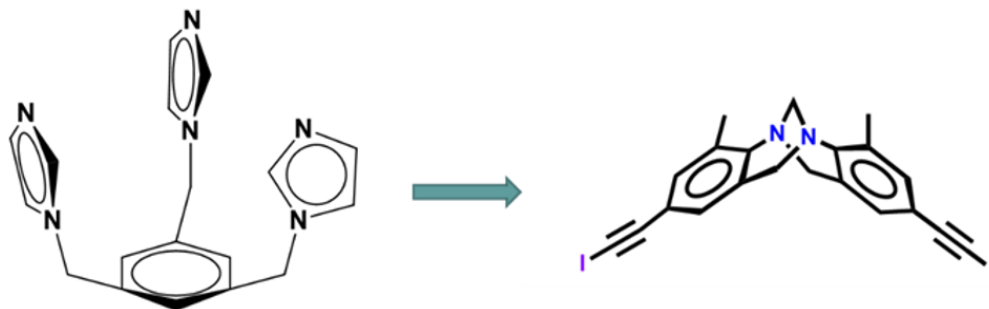


**Figure 7.3** A flexible tritopic acceptor compared to a rigid ditopic donor

However, there is much to be done to extend some of the systems to the next phase. The complexity of the tritopic acceptors can be increased by introducing asymmetric tritopic acceptors. This can be done by either introducing two or three structurally and electrostatically diverse binding sites, Figure.

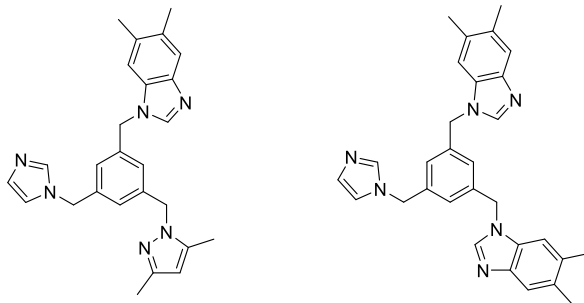


**Figure 7.4** Asymmetric tritopic acceptors

Furthermore, conformational rigidity can be introduced to a tritopic acceptor by replacing the flexible methylene bridge connecting the heterocycle to the benzene core. By reducing conformational flexibility, the complexity of the system can be reduced, which is as similar to a pre-organized biotic system.

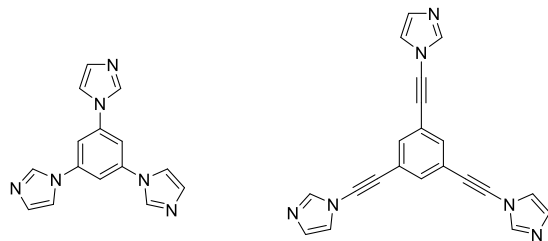


**Figure 7.5** Conformationally rigid tritopic acceptors

## Appendix A - $^1\text{H}$ NMR and $^{13}\text{C}$ NMR spectra

